

# **Reaction kinetics in formulated industrial catalysts**

By

Sam K. Wilkinson

A thesis submitted to the School of Chemical Engineering of the  
University of Birmingham for the degree of  
**DOCTORATE IN ENGINEERING EngD**

School of Chemical Engineering  
Faculty of Engineering  
The University of Birmingham  
B15 2TT, UK

UNIVERSITY OF  
BIRMINGHAM

**University of Birmingham Research Archive**

**e-theses repository**

This unpublished thesis/dissertation is copyright of the author and/or third parties. The intellectual property rights of the author or third parties in respect of this work are as defined by The Copyright Designs and Patents Act 1988 or as modified by any successor legislation.

Any use made of information contained in this thesis/dissertation must be in accordance with that legislation and must be properly acknowledged. Further distribution or reproduction in any format is prohibited without the permission of the copyright holder.

## Abstract

In heterogeneous catalysis, a fundamental understanding of the necessary physico-chemical requirements for a catalyst formulation is essential to its success, both in terms of performance and longevity. Understanding of reaction kinetics via modelling is essential for fundamental understanding of how catalysts work, providing functional information around surface active sites and details of reaction mechanism. This tool, combined with well-designed laboratory experiments to test a catalyst under steady and/or non-steady state conditions, can provide insight into the links between catalyst formulation and reaction performance. The aim of this project is to develop novel strategies and methods in these areas utilising a range of Johnson Matthey catalysts and reaction systems.

This thesis places significant focus on obtaining mechanistically and statistically sound kinetic models with reliable model parameter estimates. Methods for this are developed using a batch liquid phase hydrogenation system using a Pt/TiO<sub>2</sub> catalyst and are subsequently applied throughout the thesis.

Non-steady state analysis of catalyst formulations has been explored successfully under a number of distinct situations. Kinetic analysis of the initial transient behaviour of a fresh vanadium phosphorus oxide selective oxidation catalyst under reaction conditions was highly effective at understanding the evolution of distinct active site populations on the catalyst surface with time on stream. A subsequent study of copper-based methanol synthesis catalysts explored the impact of gas phase conditions on the catalyst state. A mixture of steady-state testing and transient response experiments (i.e. via an imposed change in gas phase conditions over the catalyst) provided not only a robust and mechanistic kinetic model for catalyst performance but also new insights into the evolution of active site populations and populations of surface species on the catalyst surface.

Overall, the reaction kinetics studies demonstrated across this thesis demonstrate not only a series of methods to understand catalyst behaviour in greater depth but also to understand the key functional requirements for an effective industrial catalyst.

## Acknowledgments

The four years of my EngD project with the University of Birmingham and Johnson Matthey has been a fantastic experience and (steep) learning curve for me in the field of reaction engineering and research in general. I'd firstly like to acknowledge my supervisors Prof. Mark Simmons, Dr. Mike Watson, Prof. Hugh Stitt and Dr. Phil Robbins.:

Firstly Mark, a huge thank-you for the boundless support you have given me in all aspects of my work during the doctorate. You've always gone the extra mile for me with the project and I also appreciate the critical eye you've given to my written work and presentations. Many good memories – particularly the wine and poster session at JMAC 2012...although the next day was a little difficult!

Mike – the ideas and premise you provided to my project were great and laid the foundations for an exciting set of studies. I also greatly appreciate the support you have given me during the project and in integrating into the Catalyst Research group at JMTC-North. Thanks also for the excellent tutelage I have received from you in catalysis and chemistry – many aspects of both were largely a blank slate for me when I first began my project here.

Hugh – the enthusiasm and ideas you have brought to my project have been fantastic. I've really enjoyed the in-depth scientific discussions we have (often running till late on a Friday afternoon or over a few beers!) I also appreciate the wider opportunities you have given me within my project at JM and with the reaction engineering conferences I have attended. Many good memories, particularly of meetings filled with puns (I can see Mike holding his head in despair!) and frequent quotations of the Yorkshireman's 2<sup>nd</sup> Law of Thermodynamics ('ye don't get 'art fer nart')

Thanks also to you Phil for your help in my project. I've always enjoyed working with you, going back to my undergrad days and it was good to have you around for my EngD reviews and to check over my written work! A big thank-you also to Dr. Richard Greenwood (EngD co-ordinator in the Centre for Formulation Engineering). Cheers Richard for doing a stellar job in running the EngD programme and thanks for enabling me to attend three international conferences! I have some great memories of the quarterly EngD reviews in Birmingham and Teesside interchanging between legendary currys and the Wynyard!

On a day-to-day basis I had the fortune of working with Drs Xavier Baucherel, Leon van de Water and John West (all at JM). Xavier – thanks for the support you gave me in the early stages of the project and your help in getting my experimental work going. We certainly had some (frustrating!) challenges on the VPO rig but it was all worth it in the end! Leon – working with you on the methanol synthesis project has been fantastic; I've always enjoyed how we've combined a passion for the topic with plenty of jokes at the same time. I also appreciated all of the chemistry and in-depth catalysis I've learnt off you – Dank je wel! John – thanks for all of your help and training on my thermal analysis work and for the flexibility in building in my experiments to your setup. I thoroughly enjoyed the 3 months we worked together on the ammonia SCR project!

I also extend a big thanks to many of my friends who have supported me over the past four years. Pete (Clark) – cheers for being a great housemate over the past two years – hopefully we've kept each other sane enough to get through our respective EngD endeavours – good luck over the rest of your project. Iain (Hitchcock) – always enjoy our big scientific discussions, long may they continue! Michele (Marigo) – as a fellow EngD, always good to talk to you about the project, the future and 'massive' ideas, with a good dose of banter thrown in! Jeroen (ten Dam) – great memories from our thesis weekends, particularly with the rewards for (completing) some work in the form of club sandwiches and Belgian beer! Lockhart (Horsburgh) for our countless discussions about heavy metal, cheese and pub quizzes! Also thanking Dilip (Poduval), my office 'neighbour' for three years and the many cricket matches and concerts we've been to. I'd also like to mention the friendship of my undergraduate/school friends Jon Blake, Robert Osborne, Rebecca Sindall, Richard Webster, Sam Lythe and Robert Wright over the years, cheers. Thanks to all of my other friends who have supported me as well – you know who you are!

Last but not definitely not least, thank you to my loved ones for your endless support and patience throughout my doctorate – my girlfriend Lou, mum Michele, step-dad Alan and grandparents Ken and Sylvia. You guys have played a huge part in supporting me in getting to where I am today!

I am also indebted to the specific contribution of the following individuals to the results chapters:

#### **Chapter 3:**

- Prof. Chris Hardacre, Dr. Jillian Thompson, Dr. Helen Daly, Ian McManus (Queen's University Belfast) for the background work and experimental data generated which were utilised in this chapter.
- Nazita Sedaie Bonab (University of Birmingham) whose PhD work on this topic ran in parallel to my work in this chapter.
- Jeroen ten Dam (JM) – many thanks for your insight on catalytic hydrogenation chemistries and some fantastic discussions over a coffee or three!

#### **Chapter 4:**

- Dr. Xavier Baucherel (JM)
- Dr. Richard Smith (XPS analysis and interpretation) (JM) – it was great to understand the workings of this technique from you and many thanks for your help in designing some very interesting XPS experiments on this system, the results of which go much further than presented in this chapter.
- Malcolm Kett (XRD and Raman Spectroscopy experiments) (JM)

- Rob Fletcher (Mercury porosimetry and BET surface area experiments) (JM)
- Colin Baptist (JM) – the rig gas chromatograph and I are very thankful to your help at times of crisis!

#### **Chapter 5:**

- Dr. Andy York (JM) – your idea to look at the ‘start-up’ of these selective catalytic reduction catalysts was an excellent one and led to a fascinating project. Thanks for the support and discussions we have had.
- Dr. Jörg Münch (JM) – many thanks for the experimental catalyst testing data and full support on this work.
- Dr. John West (JM)
- Dr. Iain Hitchcock (BET surface area experiments and analysis) (JM)
- Malcolm Kett (XRD and Raman Spectroscopy experiments) (JM)

#### **Chapters 6 and 7:**

- Dr. Leon van de Water (JM)
- Colin Ranson (N<sub>2</sub>O reactive titration experiments and for providing background property data to the catalysts tested) (JM)
- Rob Fletcher (BET surface area experiments) (JM)

Sam K. Wilkinson – February 2014

# Table of contents

## Chapter 1: Reaction kinetics in formulated industrial catalysts: *Introduction and business case*

1. Introduction: ‘ <i>Reaction kinetics in formulated industrial catalysts</i> ’ .....	30
1.1 Formulated industrial catalysts in context .....	32
1.2 Levels of complexity in kinetic modelling studies in heterogeneous catalysis...	34
1.2.1 Steady state vs. non-steady state.....	35
1.2.2 Statistical analysis and confidence in kinetic models.....	37
1.2.3 Theoretical approaches.....	38
1.3 Company background: Johnson Matthey plc .....	39
1.4 Business case .....	40
1.5 Thesis objectives.....	41
1.6 Structure of the thesis .....	43
1.7 Appendix: List of publications and conferences .....	47
1.8 References .....	48
2. Introduction: ‘ <i>Linking catalyst functionality under reaction conditions to formulation</i> ’ .....	52
2.1 Catalyst testing.....	54
2.1.1 The ten commandments of catalyst testing .....	54
2.1.2 Experimental techniques to understand catalyst performance evolution..	62
2.1.2.1 Accelerated decay tests .....	62
2.1.2.2 Parallel difference tests.....	63
2.1.2.3 Transient response tests.....	66
2.2 Catalyst characterisation .....	67
2.2.1 <i>Ex situ</i> techniques.....	67
2.2.2 <i>In situ</i> and <i>operando</i> techniques .....	68
2.3 Kinetic and activity-time modelling .....	69
2.3.1 Time dependent adsorption-desorption-(reaction) kinetic modelling.....	69
2.3.2 Activity-time modelling.....	71
2.3.2.1 Empirical approaches .....	71
2.3.2.2 Semi-empirical approaches.....	74
2.3.2.3 Fundamental approaches.....	74

2.4	Conclusions.....	76
2.5	References .....	77
3.	Introduction: ‘ <i>Solvation, Adsorption and Selectivity</i> ’ .....	82
3.1	Kinetic modelling of solvent effects in literature .....	83
3.1.1	Complementary approaches for elucidating solvent effects .....	85
3.1.2	Study of 4-phenyl-2-butanone hydrogenation over a Pt/TiO <sub>2</sub> catalyst .....	86
3.1.3	Chapter Objectives .....	86
3.2	Materials and methods.....	87
3.2.1	Experimental: Autoclave reaction studies .....	87
3.2.2	Kinetic modelling procedure .....	89
3.3	Results .....	91
3.3.1	Effect of temperature.....	91
3.3.2	Effect of 4-phenyl-2-butanone concentration.....	93
3.3.3	Effect of solvent choice.....	94
3.4	Kinetic Modelling.....	96
3.4.1	Model refinement: Parameter reduction example.....	98
3.4.2	Comparison and selection from refined models.....	107
3.4.3	Kinetic model application to a range of solvents .....	111
3.5	Discussion .....	113
3.6	Conclusions.....	114
3.7	Appendices - Experimental and <i>a priori</i> checks for mass transport limitations ... .....	116
3.7.1	Experimental checks for mass transport limitations.....	116
3.8	References .....	117
4.	Introduction: ‘ <i>Catalyst conditioning – The final stage of catalyst activation?</i> ’ .....	122
4.1	Vanadium phosphorus oxide catalysts for <i>n</i> -butane selective oxidation.....	123
4.1.1	Chapter Objectives .....	126
4.2	Materials and methods.....	126
4.2.1	Sample preparation and properties.....	126
4.2.2	Micro-reactor test rig.....	127
4.2.3	Catalyst characterisation .....	130
4.2.4	Kinetic modelling .....	130
4.3	Results .....	131
4.3.1	Parallel difference testing .....	131

4.3.2	Characterisation.....	136
4.3.3	Testing in differential mode.....	141
4.4	Kinetic modelling .....	143
4.4.1	Apparent kinetics .....	143
4.4.2	Triangular networks .....	145
4.4.2.1	6-parameter model of Escardino <i>et al.</i> , (1973) .....	146
4.4.3	Activity-time modelling.....	150
4.5	Discussion .....	153
4.5.1	Methodology development.....	153
4.5.2	Critically assessment of the impact of activation and conditioning periods .. .....	154
4.5.3	Insight into reaction mechanisms .....	155
4.6	Conclusions.....	156
4.7	Appendices .....	158
4.7.1	Other kinetic models tested in section 4.4 .....	158
4.8	References .....	159
5.	Introduction: ‘ <i>Stability, storage and reaction</i> ’ .....	165
5.1	Kinetics and mechanism .....	167
5.1.1	Steady state kinetic studies in literature for NH <sub>3</sub> SCR of NO .....	167
5.1.2	Adsorption-desorption kinetic studies using NH <sub>3</sub> and/or NO .....	169
5.1.3	Chapter Objectives .....	172
5.2	Materials and methods.....	172
5.2.1	Sample preparation and properties.....	172
5.2.2	Catalyst characterisation .....	173
5.2.3	Steady-state reaction studies.....	173
5.2.4	NH <sub>3</sub> temperature programmed desorption (TPD) studies .....	175
5.2.5	Kinetic modelling procedure .....	178
5.3	Results and discussion.....	181
5.3.1	Catalyst characterisation .....	181
5.3.2	Steady state results.....	183
5.3.3	Steady state kinetic modelling .....	185
5.3.3.1	Kinetic analysis using the model of Lintz and Turek .....	185
5.3.3.2	Kinetic analysis using the model of Dumesic <i>et al.</i> .....	187
5.3.4	TPD studies .....	193

5.4	Conclusions.....	199
5.5	References .....	201
6.	Introduction: ‘ <i>Functionality, feed and formulation</i> ’ .....	206
6.1	Kinetics and reaction mechanisms for copper-based catalysts in literature... 208	
6.1.1	CO/CO <sub>2</sub> /H <sub>2</sub> conditions .....	208
6.1.2	Chapter Objectives .....	212
6.2	Materials and methods.....	213
6.2.1	Sample preparation and properties.....	213
6.2.2	Micro-reactor test rig.....	214
6.2.3	Kinetic modelling .....	218
6.3	Results and discussion.....	220
6.3.1	Initial reduction of CuO/ZnO/Al <sub>2</sub> O <sub>3</sub> in H <sub>2</sub> /N <sub>2</sub> .....	221
6.3.2	Kinetic analysis of Cu/ZnO/Al <sub>2</sub> O <sub>3</sub> under CO/CO <sub>2</sub> /H <sub>2</sub> feeds.....	223
6.3.2.1	Steady state experimental.....	223
6.3.2.2	Steady state kinetic modelling .....	229
6.3.2.3	Start-up in CO/CO <sub>2</sub> /H <sub>2</sub> feeds.....	234
6.3.3	Binary formulations .....	238
6.4	Conclusions.....	240
6.5	Appendices .....	242
6.6	References .....	246
7.	Introduction: ‘ <i>New active sites or old surface species?</i> ’ .....	251
7.1	Approaches to examining the generation and loss of methanol synthesis functionality over copper-based formulations.....	252
7.1.1	Steady-state kinetics under CO/H <sub>2</sub> .....	252
7.1.2	<i>In situ</i> gas-phase pre-treatments .....	255
7.1.3	Dynamic kinetic modelling .....	257
7.1.4	Co-adsorption and temperature programmed desorption (TPD) studies	258
7.1.5	<i>In situ</i> characterisation studies .....	259
7.1.6	Chapter Objectives .....	260
7.2	Materials and methods.....	261
7.2.1	Sample preparation and properties.....	261
7.2.2	Micro-reactor test rig.....	261
7.3	Results and discussion.....	262
7.3.1	Kinetic analysis of Cu/ZnO/Al <sub>2</sub> O <sub>3</sub> under CO/H <sub>2</sub> feeds.....	263

7.3.1.1	Start-up in CO/H <sub>2</sub> feeds.....	263
7.3.1.2	Steady state apparent kinetics .....	270
7.3.2	Dynamic analysis under CO/CO <sub>2</sub> /H <sub>2</sub> conditions following CO/H <sub>2</sub> pre-treatments over a Cu/ZnO/Al <sub>2</sub> O <sub>3</sub> catalyst.....	272
7.3.2.1	Initial parallel difference test analysis.....	272
7.3.2.2	Reversibility and stability .....	278
7.3.2.3	Impact of pre-treatment temperature .....	279
7.3.3	Binary formulations .....	285
7.4	Conclusions.....	286
7.5	References .....	289
8.	Conclusions Overview.....	293
8.1	Reflection on the specific project aims .....	293
8.2	Reflection on the overall project aims: ' <i>A tale of two active sites</i> ' .....	297
8.3	Context and future work .....	300

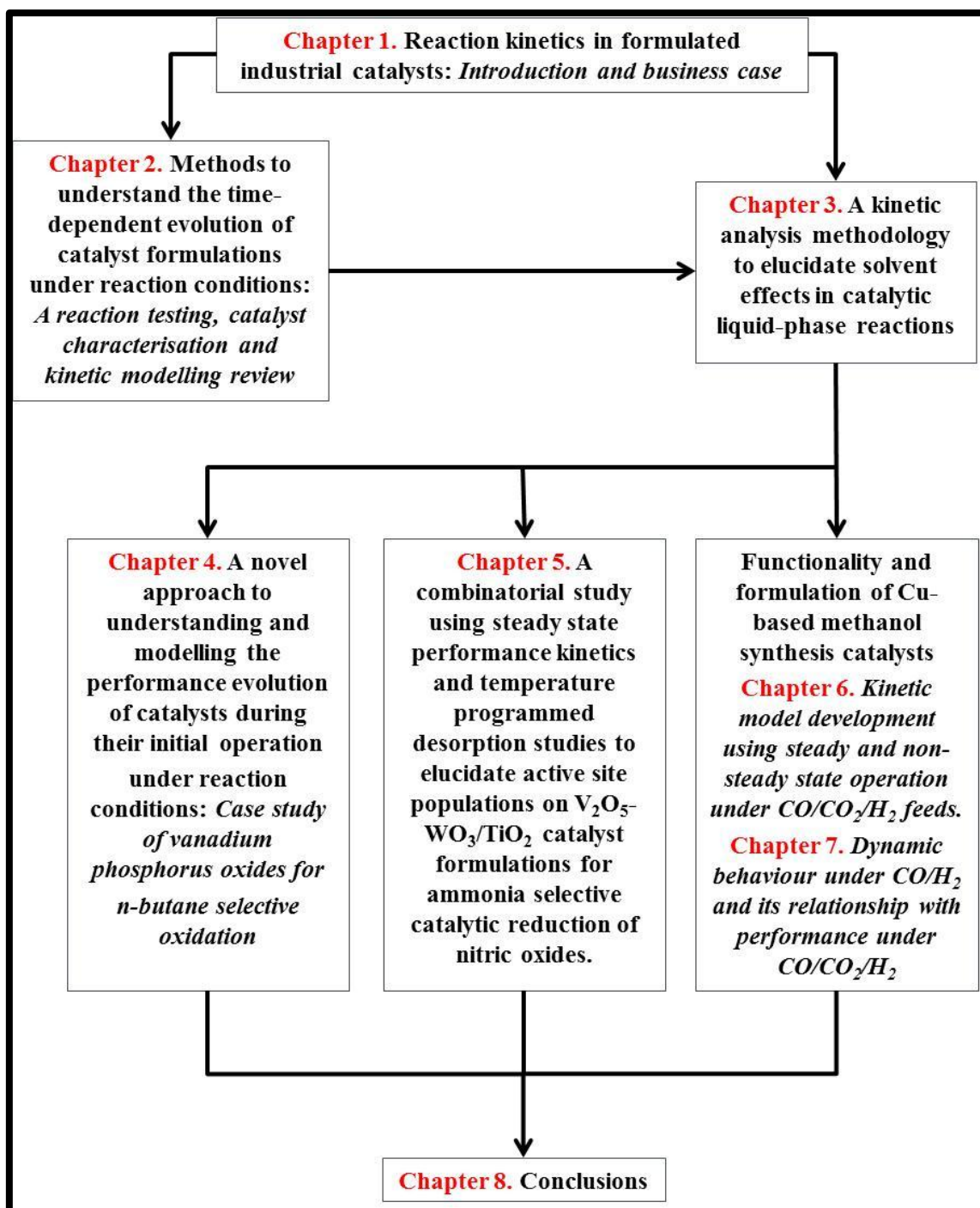


Diagram of the thesis structure

## List of figures

### Chapter 1:

Figure 1.1: Figure 1.1: Examples of formulated catalysts: A) Heavy duty diesel emissions control catalyst, B) Polymer electrolyte fuel cells, C) Methanol synthesis catalyst.

Figure 1.2: A generalised flow chart for a catalyst formulation process, through to a ‘finished’ product operating at quasi-steady state (QSS) under reaction conditions.

Figure 1.3: Graph of observed methanol synthesis activity plotted against copper metal surface area of different Cu-based catalyst formulations.

Figure 1.4: Thesis structure

### Chapter 2:

Figure 2.1: Generalised flow diagram to understand time-dependent evolution of catalyst formulations under reaction conditions.

Figure 2.2: Common laboratory flow micro-reactors used for kinetic measurements.

Figure 2.3: Example of a parallel difference test setup using 4 micro-reactors in parallel filled with catalyst and inert silicon carbide packing.

Figure 2.4: Characteristic catalyst performance evolution plots for parallel difference testing.

Figure 2.5: Examples of step-change transient response tests: (left) CO<sub>2</sub> product response over a MnO<sub>2</sub> catalyst when an O<sub>2</sub>/N<sub>2</sub> feed is switched to either a CO/He or CO/O<sub>2</sub>/N<sub>2</sub> feed (right) NO and NH<sub>3</sub> concentration response over two different catalyst formulations.

### Chapter 3:

Figure 3.1: Reaction network for 4-phenyl-2-butanone (PBN) hydrogenation.

Figure 3.2: Schematic for reaction testing equipment in this study.

Figure 3.3: A) Evolution of PBN concentration with reaction time at different reaction temperatures in hexane solvent. B) Selectivity of products at different temperatures at 10 min and 120 min reaction time.

Figure 3.4: A) Evolution of PBN hydrogenated with reaction time using different starting concentrations of PBN at 343 K. B) Variation in initial rate behaviour against starting concentration of PBN.

Figure 3.5: Reaction time concentration profiles for different solvents at 343 K.

Figure 3.6: PBN Conversion plotted against Henry's Constant for H<sub>2</sub> solubility in each solvent experiment after 30 min and 120 min.

Figure 3.7: A) Normalised Jacobian norms for all model responses with respect to model parameters and B) for individual responses.

Figure 3.8: A) Calculated *F*-statistic for successive parameter removal across the entire system response and B) with respect to individual model responses.

Figure 3.9: Calculated *F*-statistic for successive parameter removals across the entire system response for different models.

Figure 3.10: Change in condition number with number of parameters in models.

Figure 3.11: Estimated parameter values for  $k_{ket}$ ,  $k_{arom}$  and  $K_{CBN}$  using the surface reaction r.d.s model with product desorption for experimental data using different starting concentrations of PBN at 343 K.

Figure 3.12: A) Magnitude of CBN adsorption constant against selectivity for PBN hydrogenation in different solvents and B) Summated rate constant  $k_{arom} + k_{ket}$  plotted against  $k_H$  for H<sub>2</sub> solubility at 5 bar, 343 K in various solvents.

Figure 3.13: Effect of stirrer speed on initial reaction rate of PBN.

Figure 3.14: Effect of catalyst mass on initial reaction rate of PBN.

#### **Chapter 4:**

Figure 4.1: Time on stream intrinsic rate evolution for individual sectors of an example run for (A) *n*-butane consumption, (B) MA formation, (C) CO<sub>x</sub> formation over a VPO catalyst.

Figure 4.2: Evolution of *n*-butane conversion over the full catalyst bed between initial reading (t = 0.4 h); 17 h on stream for different reaction temperatures; and adjusted reactor inlet flow

rates required at 17 h on stream to achieve initial *n*-butane conversion over the full catalyst bed.

Figure 4.3: Performance evolution of MA and CO<sub>x</sub> yields over A) Sector 1, B) Sectors 2-4 combined.

Figure 4.4: Evolution of MA intrinsic selectivity of a VPO catalyst across a full catalyst bed for different reaction temperatures.

Figure 4.5: XRD analysis of VPO catalyst from the 1<sup>st</sup> sector of the catalyst bed, before and after testing at under 653 K, 2% *n*-butane in air reactor inlet conditions, 30 ml min<sup>-1</sup> flow.

Figure 4.6: Raman analysis of VPO catalyst from the 1<sup>st</sup> sector of the catalyst bed, before and after testing at 653 K, 2% *n*-butane in air reactor inlet conditions, 30 ml min<sup>-1</sup> flow.

Figure 4.7: Measured bulk  $V_{ox}$  via auto-titration of VPO catalyst before and after testing at 653 K, 2% *n*-butane in air reactor inlet conditions, 30 ml min<sup>-1</sup> flow.

Figure 4.8: XPS analysis of VPO catalyst from the 1<sup>st</sup> sector of the catalyst bed, before and after testing at 653 K, 2% *n*-butane in air reactor inlet conditions, 30 ml min<sup>-1</sup> flow.

Figure 4.9: Differential mode testing of VPO catalyst under steady state performance following 48 hours conditioning.

Figure 4.10: Evolution in apparent reaction order in *n*-butane with time on stream for A) MA formation, B) CO<sub>x</sub> formation.

Figure 4.11: Schematic of triangular reaction network.

Figure 4.12: Fitted parameters against time on stream for 5-parameter model using pseudo-first order relationships. A) Activation energies B) Re-parameterised pre-exponential factors.

Figure 4.13: Parity plots of predicted concentrations (from 5-parameter model) against experimental concentrations of A) *n*-butane, B) MA, C) CO<sub>x</sub>/4. Data from 3 different time on stream points are shown: 0.4 h, 2.1 h, 11.4 h.

Figure 4.14: Evolution of normalised pre-exponential factors ('activity') with time on stream for the 5 parameter kinetic model. Lines denote fitted 1<sup>st</sup> order activity-time models.

Figure 4.15: Calculated norms of the Jacobean matrix for each parameter in the activity evolution model network.

## Chapter 5:

Figure 5.1: Examples of commercial  $V_2O_5$ - $WO_3$ / $TiO_2$  catalysts.

Figure 5.2: Schematic for the  $NH_3$  SCR of NO over a  $V_2O_5$ / $TiO_2$  catalyst (taken from Dumesic *et al.*, 1996).

Figure 5.3: Dynamic adsorption-desorption of  $NH_3$  and NO on a model  $V_2O_5$ - $WO_3$ / $TiO_2$  catalyst.

Figure 5.4: Proposed structures for ammonia adsorbed on  $V_2O_5$ / $TiO_2$ : a) Lewis-bonded  $NH_3$  at Ti sites; b) H-bonded  $NH_3$  at oxide sites; c) Lewis-bonded  $NH_3$  at vanadyl sites; d) ammonium ions bonded at V Brønsted acid sites.

Figure 5.5: XRD analysis of fresh and aged SCR1 and SCR 2 catalyst powders. All reflections are assigned to  $TiO_2$ -anatase.

Figure 5.6: Raman spectroscopy analysis of fresh and aged SCR1 and SCR2 catalyst powders.

Figure 5.7:  $NO_x$  removal performance of fresh and 200 hours 873 K aged for SCR1 and SCR2 catalysts in the 453 – 773 K temperature range.

Figure 5.8: Ratio of  $NO_x$  to  $NH_3$  consumption at different temperatures and aged state of catalysts.

Figure 5.9: Parameter estimates for energies of model reaction steps and their re-parameterised pre-exponential factors. Ageing conditions were 873 K and  $T_{base} = 423K$  for re-parameterisation.

Figure 5.10: Parameter estimates for re-parameterised pre-exponential factors ( $T_{base} = 348K$ ) of  $K_{NH_3}$  (Graph A) and  $k_2$  (Graph B) for SCR1 and SCR2 catalysts. Ageing conditions were 873 K.

Figure 5.11: Comparison of parametric evolution ( $T_{base} = 348K$ ) of  $A_{NH_3}$  (graph A) and  $A_2$  (graph B) for SCR1 and SCR2 at different ageing temperatures against ageing time.

Figure 5.12: Raw exit stream ammonia response during TPD for all four SCR catalysts tested.

Figure 5.13: Ammonia TPD over 0.1 g of A) Fresh SCR1 and SCR2 and B) 200 h 873 K aged SCR1 and SCR2 using a temperature ramp rate of 15 K min<sup>-1</sup>.

## Chapter 6:

Figure 6.1: Methanol production rates from CO/CO<sub>2</sub>/H<sub>2</sub> gas mixtures under differential and finite conversion over Cu/ZnO/Al<sub>2</sub>O<sub>3</sub> at 523 K.

Figure 6.2: Reaction scheme for the synthesis of methanol and WGS reaction (taken from Vanden Bussche and Froment, 1996).

Figure 6.3: Parallel difference setup for testing copper-based catalysts.

Figure 6.4: Transitions of gas-phase conditions over copper-based catalysts explored in Chapter 6 and Chapter 7.

Figure 6.5: Evolution of A) H<sub>2</sub>O and B) CO<sub>2</sub> during the initial CuO/ZnO/Al<sub>2</sub>O<sub>3</sub> reduction step under 2% H<sub>2</sub>/N<sub>2</sub> at 10 bar.

Figure 6.6: Catalyst stability example during steady state testing.

Figure 6.7: Steady-state axial concentration plots for a Cu/ZnO/Al<sub>2</sub>O<sub>3</sub> catalyst operating under 473 K, 7.5 L h<sup>-1</sup> conditions with CO/CO<sub>2</sub> inlet ratios of A) 10:1, B) 3:1 and C) 1:1.

Figure 6.8: Values of equilibrium terms A)  $\beta_1^*$  and B)  $\beta_2^*$  at individual sector outlets for all experimental steady state data points (temperature/pressure/feed conditions inclusive) in the kinetic study.

Figure 6.9: Extended reaction network for methanol synthesis and WGS catalysis over a Cu/ZnO/Al<sub>2</sub>O<sub>3</sub> catalyst.

Figure 6.10: Reaction performance of A) 250 mg, B) 500 mg of Cu/ZnO/Al<sub>2</sub>O<sub>3</sub> catalyst upon feeding CO/CO<sub>2</sub>/H<sub>2</sub>/N<sub>2</sub> (3:3:67:27) at 7.5 L h<sup>-1</sup> (STP) at 25 bar, 473 K.

Figure 6.11: A) Cumulative missing carbon and oxygen over a Cu/ZnO/Al<sub>2</sub>O<sub>3</sub> catalyst during the first 30 min operation under CO/CO<sub>2</sub>/H<sub>2</sub>/N<sub>2</sub> (3:3:67:27) at 7.5 L h<sup>-1</sup> (STP) at 25 bar, 473 K. B) Calculated O/C ratio and RWGS equilibrium term at bed exits.

Figure 6.12: Comparison on H<sub>2</sub>O productivity and rate of carbon and oxygen lost over the front 250 mg of a Cu/ZnO/Al<sub>2</sub>O<sub>3</sub> catalyst bed during the first 15 min operation under CO/CO<sub>2</sub>/H<sub>2</sub>/N<sub>2</sub> (3:3:67:27) at 7.5 L h<sup>-1</sup> (STP) at 25 bar, 473 K.

Figure 6.13: Parity plots for response variables A) CO, B) CO<sub>2</sub> C) CH<sub>3</sub>OH and D) H<sub>2</sub>O. Response variable predictions are provided by the 7-parameter, 3 reaction pathway model based on Vanden Bussche and Froment, 1996.

## Chapter 7:

Figure 7.1: Potential energy diagram for the methanol synthesis reaction on the Cu/ZnO interface (1 0 1 0) from CO hydrogenation.

Figure 7.2: Normalised methanol production rate in a tubular reactor after pre-treatment of a Cu/ZnO/Al<sub>2</sub>O<sub>3</sub> catalyst for 0.5 h with (A) CO/He, (B) He, (C) pure H<sub>2</sub> and (D) CO<sub>2</sub>/He with a subsequent switch to syngas (CO/CO<sub>2</sub>/H<sub>2</sub>/He).

Figure 7.3: Methanol production over a Cu/ZnO/Al<sub>2</sub>O<sub>3</sub> catalyst in a tubular reactor as a function of time following different 2 h pre-treatments comprising mixtures of CO and H<sub>2</sub>. After the pre-treatment (t = 0 min), the gas mixture is changed to syngas (CO/CO<sub>2</sub>/H<sub>2</sub>/He).

Figure 7.4: Model diagram for the wetting/non-wetting of Cu-particles on a Zn support, surface alloying and bulk alloy formation: a) round shaped particle under oxidising syngas conditions, b) disk-like particle under more reducing conditions, c) surface Zn-Cu alloying due to stronger reducing conditions, d) brass alloy formation due to severe reducing conditions.

Figure 7.5: TPD profiles obtained after coadsorption of CO<sub>2</sub> and H<sub>2</sub> (1:9) at 100°C, 8 bar on a reduced commercial Cu/ZnO/Al<sub>2</sub>O<sub>3</sub> catalyst with a heating rate of 3 K min<sup>-1</sup>.

Figure 7.6: Transitions of gas-phase conditions over copper-based catalysts explored in Chapter 6 and Chapter 7.

Figure 7.7: A) Reaction performance of Cu/ZnO/Al<sub>2</sub>O<sub>3</sub> catalyst upon feeding CO/H<sub>2</sub>/N<sub>2</sub>. B) Comparison of normalised carbon loss rates with CO<sub>2</sub> and H<sub>2</sub>O elution in the same experiment.

Figure 7.8: Reactor outlet observations of A) CO<sub>2</sub>, B) H<sub>2</sub>O and C) CH<sub>3</sub>OH of 125 mg, 250 mg, 375 mg and 500 mg of Cu/ZnO/Al<sub>2</sub>O<sub>3</sub> catalyst upon feeding CO/H<sub>2</sub>/N<sub>2</sub>.

Figure 7.9: Outlet methanol profiles for a 500 mg Cu/ZnO/Al<sub>2</sub>O<sub>3</sub> catalyst bed upon feeding CO/H<sub>2</sub>/N<sub>2</sub>.

Figure 7.10: Apparent  $E_a$  values for methanol formation across 125 and 500 mg Cu/ZnO/Al<sub>2</sub>O<sub>3</sub> catalyst beds under 3% CO/ X% CO<sub>2</sub>/ 67% H<sub>2</sub>/ 30-X% N<sub>2</sub> at 7.5 L h<sup>-1</sup> (STP) at 25 bar in the temperature range 453 – 493 K.

Figure 7.11: Start-up comparison of 500 mg Cu/ZnO/Al<sub>2</sub>O<sub>3</sub> catalyst pre-treated in A) CO/H<sub>2</sub>/N<sub>2</sub> and B) H<sub>2</sub>/N<sub>2</sub>: 2/98. Start-up conditions were 473 K, 25 bar, 7.5 L h<sup>-1</sup> using feed gas (CO/CO<sub>2</sub>/H<sub>2</sub>/N<sub>2</sub>).

Figure 7.12: Comparison of normalised ‘additional’ CH<sub>3</sub>OH and H<sub>2</sub>O production and CO<sub>2</sub> consumption rates over a CO/H<sub>2</sub> pre-treated 500 mg Cu/ZnO/Al<sub>2</sub>O<sub>3</sub> catalyst in comparison to a H<sub>2</sub>/N<sub>2</sub> pre-treatment at 473 K, 25 bar, 7.5 L h<sup>-1</sup> using feed gas (CO/CO<sub>2</sub>/H<sub>2</sub>/N<sub>2</sub>).

Figure 7.13: Time on stream sector evolution of A) Methanol productivity, B) Apparent methanol synthesis first order rate constant of a Cu/ZnO/Al<sub>2</sub>O<sub>3</sub> catalyst (500 mg total bed) during start-up under CO/CO<sub>2</sub>/H<sub>2</sub>/N<sub>2</sub> following a 6 h pre-treatment under CO/H<sub>2</sub>/N<sub>2</sub> and H<sub>2</sub>/N<sub>2</sub>.

Figure 7.14: Measured changes in molar surface population of carbon and oxygen species during start-up under CO/CO<sub>2</sub>/H<sub>2</sub>/N<sub>2</sub> following a 6 h pre-treatment under CO/H<sub>2</sub>/N<sub>2</sub>.

Figure 7.15: A) Outlet CH<sub>3</sub>OH and B) Outlet H<sub>2</sub>O partial pressures of four Cu/ZnO/Al<sub>2</sub>O<sub>3</sub> catalyst beds of different masses during start-up under CO/CO<sub>2</sub>/H<sub>2</sub>/N<sub>2</sub> following a 6 h pre-treatment under CO/H<sub>2</sub>/N<sub>2</sub>. Solid lines denote results following first pre-treatment and dotted lines results following a second successive pre-treatment in the same experiment.

Figure 7.16: Outlet CH<sub>3</sub>OH and H<sub>2</sub>O partial pressures at the reactor outlets of a 125 mg Cu/ZnO/Al<sub>2</sub>O<sub>3</sub> catalyst bed under CO/CO<sub>2</sub>/H<sub>2</sub>/N<sub>2</sub> over 30 h on stream following a 6 h pre-treatment under CO/H<sub>2</sub>/N<sub>2</sub> or H<sub>2</sub>/N<sub>2</sub>.

Figure 7.17: Partial pressure outlet responses over a 500 mg Cu/ZnO/Al<sub>2</sub>O<sub>3</sub> catalyst bed for A) CO, B) CO<sub>2</sub>, C) CH<sub>3</sub>OH, D) H<sub>2</sub>O with time on stream under CO/CO<sub>2</sub>/H<sub>2</sub>/N<sub>2</sub> at 473 K, 25 bar, 7.5 L h<sup>-1</sup> following 30 min pre-treatments using CO/H<sub>2</sub>/N<sub>2</sub> at different temperatures.

Figure 7.18: Comparison of total oxygen lost from catalyst during pre-treatments in CO/H<sub>2</sub>/N<sub>2</sub> at different temperatures for 30 min with subsequent ‘additional methanol’ produced during the first 30 min operation under CO/CO<sub>2</sub>/H<sub>2</sub>/N<sub>2</sub> over 500 mg Cu/ZnO/Al<sub>2</sub>O<sub>3</sub>.

Figure 7.19: Start-up of 500 mg Cu/ZnO and Cu/Al<sub>2</sub>O<sub>3</sub> in CO/CO<sub>2</sub>/H<sub>2</sub>/N<sub>2</sub> following pre-treatment in CO/H<sub>2</sub>/N<sub>2</sub>.

## **Chapter 8:**

No figures.

## List of tables

### Chapter 1:

Table 1.1: Classification of kinetic models (taken from Bos *et al.*, 1997).

### Chapter 2:

Table 2.1: Empirical power law expressions for catalyst performance evolution (taken from Levenspiel, 1972).

Table 2.2: Integral and differential expressions for a concentration independent mechanism.

Table 2.3: Power law expressions with residual activity.

Table 2.4: Fundamental LHHW-based ‘balance of sites’ activity evolution expressions (taken from Wolf and Petersen, 1977).

### Chapter 3:

Table 3.1: Rate model approaches previously employed to model kinetics of solvent effects within liquid phase hydrogenations in literature.

Table 3.2: Properties of solvents used in this study.

Table 3.3: Experimental series undertaken for this study.

Table 3.4: Apparent reaction order dependency on PBN at different temperatures using a simple linear fit.

Table 3.5: Candidate rate models for describing reactions in the PBN hydrogenation network.

Table 3.6: Estimated parameter values, confidence intervals and t-values from non-linear least squares fitting of a 12 parameter surface reaction r.d.s model with product desorption.

Table 3.7: Cross correlation matrix for 12 model parameters.

Table 3.8: Parameters removed in surface reaction limited model with product desorption.

Table 3.9: Parameter estimates and 95% confidence intervals remaining kinetic models.

Table 3.10: Estimated parameters for Eq. (3.13) using  $n = 2$ .

## **Chapter 4:**

Table 4.1: List of properties of catalyst and experimental setup conditions.

Table 4.2: Apparent activation energies for MA and CO<sub>x</sub> product formation in the 1<sup>st</sup> sector obtained via Arrhenius Plot.

Table 4.3: Selected kinetic models from literature applied in this study.

Table 4.4: 6-parameter model of Escardino *et al.* at 0.4 and 11.4 h.

Table 4.5: 1<sup>st</sup> order activity-time model parameters for each reaction pathway.

Table 4.6: 8-parameter model of Sharma and Cresswell at 0.4 and 11.4 h.

## **Chapter 5:**

Table 5.1: Feed conditions used for collection of steady-state data in this study.

Table 5.2: Estimated mass transport criteria and efficiency values for a flow through monolith V<sub>2</sub>O<sub>5</sub>-WO<sub>3</sub>/TiO<sub>2</sub> catalyst under operating conditions in Table 5.1.

Table 5.3: Typical experimental program used in NH<sub>3</sub> adsorption-desorption experiments in this study.

Table 5.4: Estimated mass transport criteria and efficiency values for a 0.1 g V<sub>2</sub>O<sub>5</sub>-WO<sub>3</sub>/TiO<sub>2</sub> catalyst powder fixed bed during step 5 in Table 5.3 at 1023 K.

Table 5.5: Kinetic parameters quoted in Dumesic *et al.*, (1996) used in this study.

Table 5.6: Ammonia desorbed during TPD and calculated ammonia surface coverage and catalyst storage capacity prior to TPD step.

Table 5.7: Final  $E_d$  models and estimated parameters to describe TPD profiles for the four SCR catalysts tested.

## **Chapter 6:**

Table 6.1: Selected kinetic models for methanol synthesis under CO/CO<sub>2</sub>/H<sub>2</sub> conditions taken from literature.

Table 6.2: Compositional and structural data of catalyst precursor formulations used in this study.

Table 6.3: List of properties of catalyst and experimental setup conditions.

Table 6.4: Standard catalyst precursor reduction procedure employed in this study.

Table 6.5: Comparison of measured mass losses of CuO/ZnO/Al<sub>2</sub>O<sub>3</sub> during reduction with calculated values.

Table 6.6: 9 parameter model of Graaf *et al.*, (1988).

Table 6.7: Parameter estimation results using a 5- and 7- parameter model based on the model of vanden Bussche and Froment, (1996).

Table 6.8: F-test analysis to verify significance of extra parameters in the 7-parameter model.

Table 6.9: Comparison of binary and ternary copper-based formulations during reduction step and under CO/CO<sub>2</sub>/H<sub>2</sub>-feed reaction conditions.

Table 6.10: Application of steady state parallel difference test data for binary and ternary copper-based formulations under reaction conditions using the kinetic model developed in this study.

Table 6.11: Steady state testing results for parallel difference testing of Cu/ZnO/Al<sub>2</sub>O<sub>3</sub> under CO/CO<sub>2</sub>/H<sub>2</sub> conditions

## **Chapter 7:**

Table 7.1: Kinetic models for methanol synthesis under CO/H<sub>2</sub> conditions over Cu/ZnO/(Al<sub>2</sub>O<sub>3</sub>) taken from literature.

Table 7.2: List of feed-gas compositions used in this study.

Table 7.3: Calculated surface coverage of oxygen removed and carbon adsorbed onto a Cu/ZnO/Al<sub>2</sub>O<sub>3</sub> catalyst surface during the first 30 min operation under CO/H<sub>2</sub>.

Table 7.4: Carbon and oxygen surface population balance evaluation over 500 mg Cu/ZnO/Al<sub>2</sub>O<sub>3</sub> during CO/H<sub>2</sub>/N<sub>2</sub> pre-treatment and subsequent CO/CO<sub>2</sub>/H<sub>2</sub>/N<sub>2</sub> exposure step.

A comparison is made with the same catalyst, pre-treated in  $\text{H}_2/\text{N}_2$  and exposed to  $\text{CO}/\text{CO}_2/\text{H}_2/\text{N}_2$  at 473 K.

Table 7.5: Comparison of performance of 500 mg of copper-based formulations under  $\text{CO}/\text{H}_2/\text{N}_2$ .

### **Chapter 8:**

No tables.

## Thesis table of nomenclature

Symbol	Description	SI Units
a	Activity	-
a'	Specific surface area	$\text{m}^2 \text{m}^{-3}$
A	Pre-exponential factor	$\text{s}^{-1}$ (for 1 <sup>st</sup> order reaction)
b	Degree of catalyst bed dilution	-
B(t)	Sensitivity function	-
C	Concentration	$\text{mol m}^{-3}$
C <sub>p</sub>	Specific heat capacity	$\text{J K}^{-1}$
CC	Cross correlation coefficient	-
C(J <sub>K</sub> )	Condition number	-
d	Diameter	m
D <sub>eff</sub>	Effective diffusivity	$\text{m}^2 \text{s}^{-1}$
E <sub>a</sub>	Activation energy	$\text{kJ mol}^{-1}$
F	F-statistic	-
h	Heat transfer coefficient	$\text{W m}^{-2} \text{K}^{-1}$
J <sub>K</sub>	Jacobian matrix	-
k <sub>f</sub>	Mass transfer coefficient	$\text{m s}^{-1}$
k <sub>H</sub>	Henry's constant	$\text{m}^3 \text{Pa mol}^{-1}$
k <sub>i</sub>	Rate constant of reaction i	$\text{s}^{-1}$ (for 1 <sup>st</sup> order)
K <sub>i</sub>	Adsorption equilibrium constant	$\text{Pa}^{-1}$ (for 1 <sup>st</sup> order)

$K_i^*$	Thermodynamic equilibrium constant	-
$K_{\text{shape}}$	Shape factor (in XRD crystallite size calculations)	-
L	Length	m
m	Order of catalyst activity evolution	
n	Reaction order	-
norm( $J_K$ )	Norm of the Jacobian matrix	-
p	p-value	-
P	Partial pressure	Pa
r	Rate of reaction	Varies
R	Molar gas constant	$\text{J mol}^{-1} \text{K}^{-1}$
$R^2$	Coefficient of determination	-
t	Time	s
T	Temperature	K
u	Superficial gas velocity	$\text{m s}^{-1}$
$v_m$	Molar volume	$\text{m}^3 \text{mol}^{-1}$
X	Reactant conversion	-
y	Response variable	-
z	Axial co-ordinate	m
Z	Compressibility factor	-

---

*Greek letters and others:*

---

$\alpha$	Constant used in Temkin and Freundlich adsorption isotherm models	-
$\alpha_{1,2}$	Hydrogen bond acceptor and donor parameters	-
$\beta_i^*$	Equilibrium term of reaction i (product of thermodynamic equilibrium constant and driving forces)	-
$\beta_j$	Of model parameter j	-
$\Delta H_r$	Heat of reaction	$\text{kJ mol}^{-1}$
$\Delta P$	Pressure drop	Pa
$\Delta T_{ad}$	Adiabatic temperature rise	K
$\varepsilon$	Bed voidage	-
$\varepsilon_r$	Relative permittivity	-
$\eta$	Effectiveness factor	-
$\theta_B$	Bragg angle (in XRD crystallite size calculations)	$^\circ$
$\theta_i$	Fractional surface coverage of species i	-
$\Theta$	Catalyst activity	-
$\lambda$	Thermal conductivity	$\text{W m}^{-1} \text{K}^{-1}$
$\mu(\text{Debye})$	Dipole moment	-
$\mu_g$	Dynamic gas viscosity	$\text{Pa s}^{-1}$
$v$	Interstitial gas velocity	$\text{m s}^{-1}$
$\rho_g$	Gas density	$\text{kg m}^{-3}$

---

$\tau$	Mean size of ordered crystal domains	m
$\Gamma$	Dimensionless monolith channel concentration	-
$\varphi$	Thiele modulus	-
$\Phi$	Wheeler-Weisz modulus	-
$\Psi$	Catalyst activity evolution function	-
$\Omega$	Catalyst adsorption capacity	mol m <sup>-3</sup>
*	Active site	-
[ ]	Concentration term	mol m <sup>-3</sup>

*Subscripts:*

ads	Of adsorption	-
app	Apparent	-
arom	Aromatic ring	-
base	At base temperature	-
bed, b	Of catalyst bed	-
bulk	In the bulk phase	-
c	Of coke	-
crit	Critical	-
deac, d	Of deactivation	-
des	Of desorption	-
eff	Effective	-

extra	Extra-particle	-
grad	Gradient	-
intra	Intra-particle	-
ket	Ketone group	-
lump	Of a lumped reaction term	-
obs	Observed	-
p	particle	-
pois	Poison	-
prod	Product	-
qss, ss	(Quasi) steady state	-
reac	Reactant	-
solv	Of solvent	-
surf, s	At the surface	-
tot	Total	-
tube	In the tube	-
wall, w	At the wall	-

---

*Dimensionless numbers*

Bi	Biot number	-
Bo	Bodenstein number	-
Ca	Carberry number	-
Da	Damköhler number	-

---

---

Sh

Sherwood number

-

---

## Chapter 1:

### Reaction kinetics in formulated industrial catalysts:

#### Introduction and business case

*Catalytic solutions are gaining increased importance as the 21<sup>st</sup> century progresses, owing to growing demands for transportation fuels, polymers and chemicals, tightening environmental emissions controls and increased sustainability drivers. As of 2012, solid catalysts for heterogeneous applications in many of these areas comprise a global market worth ~\$16 billion. Development and innovation of catalysts and their associated processes, both within industry and academia, are critical to keeping pace with these demands. In heterogeneous catalysis, a fundamental understanding of the necessary physico-chemical requirements for a catalyst formulation is essential to its success, both in terms of performance and longevity.*

*Understanding of reaction kinetics is essential for fundamental understanding of how catalysts work, providing functional information around surface active sites and details of mechanism. This tool, combined with well-designed laboratory experiments to test a catalyst under steady and/or non-steady state conditions, can provide insight into the links between catalyst formulation and reaction performance. There is still considerable room for development in this area particularly with non-steady state operation. Non-steady state catalyst performance may occur as a function of a step change in reaction conditions and/or due to physico-chemical transformations of the catalyst itself. Kinetic analysis of this behaviour, for example of transient performance of a fresh catalyst during reactor start-up, has great potential to provide clarity around the generation and loss of catalytically active sites, which can be linked to a reaction mechanism and ultimately to the catalyst formulation itself.*

## 1. Introduction: ‘Reaction kinetics in formulated industrial catalysts’

Solid catalysts are structured products which are invaluable in assisting a wide range of chemical processes on an industrial scale (Figure 1.1). Important benefits include lowering the energetics of a reaction pathway so that it is more favourable and increasing selectivity towards desired products vs. unwanted by-products. A multi-scale understanding is required to formulate effective catalysts for industrial processes, from the nm scale catalyst microstructure through to mm/cm scale catalyst pellet structure to the scale of the reactor in the overall process. It is also critical to understand catalytic processes on a molecular level, such as understanding how reactants approach and adsorb onto a catalyst surface in the desired manner and how subsequent reactions can take place. It can be seen in Figure 1.1 that catalysts can take a variety of structural forms, a factor which is strongly influenced by the application in which they are used (e.g. monolith structured supports for vehicle emissions control, large cylindrical reactors for many industrial catalysts) as well as the reaction conditions they are exposed to.

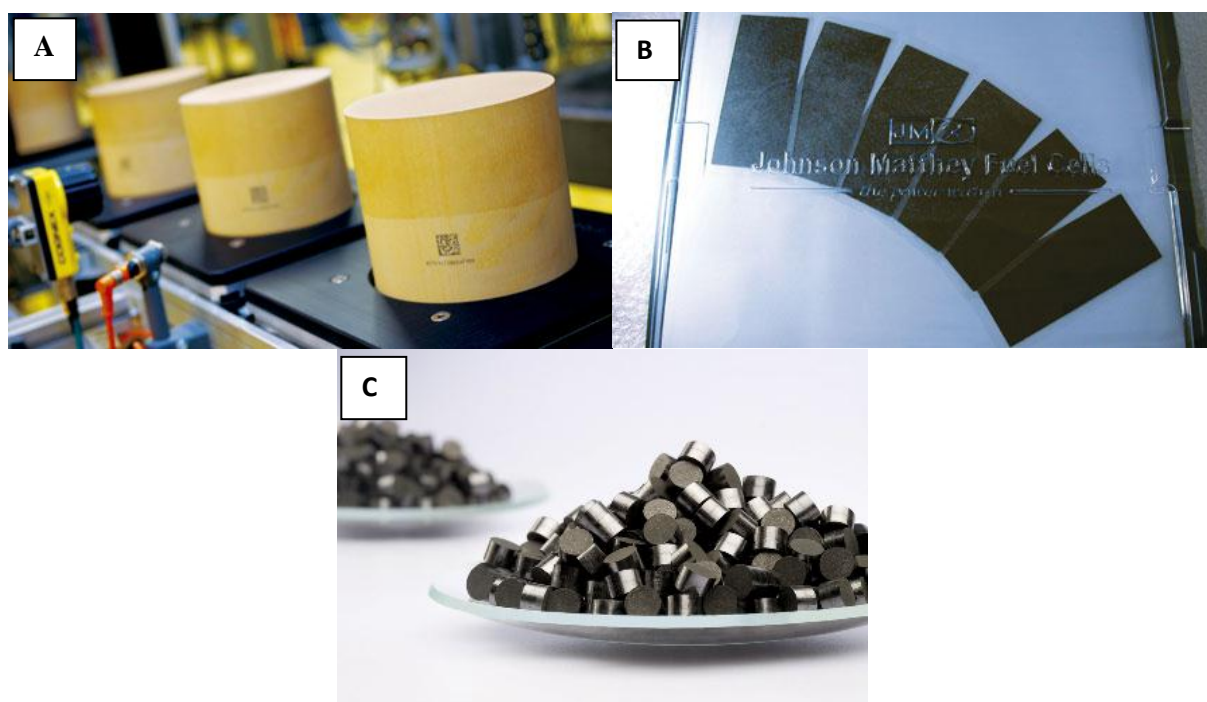


**Figure 1.1: Examples of formulated catalysts: A) Heavy duty diesel emissions control catalyst, B) Polymer electrolyte fuel cells, C) Methanol synthesis catalysts<sup>1</sup>**

Under operating conditions, *active sites* on the catalyst surface form the heart of the catalytic process. These are functional centres whereby specific reactions (whether desired or

<sup>1</sup> <http://www.matthey.com/> [Accessed: 22<sup>nd</sup> Feb 2013]

undesired) can take place; understanding their development during the catalyst formulation process is critical. The catalyst formulation process itself is multi-stage, incorporating formulation of a catalyst precursor, activation of that precursor (typically in a controlled gas atmosphere) and final conditioning of the ‘activated’ catalyst under operating conditions (see Figure 1.2).

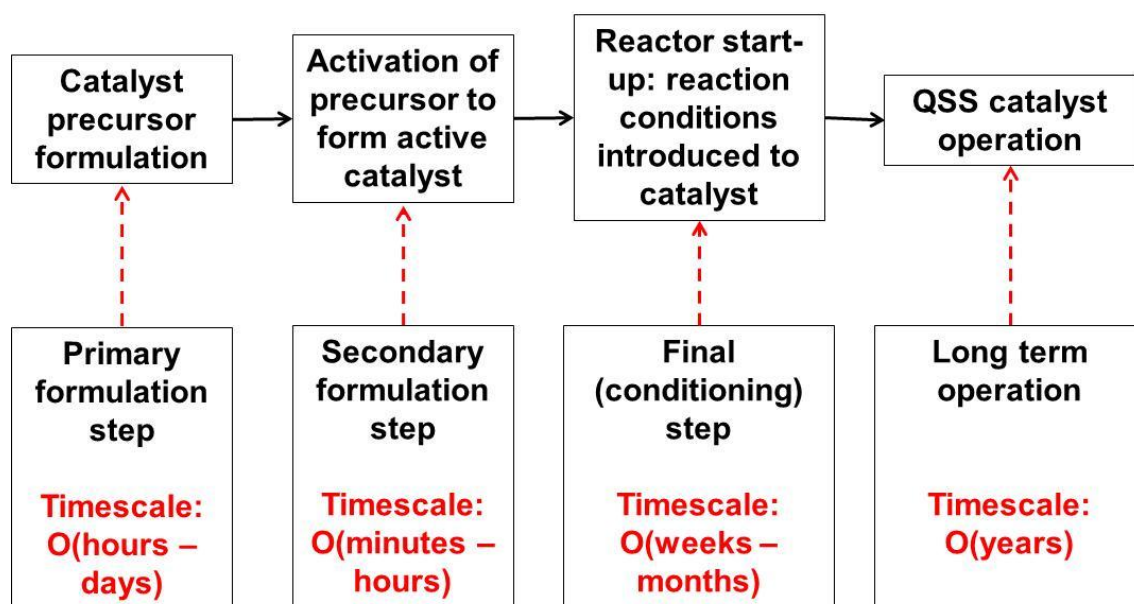


**Figure 1.2: A generalised flow chart for a catalyst formulation process, through to a ‘finished’ product operating at quasi-steady state (QSS) under reaction conditions**

As a result of these factors, developing effective catalyst formulations goes above and beyond simple use of relevant compounds and materials that are known to be catalytically active. Examples of this are catalysts used in the industrial methanol synthesis reaction (Figure 1.1C). Copper metal ( $\text{Cu}^0$ ) is known to be the catalytically active site to allow this reaction to proceed however simple use of copper on its own will yield little or no catalytic activity under reaction conditions. Instead, the metal itself is supported in a finely dispersed form (such as crystallites of the order of 10 nm) on other materials (such as alumina,  $\text{Al}_2\text{O}_3$  and zinc oxide,  $\text{ZnO}$ ) leading to an effective industrial catalyst (Kung, 1992). In general, the pursuit of designing active catalysts involves not only an understanding of active sites for the desired chemistry but also careful positioning of them. Many catalysts are also intended for many years of use, both in stationary and vehicle applications. A challenge exists to deliver a catalyst product that achieves desired performance not only at the start but also over several years of operation.

The overall stages of catalyst formulation are demonstrated in Figure 1.2, which depicts these stages as part of the catalyst life-cycle. It is noted, in the case of many catalysts, that the earlier stages of formulation are short in comparison to the long term operation but are critical in ensuring that the desired performance in the latter is achieved.

During the development of industrial catalyst formulations, it is critical to test their reaction performance and long-term stability (Berger *et al.*, 2001). In the former, a set of targeted reaction performance experiments on a handful of candidate catalyst formulations can be used for a reaction kinetics studies. Candidate formulations may be chosen due to good reaction selectivity or activity in preliminary reactor trials or alternatively may probe a range of interest of catalyst formulation parameters (such as metal dispersion or loading) in the pursuit of optimum performance. Reaction kinetics is a powerful tool in understanding the functional behaviour of a catalyst under reaction conditions. Reaction kinetic modelling encompasses building mechanistically based mathematical descriptions of catalyst behaviour. These descriptions involve fitting parameters based on physical and chemical understanding (such as pre-exponentials and activation energies from Arrhenius-type relationships) which are estimated when experimental data are fitted. A good kinetic model reveals the rate determining step in a catalytic reaction and alludes to quantities of active sites on a catalyst surface that permit specific reactions (i.e. functional behaviour) and this can be linked to the formulation of the catalyst itself.

There is considerable academic and industrial scope in the investigation of reaction kinetics of formulated catalysts and this will be demonstrated throughout this thesis. The thesis will approach a number of challenges in this area and develop appropriate methods to greatly increase fundamental understanding of the link between reaction kinetics and catalyst formulation.

### **1.1 Formulated industrial catalysts in context**

Industrial catalysis has garnered a rich history in the past 250 years (Armor, 2011). Catalytic processes, following discoveries by key academics of the time, were able to realise significantly improved bulk production levels of important industrial chemicals. Some early examples include:

- Sulphuric acid production using vanadia ( $V_2O_5$ ) (1875).
- Nitric acid production using platinum (Pt) gauzes (1904).

- Methanol synthesis under high pressure conditions over zinc oxide-chromia (ZnO-Cr<sub>2</sub>O<sub>3</sub>) (1923).

The development of many of these initial catalysts was on a purely practical basis. Very little work at the time was put into gaining fundamental understanding of how these catalysts work which could lead to improvements in their design and operation. In the past 50 years, this outlook has changed considerably, due to many new industrial drivers for improving the performance of catalytic processes. These include, but are not limited to, rising materials costs, increased demand for transportation fuels, strong growth of chemicals and polymers sectors, emissions legislation and sustainability factors. The net result is a global catalyst market worth ~\$16 billion in 2012 that is highly competitive between key industrial players (Armor, 2011). The need to innovate and improve catalyst design and an understanding of their operation is therefore critical to the competitiveness of any industry in this field.

Many prior works exist that demonstrate innovation in understanding the importance of obtaining the right formulation when designing and manufacturing catalysts as mentioned in Section 1. A well-known example of this can be found in the work carried out by ICI in the 1980s on the low pressure Cu/ZnO/Al<sub>2</sub>O<sub>3</sub> methanol synthesis catalyst and related formulations (Chinchen *et al.*, 1986). It was found that the copper metal surface area of each catalyst formulation tested was directly proportional to its methanol synthesis activity observed under reaction conditions, regardless of support material used (see Figure 1.3).

Elsewhere, another fine example of the importance of catalyst structure in reaction performance can be found in Froment *et al.*, (1990). The study tested three different zeolites under *n*-hexane cracking conditions (ZSM-5, -11, -48); all of which featured different channel structures. The effect of coke formation on *n*-hexane cracking performance was observed and was directly linked to catalyst structure.

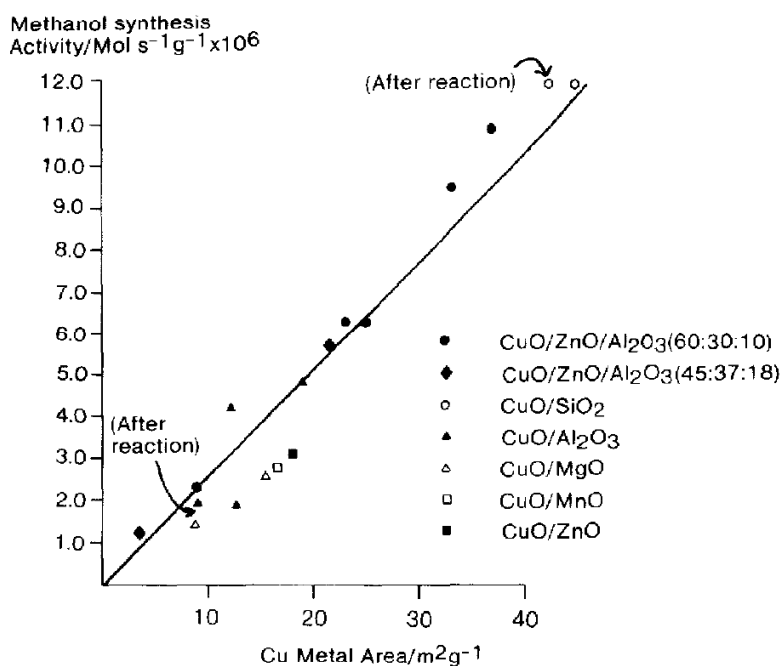


**Figure 1.3: Graph of observed methanol synthesis activity plotted against copper metal surface area of different Cu-based catalyst formulation (Chinchen *et al.*, 1986)**

### 1.2 Levels of complexity in kinetic modelling studies in heterogeneous catalysis

Kinetic modelling studies are central to studies such as these in identifying the links between reaction behaviour and formulation of catalysts. The pursuit of understanding reaction kinetics in heterogeneous catalytic systems can be approached on a number of levels of complexity. Table 1.1, shows a broad classification of kinetic models:

**Table 1.1: Classification of kinetic models (taken from Bos *et al.*, 1997)**

	Model Complexity		Model Level
1.	Simple first order or power law	A.	Intrinsic kinetic models excluding all transport effects
2.	Langmuir-Hinshelwood-Hougen-Watson (LHHW)	B.	Apparent kinetic models that include internal transport effects
3.	n-lumped models (for complex systems)	C.	Extrinsic models including all transport effects plus kinetic
4.	Detailed mechanistic model		
5.	Ab initio, molecular dynamics		

In Table 1.1, it is observed that models feature different degrees of complexity (i.e. power law: simplest, ab initio: most complex) but also can be defined on different model levels depending on how effectively kinetics have been separated from mass and heat transport effects. Indeed, transport effects can be ‘designed out’ of a kinetic study, allowing intrinsic measurements. This will be discussed in Chapter 2.

The ‘complexity’ and ‘level’ of model required ultimately depends on the requirements for the study. Investigating and elucidating more complex models may present a difficult challenge but the potential for greater fundamental understanding is increased significantly.

A recent presentation given by Prof. Gregory Yablonsky at the MaCKiE-3 conference in Chennai, India broached the topic of ‘*Grasping complexity in chemical kinetics*’ (Yablonsky, 2013). A key point noted was that it is common in heterogeneous catalysis to approach a reaction kinetics problem by simplifying it (e.g. 1<sup>st</sup> order assumptions, irreversibility, QSS analysis to neglect changes in surface intermediate populations, using a rate determining step). Whilst this may frequently lead to pragmatic and effective results it is different to grasping the complexity of a problem, whereby kinetics of catalytic systems can be understood on a more detailed level, which could lead to improved approaches to formulating industrial catalysts. Advanced approaches which can potentially ‘grasp’ complexity are briefly discussed in sections 1.2.1 and 1.2.3.

### **1.2.1 Steady state vs. non-steady state**

In heterogeneous catalysis, choice of steady or non-steady state testing of a catalyst is strongly driven by the objective of the study. In a review of heterogeneous catalytic kinetics, Weller, (1992), provides a history and overview of both types of technique. In general, steady-state testing of catalysts has a focus on understanding overall, ‘global’, reaction kinetics. Steady state models generally fall back on assumptions of a rate determining step in a reaction, adsorption-desorption equilibrium of reactants and products, and a constant surface species population. As many industrial catalysts spend the majority of their working life under quasi-steady state conditions, developing models in this mode of operation has great value. Indeed, different catalyst formulations can be compared using steady state models and differences in estimated model parameters linked through to the functional structure of the catalyst. Some excellent and mechanistically sound steady state models exist in literature including:

- Methanol synthesis over a copper-zinc oxide-alumina catalyst (Vanden Bussche and Froment, 1996)
- Selective catalytic reduction of nitric oxide by ammonia over vanadia/titania (Dumesic *et al.*, 1996)
- Carbon monoxide conversion over a copper-ceria catalyst (Quiney and Schuurman, 2007)

Non-steady state methods often focus on some/all elementary steps in a reaction mechanism. These methods typically probe behaviour of a catalyst following a measurable change in process conditions (temperature, pressure, flow rate etc.) and can lead to a greater mechanistic understanding of catalyst behaviour. Reaction testing systems utilising these methods are typically more complex in nature than those used in steady state testing and include:

- Temporal analysis of products (TAP) which examines the response of a catalyst to a short ‘pulse’ of reactants. Examples include selective oxidation of n-butane over vanadium phosphorus oxides (Schuurman and Gleaves, 1997).
- Step-change response method which examines response of a catalyst following a ‘step’ in feed concentration. Examples include CO oxidation over manganese dioxide (Kobayashi and Kobayashi, 1972) and selective catalytic reduction of nitric oxide by ammonia over vanadia-tungsta/titania (Lietti *et al.*, 1997). Continuous analysers for these methods have significant use at the time of writing of this thesis.
- Periodic forcing, multiple steady states and oscillatory methods. Readers are directed to works such as ‘Composition modulation of catalytic reactors’ by Silveston, (1998).

From an industrial perspective, methods such as step-change response can be used to understand fundamental differences in the reaction behaviour of catalysts which can be linked through to their structure. Methods such as periodic forcing and oscillations have been demonstrated to have great value in optimising reactor performance and avoiding unwanted reactor incidents such as wrong way behaviour in fixed bed reactors (Luss, 1997).

### 1.2.2 Statistical analysis and confidence in kinetic models

The process of developing accurate kinetic models, on any level of complexity, to describe heterogeneous catalytic reactions can be hampered by a number of factors, including, but not limited to:

- Experimental measurement errors.
- Poor initial guesses in an iterative modelling simulation.
- Choice of solver when fitting data to a proposed kinetic model.
- Over- or under-parameterisation of kinetic models.

As a result it is very easy for a kinetic modelling study to produce misleading results or to generate kinetic models which have very little practical use outside of the results generated in a specific study.

To combat this, statistical analysis methods can be used to fully interrogate data and deliver much clearer outcomes to a kinetic modelling study or indeed provide future direction to an experimental programme. Statistical analysis procedures have seen effective use in the field of heterogeneous catalysis. A classic example of this is in the work of Corma *et al.*, (1988) which gave a comparison of models in heterogeneous catalysis for ideal and non-ideal surfaces. In this work, the authors looked at 19 different steady state datasets from previous literature studies, all of which were varied in catalyst and reaction. Each dataset was fitted to three different types of model based on an assumption of the nature of the catalyst surface:

- Langmuir (all adsorption sites are identical and have the same associated energy).
- Temkin (a linear distribution of adsorption energies).
- Freundlich (a logarithmic distribution of adsorption energies).

The end result was that in general, a similar quality of fit and set of estimated parameter values was found regardless of the surface assumption. This suggested that in most cases using models with extra parameters (Temkin and Freundlich) may not actually improve mechanistic understanding of steady state data. This links with earlier discussions by Boudart, (1986) that in many cases a LHHW approach dominates due to structure insensitive reactions occurring at high surface coverage, irrespective of ideality of surface. It also shows that the coefficient of determination,  $R^2$ , which is used to show overall quality of fit of data to a

model, is of little use in multiple parameter estimation problems.  $R^2$  provides no information as to the sensitivity of model responses with respect to fitted model parameters.

Other works have stimulated a strong drive for statistically-aware approaches to kinetic modelling. The ‘UCKRON-1’ test problem, developed by Berty *et al.*, (1989) utilised an artificial reaction mechanism and dataset for the synthesis of methanol from carbon monoxide and hydrogen. A 5% random error was applied to this dataset and was subsequently sent to 19 academic groups who were challenged with developing their own models from the data. Parts of the dataset were placed close to thermal runaway conditions however only a few groups predicted thermal runaway. On the contrary, most entries estimated similar model fitting parameters. The study stressed the importance of using appropriate solver methods, including thermodynamic expression and avoiding simplifying Arrhenius terms, particularly in sensitive reaction systems.

Elsewhere, Quiney and Schuurman, (2007) utilised a systematic method of residual and sensitivity analysis to remove weak parameters from models, compare different models and understand the influence of experimental errors on the statistical significance of proposed models. In many cases, kinetic models which are different in description initially often converge to the same final model, following the removal of statistically insignificant parameters using this method. Ultimately this greatly reduces the number of starting kinetic models that need to be tested in a kinetic study.

### **1.2.3 Theoretical approaches**

Kinetic models can also be built using a purely theoretical and mechanistic basis and could play a complementary role in studies of active sites and catalyst design. This approach to kinetic modelling of a working catalyst surface, often termed micro kinetic modelling, originates from an approach laid out in Dumesic *et al.*, (1987) but also earlier mathematical treatments described in Temkin, (1971). These methods utilise a postulated reaction mechanism (often based on prior literature) and build a model comprising all elementary steps in the reaction sequence. In effect, values for pre-exponential factors and activation energies for the Arrhenius equation for each reaction step are required. The estimations for these values are based on parameters from literature (e.g. surface bond strengths and correlations of activation energies with heat of reaction) but also activities and selectivities from process in question (Weller, 1992). The key test of this approach is in application to real

datasets. In some cases parameters may need to be adjusted to achieve this, as long as the adjustments make real, physical sense. This approach has shown success for some systems:

- Reactions of *n*-hexane over Pt(1 1 1) (Dumesic *et al.*, 1987).
- Ammonia synthesis over Fe(1 1 1) (Dumesic and Trevino, 1989)
- Water gas shift reaction over Cu/ZnO (Ovesen *et al.*, 1996)
- Kinetic analysis of cluster size dependent activity and selectivity (Murzin, 2010)

### **1.3 Company background: Johnson Matthey plc**

As mentioned in overview of their 2013 annual report, Johnson Matthey (JM) is a leading speciality chemicals company<sup>2</sup>. The company has a core focus in catalysis, precious metals, process technologies and fine chemicals. JM is a FTSE 100 company with operations in over 30 countries. In 2012-13 the company had an average of 10,500 employees, revenue of £10.73 billion and an underlying profit before tax of £389.2 million. As of July 2013, the company is organised into five divisions:

#### ***Emissions control technologies***

A world leading supplier of catalysts and related technologies for environmentally beneficial applications such as vehicle emissions control (car auto-catalysts, heavy duty diesel emissions abatement) and stationary emissions control (e.g. coal-fired power plants, waste-to-energy, marine applications).

#### ***Process technologies***

A global supplier of industrial process catalysts and technology licensing. This division comprises:

- *Process technologies*: catalysis business specialising in processes relating to syngas, ammonia, methanol etc.
- *Chemical catalysts*: catalysts for the petrochemicals industry.
- *Formox*: catalysis and process technologies for formaldehyde manufacture.
- *Davy Process Technology*: develop chemical process technologies and license them to oil, gas and petrochemical industries.

---

<sup>2</sup> [http://www.matthey.com/media\\_and\\_news/news/2013/annual\\_report\\_2013\\_published](http://www.matthey.com/media_and_news/news/2013/annual_report_2013_published) [Accessed: 17/7/13]

- *Tracerco*: a specialist measurement business that provides process diagnostic services using a wide range of analytic techniques and instruments.

### ***Precious metal products***

A metals refining and recycling business which is divided into two areas:

- *Services*: precious metals refining and recycling and the marketing and distribution of platinum group metals (PGMs).
- *Manufacturing*: making products using precious metals and related materials. Noble metals, colour technologies and chemical products all fall under this business.

### ***Fine chemicals***

A global supplier of active pharmaceutical ingredients (e.g. MacFarlan Smith), catalysis and chiral technologies and research chemicals (under the Alpha Aesar brand).

### ***New businesses***

Comprises the fuel cells and batteries businesses as well as business development programmes.

## **1.4 Business case**

For JM, an improved scientific understanding of formulated industrial catalysis is desirable in a number of areas:

- Understand the fundamentals behind the changes which occur in early stages of operation in industrial and automotive catalytic processes (e.g. reactor start-up). This represents an opportunity to produce catalysts with enhanced performance via control of catalyst formulation process and/or start-up conditions. This may further extend to an improved understanding of catalyst pre-cursor activation procedures, which deliver the catalyst in an active state for a process.
- Develop catalyst testing and kinetic modelling methods to understand longer-term catalyst stability and deactivation modes. By linking findings with physical and

chemical characteristics of catalyst formulations this presents an opportunity for JM to improve catalyst design.

- Develop experimental and modelling methodologies/capabilities that can be applied to future catalyst research and development programmes. This may enable a more efficient and effective development time of new catalyst technologies, decreasing the overall time to market of the product. In effect, instigating a holistic approach to catalyst design could be a powerful tool in their development.

Increased understanding and potential formulation improvements from these areas using model systems will give JM a commercial advantage in areas of catalyst performance over their competitors. These benefits could be long term, as the project will allow JM to take a lead in a less explored area within the field of catalysis. Furthermore, a sustainability business need is prevalent, as factors involved in improving catalyst product performance may, for example, reduce resource use, energy inputs and CO<sub>2</sub> emissions per unit of product produced.

Academically, outcomes from this thesis will provide a furthered knowledge base for both JM and the University of Birmingham. This will strengthen links between the two establishments, which is beneficial for any future co-operative work that is carried out between them. Journal papers and conference presentations arising from this project will serve to show this work to the wider scientific community which will enhance the impact of the work.

### **1.5 Thesis objectives**

In light of the background to opportunities in reaction kinetics in industrial catalysis as well as the business drivers for JM, the overall thesis objectives are thus:

#### ***Overall aims:***

- A. Combine experimental, characterisation and kinetic modelling approaches to fundamentally understand reaction pathway functionality and the nature of active sites on the surfaces of catalyst formulations.
- B. By examining a range of catalyst formulations for use in a particular reaction system, understand the critical structural components that deliver catalytic functionality in

these formulations. This should be linked with the scope of reaction conditions employed for the catalytic process in question.

- C. By studying a range of catalyst systems and meeting the above aims assess common themes and differences between different types of catalytic system both in terms of physico-chemical observations but also methodologies and analytical techniques used.

*Specific aims:*

- i) In the pursuit of understanding reaction kinetics of formulated industrial catalysts, develop experimental methods to rigorously probe catalysts under reaction conditions.
  - a. Design lab-based experiments to ensure the absence of heat/mass transport and flow regime limitations so that catalyst testing data are intrinsic in nature and explore ‘true’ reaction behaviour.
  - b. Design experimental methods that are simple to implement so that they can have wider use in future industrial catalyst development programmes or academic studies.
- ii) Develop non-steady state experimental approaches which can provide further depth of understanding of catalyst systems, in particular to probe the following:
  - a. Generation and loss of catalytically active sites during catalyst pre-cursor activation and/or initial operation under reaction conditions (reactor start-up).
  - b. Dynamic behaviour of catalysts following a change in process conditions (transient response experiments).
  - c. Generation and loss of catalytically active sites during longer-term ageing of catalyst formulations.

These three areas have typically different relaxation times (e.g. longer-term ageing is typically much slower than a transient response experiment). As a result, different experimental approaches may be required.

- iii) Develop appropriate steady-state and dynamic kinetic modelling techniques in order to fit experimental data to mechanistically-based kinetic models and estimate key parameters surrounding catalytic reaction behaviour (e.g. activation energies).

- iv) Develop rigorous statistical analysis methods to interrogate both quality of data and kinetic modelling parameter estimation results in order to develop more robust model descriptions of catalyst reaction performance.
  - a. Include critical examination of estimated parameters from kinetic modelling studies to understand these outputs in a real, physical sense.
- v) Employ appropriate catalyst characterisation methods to provide supporting evidence to kinetic models and findings from experimental reaction studies.

## 1.6 Structure of the thesis

Due to the broad nature of the objectives described in Section 1.5 and the large and varied catalyst portfolio available at JM, this thesis will incorporate a number of different catalyst studies, each intended for different applications, which will be explored in pursuit of the aims described in Section 1.5. The studies are thus:

### **Solvent effects in the liquid phase hydrogenation of 4-phenyl-2-butanone over a platinum supported on titania catalyst**

Development of kinetic analysis methods is a key aim of this study, which will employ batch reactor data provided by Queen's University, Belfast. Specific aims (iii) and (iv), described in Section 1.5 will be approached in this chapter which will apply kinetic modelling techniques and use statistical analysis methods to develop accurate model descriptions of catalyst performance. Overall aim (B) can be applied to this work as catalyst active sites, reaction pathway kinetics and the impact of solvent choice on reaction rates and selectivity will be linked.

### **Vanadium phosphorus oxide catalysts for selective oxidation of *n*-butane**

Fresh vanadium phosphorus oxide catalysts show time-dependent reactor performance behaviour when initially exposed to *n*-butane/air reaction conditions. The time scale of this process is of the order of 10 – 100 h. The catalyst appears to lose overall activity with time on stream but become more selective to the desired reaction product, maleic anhydride. This study is an excellent opportunity to meet all of the specific aims. The reactions in this catalytic system are strongly exothermic and careful experimental design is needed to obtain intrinsic reaction conditions (Aim i)) and the dynamic behaviour of the catalyst during initial operation will allow development of non-steady state analytical methods (Aim ii)).

Appropriate kinetic models can be developed, tested and critically assessed using statistical methods (Aims iii) and iv)) and catalyst characterisation methods can be developed to track the evolution of catalyst performance to real physical parameters.

This study should provide great insight into overall aims A and B. Experimental, modelling and characterisation techniques will be combined and the dynamic initial operation of the catalyst is seen as an opportunity to track the development of different active sites on the catalyst surface and link changes in their quantities to catalyst formulation.

### **Vanadia-tungsta-titania catalysts for the selective catalytic reduction of nitric oxide by ammonia**

Vanadia-tungsta-titania catalysts are used for stationary NO<sub>x</sub> emissions control purposes and have an intended operating life time in the order of years. An ideal catalyst formulation for this purpose will show a specified de-NO<sub>x</sub> performance level from the first day of operation and maintain this performance with age. Designing a formulation to meet this aim is a difficult task and it is of interest to analyse the performance of different fresh formulations and how activity of the de-NO<sub>x</sub> reaction pathways change with age. Understanding can be applied to the design of these catalysts to enable improved formulation performance.

As with the vanadium phosphorus oxide catalyst study, all specific aims will be encompassed in this study. In particular, steady state, ‘product performance’ experiments using monolithic catalysts will be complemented by non-steady state, mechanistically driven, temperature programmed desorption studies on catalyst powders. Kinetic modelling from both approaches will be used to gain fundamental understanding of the relative levels of active sites in fresh and aged catalyst formulations and link with physical structure. This work will strengthen the understanding of the links between catalyst functionality and formulation and combine findings from two scales of experiment, leading to stronger conclusions.

### **Copper-based catalysts for methanol synthesis**

Copper-based catalysts, such as copper-zinc oxide-alumina, are functional for methanol synthesis and the water gas shift reaction under mixtures of comprising CO/CO<sub>2</sub>/H<sub>2</sub>. The specific nature of this functionality and the associated active sites are complex to

elucidate and can change significantly based on factors such as catalyst support, metal and gas atmosphere conditions. This study will build on all of the previous areas of this thesis and explore steady and non-steady state kinetics under a wide range of conditions and also examine the effect of step changes in conditions to catalyst behaviour. As a result, a sophisticated approach will be needed to tackle the specific experimental aims (i) and (ii) but also the approach of the kinetic modelling aspect (aim (iii)), in light of an extensive literature background on the topic which still contains many areas of disagreement around the functionality and nature of active sites on these catalysts.

Figure 1.4 (overleaf) provides a road map of the thesis, to guide readers to appropriate chapters based on their interests. For those who are unfamiliar with the literature background to the experimental, characterisation or modelling techniques utilised in this work, Chapter 2 is a recommended start point. Chapter 3 is a full reaction kinetics study in its own right but is also intended as a detailed demonstration of the modelling and statistical analysis approaches used throughout the thesis. Readers without a modelling background are strongly advised to read this chapter before reading the rest of the thesis. Chapters 4-7 all investigate catalyst systems which display varying degrees of dynamic behaviour. Chapters 4-5 each address specific catalysis topics and challenges and can be read on an individual basis. Chapters 6-7 are related and should be read as a pair.

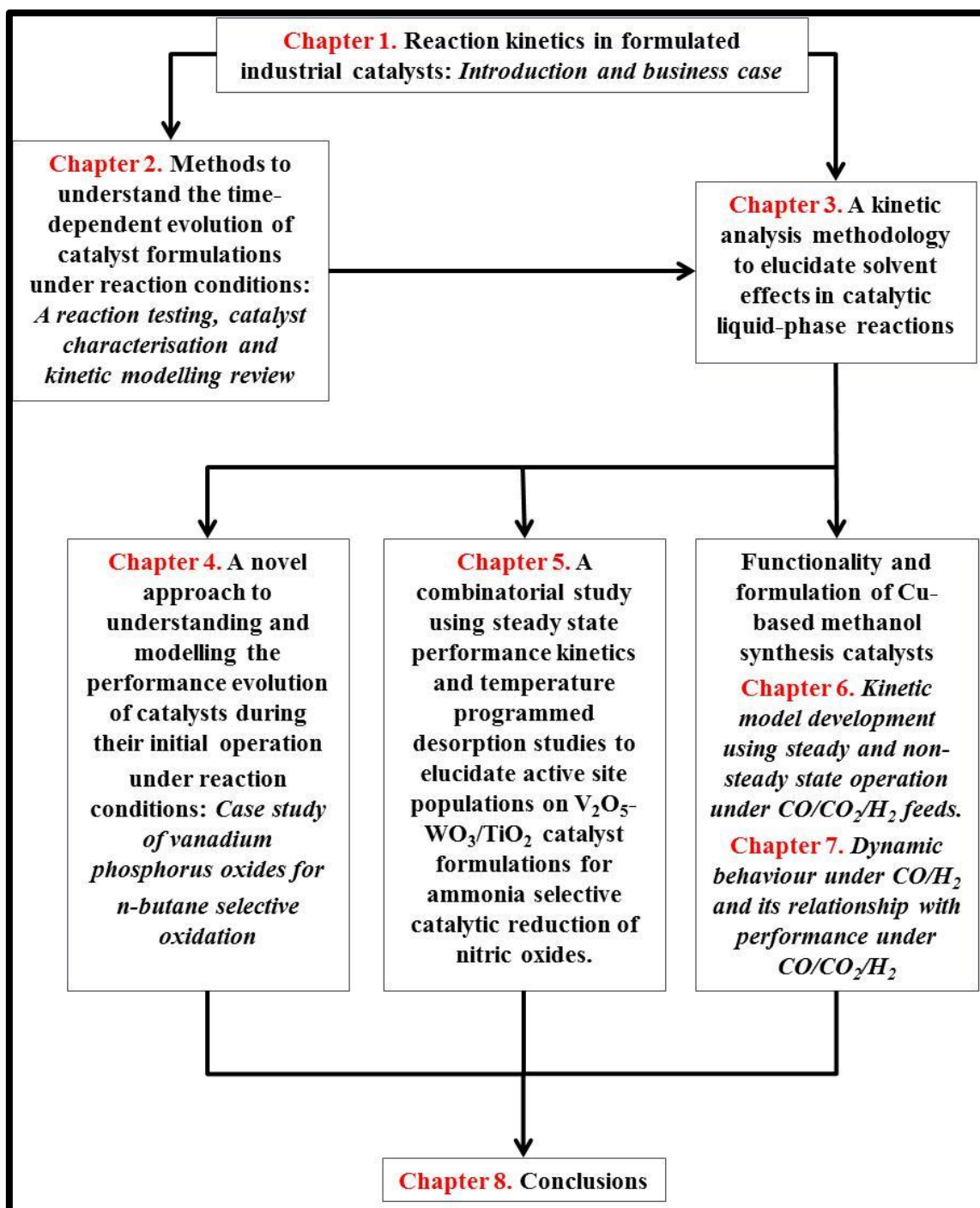


Figure 1.4: Thesis structure

## 1.7 Appendix: List of publications and conferences

### *Publications (chronological):*

- a. Clark P.J., Wilkinson S.K., (2012), 'Why not EngD?', *The Chemical Engineer*, **849**, 44-47
- b. Wilkinson S.K., Simmons M.J.H., Stitt E.H., Baucherel X., Watson M.J., (2013), 'A novel approach to understanding and modelling performance evolution of catalysts during their initial operation under reaction conditions – Case study of vanadium phosphorus oxides for n-butane selective oxidation', *Journal of Catalysis*, **299**, 249-260
- c. McManus I., Wilkinson S.K., Thompson J.M., Daly H., Sedaie Bonab N., ten Dam J., Simmons M.J.H., Stitt E.H., D'Agostino C., McGregor J., Gladden L.F., Hardacre C., (2014), 'Solvent effects in the liquid phase hydrogenation of 4-phenyl-2-butanone over Pt/TiO<sub>2</sub> – Part A', **paper in preparation**
- d. Wilkinson S.K., McManus I., Thompson J.M., Daly H., Sedaie Bonab N., ten Dam J., Simmons M.J.H., , D'Agostino C., McGregor J., Gladden L.F., Hardacre C., Stitt E.H., (2014), 'Solvent effects in the liquid phase hydrogenation of 4-phenyl-2-butanone over Pt/TiO<sub>2</sub> – Part B: A kinetic analysis methodology to elucidate the roles of metal, support and solvent', **paper ready for publication**

### *Conferences (chronological):*

- a. *Rational Catalysis and Process Design*; held at University College, Oxford, UK, 19-20 Sep 2011.
  - *Understanding catalyst performance evolution during reactor start-up* – poster
- b. *International Symposium of Chemical Reaction Engineering (ISCRE-22)*; held at Maastricht, the Netherlands, 2-5 Sep 2012.
  - *Techniques to understand and model catalyst performance evolution during reactor start-up* – presentation
- c. *1<sup>st</sup> Annual EPSRC Manufacturing The Future Conference*; held at Loughborough, UK, 19-20 Sep 2012.
  - *Understanding the impact of reactor start-up methods on the longer term performance of industrial catalysts* – poster

- d. *Mathematics in Chemical Kinetics and Engineering (MaCKiE-3)*, held at IIT Madras, Chennai, India, 4-6 Feb 2013.
- *Kinetic analysis during catalyst conditioning: A methodology to understand the evolution of active sites* – presentation
- e. *North American Symposium on Chemical Reaction Engineering (NASCRE-3)*, held at Houston, Texas, USA, 17-20 Mar 2013.
- *A kinetic analysis methodology to elucidate solvent effects in catalytic liquid phase reactions* – presentation

## 1.8 References

- Armor J.N., (2011), '*A history of industrial catalysis*', Catal. Today, 163, 3-9
- Berger R.J., Stitt E.H., Marin G.B., Kapteijn F., Moulijn J.A., (2001), '*Chemical reaction kinetics in practise*' Eurokin, 5, 1, 30-60
- Berty J.M., Lee S., Szeifert F., Cropley J.B., (1989), '*The "UCKRON-1" test problem for reaction engineering modelling*', Chem. Eng. Comm., 76, 9-33
- Bos A.N.R., Lefferts L., Marin G.B., Steijns M.H.G.M., (1997), '*Kinetic research on heterogeneously catalysed processes: A questionnaire on the state-of-the-art in industry*', App. Cat. A: Gen, 160, 185-190
- Boudart M., (1986), '*Classical catalytic kinetics: a placebo or the real thing?*', Ind. Eng. Chem. Fund., 25, 656-659
- Chinchen G.C., Waugh K.C., Whan D.A., (1986), '*The activity and state of the copper surface in methanol synthesis catalysts*', App. Cat., 25, 101-107
- Corma A., Llopis F., Monton J.B., Weller S.W., (1988), '*Comparison of models in heterogeneous catalysis for ideal and non-ideal surfaces*', Chem. Eng. Sci., 43, 4, 785-792
- Dumesic J.A., Milligan B.A., Greppi A.A., Balse V.R., Sarnowsky K.T., Bell C.E., Kataoka T., Rudd D.F., Trevino A. A., (1987), IEC Res., 26, 1399
- Dumesic J.A., Trevino A.A., (1989), '*Kinetic simulation of ammonia simulation catalysts*', J. Catal., 116, 119-129

- Dumesic J.A., Topsøe N-Y., Topsøe H., Chen Y., Slabiak T., (1996), '*Kinetics of selective catalytic reduction of nitric oxide by ammonia over vanadia/titania*', J. Catal., 163, 409-417
- Froment G.F., De Meyer J., Derouane E.G., (1990), '*Deactivation of zeolite catalysts by coke formation*', J. Catal., 124, 391-400
- Kobayashi M., Kobayashi H., (1972), '*Application of transient response method to the study of heterogeneous catalysis – 3 parts*', J. Catal., 27, 100-119
- Kung H.H., (1992), '*Deactivation of methanol synthesis catalysts: A review*', Catal. Today, 11, 443-453
- Lietti L, Nova I, Camurri S., Tronconi E., Forzatti P., (1997), '*Dynamics of the SCR-DeNO<sub>x</sub> reaction by the transient response method*', AIChE Jnl., 43, 10, 2259
- Luss D., (1997), '*Temperature fronts and patterns in catalytic systems*', Ind. Eng. Chem. Res., 36, 2931-2944
- Murzin D.Y., (2010), '*Kinetic analysis of cluster size dependent activity and selectivity*', J. Catal., 276, 85-91
- Ovesen C.V., Clausen B.S., Hammershøi B.S., Steffensen G., Askgaard T., Chrokendorff I., Nørskov J.K., Rasmussen P.B., Stoltze P., Taylor P., (1996), '*A micro kinetic analysis of the water gas shift reaction under industrial conditions*', J. Catal., 158, 524-535
- Quiney A.S., Schuurman Y., (2007), '*Kinetic modelling of CO conversion over a Cu/ceria catalyst*', Chem. Eng. Sci., 62, 5026-5032
- Schuurman Y., Gleaves J.T., (1997), '*A comparison of steady-state and unsteady-state reaction kinetics of n-butane oxidation over VPO catalysts using a TAP-2 reactor system*', Catal. Today, 33, 25-37
- Silveston P.L., (1998), '*Composition modulation of catalytic reactors*', Overseas Publishers Association
- Temkin M.I., (1971), '*The kinetics of steady state complex reactions*', Int. Chem. Eng., 11, 709-717

Vanden Bussche K.M., Froment G.F., (1996), '*A steady state kinetic model for methanol synthesis and the water gas shift reaction on a commercial Cu/ZnO/Al<sub>2</sub>O<sub>3</sub> catalyst*', J. Catal., 161, 1-10

Weller S.W., (1992), '*Kinetics of heterogeneous catalyzed reactions*', Catal. Rev. Sci. Eng., 34, 3, 227-280

Yablonsky G.S., (2013), '*Grasping complexity in chemical kinetics*', presentation delivered at MaCKiE-3, Chennai, India, 5<sup>th</sup> Feb. 2013

## Chapter 2:

### **Methods to understand the time-dependent evolution of catalyst formulations under reaction conditions:**

#### **A reaction testing, catalyst characterisation and kinetic modelling review**

*Gaining a fundamental understanding of catalyst performance evolution via transient methods is a challenging but rewarding process. In any catalyst study of this nature, a robust strategy is required which utilises appropriate catalyst testing, characterisation and modelling methods. The rate at which a catalyst changes its behaviour and the inherent reaction conditions at which the catalyst is operable are key factors in developing such strategies. Experimentally, good catalyst testing practice is essential and a range of transient testing methods are available. For physico-chemical catalyst characterisation, appropriate choice of ex situ, in situ or operando techniques is critical. The kinetic and activity modelling approaches are dictated by the dynamics of the catalyst system; fast (second or minute) scale performance changes are likely to require unsteady state modelling procedures whilst slower (hour, day or longer) evolutions may permit global activity-time approaches and multi-reaction conditions scans of kinetic behaviour and various times on stream.*

## 2. Introduction: *'Linking catalyst functionality under reaction conditions to formulation'*

In Chapter 1, testing and modelling of formulated industrial catalyst behaviour in non-steady state (transient) operation was identified as a challenging but highly information-rich route to increase fundamental understanding. Central to this is the notion that transient operation can be used to track development of catalytically active sites with time on stream, affording a more rigorous method of testing than that of the steady-state approach. A command of catalytic reaction kinetics under these conditions can demonstrate functional behaviour of catalysts which can ultimately be traced back to their formulation.

In both industry and academia, a large amount of work has gone into exploring catalyst stability and time-dependent changes in activity (Birtill, 2003). As discussed in Chapter 1, a catalyst under reaction conditions may show changes in performance during the following stages:

- I. After steady-state reactor operation is achieved (termed 'long-term deactivation').
- II. Applying a change in feed concentrations to a catalyst operating under quasi-steady state (termed 'transient response').
- III. During initial operation of a fresh catalyst under reaction conditions before a stable, steady state reactor operation is achieved (sometimes termed 'equilibration'). Catalyst activation (i.e. the transformation of a catalyst precursor into an active catalyst under specific conditions) may be included in this category.

Many existing works describing changes in catalyst 'activity' and stability use the term '*catalyst decay/deactivation*', in part due to the prevalence of stage I-type studies in the literature (Birtill, 2004a; Birtill, 2004b). This term is somewhat misleading for this thesis, which will place much greater emphasis on stages II and III when probing catalyst formulations. Performance transformations observed during initial operation of a fresh catalyst may involve the generation of (new) active sites rather than a loss as the term *deactivation* would imply. Furthermore, transient reaction performance behaviour observed in stages II and III may not relate to a loss or gain of active sites on the catalyst and instead relate to an intrinsic rather than extrinsic relaxation process, which were originally discussed by Temkin (1976). Due to these factors, the topic will be termed '*catalyst performance*'

*evolution*' to fully encompass understanding the fundamental nature of active sites, their development with time, temporal evolution of surface intermediates, and the reaction mechanisms taking place at these sites.

Figure 2.1 depicts a generalised approach to catalyst systems explored in this thesis. Previous understanding (via literature and existing data) coupled with appropriately designed experiments are critical initial steps which will provide a strong basis for kinetic modelling (performance analysis), characterisation pursuits and ultimately, the generation of fundamentally sound catalyst activity models which can be linked to formulation.

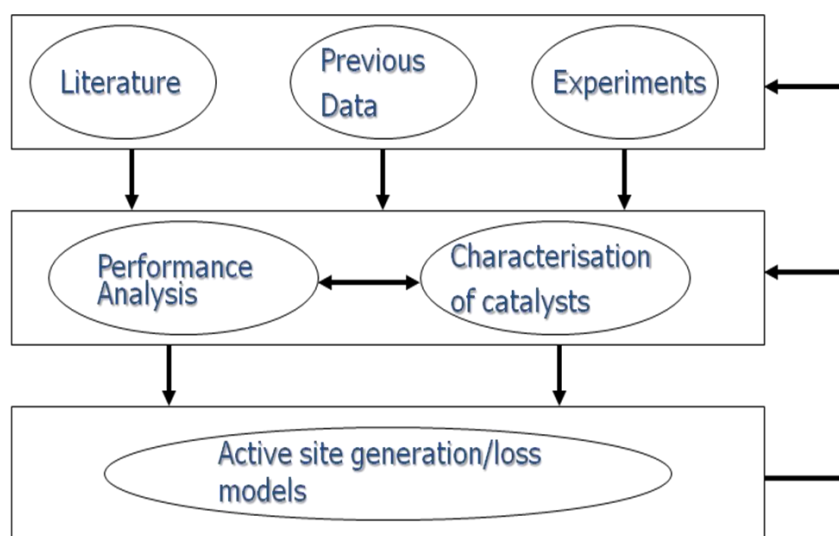


**Figure 2.1: Generalised flow diagram to understand time-dependent evolution of catalyst formulations under reaction conditions**

In this review, the above approach will be broken into three areas, based on the thesis objectives outlined in Chapter 1:

- Experimental catalyst testing methods<sup>3</sup>.
- Tracking the evolution of physico-chemical properties of a catalyst using *ex situ*, *in situ* and *operando* characterisation methods.
- Kinetic and activity-time modelling of catalyst formulations under reaction conditions to fundamentally understand and quantify evolution of surface active sites on the catalyst surface.

<sup>3</sup> Attention will be given to gas-phase fixed-bed operation which was utilised in all experiments carried out by the author in this study. Gas-liquid-solid batch experiments in Chapter 3 were not carried out by the author.

## 2.1 Catalyst testing

Choosing a suitable methodology, experimental program and range of test conditions to assess catalyst performance evolution experimentally is of critical importance to this study. Testing catalysts under intrinsic conditions (free of mass and heat transport limitations) is key to generating fundamental kinetic models which can probe confidently the nature of catalytically active sites without obfuscation. The experimental work presented in this thesis is carried out on a laboratory scale and factors ranging from the choice of lab reactor type through to choice of catalyst particle size and reactant input flow rates can all have an effect on measured variables which will ultimately be used in kinetic and activity modelling.

This section will provide an overview of catalyst testing literature, calculations and/or experiments to avoid transport limitations and how to tailor an experimental program to successfully approach a study objective. Key experimental methods and configurations to probe catalyst performance evolution will also be summarised.

### 2.1.1 The ten commandments of catalyst testing

A classic basis to undertake a catalyst testing study is to utilise the steps set out in '*The ten commandments of catalyst testing*' (Dautzenberg, 1989). The work is broadly applicable to all forms of catalyst testing and in this review is geared towards transient catalyst testing:

- I) *Specify study objective*
- and*
- II) *Use effective strategy*

The overall approach of the testing programme is dictated by the nature of the catalyst performance evolution. Whilst key outputs in all studies in this thesis are kinetic models that describe catalyst evolution phenomena, how those models are obtained will vary depending on the catalyst formulation and reaction system. For example, a study of catalyst formulation which evolves slowly, on a hour or day timescale, may require the use of discrete sweeps of reaction performance at different stages of lifetime. In a more dynamic system, such as an investigation of a catalyst's response to a feed step-change, detailed, data rich analysis techniques may be required, which can adequately describe the changes and subsequently be modelled using unsteady-state approaches. In these systems, an accurate quantification of gas

phase and surface species populations is essential. Such examples will be referred to at various points in this chapter.

### III) Select appropriate reactor

The choice of reactor for gas-solid systems on a lab scale is not straightforward. Fixed bed reactors, fluidised bed reactors and temporal analysis of products (TAP) reactors are just some examples of those available and each have their merits with regards to investigation over different reactant conversion ranges, isothermicity, easy of operability and cost. Generally no reactor exists that is right for all systems (Berger et al, 2001).

In this thesis, the author's experimental focus is primarily on fixed bed micro-reactor systems. Typically these reactors are small (<4 mm diameter) tubular reactors. Use of these reactors is highly established in industrial environments but also in academic studies. Such reactors often exist in parallel, enabling high-throughput testing and promoting improved kinetic studies and experiments comparing catalyst formulations (Perez-Ramirez *et al.*, 2000; Moulijn *et al.*, 2003). The realm of fixed bed reactors typically incorporates three types of operational mode. Figure 2.2 below shows the operation of these reactor configurations with respect to reactant conversions:

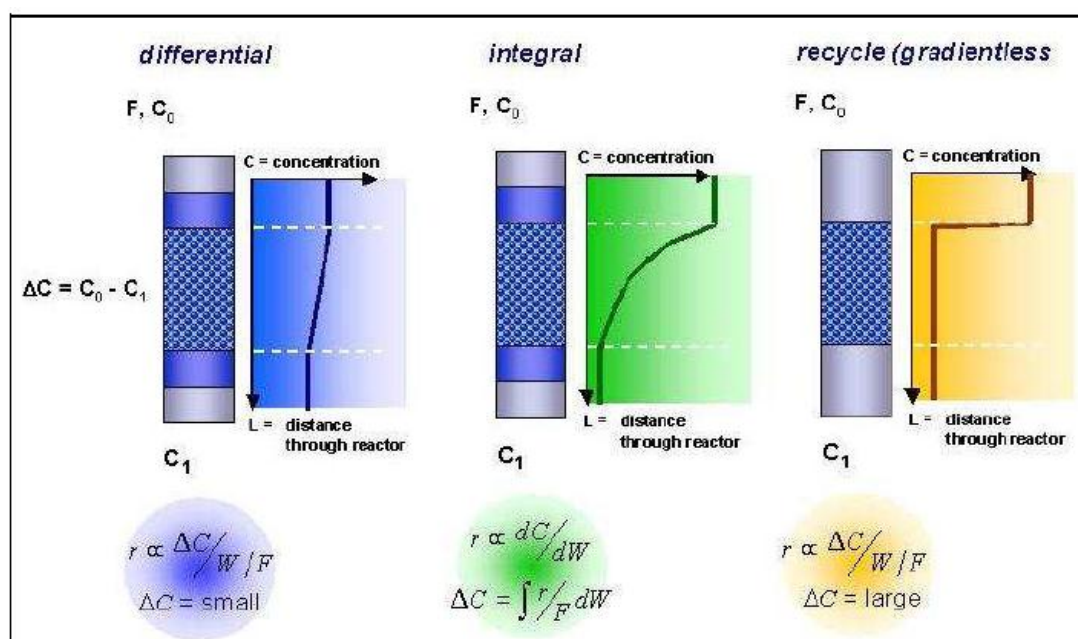


**Figure 2.2: Common laboratory flow micro-reactors used for kinetic measurements (image taken from Berger *et al.*, 2001)**

In Figure 2.2, configurations which show low (typically <5%) reactant conversions are described as *differential mode* operation. These studies are excellent for kinetics studies which purely examine the impact of input process variables. Interference in kinetic models from product concentrations is generally minimal due to the low conversions (Berger et al, 2001). *Integral mode* operation describes a configuration with higher reactant conversions (typically >10%). Significant concentration profiles may be seen along these reactors which will impact the quality of a kinetic study purely based on input process variables. This configuration can be effective in simulating typical industrial conversions (Perez-Ramirez *et al.*, 2000). *Recycle (gradientless) mode* employs a fully back-mixed operation. Full conversion is enabled and this method can provide detailed kinetic profiles with reaction time, like a batch reactor. An example of this is a Berty reactor (Berty, 1983). The development of some of these configurations into powerful methods to understand catalyst performance evolution is discussed in Section 2.1.2.

#### IV) *Establish ideal flow pattern*

In an ideal plug flow reactor (PFR), the fluid can be assumed to flow as a straight front through the reactor with zero radial velocity gradient (Perez-Ramirez *et al.*, 2000). In the laboratory micro reactor however, two key effects may be encountered which prevent ‘ideal’ plug-flow behaviour being established.

The first of these is imperfect mass transfer, caused by diffusion and localised flows around the catalyst particles and reactor walls which can cause axial dispersion effects. To combat this, a minimum ratio between catalyst bed length and particle size can be calculated by setting a maximum allowed deviation from plug flow (often 5%). This is defined below (Mears, 1971):

$$\frac{L_b}{d_p} > \frac{20n}{Bo} \ln\left(\frac{1}{1-X}\right) \quad (2.1)$$

$L_b$  denotes catalyst bed length (m),  $d_p$  denotes catalyst particle size (m),  $n$  is the reaction order (-),  $Bo$  denotes Bodenstein (or Péclet particle) number (-) and  $X$  denotes reactant conversion (-). Based on this criterion, it will be important to avoid a low catalyst bed length especially in conjunction with a low input flow rate (i.e. low  $Bo$  value) which could rapidly move a system away from conditions where axial dispersion effects can be ignored.

The second effect relates to deviations from plug flow caused by differences in reactor packing density in the interior and at the reactor walls (Perez-Ramirez *et al.*, 2000). The wall effect can cause a higher local velocity near the wall, which can prevent a plug flow regime being established. Gas bypass along the wall is another possibility. A useful criterion to neglect wall effects in a reactor tube of inner diameter,  $d_{tube}$  (m), is given below (Chu and Ng, 1989):

$$\frac{d_{tube}}{d_p} > 10 \quad (2.2)$$

Minimising pressure drop across a catalyst bed is also necessary to establish ideal flows in a reactor. This is carried out using the Ergun equation (Ergun, 1952):

$$\frac{\Delta P_b}{L_b} = \frac{150\mu_g}{d_p^2} \cdot \frac{(1-\varepsilon)^2}{\varepsilon^3} u + \frac{1.75\rho_g}{d_p} \cdot \frac{(1-\varepsilon)}{\varepsilon^3} u^2 < 0.2 \frac{P_{tot}}{L_b} \quad (2.3)$$

$\Delta P_b$  denotes pressure drop (Pa) across the catalyst bed length ( $L_b$ , m),  $u$  denotes superficial velocity ( $\text{m s}^{-1}$ ),  $\mu_g$  is the dynamic gas viscosity ( $\text{kg m}^{-1} \text{s}^{-1}$ ),  $\varepsilon$  is bed voidage fraction (-),  $\rho_g$  is gas density ( $\text{kg m}^{-3}$ ) and  $P_{tot}$  is total pressure (Pa). Based on the criterion, pressure drop across a catalyst bed should be no more than 20% of the total inlet pressure for laboratory reactors testing.

#### V) *Ensure isothermal conditions*

This criterion refers to obtaining a constant bulk fluid temperature throughout a catalytic bed. For radial temperature gradients in a packed bed, a criterion has been derived for a PFR (Mears, 1971):

$$\frac{E_a}{RT_W} \left| \frac{(-\Delta H_r) r_{v,obs} (1-\varepsilon)(1-b) r_t^2}{\lambda_{eff,b} T_W} \right| \times \left( \frac{1}{8} + \frac{1}{Bi_W} \cdot \frac{d_p}{d_{tube}} \right) < 0.05 \quad (2.4)$$

$E_a$  refers to activation energy ( $\text{kJ mol}^{-1}$ ),  $R$  is the universal gas constant ( $\text{J mol}^{-1} \text{K}^{-1}$ ),  $T_W$  is reactor wall temperature (K),  $\Delta H_r$  is heat of reaction ( $\text{kJ mol}^{-1}$ ),  $r_{v,obs}$  is observed rate of reaction ( $\text{mol s}^{-1} \text{kg}^{-1}$ ),  $b$  is degree of dilution (-),  $r_t$  is reactor tube inner radius (m),  $\lambda_{eff,b}$  is the effective thermal conductivity of the catalyst bed ( $\text{J m}^{-1} \text{s}^{-1} \text{K}^{-1}$ ) and  $Bi_w$  is the Biot number at the reactor wall.

In Eq. (2.4) deviation from the desired temperature is set at a maximum 5%. The criterion considers heat production and conduction rates in the radial direction and the relative contributions of the radial conductivity and heat transfer at the reactor wall. Typically, diluting the catalyst bed or using a smaller tube diameter will reduce the radial temperature gradient in the catalyst bed.

Axial temperature gradients may also be discovered across a catalyst bed. The usage of thermocouples at the inlet and outlet of a catalyst bed can identify this. Outside of experimental findings, a calculation of the adiabatic temperature rise within a system can be used:

$$\Delta T_{ad} = (\text{Fraction reactant conversion}) \cdot (\text{Fraction reactant in feed}) \cdot (-\Delta H_r) / (C_{p,mix}) \quad (2.5)$$

This crude but pragmatic calculation shows the change in temperature caused by a specified reaction. The calculation takes the circumstance that the heat released by the reaction is retained in the system and is used to heat up remaining reactants and products. In a strongly exothermic system, adiabatic temperature rise values measured can be very high (order of  $10^2$  K) however in practice the real temperature rise is lower due to heat loss from the reactor.

$\Delta T_{ad}$  refers to adiabatic temperature rise (K),  $C_{p,mix}$  refers to specific heat capacity of the gas mixture ( $\text{J mol}^{-1} \text{K}^{-1}$ ). Axial temperature gradients can be reduced in reaction systems by operation at low conversion, using smaller catalyst particles and by using a high conductivity, inert diluent.

#### VI) *Diagnose and minimise heat and mass transport disguises*

The effect of transport limitations in heterogeneously catalysed reactions has been heavily studied in literature (Perez-Ramirez *et al*, 2000) and it is highly important to check for their presence or absence when testing catalysts, an essential of intrinsic kinetics investigations. For laboratory gas-solid systems, there are five gradients which often have the following order of importance (Kapteijn and Moulijn, 1996):

$$(T_{grad})_{bed} > (T_{grad})_{extra} > (c_{grad})_{intra} > (T_{grad})_{intra} > (c_{grad})_{extra} \quad (2.6)$$

$c$  refers to gas concentration ( $\text{mol m}^{-3}$ ) and  $T$  is temperature (K). Axial and radial reactor scale temperature gradients  $(T_{-grad})_{bed}$  are often the most critical transport phenomena due to poor heat conductivity of gas-solid fixed beds, an effect that can be exacerbated in highly exothermic or endothermic systems. Significant concentration gradients often prevail within a particle (*intra-particle*) or at the interface with an external fluid phase (*extra-particle*). The four extra and intra particle gradients can be estimated *a priori* using the following equations:

- Extra-particle mass transfer: Carberry number ( $Ca$ ) (Carberry 1987):

$$Ca = \frac{r_{v,obs}}{a'k_f c_{bulk}} < \frac{0.05}{n} \quad (2.7)$$

$Ca$  relates the concentration difference over the film to procurable quantities.  $a'$  is the specific surface area of the catalyst particle ( $\text{m}^2 \text{m}^{-3}$ ),  $k_f$  is the mass transfer coefficient ( $\text{m s}^{-1}$ ),  $c_{bulk}$  is bulk phase concentration ( $\text{mol m}^{-3}$ ) and  $n$  is order of reaction.

- Extra-particle heat transport gradients (Mears, 1971):

$$\gamma\beta_{extra} Ca = \left( \frac{E_a}{RT_b} \right) \left| \frac{(-\Delta H_r)k_f c_b}{hT_b} \right| \times \left( \frac{r_{v,obs}}{a'k_f c_b} \right) < 0.05 \quad (2.8)$$

$T_b$  refers to bed temperature (K),  $h$  the gas-solid heat transfer coefficient ( $\text{W m}^{-2} \text{K}^{-1}$ ),  $\gamma$  and  $\beta_{extra}$  are constants based on correlations in literature (-).

- Intra-particle diffusional gradients (Weisz, 1957):

$$\Phi = \eta\phi^2 = \left( \frac{r_{v,obs}L^2}{D_{eff}c_s} \right) \left( \frac{n+1}{2} \right) < 0.15 \quad (2.9)$$

$\Phi$  refers to the Wheeler-Weisz modulus (-),  $\eta$  is particle effectiveness factor (-),  $\phi$  is the Thiele modulus (-),  $L$  is a characteristic catalyst dimension (m),  $D_{eff}$  is the effective diffusivity in a particle ( $\text{m}^2 \text{s}^{-1}$ ) and  $c_s$  is catalyst particle surface concentration ( $\text{mol m}^{-3}$ ).

- Intra-particle heat transport gradients (Mears, 1971):

$$\gamma\beta_{intra}(\eta\phi^2) = \left( \frac{E_a}{RT_b} \right) \left| \frac{(-\Delta H_r)D_{eff}c_s}{\lambda_{eff,p}T_b} \right| \times \left( \frac{r_{v,obs}L^2}{D_{eff}c_s} \right) < 0.05 \quad (2.10)$$

$\gamma$  and  $\beta_{intra}$  refer to constants based on correlations in literature (-),  $\lambda_{eff,p}$  is effective thermal conductivity of a particle ( $\text{J m}^{-1} \text{s}^{-1} \text{K}^{-1}$ ). This gives an approximation for the maximum allowable temperature rise in the catalyst bed and is often set at a 5% deviation from desired isothermal conditions

#### VII) *Gather meaningful catalyst performance data*

Selection of an appropriate gas-phase reactor outlet analysis method is essential. Two key considerations should be made for a transient performance study, firstly whether the technique can analyse accurately the necessary reactants and products in the chosen system and secondly whether the chosen technique can gather data fast and accurately enough to show transient catalyst behaviour.

Gas chromatography (GC) methods are effective at analysing many inorganic and organic compounds but may be limited by time intervals between analysis points. Infra-red (IR) analysers can provide a fast response and detailed dataset but cannot detect compounds with symmetric vibration, such as  $\text{H}_2$ . Mass spectrometers (MS) systems provide a fast response and detailed dataset however care must be taken to decouple some responses, should compound or fragment compound masses overlap (Berger *et al.*, 2008).

#### VIII) *Establish stability early*

During a transient performance catalyst testing program it is important to establish how long it takes a catalyst to reach a ‘quasi’ steady state point of operation for given conditions. This is particularly essential before switching to a different set of conditions, such as:

- At the start of a steady state testing procedure at different process settings
- At the progression to a new set of conditions during an adsorption-desorption experiment.

Multiple but targeted assessments of catalyst stability should be undertaken, such as exploring the operational extremes (e.g. highest temperature or concentration of feed poisons).

*IX) Follow good experimental practise*

*and*

*X) Provide perspective on results*

In a study of transient catalyst behaviour, a high standard of experimental practice is essential to accurately quantify performance changes to a catalyst. An objective perspective on results is provided by this approach as the experimentalist is afforded greater command of the true values of process settings and measured output responses. These factors include:

- **Accurate calibration:** The composition range of reactants and products tested and produced within the experimental programme should be fully covered by a calibration. Certified test gases should be used to obtain a calibration.
- **Quantify blank activity:** In some systems, homogeneous reactions may take place in the absence of catalyst and should be quantified from a blank. For transient response experiments, a step change in feed compositions may not be instantaneous and a blank activity experiment for such a change can map real 'step changes' to provide more accurate feed data for subsequent kinetic modelling (Perez-Ramirez *et al*, 2000).
- **Reproducibility:** In general, it is essential to carry out 1 or 2 extra experiments under a set of 'reference' conditions during the experimental programme. This will provide a measure of 'pure error' within the experiment which provides a percentage confidence in measured data and can help identify outliers in subsequent experiments. When the data are used for model parameter estimation processes, pure error can be compared to model error via the additional sum of squares '*F*-test' (Quiney and Schuurman, 2007). This will ascertain if the data are of good enough quality to support findings from parameter estimation.
- **Reactor loading:** It is essential that catalyst, inert diluents and reactor packing materials are loaded correctly into a reactor. Ensuring thermocouples are positioned in required positions is also essential. Such procedures have been thoroughly reviewed previously (Perez-Ramirez *et al*, 2000).

- **Close out mass balances:** Assuming inlet feeds to a reactor are quantified, it is essential to understand if the elemental balance is maintained at the reactor outlet. In a steady state performance study it is required to verify that reactor outlet element balances equate to the inlet balances otherwise catalyst behaviour is not truly at steady state. For transient studies, the mass balance can provide quantification of species adsorbed/desorbed from a catalyst surface (Lietti *et al.*, 1997), build-up of carbonaceous compounds (Froment and Bischoff, 1961) or elemental losses/gains to the catalyst itself, such as during reactive frontal chromatography experiments to measure metal surface areas (Chinchen *et al.*, 1987a).
- **‘Control’ Samples:** Utilising a reference (catalyst) with known performance under the conditions tested allows for a comparison point with the other catalysts (and/or conditions) tested in the same experimental run. The reference will also act as a useful check to show that the experiment is running correctly.
- **Consider utilising tracers in feeds:** The use of a tracer (such as known concentration of inert gas) in feeds is particularly useful during transient kinetic studies. Tracers act as an internal standard to quantify the incoming gas composition, in particular during a step change in feed conditions. This allows full characterisation of the dynamics of experimental reactors and correct estimations of adsorbed or desorbed species.

## 2.1.2 Experimental techniques to understand catalyst performance evolution

### 2.1.2.1 Accelerated decay tests

Accelerated decay tests are commonly used in industry as a pragmatic method to examine long term stability and performance of catalyst formulations. Levenspiel (1972) divides the concept of catalytic performance evolution into five key categories, the effects of which can be promoted by accelerated ageing:

- **Parallel:** Depends on concentrations of reactants,  $C_{reac}$  (such as poisoning or fouling due to deposition of side-products from main reaction).
- **Series:** Depends on concentrations of reaction products  $C_{prod}$  (such as poisoning, fouling or structural changes caused by decomposition of main reaction products).
- **Side-by-side:** Depends on concentrations of other components,  $C_{pois}$  that are not involved in the main reaction (such as a feedstock impurity).

- **Independent:** Driven by structural transformations occurring at reaction temperature. These are independent of fluid composition.
- **Multi-component:** Catalytic performance evolution due to more than one of the above effects.

These mechanisms are probed by harsher conditions than would be experienced in actual plant operation (e.g. higher temperatures, greater concentration of feed poisons). These tests are most effective when one particular mode of decay dominates, however, care must be taken when designing these tests to ensure that operational conditions do not stray too far from typical process settings (Birtill, 2004a). For example, in an investigation of poison effects, a large increase in reaction temperature may induce sintering effects whilst reducing the effect of the poison (e.g. promoting desorption). In short, these tests are useful but require clear initial thinking before they are carried out.

Such catalyst performance evolution processes can be further demonstrated by an examination of selectivity evolution across the catalyst beds (Birtill, 2003). This is tested by modifying the flow rate over the largest catalyst bed so that a reference initial reactant conversion is restored. All smaller catalyst beds are then exposed to same flow rate and a shift in product selectivity can be compared. Often selectivity evolution is linked directly to overall catalyst activity: active sites do not fundamentally change but are simply lost or gained over time. In these situations *intrinsic* selectivity of the catalyst is constant but *observed* selectivity may still change, as a function of conversion.

In some systems, *intrinsic* selectivity may change, with no simple direct link to overall catalyst activity. In these situations, modelling activity evolution will be more complex; multiple mechanisms may be prevalent and relative quantities of active sites may shift.

#### 2.1.2.2 Parallel difference tests

Parallel difference testing of catalyst formulations using multi-tube, fixed-bed reactor units is a strong candidate for analysing catalyst performance evolution in detail. Parallel difference testing of a single catalyst provides the capability to estimate performance of discrete segments of a catalyst bed (see Figure 2.3). Multiple reactors are operated using identical feedstock concentrations, flow rates and temperature, but with different catalyst

masses. The approach is data rich and effectively tracks kinetic profiles of an integral bed with time on stream, which is excellent for kinetic modelling purposes.

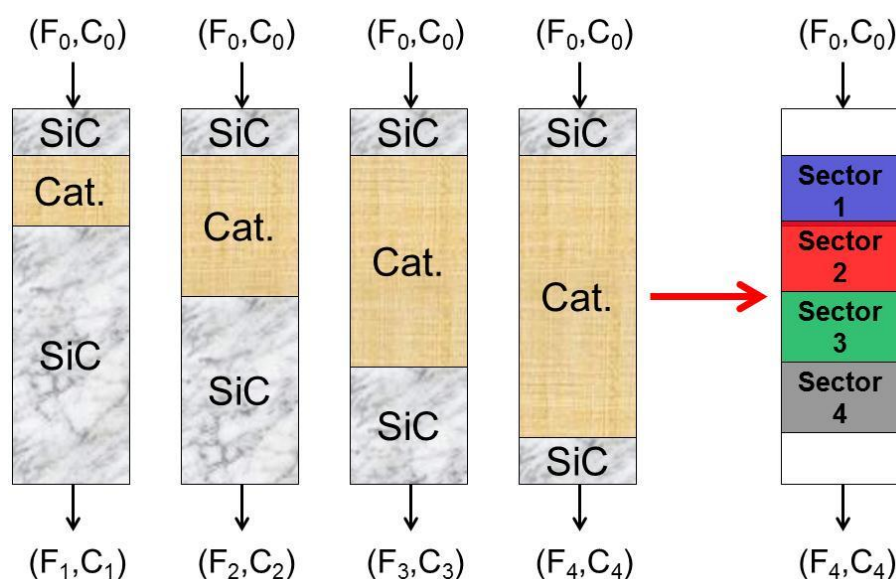


**Figure 2.3: Example of a parallel difference test setup using 4 micro-reactors in parallel filled with catalyst and inert silicon carbide packing**

Example data (Figure 2.4, overleaf) shows a test whereby three catalyst beds are utilised and performance over time is calculated for each segment. It is essential to carry out repeats for this kind of experiment, as error can be propagated in the species concentration changes between segments. This is due to subtraction of one value from another, both of which will have a degree of uncertainty, dependent of the quality of experimental measurements.

Parallel difference testing can provide clues as to the type of evolution mechanism observed over time on stream. The graphs in Figure 2.4 provide simple examples of the four mechanisms previously discussed. Upon restoration of initial reactant conversion across the 100% length bed the following typical behaviours can be observed:

- **Parallel:** Large changes are seen in performance at the front of bed resulting from high reactant concentrations at this point. Subsequent parts of the catalyst bed accommodate for these changes over time. A return to initial conversion reveals a large performance evolution at the front of the catalyst bed.

- **Series:** Front of catalyst bed slowly changes in activity however subsequent catalyst bed sectors do not compromise this change due to the effect of product concentrations.
- **Side-by-side:** Performance profiles are often similar to those seen for a parallel mechanism. Further testing using high purity feedstock may be required to fully decouple these mechanisms.
- **Independent:** Changes in segment performance are often similar to those for a series mechanism, however a return to initial overall conversion sees each bed segment return to its initial conversion also. Catalyst performance evolution is uniform along the catalyst bed.

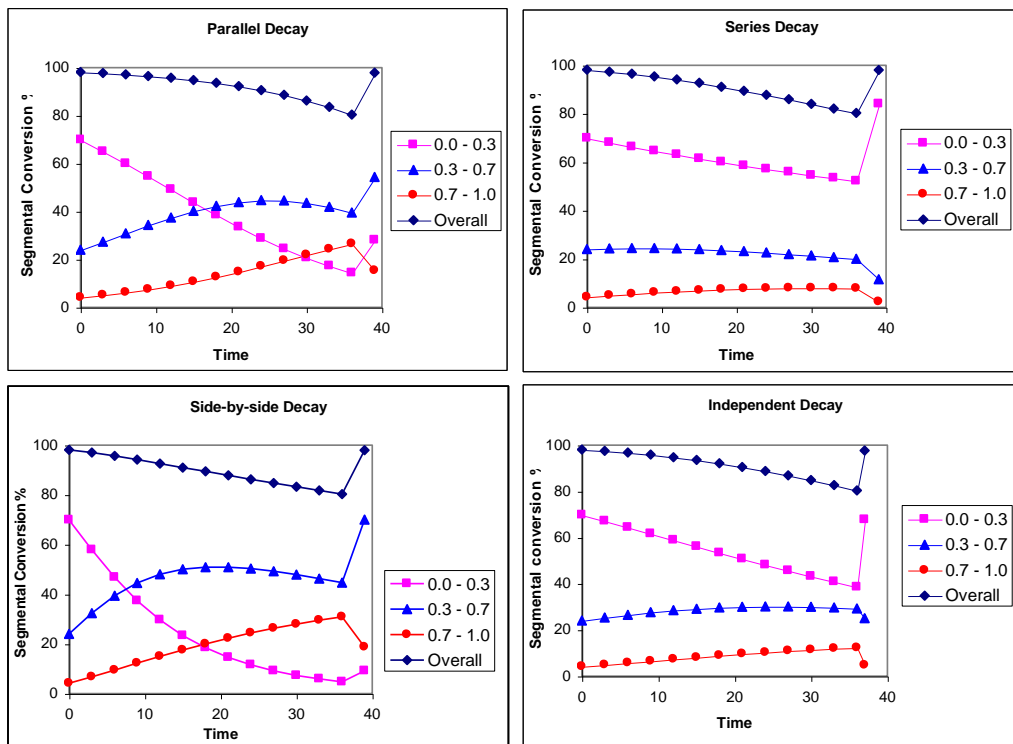


**Figure 2.4: Characteristic catalyst performance evolution plots for parallel difference testing. In each case all beds receive identical feeds for the entire test except for the final data points at time = 40 h. At time = 40 h, the feed-rates to the 100% length beds are reduced so as to restore conversion to the initial value of 98% and the feed-rates to the shorter beds are reduced to the same extent (taken from Birtill, 2004a). Source does not describe the origin of the data presented. 0.0 – 0.3, 0.3 – 0.7, 0.7 – 1.0 denotes the fractional sections of the catalyst bed.**

### 2.1.2.3 Transient response tests

Transient response tests, such as those which incorporate step changes in feed composition over an operational catalyst, initially at steady state, can extract considerable mechanistic understanding of catalyst behaviour by probing individual steps of catalytic reaction sequences (Weller, 1992; Berger *et al.*, 2008).

As discussed in Chapter 1, the nature of these experiments can take multiple forms (e.g. choice of flow-through reactor, nature of perturbation) however in this thesis study, application will focus around flow-through, gas phase fixed beds. Examples of such operation are shown in Figure 2.5. In the example from Lietti *et al.*, (1997), catalyst formulation comparison is demonstrated. These data can be applied to non-steady state adsorption-desorption-reaction kinetic models in order to elucidate key differences in catalyst functionality and link to formulation. The background to this modelling process is discussed in Sections 2.3.1 and 2.5.1.

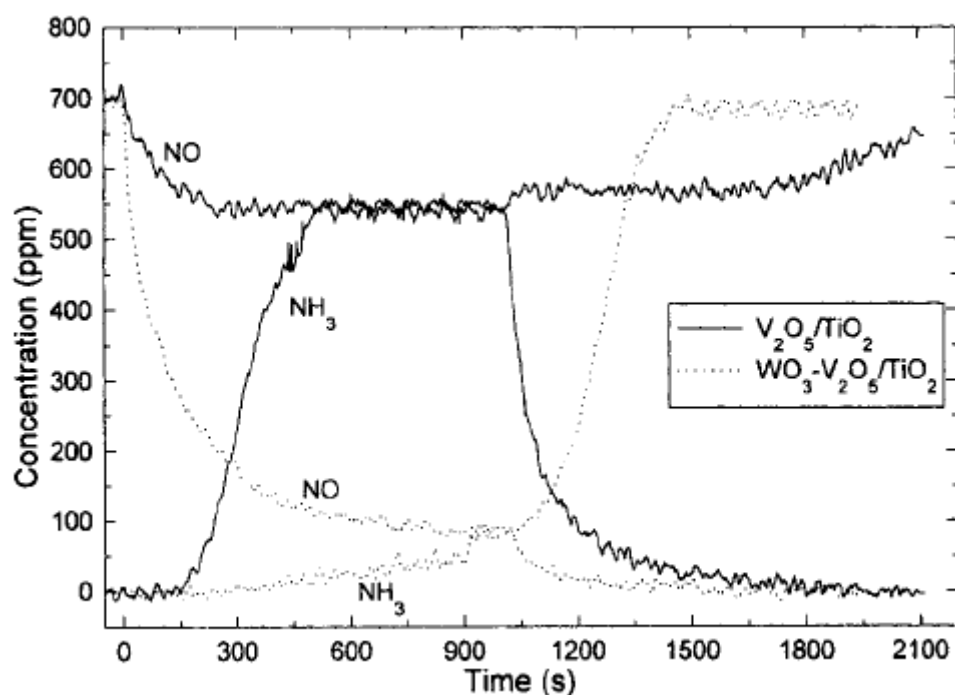


**Figure 2.5: Examples of step-change transient response tests: NO and NH<sub>3</sub> concentration response over two different catalyst formulations when a 700 ppm NO/1% O<sub>2</sub>/He feed is doped with 700 ppm NH<sub>3</sub> (at t = 0 s) which is subsequently removed at t = 1000 s at 553 K (Lietti *et al.*, 1997)**

## 2.2 Catalyst characterisation

The support of experimental catalyst performance evolution data with real physical and chemical observations on the catalyst may be used to strengthen the basis of mechanistic models generated in this study. Whilst the individual results chapters of this thesis delve into specific techniques appropriate to the catalyst system in question, this section summarises *ex situ*, *in situ* and *operando* options in this area.

### 2.2.1 *Ex situ* techniques

For some catalysts, *ex situ* analysis of physical and chemical state at various stages during catalyst performance evolution may be permissible. In previous literature, these are referred to as post-mortem studies whereby the catalyst under scrutiny is characterised by a set of techniques following reactor discharge. Birtill (2003) summarises a range of characterisation techniques which could be used:

- **Sample sizing:** Is there sizing variation between discharged catalyst powder/pellets?
- **Bulk chemical analysis:** Such as X-ray fluorescence (XRF) on catalyst and potential deposits.
- **Phase identification/morphology:** Such as X-ray diffraction (XRD), Raman spectroscopy or scanning electron microscopy (SEM).
- **Surface area:** Sorption techniques
- **Crystallite size:** XRD, SEM, transmission electron microscopy (TEM)
- **Pore structure:** Mercury porosimetry, sorption techniques
- **Surface composition or structure:** X-ray photoelectron spectroscopy (XPS)

In the literature, such an approach is generally seen for catalysts whose rate of performance evolution is sufficiently slow that the catalysts in question can be removed from reactor operation without further change to physico-chemical state. An initial reactor operation example of this is the evolution of a vanadium phosphorus oxide selective oxidation catalyst, whose evolution was tracked by XRD, Raman and XPS during a ~150 h period of performance change (Abon *et al.*, 1995). Long-term deactivation examples include analysis of the impact of accelerated (hydro)thermal ageing of diesel oxidation (Wiebanga *et al.*, 2012) and ammonia selective catalytic reduction (Madia *et al.*, 2002) catalysts using XRD, Raman, XPS, XRF and SEM.

The utilisation of characterisation data within catalyst performance evolution models is seldom explored, but examples do exist, including a sulphation study (Quet *et al.*, 1980) and hydrocarbon reforming study (Christensen, 1996). A greater number of examples exist for purely mechanistic studies, such as a study of segregation in vanadia-molybdena catalyst during redox processes (Bielanski *et al.*, 1979).

### 2.2.2 *In situ* and *operando* techniques

The post-mortem approach may be of limited use for catalyst systems where either performance changes are occurring too quickly or the active catalyst state is formed *in situ* (e.g. reduction of a metal oxide precursor to a catalytically active metal state). In such circumstances, *in situ* and *operando* techniques may have considerably more value. Both types of technique involve analysis of the physico-chemical state of a catalyst under the influence of reaction conditions. *Operando* techniques are highly desirable as the catalyst is operated under working conditions (e.g. temperature, flow, pressure) whilst undergoing analysis of reaction products in real time. Hence *operando* techniques can be linked directly with catalyst performance during testing. The following example techniques can be operated either *in situ* or *operando*:

- **Environmental TEM:** Using high-resolution, aberration corrected techniques, environmental TEM can be applied to samples of catalyst sampled from working conditions. A catalyst evolution application example is the sintering of Pt/Pd nanoparticles on carbon (Gai and Boyes, 2009).
- **XRD and XPS:** Catalysts under reaction conditions can be periodically sampled, retained under vacuum and analysed via these techniques. The working scope before sampling, particularly with respect to operating pressure, is limited.
- **Tapered element oscillating micro-balance (TEOM):** A technique designed to detect changes in mass of a catalyst under working conditions. Sensitivity is typically on a microgram scale. Examples include use as a coke-microbalance (Chen *et al.*, 1996) and to assess catalyst reduction and oxidation (Wang and Barteau, 2000).
- **Atomic labelling studies:** Elemental labelling of specific feed gases can enhance mechanistic understanding of catalytic reactions. An example is the use of labelled  $^{14}\text{CO}_2$  (in a mixture with CO/H<sub>2</sub>) over Cu-based methanol synthesis catalysts to elucidate the roles of CO and CO<sub>2</sub> in methanol formation (Kagan *et al.*, 1975; Chinchén *et al.*, 1987b).

- **Diffuse reflectance infra-red Fourier transform spectroscopy (DRIFTS):** A technique designed to analyse surface species on a catalyst under reaction conditions via detection of functional groups at different wavelengths. The technique has seen development for operation in flow through reactor operation (coupled with outlet gas analysis), high pressure operation and application of feed step changes enabling quantitative analysis of surface species evolution on a catalyst surface with time on stream (Meunier *et al.*, 2007).

## 2.3 Kinetic and activity-time modelling

In general, there are two key methods for modelling catalyst performance evolution. For fast, dynamic systems (second or min scale evolution), such as those impacted by a step change response, unsteady-state models are appropriate. These incorporate adsorption, desorption and reaction steps. This method is necessary, often due to fast shifts in population of species on the catalyst surface. For slower evolving catalysts (hour, day or longer evolution), ‘activity’-time models are generally more appropriate and can track active site evolution, provided the steady-state kinetics of the system are sufficiently understood.

### 2.3.1 Time dependent adsorption-desorption-(reaction) kinetic modelling

A proposed series of mechanistic steps is the start point for any unsteady-state kinetic modelling investigation. To illustrate for future application in this thesis, a simple two-step sequence for the reaction  $A + B \rightarrow C$  is demonstrated:



Where  $k_i$  and  $k_{-i}$  denotes forwards and backwards rate constants and  $S_i$  denotes an active site. This example, which follows an Eley-Rideal-type sequence, is then presented as an unsteady-state material balance for gas-phase and adsorbed species (examples of the fully development of these model types can be found in Kobayashi and Kobayashi, (1972)):

$$\frac{dC_A}{dt} = -v \frac{dC_A}{dz} + \Omega(r_{-1} - r_1) \quad (2.13)$$

$$\frac{dC_B}{dt} = -v \frac{dC_B}{dz} - \Omega(r_2) \quad (2.14)$$

$$\frac{dC_C}{dt} = -v \frac{dC_C}{dz} + \Omega(r_2) \quad (2.15)$$

$$\frac{d\theta_A}{dt} = r_1 - r_{-1} - r_2 \quad (2.16)$$

Where  $C_i$  denotes gas phase concentrations,  $\theta_i$  surface species coverage,  $\Omega$  adsorption capacity of catalyst,  $z$  reactor axial coordinate,  $v$  interstitial gas velocity,  $r_1$  adsorption rate of A,  $r_{-1}$  desorption rate of A and  $r_2$  reaction rate of A with B. The rate terms themselves are expanded into rate equations based on the specific steps. Whilst the possibilities here are numerous, specific mention should be given to models applied in the desorption step which can provide insight into the degree of heterogeneity of the active catalyst surface and the spread of desorption energies ( $E_{des}$ ) of active sites. These include Langmuir (Eq. (2.17);  $E_{des}$  constant), Temkin (Eq. (2.18);  $E_{des}$  decreases linearly with surface coverage) and Freundlich (Eq. (2.19);  $E_{des}$  decreases logarithmically with surface coverage) (Corma *et al.*, 1988; Lietti *et al.*, 1997):

$$r_{des} = k_{des}^0 \exp\left(\frac{-E_{des}}{RT}\right) \theta_i \quad (2.17)$$

$$r_{des} = k_{des}^0 \exp\left(\frac{-E_{des}^0(1-\alpha\theta_i)}{RT}\right) \theta_i \quad (2.18)$$

$$r_{des} = k_{des}^0 \exp\left(\frac{-E_{des}^0 \exp(-\alpha\theta_i)}{RT}\right) \theta_i \quad (2.19)$$

Where  $\alpha$  is a fitted constant (-). By solving equations such as (2.13-16) with the application of appropriate rate terms, dynamic behaviour of catalyst formulations can be described. Fitted parameters from this process can be linked to the fundamental nature of active site populations on a given catalyst surface.

### 2.3.2 Activity-time modelling

Activity evolution of a catalyst can be studied at three levels, fundamental, semi-empirical and empirical (Birtill, 2003). Fundamental studies involve a direct link to changes in active sites of a catalyst, such as utilising Langmuir-Hinshelwood-Hougen-Watson (LHHW) expressions, which incorporate a balance of sites (Wolf and Petersen, 1977). In a semi-empirical approach, catalyst performance evolution is tracked by an empirical expression but is linked to some measurable change on the catalyst (e.g. coke laydown (Froment and Bischoff, 1961), changes in catalyst mass (Wang and Barteau, 2000)). In an empirical approach, catalyst evolution is described directly in terms of local reaction environment by power law expressions (Levenspiel, 1972).

Catalyst activity will evolve as a consequence of physical and chemical changes impacted by the reaction environment. The principal of separability is used in many studies as it allows main reaction kinetics and catalyst performance evolution kinetics to be resolved. This was originally described in Szépe and Levenspiel (1968):

$$r = f_1(C, T) \cdot f_2(\Theta) \quad (2.20)$$

By this general formula, the rate of main reaction,  $r$  at time  $t$  is the product of two separable terms.  $f_1$  refers to the true catalytic reaction kinetics and is assumed *time independent*.  $f_2$  refers to current activity (or population of active sites),  $\Theta$  and is *time dependent*.  $\Theta$  is measured relative to a standard condition  $\Theta_0$ . The basis of Eq. (2.20) is that there is little or no linkage between  $f_1$  and  $f_2$  and so a change in activity will result in no change to true catalytic reaction kinetics. Butt *et al.*, (1978) critically examined this relationship, concluding it is only truly correct for an ideal surface. Care must therefore be taken in its use. The ‘level’ of approach, described in the following sections will also be significant in the decision to utilise the relationship.

#### 2.3.2.1 Empirical approaches

On an empirical level, evolution of catalyst performance (such as conversion of reactants or yield of specific products) can be tracked as a function of the local environment. The  $f_2(\Theta)$  term in Eq. (2.20) can be expressed in a general form using simple power law expressions (Levenspiel, 1972):

$$-\frac{d\Theta}{dt} = k_d (c_1^{n_1} c_2^{n_2} \dots c_i^{n_i}) \Theta^m \quad (2.21)$$

$k_d$  represents a catalytic performance evolution rate constant (itself an Arrhenius function term with activation energy,  $E_d$ ),  $m$  is the order of catalytic performance evolution,  $c_1-c_i$  are concentrations of fluid phase components,  $n_1-n_i$  are orders of concentration dependencies. Levenspiel (1972) applied this relationship to the five causes of catalyst performance evolution (Section 2.1.2.1) to yield the following equations in Table 2.1:

The relationships in Table 2.1 will often arise from analysis of an accelerated ageing or parallel difference study. The mechanisms described here are pragmatic and may serve as an initial probe for catalyst performance evolution, particularly for initial operation and long term deactivation mechanisms.

**Table 2.1: Empirical power law expressions for catalyst performance evolution (Levenspiel, 1972)**

Mechanism	Equation No.	Model
Parallel	(2.22)	$-\frac{d\Theta}{dt} = k_d c_{reac}^n \Theta^m = A \exp\left(\frac{-E_d}{RT}\right) c_{reac}^n \Theta^m$
Series	(2.23)	$-\frac{d\Theta}{dt} = k_d c_{prod}^n \Theta^m = A \exp\left(\frac{-E_d}{RT}\right) c_{prod}^n \Theta^m$
Side-by-side	(2.24)	$-\frac{d\Theta}{dt} = k_d c_{pois}^n \Theta^m = A \exp\left(\frac{-E_d}{RT}\right) c_{pois}^n \Theta^m$
Independent	(2.25)	$-\frac{d\Theta}{dt} = k_d \Theta^m = A \exp\left(\frac{-E_d}{RT}\right) \Theta^m$
Multi-component	(2.26)	$-\frac{d\Theta}{dt} = A \exp\left(\frac{-E_d}{RT}\right) (c_1^{n_1} c_2^{n_2} \dots c_i^{n_3}) \Theta^m$

The value of  $m$  may also vary for different catalytic phenomena. Table 2.2 shows the appearance of catalyst performance evolution equations based on the value of  $m$ , using an independent mechanism example:

**Table 2.2: Integral and differential expressions for a concentration independent mechanism (Birtill, 2004b)**

	Equation	Activity-time dependence	Equation	Activity decay rate
Linear	(2.27a)	$\Theta = 1 - k_d.t$	(2.27b)	$-d\Theta/dt = k_d$
Exponential	(2.28a)	$\Theta = \exp(-k_d.t)$	(2.28b)	$-d\Theta/dt = k_d.\Theta$
Hyperbolic	(2.29a)	$\Theta = 1/(1+k_d.t)$	(2.29b)	$-d\Theta/dt = k_d.\Theta^2$
Reciprocal Power	(2.30a)	$\Theta = t^{-0.5}/k_d$	(2.30b)	$-d\Theta/dt = k_d.\Theta^3$
Wojciechowski	(2.31a)	$\Theta = (1+(m-1).k_d.t)^{-1/(m-1)}$	(2.31b)	$-d\Theta/dt = k_d.\Theta^m$

Eqs. (2.27-30) represents solutions where  $m$  is fixed. The real physical meaning of  $m$  is debatable, particularly for higher order ( $m \geq 2$ ) relationships. Such empirical fits are likely to act as a mask for multiple catalyst performance evolution phenomena which will require more detailed fundamental kinetic analysis. Eq. (2.31) (Wojciechowski, 1968), is based on pseudo-concentration-independent performance evolution kinetics and  $m$  can be fitted to incorporate concentration dependent changes. Utilising this model to mirror concentration dependent evolution lacks sound mechanistic basis and functions simply as a pragmatic fit.

Eqs. (2.22-31) all describe empirical activity evolution that is tending towards a zero value. In some situations, particularly during initial operation of a fresh catalyst under reaction conditions, activity may instead tend towards a steady state (residual) activity term,  $\Theta_{ss}$ . Table 2.3 (overleaf) denotes examples of these models in Eqs. (2.32-34). Fuentes, (1985) and Corella *et al.*, (1988) have developed this steady state term into power law models when attempting to describe catalyst performance evolution through to a residual steady state.

Feasibly, a  $\Theta_{ss}$  term can be incorporated into most mechanistic models, whether empirical or fundamentally based. The key challenge to this approach may be establishing the  $\Theta_{ss}$  baseline. Estimation of  $\Theta_{ss}$  could be problematic if the catalyst does not reach steady state, or if start-up evolution mechanisms are interlinked with long term deactivation mechanisms. Providing a physical explanation for residual activity may be further complicated if  $\Theta_{ss}$  has a

non-linear relationship with reaction conditions, or if the catalyst shows non-separable behaviour.

**Table 2.3: Power law expressions with residual activity (Birtill, 2004b)**

Equation	Model
(2.32)	$-\frac{d\Theta}{dt} = k_d \{c_A^n\} (\Theta - \Theta_{ss})^m$
(2.33)	$-\frac{d\Theta}{dt} = k_d \{c_A^n\} (\Theta^m - \Theta_{ss}^m)$
(2.34)	$-\frac{d\Theta}{dt} = k_d \{c_A^n\} (\Theta - \Theta_{ss}) / (1 - \Theta_{ss})$

A number of examples exist in literature; Forzatti and Buzzi-Ferraris (1982) examined methanol oxidation utilising a redox model with residual activity, Wanke and Flynn (1975) have investigated sintering of supported metal catalysts, Borgna *et al.* (2001) used power-law residual activity models for reversible acid poisoning of Cs-Y zeolite catalysts.

### 2.3.2.2 Semi-empirical approaches

The addition of a measureable physical quantity to the empirical equations described in Section 2.3.2.1 has also received considerable literature attention. The classic example of this is in studies of activity-coke relationships. Studies in this area are rooted in the techniques laid down for parallel and series coking by Froment and Bischoff, (1961). The relationships in these studies take a similar form to equations in Table 2.2 and replace time on stream ( $t$ ) with measured coke content ( $C_C$ ) and deactivation rate constant ( $k_d$ ) with coking rate constant ( $k_c$ ) (Rieff and Kittrell, 1980). Zeolite catalyst formulations have been compared using this method; Froment *et al.*, (1990) tracked the rate constant evolution of hexane cracking and coking reactions over ZSM-5, 11 and 48.

### 2.3.2.3 Fundamental approaches

In more complex catalyst systems, utilisation of the principle of separability is more challenging. Examples includes systems with physical non-equivalence of active sites, such as a non-homogeneous surface which features more than one active site, each different in activity. In such systems, considerable steady state and transient kinetic analysis will be

needed to fully elucidate active sites and reaction pathways. Processes which modify active sites can result in a change to  $f_l$  which again creates non-separable behaviour.

The approach of Wolf and Petersen, (1977) utilised LHHW-type expressions to maintain a balance of sites with time on stream. Examples, shown in Table 2.4, feature both a reaction pathway rate constant,  $k_i$  and a fraction of remaining active sites for that pathway,  $\Theta$ . Lumping of these values affords an evolution of pre-exponential factor,  $A_i$ , with time which itself can be related back to active site quantities on a fundamental level:

**Table 2.4: Fundamental LHHW-based ‘balance of sites’ activity evolution expressions (taken from Wolf and Petersen, 1977)**

Mechanism	Equation No.	Model
Parallel	(2.35)	$-\frac{d\Theta}{dt} = \frac{k_i K_i \Theta C_{\text{reac}}}{(1 + K_{\text{reac}} C_{\text{reac}} + K_{\text{prod}} C_{\text{prod}})}$
Series	(2.36)	$-\frac{d\Theta}{dt} = \frac{k_i K_i \Theta C_{\text{prod}}}{(1 + K_{\text{reac}} C_{\text{reac}} + K_{\text{prod}} C_{\text{prod}})}$
Side-by-side	(2.37)	$-\frac{d\Theta}{dt} = \frac{k_i K_i \Theta C_{\text{pois}}}{(1 + K_{\text{reac}} C_{\text{reac}} + K_{\text{prod}} C_{\text{prod}} + K_{\text{pois}} C_{\text{pois}})}$
Independent	(2.38)	$-\frac{d\Theta}{dt} = \frac{k_i K_i \Theta}{(1 + K_{\text{reac}} C_{\text{reac}} + K_{\text{prod}} C_{\text{prod}})}$

The approach in Table 2.4 can be developed in multiple ways, dependent on the complexity of the reaction network involved and/or the level of heterogeneity on the catalyst surface. On a single site basis, multiple catalyst performance evolution phenomena may take place giving rise to the following type of equations (Birtill, 2004a):

$$-\frac{d\Theta}{dt} = k_{d1} (\psi_{d1}) \Theta^{m1} + k_{d2} (\psi_{d2}) \Theta^{m2} \quad (2.39)$$

$\psi_{di}$  refers to the catalyst performance evolution functions for each particular mechanism. Corella and Monzon (1988) provide a detailed modelling review for such systems.

Alternatively, catalyst performance evolution may be due to combined mechanisms which are *interdependent*. Eq. (2.40) describes a simple model for this:

$$\Theta = \Theta_1 \cdot \Theta_2 \quad (2.40)$$

In this example, a particular reaction mechanism involves two sites and cannot be modelled via an additive method. An example would be a sintering process which is slowed by active site loss due to poisoning. Butt *et al.*, (1978) provides a review of interdependent mechanisms. Similarly, a two site basis can be used where both reversible and irreversible modes of deactivation prevail in one reaction mechanism (Eq. 2.41) (Schipper and Krambeck, 1986). An example would be a reversible coking mechanism coupled with longer term, irreversible sintering effects.

$$\Theta_1 = \frac{\text{current rate}}{\text{recoverable rate}} \quad (2.41)$$

$$\Theta_2 = \frac{\text{recoverable rate}}{\text{initial rate}}$$

Catalyst performance evolution mechanisms may be further complicated when product formation is a product of different reaction pathways (over different active sites). If the nature and/or number of these active sites changes at different rates (but in a similar order of magnitude), additive mechanisms may again be considered:

$$\frac{d\Theta}{dt} = \frac{d\Theta_1}{dt} + \frac{d\Theta_2}{dt} \quad (2.42)$$

Such an approach in Eq. (2.42) will require rigorous kinetic modelling of the reaction network of the catalyst system in question, at multiple stages in the life of the catalyst, to fully understand development of active sites in this case.

## 2.4 Conclusions

Gaining a fundamental understanding of catalyst performance evolution via transient methods is a challenging but rewarding process. In any catalyst study of this nature, a robust strategy is required which utilises appropriate catalyst testing, characterisation and modelling methods. The rate at which a catalyst changes in behaviour and the inherent reaction conditions at which the catalyst is operable are key factors in developing such strategies. Experimentally, good catalyst testing practise is essential and a range of transient testing methods are available. For physico-chemical catalyst characterisation, appropriate choice of *ex situ*, *in situ* or *operando* techniques is critical. The kinetic and activity modelling

approaches are dictated by how dynamic the catalyst system is; fast (second or min) scale performance changes are likely to require unsteady state modelling procedures whilst slower (hour, day or longer) evolutions may permit global activity-time approaches and multi-reaction conditions scans of kinetic behaviour and various times on stream.

## 2.5 References

Abon M., Bere K.E., Tuel A., Delichere P., (1995), '*Evolution of a VPO catalyst in n-butane oxidation reaction during the activation time*', J. Catal., 156, 28-36

Berger R.J., Stitt E.H., Marin G.B., Kapteijn F., Moulijn J.A., (2001), '*Chemical reaction kinetics in practice*' Eurokin, 5, 1, 30-60

Berger R.J., Kapteijn F., Moulijn J.A., Marin G.B., De Wilde J., Olea M., Chen D., Holmen A., Lietti L., Tronconi E., Schuurman Y., (2008), '*Dynamic methods for catalytic kinetics*', App. Cat. A: Gen., 342, 3-28

Berty J.M., (1983), '*Chapter 3 – Laboratory reactors for catalytic studies*', App. Ind. Cat, 1, 41-67

Bielanski A., Camra J., Najbar M., (1979) '*Segregation in vanadia-molybdena catalysts in the course of oxidation and reduction processes*', J. Catal., 57, 326-330

Birtill J.J., (2003) '*But will it last until shutdown? Deciphering catalyst decay!*', Catal. Today 81, 531-545

Birtill J.J., (2004a) '*Industrial catalyst decay. Part I: Review of test methods*', EUROKIN consortium internal document

Birtill J.J., (2004b) '*Industrial catalyst decay. Part II: Literature review, gaps and needs*', EUROKIN consortium internal document

Borgna A., Magni S., Sepulveda J., Apesteguia C., (2001) '*Selective acid-base poisoning on bifunctional alkylation reaction*', Stud. Surf. Sci. Catal., 139, 213-220

Dautzenberg F.M., (1989), '*Ten guidelines for catalyst testing*', ACS Symposium Series, No. 411, Characterisation and catalyst development, Bradley S.A., Galhuso M.J., Bertolacini R.J. (Eds.)

Butt J.B., Wachter C.K., Billimoria R.M., (1978) '*On the separability of catalyst deactivation kinetics*', Chem. Eng. Sci., 13, 1321-1329

Carberry J.J., in: Anderson J.R., Boudart M., (eds), (1987) '*Catalysis: Science and Technology, Vol. 8*' Springer, Berlin, p. 131

Chen D., Grønvold A., Rebo H.P., Moljord K., Holmen A., (1996), '*Catalyst deactivation studied by conventional and oscillating microbalance reactors*', App Cat A: Gen, 137, L1-L8

Chinchen G.C., Hay C.M., Vandervell H.M., Waugh K.C., (1987a), '*The measurement of copper surface areas by reactive frontal chromatography*', J. Catal., 103, 79-86

Chinchen G.C., Denny P.J., Parker D.G., Spencer M.S., Whan D.A., (1987b), '*Mechanism of methanol synthesis from CO<sub>2</sub>/CO/H<sub>2</sub> mixtures over copper/zinc oxide/alumina catalysts: Use of <sup>14</sup>C labelled reactants*', App. Cat., 30, 333-338

Christensen T.S., (1996) '*Adiabatic pre-reforming of hydrocarbons – An important step in syngas production*', App. Cat. A:Gen, 138 (2), 285-309

Chu C.F. and Ng K.M., (1989), '*Flow in packed tubes with a small tube to particle diameter ratio*' AIChE Jnl., 35, 148

Corella J., Adanez J., Monzon A., (1988) '*Some intrinsic kinetic equations and deactivation mechanisms leading to deactivation curves with a residual activity*', Ind. Eng. Chem. Res., 27, 375-381

Corella J., Monzon A., (1988) '*Modelling of the deactivation kinetics of solid catalysts by two or more simultaneous and different causes*', Ind. Eng. Chem. Res., 27, 369-374

Corma A., Llopis F., Monto J.B., Weller S.W., (1988), '*Comparison of models in heterogeneous catalysis for ideal and non-ideal surfaces*', Chem. Eng. Sci., 43, 4, 785-792

Ergun S., (1952) '*Fluid flow through packed columns*' Chem. Eng. Prog., 49, 89-94

Flynn P.C., Wanke S.E., (1975) '*A model for supported metal catalyst sintering I. Development of model II. Application of model*', J. Catal., 34, 390-410

Forzatti P., Buzzi-Ferraris G., (1982) '*Reaction-deactivation kinetics of methanol oxidation over a silica-supported Fe<sub>2</sub>O<sub>3</sub>-MoO<sub>3</sub> catalyst*', Ind. Eng. Chem. Process. Des. Dev., 21, 67-73

Froment G.F., Bischoff K.B., (1961), '*Non steady-state behaviour fixed bed catalytic reactors due to catalyst fouling*', Chem. Eng. Sci., 16, 189-201

Froment G.F., De Meyer G., Derouane E.G., (1990), '*Deactivation of zeolite catalysts by coke formation*', J. Catal., 124, 391-400

Fuentes G.A., (1985) '*Catalyst deactivation and steady-state activity: A generalised power-law equation model*', App. Cat., 15, 33-40

Gai P.L., Boyes E.D., (2009), '*Advances in atomic resolution in situ environmental transmission electron microscopy and 1Å aberration corrected in situ electron microscopy*', Micro. Res. and Tech., 72, 153-164

Kagan Y.B., Rozovskii A.Y., Liberov L.G., Slivinskii E.V., Lin G.I., Loktev S.M., Bashkirov A.N., (1975), Dokl. Akad. Nauk. SSSR, 224, 1081

Kapteijn F., Moulijn J.A., in: Ertl G., Knözinger H., Weitkamp J., (eds), (1996), '*Handbook of heterogeneous catalysis, Vol. 3*' VCH, Weinheim, p. 1359

Kobayashi M., Kobayashi H., (1972), '*Application of transient response method to the study of heterogeneous catalysis: I. Nature of catalytically active oxygen on manganese dioxide for the oxidation of carbon monoxide at low temperatures*', J. Catal., 27, 100-107

Lietti L, Nova I, Camurri S., Tronconi E., Forzatti P., (1997), '*Dynamics of the SCR-DeNO<sub>x</sub> reaction by the transient response method*', AIChE Jnl., 43, 10, 2259

Madia G., Elsener M., Koebel M., Raimondi F., Wokaun A., (2002), '*Thermal stability of vanadia-tungsta-titania catalysts in the SCR process*', App. Cat. B: Env, 39, 181-190

Mears D.E., (1971) '*The role of axial dispersion in trickle-flow laboratory reactors*' Chem. Eng. Sci. 26, 1361

Meunier F.C., Goguet A., Hardacre C., Burch R., Thomsett D., (2007), '*Quantitative DRIFTS investigation of possible reaction mechanisms for the water-gas shift reaction on high-activity Pt- and Au-based catalysts*', J. Catal., 252, 18-22

- Moulijn J.A., Perez-Ramirez J., Berger R.J., Hamminga G., Mul G., Kapteijn F., (2003), *'High-throughput experimentation in catalyst testing and in kinetic studies for heterogeneous catalysis'*, Catal. Today, 81, 457-471
- Perez-Ramirez J., Berger R.J., Mul G., Kapteijn F., Moulijn J.A., (2000), *'The six-flow reactor technology: A review on fast catalyst screening and kinetic studies'* Catal. Today, 60, 93-109
- Quet C., Tellier J., Voirin R., (1980) *'Poisoning of Claus catalyst by sulphation; from Catalyst Deactivation'*, Elsevier, 323-329
- Quiney A.S., Schuurman Y., (2007), *'Kinetic modelling of CO conversion over Cu/Ceria catalyst'*, Chem. Eng. Sci., 62, 5026-5032
- Reiff, E.K. Jr., Kittrell J.R., (1980), *'Use of active site balances for catalyst deactivation models'*, Ind. & Eng. Chem. Fundamentals, 19, 1, 126-128
- Schipper P.H., Krambeck P.J., (1986) *'A reactor design simulation with reversible and irreversible catalyst deactivation'*, Chem. Eng. Sci., 41, 4, 1013-1019
- Temkin M.I., (1976), *'The kinetics of steady-state complex reactions'*, Kinet. Katal., 17, 1095
- Wang D., Kung H.H., Barteau M.A., (2000), *'Identification of vanadium species involved in sequential redox operation of VPO catalysts'*, App. Cat. A: Gen., 201, 203-213
- Weisz P.B., (1957), Z. Phys. Chem. (Frankfurt Am Main), 11, 1
- Weller S.W., (1992), *'Kinetics of heterogeneous catalysed reactions'*, Catal. Rev. Sci. Eng., 34, 3, 227-280
- Wiebanga M.H., Kim C.H., Schmiege S.J., Oh S.H., Brown D.B., Kim D.H., Lee J.-H., Peden C.H.F., (2012), *'Deactivation mechanisms of Pt/Pd-based diesel oxidation catalysts'*, Catal. Today, 184, 197-204
- Wojciechowski B.W., (1968) *'A theoretical treatment of catalyst decay'*, Canadian J. Chem. Eng., 46, 48-52
- Wolf E.E., Petersen E.E., (1977) *'On the kinetics of self-poisoning catalytic reactions'*, J. Catal., 47, 28-32

## **Chapter 3:**

### **A kinetic analysis methodology to elucidate solvent effects in catalytic liquid-phase reactions**

*Solvents are an indispensable presence in many catalytic liquid-phase reactions. The choice of solvent should not be arbitrary and is one which can be highly beneficial or detrimental to both activity and selectivity of catalytic reactions. A kinetic analysis methodology, which utilises a statistical analysis procedure to eliminate non-influential parameters from proposed models, is applied to 4-phenyl-2-butanone hydrogenation data. Choice of solvent strongly influences selectivity towards aromatic ring or ketone group hydrogenation of this species. The final kinetic model incorporates a dominant adsorption term for the selective product species which shows a strong correlation with selectivity of that particular product.*

### 3. Introduction: ‘Solvation, Adsorption and Selectivity’

Solvents are an indispensable presence in many catalytic liquid-phase reactions. The choice of solvent should not be arbitrary and is one which can be highly beneficial or detrimental to both activity and selectivity of catalytic reactions. Such a fact is well known, with observations of solvent effects originating in works such as those by Menshutkin, who in 1890 stated: ‘By means of a proper choice of solvent, decisive acceleration or deceleration of a chemical reaction can be achieved’ (Menshutkin, 1890).

Consequently, solvent effects have become very well documented in organic synthesis literature (Carey and Sundberg, 1990) and, in the past 50 years have been reported in heterogeneous catalysis (Singh and Vannice, 2001). Properties of the solvent such as relative permittivity and polarity play a role in gas solubility (such as hydrogen), solvation of reactants and products as well as other mass transfer effects (Akpa *et al.*, 2012). As well as influencing reactant and product behaviour, the solvent may also interact with the metal and/or support of the catalyst. A classic example of this is shown in the work by Boudart and co-workers (Madon *et al.*, 1978; Gonzo and Boudart, 1978; Boudart and Cheng, 1987) which explored the liquid phase hydrogenation of cyclohexene using a variety of silica (SiO<sub>2</sub>) supported catalysts with a range of solvents. To illustrate, the turn-over frequency (TOF) for Pd/SiO<sub>2</sub> was found to be solvent insensitive whilst in contrast, when using a Ni/SiO<sub>2</sub> catalyst, the use of polar or oxygenated solvents resulted in a marked decrease in TOF and a strong adsorption of the solvent itself on the nickel metal.

Ultimately, the numerous effects that can arise between solvent, catalyst and substrate result in catalytic reaction systems whose behaviour can be very difficult to predict. This presents a particular challenge to industry where the following problems can be manifested as a result of these difficulties:

- High E-factors (kg by-products/kg products), in particular in the pharmaceutical industry.
- ‘Scale-up confidence’ – prediction of plant scale reactor performance.
- Catalyst, feedstock and solvent choice constraints due to economic feasibility and environmental restrictions.

To understand and predict solvent effects, methodologies are needed that probe reaction behaviour from a fundamental physical and chemical standpoint but are also pragmatic in nature so that a broad spectrum of application is possible.

### 3.1 Kinetic modelling of solvent effects in literature

When modelling kinetics to describe solvent effects in catalytic liquid phase hydrogenations, it is essential that proposed models have a fundamental mechanistic basis and include estimated parameters that are physically meaningful in value and are statistically significant to justify their presence. Table 3.1 provides a summary of rate models that have previously been used in the literature for this area of study.

**Table 3.1: Rate model approaches previously employed to model kinetics of solvent effects within liquid phase hydrogenations in literature.**

References	Rate Model	Mechanistic Basis
<ul style="list-style-type: none"> <li>Bertero <i>et al.</i></li> <li>Mathew <i>et al.</i></li> </ul>	$r = \frac{k_b \cdot K_a \cdot [R]}{(1 + K_a \cdot [R] + \sum K_d [I])^n}$	<ul style="list-style-type: none"> <li>LH approach with competitive adsorption of organics.</li> <li>Surface reaction r.d.s.</li> </ul>
<ul style="list-style-type: none"> <li>Mounzer <i>et al.</i></li> </ul>	$r = \frac{k_b \cdot K_a \cdot [R]}{\left(1 + K_a \cdot [R] + \frac{[P]}{K_c}\right)^n}$	<ul style="list-style-type: none"> <li>LH approach with product desorption term.</li> <li>Surface reaction r.d.s.</li> </ul>
<ul style="list-style-type: none"> <li>Gamez <i>et al.</i></li> </ul>	$r = \frac{K_{a,b,c} \cdot [R]}{(1 + K_{a,c} [R])}$	<ul style="list-style-type: none"> <li>Michaelis-Menten approach.</li> </ul>
<ul style="list-style-type: none"> <li>Kishida and Teranishi</li> <li>Lemcoff</li> <li>Mukherjee and Vannice</li> </ul>	$r = \frac{k_b \cdot K_a \cdot [R]}{(1 + K_a \cdot [R] + K_{solv} [S])^n}$	<ul style="list-style-type: none"> <li>LH approach with a competitive solvent adsorption term.</li> <li>Assumes solvent interacts with catalyst surface.</li> <li>Surface reaction r.d.s.</li> </ul>

Symbols denote:

- $r$ : rate of reaction ( $\text{mol L}^{-1} \text{min}^{-1}$ ),  $k$ : rate constant:  $\text{min}^{-1}$  (1<sup>st</sup> order),  $K$ : equilibrium constant ( $\text{L mol}^{-1}$ )
- $[ ]$ : concentration ( $\text{mol L}^{-1}$ ),  $R$ ,  $P$ ,  $I$  and  $S$ : reactant, product, inhibiting species and solvent respectively
- Subscripts  $a$ ,  $b$ ,  $c$ ,  $d$  and  $s$ : reactant adsorption, surface reaction, product desorption, inhibition and solvent adsorption steps respectively.
- Superscript,  $n$  denotes order of reaction.

Bertero *et al.*, (2008) considered a wide range of Langmuir-Hinshelwood (LH) expressions to describe the hydrogenation of acetophenone. Quality of fit ( $R^2$ ) for all models in this work was very high (0.999) suggesting at least some were parametrically over-determined. Optimal model choice was therefore based on the physical meaning of measured parameters (such as discounting models with negative adsorption constants) and using a model selection criteria based on a comparison of residuals and degrees of freedom in each final model. Mathew *et al.*, (1999) utilised a similar approach and also checked adsorption parameters for thermodynamic consistency. This is achieved by equating the pre-exponential term in the adsorption constant to  $e^{\Delta S_{ads}/R}$ .  $(-\Delta S_{ads})$  must remain positive and not exceed the entropy of the gas,  $S^0$  at a given temperature and pressure.

Mounzer *et al.*, (2010) modelled the kinetics of 2-octanol oxidation performed using a variety of heptane/dioxane mixtures. A LH approach including a product ketone desorption parameter, which was experimentally measured, provided the best description. This model was found to be statistically significant via both the *F*- and *T*-test and showed an excellent correlation between solvent compositions, oxidation rate and the ketone desorption parameter.

Other approaches include the use of Michaelis-Menten-type expressions (Gamez *et al.*, 1998). This method was shown to be pragmatic in describing solvent effects in ethyl pyruvate hydrogenation by discriminating a lumped reaction term from one relating to adsorption. The limited number of parameters in this model compromises quality of fit and may be difficult to implement in multi-response systems.

A number of works have attempted to include a competitive solvent adsorption term,  $K_{Solv}$ , in their models. Early works focused on acetone hydrogenation; Kishida and Teranishi, (1968) developed a model using an *n*-hexane solvent and subsequently fixed rate constants to measure  $K_{Solv}$  for other solvents. The assumption that the solvent does not influence rate constants was not justified in the work; neither was the effect of hydrogen solubility considered. Lemcoff, (1977) did not make this assumption and developed models with thermodynamically sound adsorption parameters for a mixture of polar and apolar solvents. Recently, Mukherjee and Vannice, (2006a) demonstrated a similar approach for citral hydrogenation. Their model was developed around citral conversion and validated against prediction of product formation. In this work, the assumption that the solvent competes for an active site is based around the fact that other possible solvent effects. These are namely mass transport limitation, liquid phase H<sub>2</sub> solubility and liquid-phase non-ideality were found

to be insignificant in terms of influencing the large changes in rate behaviour observed between different solvents. In all cases, the lack of experimental validation for  $K_S$  and the fact that solvent concentrations were not varied during testing calls into question the physical meaning of this estimated parameter.

A key element which is missing from these studies is a detailed statistical analysis which can ascertain the significance of parameters and the models themselves. This will take model critique beyond  $R^2$  and the removal of parameters due to lower or upper bound constraints. A possible approach is afforded by Quiney and Schuurman, (2007). This work describes the modelling of the kinetics of the water gas shift reaction under continuous flow and used a methodology which examined parameter sensitivities, parameter cross correlation and influence of parameter removal on  $R^2$  values via use of the F-test.

### **3.1.1 Complementary approaches for elucidating solvent effects**

Other experimental and modelling techniques exist to elucidate solvent effects and are complementary to the findings of kinetic studies. Density functional theory (DFT) calculations, chiefly via the work of Neurock and co-workers (Akpa *et al.*, 2012; Sinha and Neurock, 2012) have been shown to be effective in simulating solvent effects in heterogeneous catalysis. In these examples, molecular simulation of the hydrogenation of  $C_1$  to  $C_4$  aldehydes and ketones over a Ru(0 0 0 1) surface was used to understand key energy barriers to the reaction. DFT was used to study 2-butanone hydrogenation in the presence of water and isopropanol (2-PrOH) solvent mixtures to understand the complex variance in rate behaviour observed experimentally.

Gas-liquid mass transport effects in liquid phase hydrogenations are also important in determining reaction rate and selectivity, particularly in larger scale reaction vessels. Choice of solvent can further influence this effect and has been demonstrated (Hu *et al.*, 2007). Bubble sizes were measured in a stirred tank vessel using a video-microscope-computer system. Reaction rate and hydrogen solubility-bubble size ratio were found to be strongly correlated across a range of 2-PrOH and water solvent mixtures for 2-butyne-1,4-diol hydrogenation.

### 3.1.2 Study of 4-phenyl-2-butanone hydrogenation over a Pt/TiO<sub>2</sub> catalyst

The hydrogenation of 4-phenyl-2-butanone (PBN) has two distinctive routes to produce the fully hydrogenated product, 4-cyclohexyl-2-butanol (CBL). Intermediate compounds are 4-phenyl-2-butanol (PBL), produced by hydrogenation of the carbonyl C=O group and 4-cyclohexyl-2-butanone (CBN) by hydrogenation of the aromatic ring. The reaction scheme is shown in Figure 3.1 and features two reaction types, namely ketone (blue arrow) or aromatic ring (red arrow) hydrogenation.

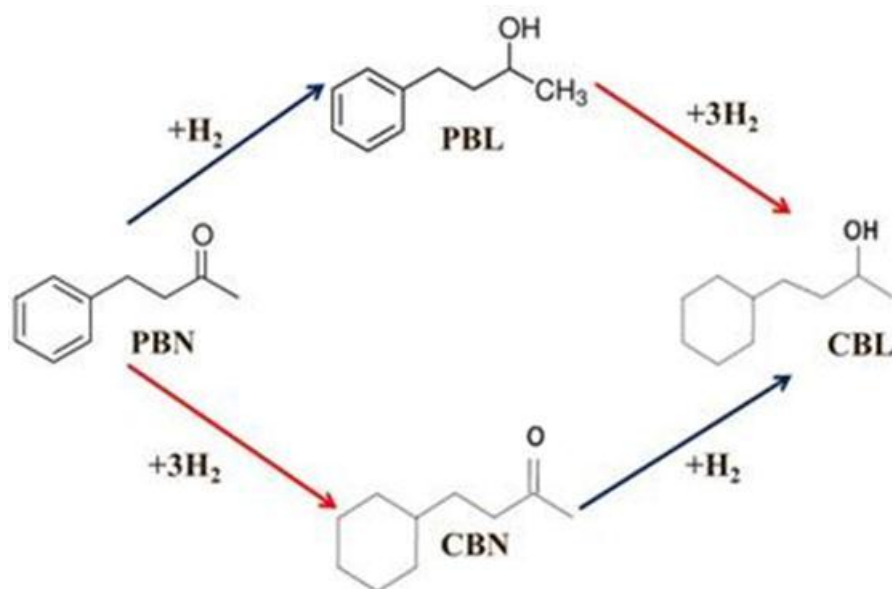


**Figure 3.1: Reaction network for 4-phenyl-2-butanone (PBN) hydrogenation.**

The above reaction system was chosen as the selectivity of the two routes taken from the original PBN reactant can be influenced by choice of solvent. Hence, this reaction system is a good choice for methodology development. At the time of writing no kinetic studies exist in literature for PBN hydrogenation; however the literature reviewed in section 3.1 has shown that aromatic ring and C=O bond hydrogenations are well studied reactions.

### 3.1.3 Chapter Objectives

In this chapter, the PBN hydrogenation system will be used to satisfy three key aims:

- Develop a methodology to critically examine the significance of estimated parameters in mechanistically based kinetic models.

- Use the methodology to reduce the number of parameters in model descriptions to a level that does not compromise their statistical and fundamental integrity.
- Apply the best model description(s) to PBN hydrogenation data using a range of solvents to examine the relationship between model adsorption constants and observed reaction pathway selectivity.

## 3.2 Materials and methods

### 3.2.1 Experimental: Autoclave reaction studies

Kinetic data for this study were obtained using a 100 mL autoclave with dead end operation (see Figure 3.2) and were supplied by Queen's University Belfast<sup>4</sup>. The catalyst used was 4% Pt/TiO<sub>2</sub>. Prior to reaction testing the catalyst was reduced in 1 bar H<sub>2</sub> at 333 K for 1 h.

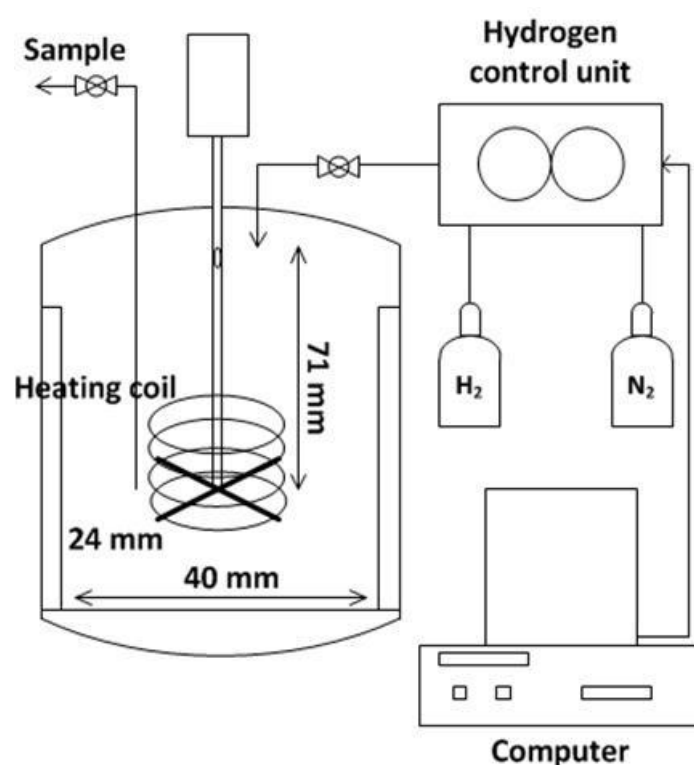


**Figure 3.2: Schematic for reaction testing equipment in this study<sup>5</sup>**

<sup>4</sup> Data supplied by Daly H., Thompson J.M., McManus I., Hardacre C. (CenTACat, Queen's University Belfast) and Sedaie Bonab N. (Department of Chemical Engineering, University of Birmingham), August 2012

<sup>5</sup> Schematic supplied from correspondence with Sedaie Bonab N., December 2012

In all experiments, a slurry comprising 0.1 g catalyst (particle size 5  $\mu\text{m}$ , mean pore size 25  $\text{\AA}$ ) and 50 mL combined solvent and reactant was used. The starting reactant in all cases was PBN in the concentration range of 0.13 – 0.39 mol L<sup>-1</sup>. H<sub>2</sub> pressure and impeller speed,  $N$ , were kept constant at 5 bar and 1400 rpm respectively for all tests. This was chosen based on experiments shown in Figure 3.13 (Section 3.7.1), which explored the effect of stirrer speed on liquid-gas mass transport. All reaction tests were found to be performed in a kinetic rather than mass transfer controlled regime. Relevant experiments<sup>6</sup> are shown in section 3.7.1 (appendix). All experimental runs lasted for 120 min with 2 cm<sup>3</sup> liquid samples taken at 10, 20, 30, 60 and 120, min respectively. The samples were passed through a syringe filter to remove the catalyst before being diluted with solvent in a 1:10 ratio. The samples were analysed using a Perkin-Elmer Clarus 500 gas chromatograph equipped with a FID with an Agilent HP-5 column.

Four different solvents were tested whose properties are documented in Table 3.2. The wide difference in characteristics between protic and aprotic polar solvents may assist in rationalising differences observed in reaction selectivity, rate constants and dominant adsorption constants estimated from the kinetic modelling process described in section 3.4.

**Table 3.2: Properties of solvents used in this study.  $\epsilon_{\text{di}}$  denotes relative permittivity,  $\mu$  denotes dipole moment,  $\alpha_1$  denotes hydrogen bond donor parameter,  $\alpha_2$  denotes hydrogen bond acceptor parameter,  $k_{\text{H}}$  denotes Henry's Constant**

Solvent	Type	$\epsilon_r$ <sup>a</sup>	$\mu$ (Debye) <sup>a</sup>	$\alpha_1$ <sup>a</sup>	$\alpha_2$ <sup>a</sup>	$k_{\text{H}}$ for H <sub>2</sub> at 5 bar <sup>b</sup>
<b>Hexane (HEX)</b>	Aprotic apolar	2.02	0.08	0	0	1391 (303K) 1262 (323K) 1133 (343K)
<b>t-butyl toluene (TBT)</b>	Aprotic apolar	2.38	0.37	0	0.11	1374 (343K)
<b>1-propanol (1-PrOH)</b>	Protic	20.1	1.68	0.84	0.9	2415 (343K)
<b>2-propanol (2-PrOH)</b>	Protic	19.9	1.66	0.76	0.84	1486 (343K)

<sup>a</sup> Values taken from Bertero *et al.*, 2011.

<sup>b</sup> Values calculated using data from Bertero *et al.*, 2011; Katayama and Nitta, 1978; Chang *et al.*, 1991; Tsuji *et al.*, 2005.

Table 3.3 summarises the three stage approach of the experimental programme to provide sufficient experimental data to build a mechanistically sound kinetic model that will

<sup>6</sup> Sedaie Bonab N., Ph. D. thesis, The University of Birmingham, UK, currently in writing

link selectivity and adsorption constants to choice of solvent. Series A, utilising multi-temperature data will be utilised for refinement of candidate models. This will both remove insignificant parameters from rate expressions and identify stronger models from the initial candidates. Series B will test the best model(s) further by probing their suitability over a range of starting concentrations. This will further discriminate remaining models and potentially shed additional fundamental understanding of reaction mechanism. The most suitable model(s) will finally be tested against experiments using a range of solvents (Series C) with the aim of demonstrating the link between solvation, selectivity and the dominant adsorption constant.

**Table 3.3: Experimental series undertaken for this study**

<b>Series</b>	<b>Variables</b>	<b>Constants</b>
<b>A</b>	Effect of temperature - 303 – 353 K (6 points)	- hexane solvent - 0.26 mol L <sup>-1</sup> starting PBN concentration
<b>B</b>	Effect of PBN concentration - 0.13 – 0.39 mol L <sup>-1</sup> (5 points)	- hexane solvent - 343 K operation
<b>C</b>	Effect of solvent - hexane - t-butyl toluene - 1-propanol - 2-propanol	- 0.26 mol L <sup>-1</sup> starting PBN concentration - 343 K operation

### 3.2.2 Kinetic modelling procedure

Parameter estimation within the kinetic models was carried out using Athena Visual Studio<sup>®</sup> software<sup>7</sup>. The kinetic models tested within this work contain multiple parameters including some which are non-linear (e.g. activation energies in the Arrhenius equation). The Levenberg-Marquardt procedure, an indirect method for constrained optimisation of parameters, is appropriate for this problem (Marquardt, 1963). All response variables in the PBN hydrogenation reaction network are dependent on multiple reactions (see Figure 3.1) and so the models must be solved implicitly using a set of differential equations:

<sup>7</sup> Athena Visual Studio 14.2, Stewart & Associates Engineering Software, Inc.

$$\frac{dy}{dt} = f(y, \beta) \quad (3.1)$$

In Eq. (3.1),  $y$  denotes model responses,  $t$  denotes time and  $\beta$  denotes the model parameters. A direct decoupled method is used to estimate parametric sensitivities (Caracotsios and Stewart, 1985):

$$B(t) = \frac{\partial y(t)}{\partial \beta} \quad (3.2a)$$

$$\frac{\partial}{\partial \beta} \left( \frac{dy}{dt} \right) = \frac{d}{dt} B(t) = \frac{df}{dy} \cdot B(t) + \frac{df}{d\beta} \quad (3.2b)$$

In Eq. (3.2a),  $B(t)$  defines the sensitivity function for each model response with respect to each model parameter. In Eq. (3.2b) it can be seen that defining sensitivities as a function of time allows them to be solved alongside the main system differential equations, improving solver efficiency and performance.

To minimise cross-correlation between activation energy ( $E_a$ ) and pre-exponential factor ( $A_i$ ) parameters, a re-parameterised Arrhenius equation was used:

$$k_i = A_{i,373} \cdot \exp \left( \left( \frac{E_a}{T_{base} \cdot R} \right) \cdot \left( 1 - \frac{T_{base}}{T} \right) \right) \quad (3.3a)$$

Where base temperature,  $T_{base} = 373$  K and  $A_{i,373}$  is the value of the rate constant  $k_i$  at 373 K. The fitting process can be further improved by solving  $A_{i,373}$  as an exponential term and lumping fitted value,  $E_a$  with constants  $T_{base}$  and ideal gas constant,  $R$  ( $\text{J K}^{-1} \text{mol}^{-1}$ ) to give fitting parameter  $E_{a,lump}$ . This typically brings the values of  $A_{i,373}$  and  $E_{a,lump}$  into the same order of magnitude (typically 1 – 10) further reducing cross-correlation in this expression:

$$k_i = \exp \left( A_{i,373} + \left( E_{a,lump} \cdot \left( 1 - \frac{T_{base}}{T} \right) \right) \right) \quad (3.3b)$$

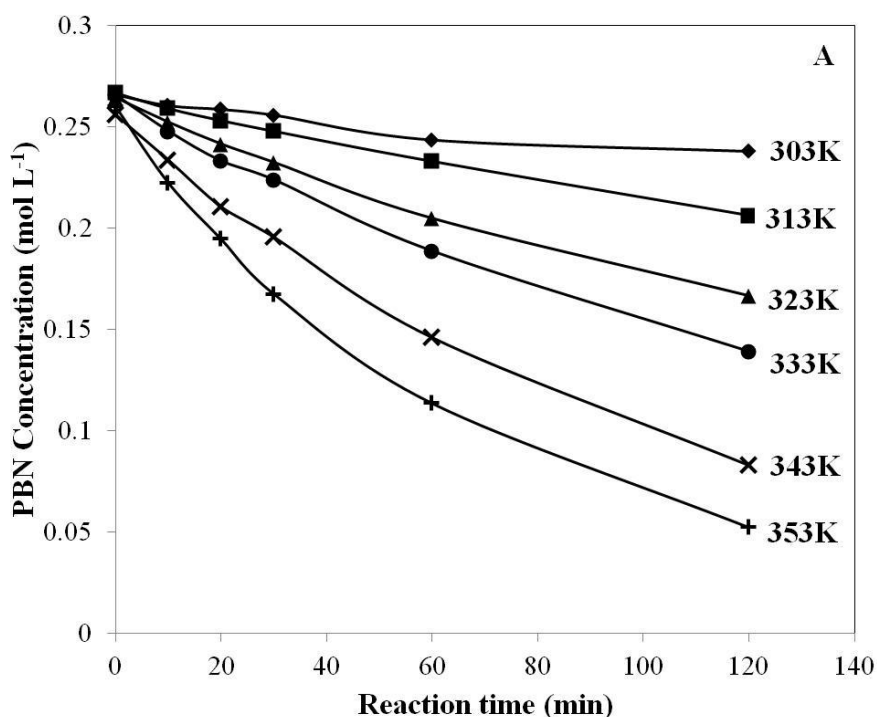
### 3.3 Results

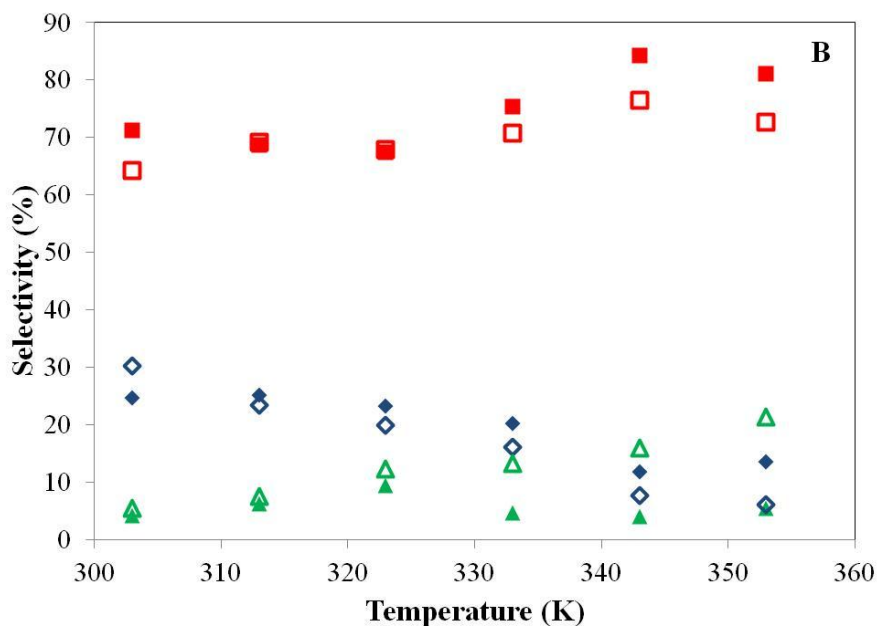
#### 3.3.1 Effect of temperature

Figure 3.3A shows the evolution of 4-phenyl-2-butanone concentration with time in a hexane solvent. PBN consumption increases with temperature; 10% conversion over 120 min is seen at 303 K through to 80% at 353 K.

In Figure 3.3B, selectivity is highest to the product CBN at all temperatures, formed via hydrogenation of the aromatic ring in PBN. This selectivity increases somewhat with temperature. Selectivity towards PBL (via ketone group hydrogenation) is considerably lower and declines with temperature. These temperature dependency observations suggest that the activation energy for aromatic ring hydrogenation is higher than that for ketone group hydrogenation, which agrees with the literature (Bergault *et al.*, 1997).

Selectivity to the fully hydrogenated product, CBL, increases with both time and temperature. In Figure 3.3B, after 120 min, CBL selectivity appears to increase with temperature at the expense of PBL selectivity.  $\text{PBL} \rightarrow \text{CBL}$  is an aromatic ring hydrogenation route, again demonstrating the prevalence of this reaction in a hexane solvent.





**Figure 3.3: A) Evolution of PBN concentration with reaction time at different reaction temperatures in hexane solvent. B) Selectivity of products at different temperatures at 10 min (closed symbols) and 120 min (open symbols) reaction time. Symbols denote: (◆,◇) PBL, (■,□) CBN, (▲,△) CBL. Each test result shown was only conducted once.**

A first approximation of the kinetics of PBN hydrogenation to products can be made using Eq. (3.4) (below). Whilst this does not consider product selectivity or further product hydrogenation it is a pragmatic way of gauging the complexity of the system kinetics:

$$r_{PBN \rightarrow products} = \frac{dC_{PBN}}{dt} = \frac{[PBN]_{t(m+1)} - [PBN]_{t(m)}}{t_{m+1} - t_m} = k[PBN]_{t(n)}^{n_{app}} \quad (3.4)$$

Where  $t_{m+1}$  is the time of concentration measurement,  $t_m$  is the time of the previous concentration measurement and  $n_{app}$  is an apparent reaction order. Plotting a linear trend line through graphs of  $\ln(r_{PBN \rightarrow products})$  against  $\ln([PBN]_{t(n)})$  reveals  $n_{app}$  (line gradient) and can be ascertained for each reaction temperature.

In Table 3.4,  $n_{app}$  decreases with increasing reaction temperature. This immediately shows the kinetics of the reaction system is non-trivial. Evolution of  $n_{app}$  with temperature in a simple power law expression is a simple indicator that species adsorption will be required in the kinetic model rate expressions. Species adsorption is exothermic and its strength decreases with temperature which lowers  $n_{app}$  in a power law expression. A further argument may be that hydrogenation of intermediates PBL and CBN may influence  $n_{app}$  in this

expression via active site competition. Whilst this cannot be ignored it is unlikely to be the sole influence on the high values of  $n_{app}$  at lower temperatures where intermediate product formation is much lower.

**Table 3.4: Apparent reaction order dependency on PBN at different temperatures using a simple linear fit**

Reaction Temperature (K)	$n_{app}$ (-)	$R^2$
303	17.1	0.66
313	3.8	0.85
323	2.5	0.97
333	2.2	0.77
343	1.4	0.90
353	1.6	0.98

### 3.3.2 Effect of 4-phenyl-2-butanone concentration

Figure 3.4a shows the amount of PBN hydrogenated against time with five different starting concentrations. The profiles are very similar for all starting concentrations up to 60 min reaction time. This similarity is further shown in Figure 3.4b whereby all initial PBN hydrogenation rates as well as PBL and CBN formation rates appear to be invariant with starting PBN concentration. This effect has been previously seen for acetophenone hydrogenation (Bergault *et al.*, 1997). It is noted that differences in the concentration profiles are evident after 120 min reaction time. This is chiefly for the experiments with 0.13 and 0.19 mol L<sup>-1</sup> PBN whereby the substrate is nearing complete conversion at this stage.

A zero order dependence of PBN concentration on reaction rate is unlikely as the individual concentration profiles over the reaction time show an apparent order that is always greater than 1. The observations in Figure 3.4b are consistent with a reaction mechanism that is rate determined, or at least strongly influenced, by product desorption.

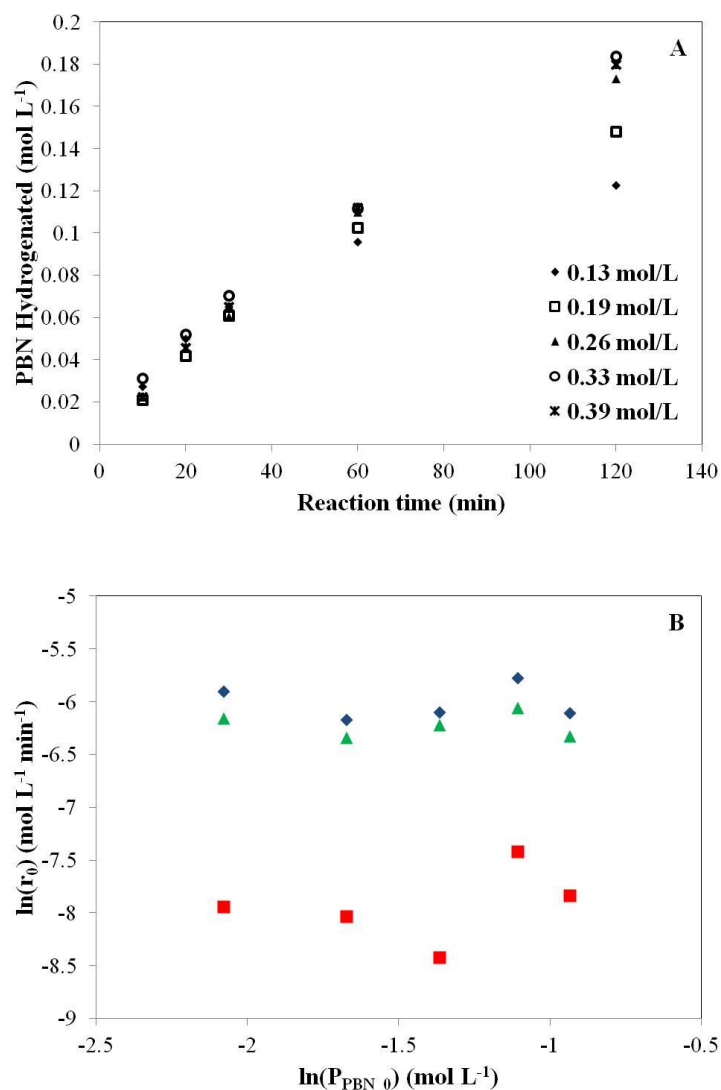


**Figure 3.4: A) Evolution of PBN hydrogenated with reaction time using different starting concentrations of PBN at 343 K. B) Variation in initial rate behaviour against starting concentration of PBN; (♦) PBN conversion, (■) PBL formation, (▲) CBN formation.**

### 3.3.3 Effect of solvent choice

Figure 3.5 shows the reaction time concentration profiles for four different solvents. These four solvents were chosen so that different categories of solvent can be compared, namely alkane (HEX), aromatic (TBT), primary alcohol (1-PrOH) and secondary alcohol (2-PrOH).

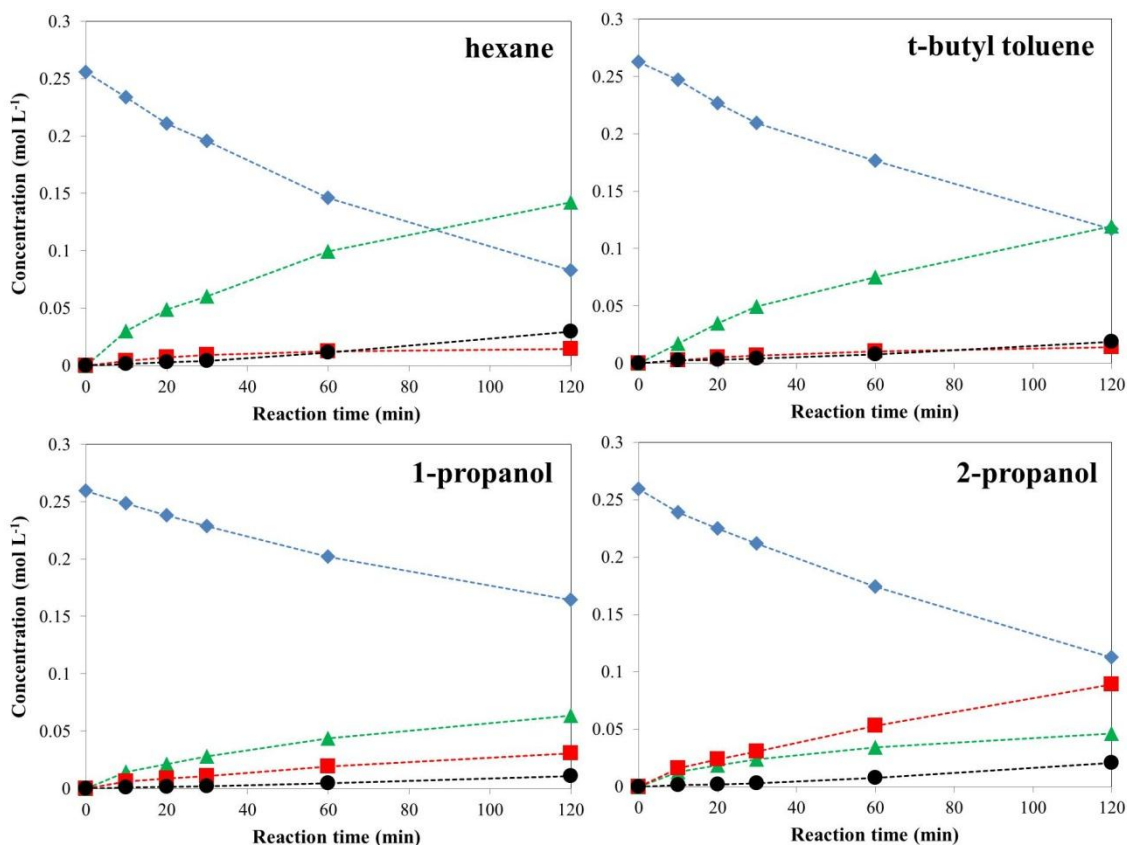


**Figure 3.5: Reaction time concentration profiles for different solvents at 343 K. Symbols denote: (♦) PBN, (■) PBL, (▲) CBN, (●) CBL. N.B.: Lines are to guide the eye**

Some marked differences are seen, in particular between the aprotic apolar (HEX, TBT) and the protic solvents (1-PrOH, 2-PrOH). The former both show significant selectivity towards CBN (aromatics hydrogenation) across the entire reaction time. The protic solvents behave somewhat differently. 2-PrOH is ultimately more selective to PBL (ketone hydrogenation) after 120 minutes although both PBN hydrogenation pathways have comparable selectivity over the first 30 minutes of reaction. 1-PrOH is more selective towards CBN than PBL although this is less marked than with the aprotic apolar solvents.

The extent of PBN converted over 120 minutes is of the order  $\text{HEX} > \text{TBT}, 2\text{-PrOH} > 1\text{PrOH}$ . Figure 3.6 shows conversion follows an inverse relationship with  $k_H$  for  $\text{H}_2$  solubility with each solvent. This suggests that a greater availability of hydrogen in the liquid phase results in an increased overall hydrogenation activity of the catalyst. This correlation does not hold for hydrogenation route selectivity however, suggesting other solvent effects may be prevalent.

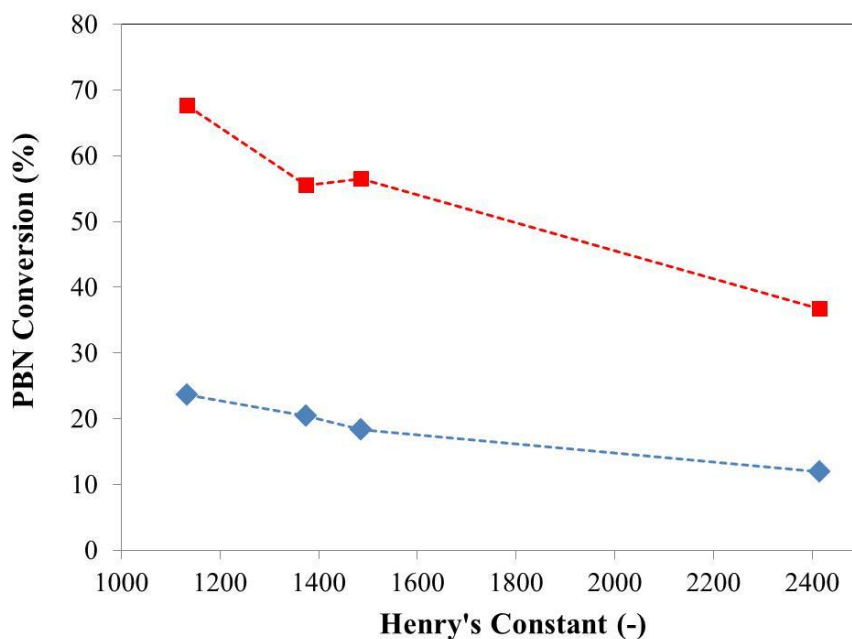


**Figure 3.6: PBN Conversion plotted against Henry's Constant for H<sub>2</sub> solubility in each solvent experiment after (♦) 30 min and (■) 120 min. Solvent Henry's Constants follow the order HEX < TBT < 2-PrOH < 1-PrOH N.B.: Lines are to guide the eye.**

### 3.4 Kinetic Modelling

The following sequence of elementary steps was used as a basis for the kinetic models in this study:



Where \* denotes active site. *R*, *P* and *I* denote reactant, product and inhibitor compounds respectively. In conjunction with this, the following are noted:

- For initial model descriptions, it is assumed that all organic reactants and products (PBN, PBL, CBN and CBL) competitively adsorb on one active site. The possibility of two or more sites is not discounted however and can be elucidated as part of the model refinement process in section 3.4.1.
- H<sub>2</sub> partial pressure is not varied during the study although Table 3.2 shows that H<sub>2</sub> solubility varies with solvent choice and temperature. Both dissociative and associative hydrogen adsorption were originally considered in the refinement of models at different temperatures in a hexane solvent. This term was always found to be indeterminate during the parameter estimation process and is not shown in the model refinement process. This does not discount the importance of hydrogen but instead acknowledges that this parameter could be explored in a wider experimental programme, particularly in light of the correlation in Figure 3.6.
- H<sub>2</sub> itself could compete for active site \* or could be associated with a different active site. Both possibilities are discussed when refined models are tested against variable initial PBN concentration data.
- Adsorption terms were originally estimated in models using a Van't Hoff-type expression however fitted adsorption energies ( $\Delta H_{\text{ads}}$ ) were always found to be insignificant in terms of statistical contribution and are not shown in the model refinement process; leaving a constant  $K$ .

Based on the elementary steps described in Eq. (3.5a-d), four candidate models were derived which may be suitable for the PBN hydrogenation system (see Table 3.5). These models have been chosen for examination on the basis of previous use in the solvent effects hydrogenation literature: Eq. (3.6a-d), but also due to initial observations of experimental data suggesting product desorption effects are significant: Eq. (3.6b,d).

It is noted that Eq. (3.6a) and (3.6d) are the same in mathematical appearance. Due to this, both equations will undergo model refinement at the same time. The magnitude of the estimated parameters in the final model and comparison with literature studies will provide direction as to whether the model is limited by surface reaction or product desorption.

**Table 3.5: Candidate rate models for describing reactions in the PBN hydrogenation network**

Equation No.	Rate Model	Basis
(3.6a)	$r = \frac{k_b \cdot K_a \cdot [R]}{\left(1 + K_a \cdot [R] + \sum K_d [I]\right)}$	<ul style="list-style-type: none"> <li>• Surface reaction between organic reactant and hydrogen is the rate determining step.</li> <li>• Competitive adsorption between organic reactants.</li> </ul>
(3.6b)	$r = \frac{k_b \cdot K_a \cdot [R]}{\left(1 + K_a \cdot [R] + \frac{[P]}{K_c} + \sum K_d [I]\right)}$	<ul style="list-style-type: none"> <li>• Same as Eq. 3.6(a) but incorporates a product desorption term.</li> </ul>
(3.6c)	$r = \frac{k_a \cdot [R]}{\left(1 + \frac{[P]}{K_{b,c}} + \sum K_d [I]\right)}$	<ul style="list-style-type: none"> <li>• Adsorption of organic reactants to the catalyst surface is the rate determining step.</li> <li>• Competitive adsorption between organic reactants.</li> </ul>
(3.6d)	$r = \frac{k_c \cdot K_{a,b} \cdot [R]}{\left(1 + K_{a,b} \cdot [R] + \sum K_d [I]\right)}$	<ul style="list-style-type: none"> <li>• Desorption of organic products is the rate determining step.</li> <li>• Equilibrium constants are lumped adsorption and reactant parameters.</li> <li>• Competitive adsorption between organic reactants.</li> </ul>

### 3.4.1 Model refinement: Parameter reduction example

In this example, statistical analysis will be carried out on the surface reaction r.d.s. model with product desorption (Eq. (3.6b)), using a methodology based on Quiney and Schuurman, (2007). The initial rate expressions, which describe the four reaction pathways detailed in Figure 3.1, are shown overleaf:

$$r_{PBN \rightarrow PBL} = r_1 = \frac{k_1 K_{PBN} [PBN]}{\left(1 + K_{PBN} [PBN] + \frac{[PBL]}{K_{PBL}} + K_{CBN} [CBN] + K_{CBL} [CBL]\right)} \quad (3.7a)$$

$$r_{PBN \rightarrow CBN} = r_2 = \frac{k_2 K_{PBN} [PBN]}{\left(1 + K_{PBN} [PBN] + \frac{[CBN]}{K_{CBN}} + K_{PBL} [PBL] + K_{CBL} [CBL]\right)} \quad (3.7b)$$

$$r_{PBL \rightarrow CBL} = r_3 = \frac{k_3 K_{PBL} [PBL]}{\left(1 + K_{PBL} [PBL] + \frac{[CBL]}{K_{CBL}} + K_{PBN} [PBN] + K_{CBN} [CBN]\right)} \quad (3.7c)$$

$$r_{CBN \rightarrow CBL} = r_4 = \frac{k_4 K_{CBN} [CBN]}{\left(1 + K_{CBN} [CBN] + \frac{[CBL]}{K_{CBL}} + K_{PBN} [PBN] + K_{PBL} [PBL]\right)} \quad (3.7d)$$

Eqs. (3.7a-d) contain 12 parameters in total:  $A_{1,373} - A_{4,373}$ ,  $E_{a1} - E_{a4}$  (each contained within  $k_1 - k_4$ ) and four adsorption constants, one for each species. To begin analysis of this kinetic model, an initial parameter estimation pass is carried out using the multi-temperature data in a hexane solvent.

Results for this initial estimation routine are shown in Table 3.6. The  $R^2$  for this model fit is 0.999. It is clear however from the estimated parameter values that the model is over parameterised, with evidence from the following observations:

- Two parameters,  $A_{2,373}$  and  $K_{CBL}$  are indeterminate; this means the solver cannot reliably iterate towards a final value for that parameter.
- The fitted value of  $E_{a4}$  is negative which is not feasible for an activation energy value.
- The critical t-value,  $t_{crit}$  for individual parameters is  $\pm 1.98$ . This is calculated assuming 108 degrees of freedom (120 observations – 12 parameters) at 95% confidence ( $p = 0.05$ ). Parameters  $A_{3,373}$ ,  $E_{a4}$  and  $K_{PBL}$  are below this threshold suggesting that they are statistically insignificant. In accordance with this, these three parameters all have 95% confidence intervals that are greater than their estimated value.

**Table 3.6: Estimated parameter values, confidence intervals and t-values from non-linear least squares fitting of a 12 parameter surface reaction r.d.s model with product desorption**

Parameter <sup>a</sup>	Result	Fitted Value	95% Confidence Interval	t-value <sup>b</sup>
$A_{1,373}$	Estimated	0.071	$\pm 0.0207$	6.79
$A_{2,373}$	Indeterminate	0.695	-	-
$A_{3,373}$	Estimated	0.084	$\pm 0.228$	0.731
$A_{4,373}$	Estimated	0.044	$\pm 0.0352$	2.50
$Ea_1$	Estimated	33.6	$\pm 6.28$	11.6
$Ea_2$	Estimated	47.0	$\pm 2.23$	41.9
$Ea_3$	Estimated	59.1	$\pm 30.1$	3.89
$Ea_4$	Estimated	-6.7	$\pm 23.5$	-0.564
$K_{PBN}$	Indeterminate	0.55	-	-
$K_{PBL}$	Estimated	8.23	$\pm 21.2$	0.771
$K_{CBN}$	Estimated	0.25	$\pm 0.199$	2.52
$K_{CBL}$	Estimated	0.71	$\pm 0.0601$	18.1

<sup>a</sup> Units are  $A_{i,373}$  (mol L<sup>-1</sup> min<sup>-1</sup>),  $E_{ai}$  (kJ mol<sup>-1</sup>),  $K_i$  (L mol<sup>-1</sup>)

<sup>b</sup>  $t_{crit}$  (measurement for parameter significance) is  $\pm 1.96$  for this dataset.

Based on these observations, three parameters in particular ( $A_{3,373}$ ,  $E_{a4}$  and  $K_{PBL}$ ) appear to have little influence on the model fitting. The same could be true for  $A_{2,373}$  and  $K_{PBN}$  however the over parameterisation of this model may have resulted in the indeterminate result returned for these parameters; ergo, these parameters may still be significant at a later point in the model refinement process.

The final steps in quantifying the significance of all 12 model parameters is to address the sensitivity,  $B(t)$ , of all model responses to model parameters as well as cross correlation between parameters themselves. This is achieved using the Jacobian Matrix for each experiment, which is a matrix of all first order partial derivatives of a vector or scalar function with respect to another vector (Caracotsios and Stewart, 1985):

$$J_k = \begin{bmatrix} \frac{dy_1}{d\beta_1} & \dots & \dots & \frac{dy_1}{d\beta_l} \\ \vdots & \ddots & \ddots & \vdots \\ \vdots & \ddots & \ddots & \vdots \\ \frac{dy_k}{d\beta_1} & \dots & \dots & \frac{dy_k}{d\beta_l} \end{bmatrix} \quad (3.8)$$

Where  $k$  denotes the number of model responses and  $l$  the number of model parameters. As  $J_k$  is generated for each of  $m$  experiments (in this example: 30 experiments composed from 6 temperature runs with 5 reaction time measurements), the overall sensitivity of model responses to parameters can be expressed as the norm of the Jacobian Matrix (Jansson, 2002):

$$\text{norm}(J_k)_m = \sqrt{\sum_i \left( \beta_j \frac{dy_i}{d\beta_j} \right)^2} \quad (3.9)$$

Where  $\text{norm}(J_k)_m$  is the norm of the Jacobian Matrix across  $m$  experiments,  $i$  and  $j$  denote correspondence to experiment  $i$  and parameter  $j$  respectively. This norm gives relative information on the influence of model parameters within the system (Quiney and Schuurman, 2007). By comparing these ‘lumped’ sensitivities, non-influential parameters can be removed systematically from the model.

Figure 3.7a shows the Jacobian norms for each parameter based over all four responses in the system. As Jacobian norms are relative values, a normalised form is shown here for clarity. Across the entire system, the most influential parameters appear to be  $A_{2,373}$ ,  $E_{a2}$  and  $K_{PBN}$ . This is not surprising as conversion of PBN to CBN ( $k_2$  route) is the most selective and dominant route across the entire dataset and the parameters which predict this route will have strong influence. Parameter  $E_{a4}$  appears to be most insignificant followed by the intermediate species hydrogenation pre-exponentials  $A_{3,373}$  and  $A_{4,373}$ .

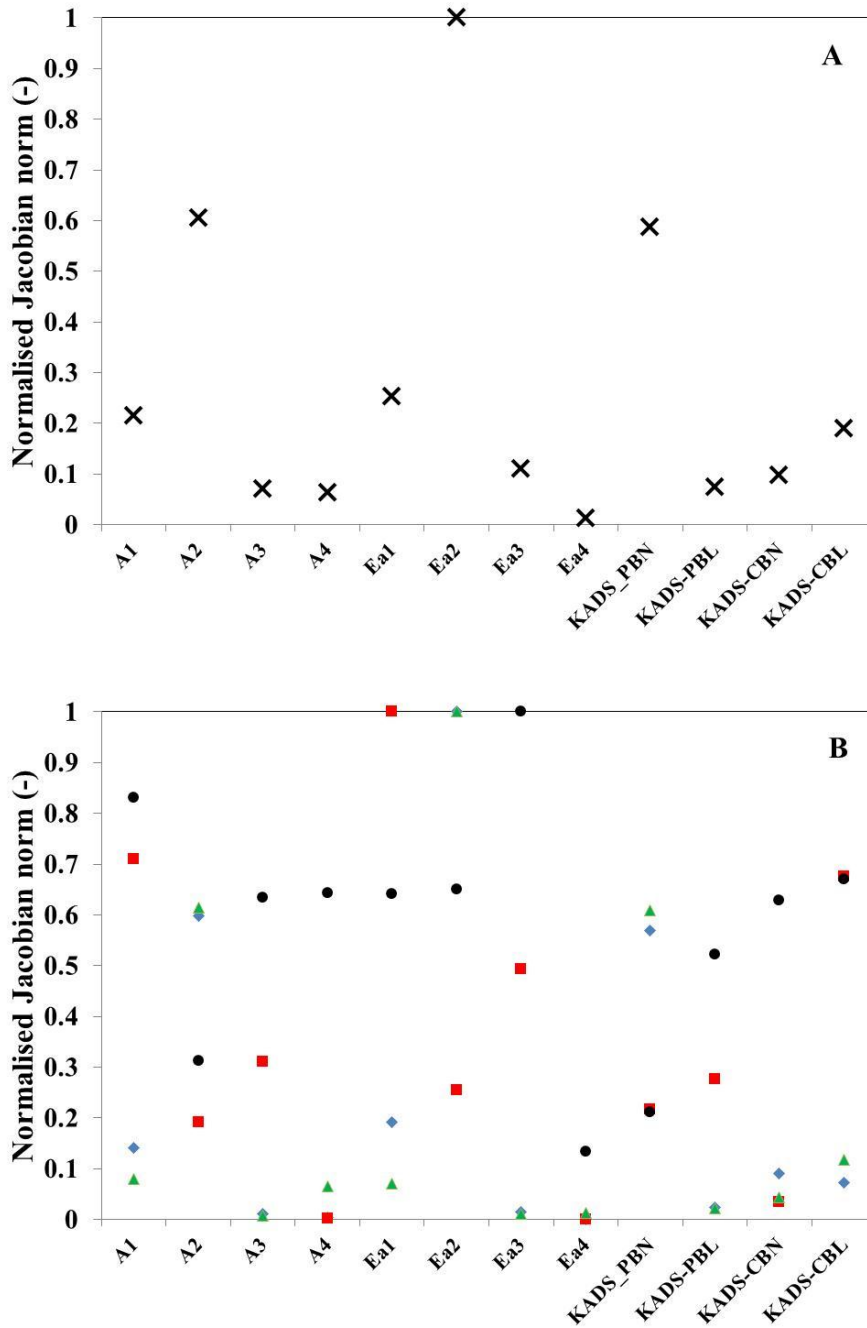


**Figure 3.7: A) Normalised Jacobian norms for all model responses with respect to model parameters and B) for individual responses (♦) PBN, (■) PBL, (▲) CBN, (●) CBL.**

It is critical to view parameter significance in terms of individual model responses (Figure 3.7b). Model responses PBL and CBL, which are much smaller in magnitude across the dataset in comparison to PBN and CBN can therefore be examined with greater clarity. In this case,  $A_{3,373}$  and  $A_{4,373}$  have a much greater impact on CBL response than the other species.  $E_{a4}$  remains low in relative significance however.

An extension of Jacobian Matrix analysis involves studying cross correlation of parameters; a further measure of over parameterisation in a model. This can be calculated for all parametric interactions using the following equation (Marquardt, 1963):

$$(CC)_{j1,j2} = \frac{(J_k^T J_k)_{j1,j2}^{-1}}{\left[ (J_k^T J_k)_{j1,j1}^{-1} \cdot (J_k^T J_k)_{j2,j2}^{-1} \right]^{0.5}} \quad (3.10)$$

Where  $CC$  denotes cross correlation coefficient, which is always in the range  $-1 < CC < +1$ , superscript  $T$  denotes matrix transpose and  $j1$  and  $j2$  are the two considered parameters respectively.  $CC$  values approaching  $-1$  or  $+1$  suggest a strong cross correlation between model parameters.

Table 3.7 shows the cross correlation coefficients for all 12 parameters during the first estimation routine.  $A_{2,373}$  and  $K_{PBN}$  return a string of zero coefficient values as both are indeterminate.  $A_{3,373}$  and  $K_{PBL}$  show a strong cross correlation suggesting their joint presence in the model may not be required, in particular in the  $r_3$  rate expression.

**Table 3.7: Cross correlation matrix for 12 model parameters**

	$A_{1,373}$	$A_{2,373}$	$A_{3,373}$	$A_{4,373}$	$E_{a1}$	$E_{a2}$	$E_{a3}$	$E_{a4}$	$K_{PBN}$	$K_{PBL}$	$K_{CBN}$	$K_{CBL}$
$A_{1,373}$	1											
$A_{2,373}$	0	0										
$A_{3,373}$	0.182	0	1									
$A_{4,373}$	-0.679	0	-0.026	1								
$E_{a1}$	0.856	0	0.307	-0.643	1							
$E_{a2}$	-0.063	0	0.221	0.502	-0.319	1						
$E_{a3}$	0.059	0	0.527	-0.244	0.403	-0.378	1					
$E_{a4}$	-0.563	0	-0.539	0.705	-0.7	0.27	-0.602	1				
$K_{PBN}$	0	0	0	0	0	0	0	0	0			
$K_{PBL}$	-0.092	0	-0.966	-0.114	-0.176	-0.338	-0.323	0.39	0	1		
$K_{CBN}$	-0.348	0	-0.768	-0.102	-0.271	-0.573	-0.156	0.434	0	-0.331	1	
$K_{CBL}$	-0.02	0	-0.251	0.429	-0.234	0.725	-0.355	0.258	0	0.207	0.775	1

At this point of analysis, the kineticist may make any of the following four decisions in order to attempt to improve the model:

- Fully or partially remove a parameter from the rate expression(s). This may involve setting an  $E_a$  value to zero or the removal of  $K$  terms from some or all of the rate expressions.
- Equate two or more model parameters, for example: two reactions may share a common reaction mechanism and equating their  $E_a$  values may be a viable step.
- Fix the value of a parameter; for example, a model may contain  $n$  as a fitting parameter which subsequently tends towards logical mechanistic values during estimation (such as 0.5 or 1) and therefore can be fixed. Also, activation energies or heats of adsorption may be fixed based on previous literature study, a common practice in micro-kinetic analysis works such as those by Dumesic and co-workers (Dumesic and Trevino, 1989).
- Make no further changes.

Consideration of the real physical and chemical implications of model parameter reduction is critical during this process. From the initial estimation process,  $E_{a4}$  appears to be a weak parameter showing low sensitivity values, an estimated value lacking physical meaning, a wide confidence interval and a low  $t$  value. Setting this value to zero would make the assumption that hydrogenation of the ketone group of CBN is a fast process with no temperature dependency. This is unlikely as ketone hydrogenation is not a selective reaction in the conditions tested and C=O bond hydrogenation will have an energy barrier that constitutes a rate determining step (Chang *et al.*, 2000; Vargas *et al.*, 2008). Equating  $E_{a4}$  to  $E_{a1}$  is more logical: both describe the activation energy for ketone hydrogenation of similar species PBN and CBN.

The next step is to rerun the parameter estimation routine with 11 fitting parameters, following equating  $E_{a1}$  and  $E_{a4}$ . This process will generate a new set of fitted parameters, sensitivities, cross correlation coefficients and residuals. A procedure known as the F-test is then invoked which addresses whether the change in residuals of model responses in the 11 parameter model in comparison to the 12 parameter one is statistically significant. This is often defined as a ‘nested model’ problem and the  $F$ -statistic can be calculated as follows:

$$F = \frac{\left( \frac{RSS_1 - RSS_2}{par_2 - par_1} \right)}{\left( \frac{RSS_2}{obs - par_2} \right)} \quad (3.11)$$

Where  $F$  is the  $F$ -statistic,  $RSS_1$  and  $RSS_2$  are the residual sum of squares in the nested and original model respective,  $par_1$  and  $par_2$  are number of parameters and  $obs$  is the total number of observations. In this study  $(par_2 - par_1)$  is always equal to 1 as parameters are removed on an individual basis. The  $F$  generated is compared to  $F_{crit}$  ( $p = 0.05$ ) under these constraints. If  $F$  is smaller than  $F_{crit}$ , the removal, equating or fixing of a parameter is deemed acceptable as a statistically significant increase in residuals has not been induced.

Figure 3.8a shows the values of  $F$  calculated for the successive removal of parameters in the model. In terms of the entire system response, seven parameters can be removed from the fitting procedure without a statistically significant effect. Individual model responses were also examined in Figure 3.8b and largely demonstrate the same result. The  $F_{crit}$  value is exceeded once for CBL and PBL respectively, however the residuals of both responses improve in subsequent parameter removals, correcting this statistically significant shift. The  $F$  value response is significant on removal of the eighth parameter however, in particular for the CBL response. Further removals, which would reduce the entire model to 3 or less parameters, amplify this effect further.

Table 3.8 documents the parameter reduction process from 12 down to 4 parameters in the entire model. The reduction contains a number of steps where an activation energy or pre-exponential is equated with another. In each case this involved ‘pairing’ of reaction pathways which have the same mechanism: ketone hydrogenation ( $r_1$  with  $r_4$ ) and aromatic ring hydrogenation ( $r_2$  with  $r_3$ ). Adsorption parameters  $K_{PBN}$ ,  $K_{PBL}$  and  $K_{CBL}$  were all removed at various stages leaving the parameter for the selective product,  $K_{CBN}$ .

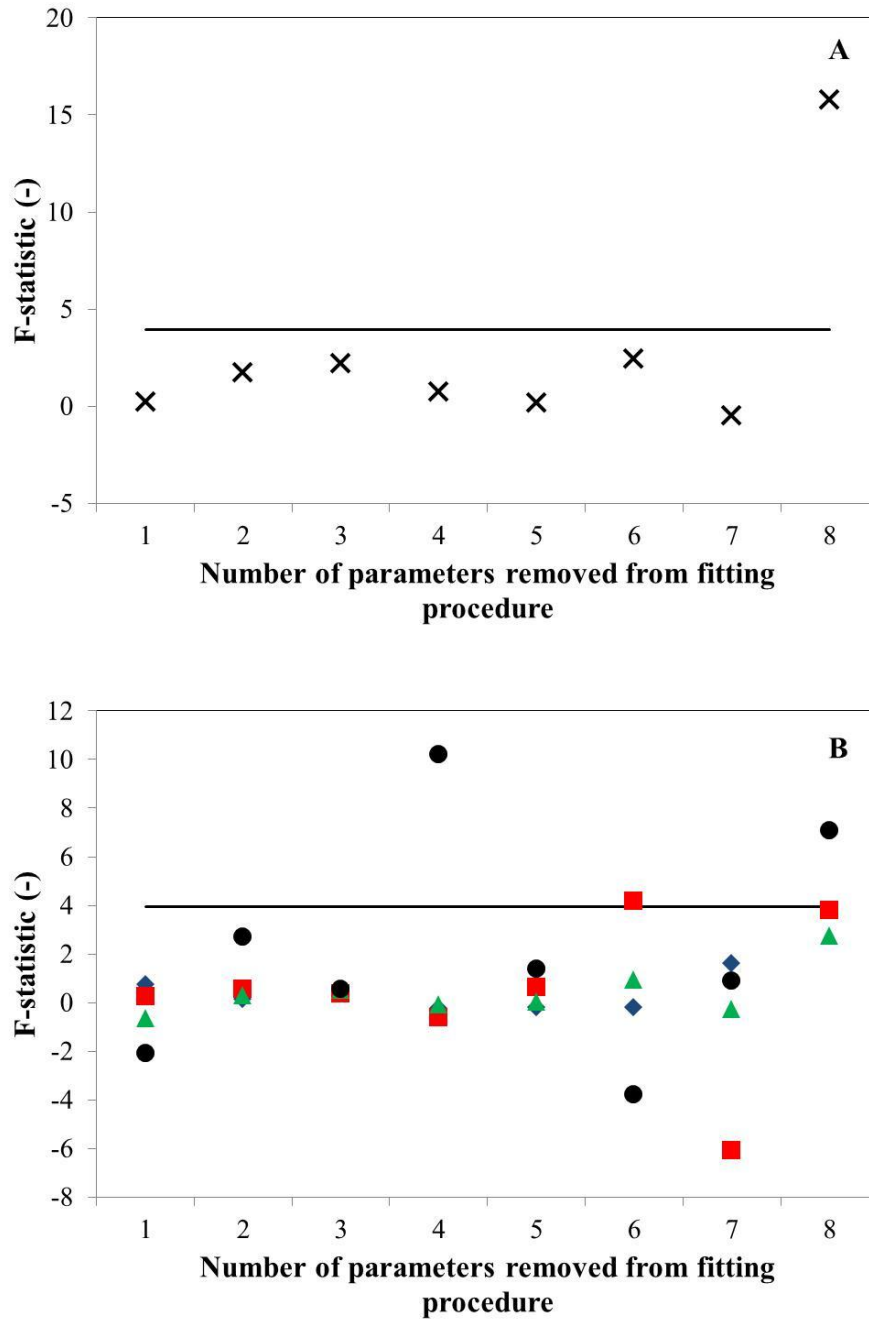


Figure 3.8: A) Calculated  $F$ -statistic for successive parameter removal across the entire system response and B) with respect to individual model responses (♦) PBN, (■) PBL, (▲) CBN, (●) CBL. N.B.: Black line denotes  $F_{crit}$

**Table 3.8: Parameters removed in surface reaction limited model with product desorption**

No. parameters in model	Most recent parameter removed	RSS ( $\times 10^4$ )	Reason for parameter removal <sup>a</sup>
12	-	6.94	-
11	$E_{a4}$	6.95	<ul style="list-style-type: none"> <li>Negative, poor confidence</li> <li>Equated to <math>E_{a1}</math>: both are ketone hydrogenation steps</li> </ul>
10	$A_{4,373}$	7.06	<ul style="list-style-type: none"> <li>Equated to <math>A_{1,373}</math>: both are available sites for ketone hydrogenation</li> </ul>
9	$K_{PBL}$	7.20	<ul style="list-style-type: none"> <li>Indeterminate</li> </ul>
8	$E_{a3}$	7.24	<ul style="list-style-type: none"> <li>Poor confidence, similar value to <math>E_{a2}</math></li> <li>Equated to <math>E_{a2}</math>: both are aromatic ring hydrogenation steps</li> </ul>
7	$A_{3,373}$	7.25	<ul style="list-style-type: none"> <li>Equated to <math>A_{2,373}</math>: both are available sites for aromatic ring hydrogenation</li> </ul>
6	$K_{CBL}$	7.41	<ul style="list-style-type: none"> <li>Lowest Jacobian norm only</li> </ul>
5	$K_{PBN}$	7.38	<ul style="list-style-type: none"> <li>Strong cross-correlation with <math>A_{2,373}</math></li> </ul>
4	$K_{CBN}$	8.38	<ul style="list-style-type: none"> <li>Statistically significant, should not be removed.</li> </ul>

<sup>a</sup> In addition to showing the lowest Jacobian norm

### 3.4.2 Comparison and selection from refined models

Once all of the models proposed in Table 3.5 have undergone parameter reduction, the next step is to discriminate between them. In Figure 3.9, variation in the  $F$ -statistic with parameter removal is shown for all three model types.

The surface reaction or product desorption r.d.s. models, which are both mathematically identical showed statistically significant changes in residuals from the removal of a 4<sup>th</sup> parameter onward. Prior to this, these models also contained indeterminate parameters when solved. These models were discarded due to both of these issues.

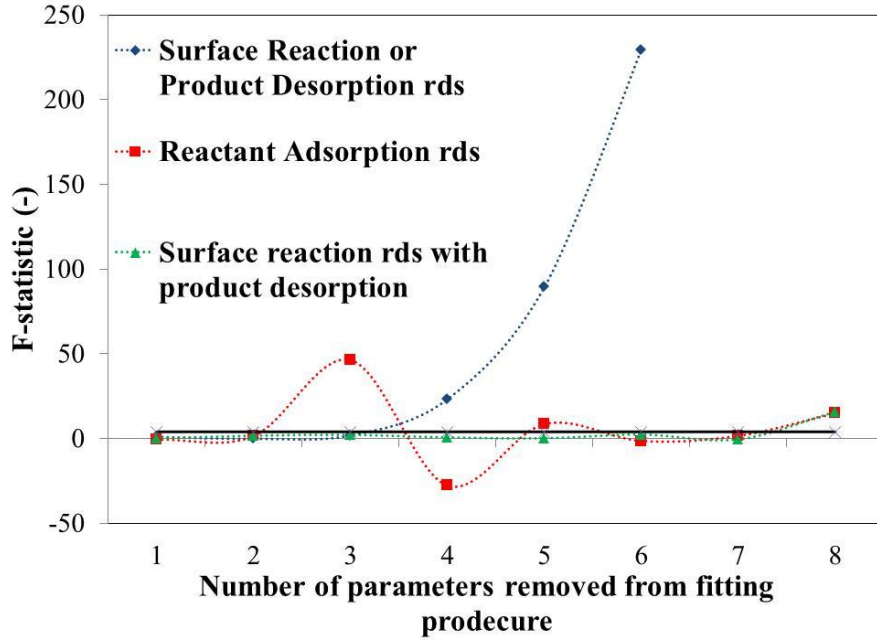


**Figure 3.9: Calculated  $F$ -statistic for successive parameter removals across the entire system response for different models**

The adsorption r.d.s. model exceeded the  $F_{crit}$  twice (3<sup>rd</sup> and 5<sup>th</sup> parameters removed) but the effect on residuals was corrected with the 4<sup>th</sup> and 6<sup>th</sup> parameters respectively. Hence it is acceptable to remove 7 parameters from this model. The surface reaction r.d.s. with product desorption model was most successful and did not exceed  $F_{crit}$  until the removal of the 8<sup>th</sup> parameter.

The condition number ( $C(J_k)$ ), which examines the overall cross correlation of parameters within each of the two remaining models can be calculated using the following:

$$C(J_k) = \|J_k\| \cdot \|J_k^{-1}\| \quad (3.12)$$

As parameters are removed from model descriptions, the number of linear dependent columns is reduced within the Jacobian matrix. Higher condition numbers reflect a greater degree of cross correlation between parameters in the system. Figure 3.10 shows that cross correlation is significantly decreased for both remaining models as parameters are removed.  $C(J_k)$  is very similar for both models with 8 parameters or less. Therefore it is not possible to discriminate the models on this basis.

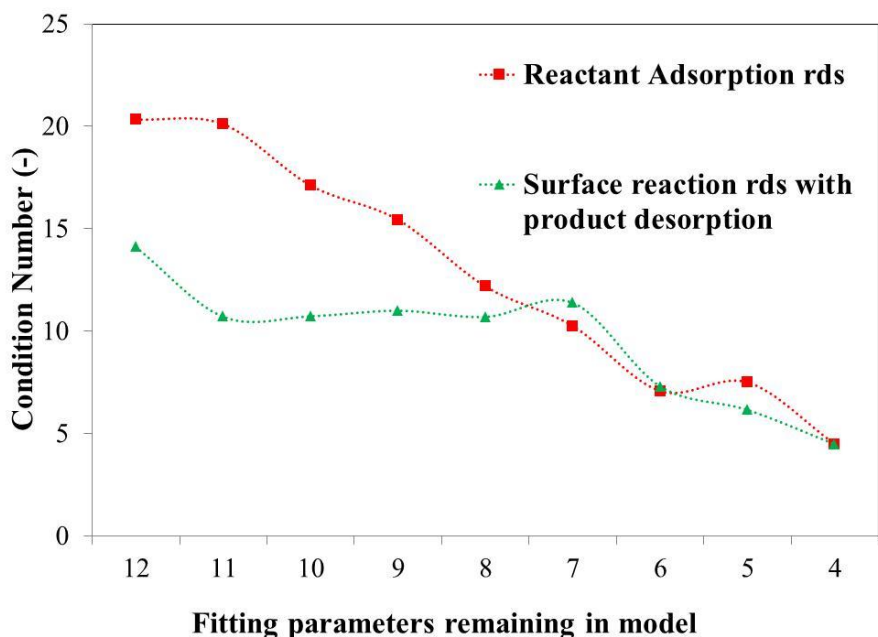


**Figure 3.10: Change in condition number with number of parameters in models**

Table 3.9 shows that the final parameter estimations for both models are very similar in value and confidence intervals. Due to the pairing of reaction pathways, subscripts 1,4 and 2,3 are now referred to as *ket* and *arom* respectively.  $E_a$  for the aromatic ring hydrogenation steps is higher than that for ketone hydrogenation, which was discussed following experimental observation in section 3.3.1. Similarly,  $A_{ket,373}$  is roughly ten times lower than  $A_{arom,373}$  which reflects the significant difference in selectivity between both hydrogenation routes observed.

**Table 3.9: Parameter estimates and 95% confidence intervals remaining kinetic models**

Parameter	Adsorption r.d.s		Surface reaction with product desorption r.d.s.	
	Estimate	95% Conf. Interval	Estimate	95% Conf. Interval
$A_{ket,373}$	0.044	0.006	0.03	0.005
$A_{arom,373}$	0.36	0.029	0.274	0.011
$E_{a,ket}$	30.3	3.4	27.9	3.9
$E_{a,arom}$	48.4	1.5	47.8	1.2
$K_{CBN}$	1.1	0.37	1.27	0.33

The key discrimination in the two models is in fact their similarity in parameter estimates. The  $E_a$  values estimated are in line with a surface reaction limited mechanism rather than an adsorption limited step. Previous work on a similar system, *p*-isobutyl acetophenone hydrogenation (Mathew *et al.*, 1999), estimated  $E_{a,ket}$  and  $E_{a,arom}$  to be 42 and 47 kJ mol<sup>-1</sup> respectively whilst heat of adsorption of the initial reactant was -5 kJ mol<sup>-1</sup>. Similarly, in a kinetic study of ketone hydrogenation (Chang *et al.*, 2000), organic heat of adsorption parameters were found to be in the -5 to -15 kJ mol<sup>-1</sup> range.

Based on the above, the surface reaction r.d.s. model is chosen on the grounds of an appropriate mechanistic basis in light of estimated parameters. Subsequently the model was then tested against data at different starting PBN concentrations for wider validity. Figure 3.11 shows a decreasing trend in  $k_{ket}$  and  $k_{arom}$  values with increasing initial PBN concentration.

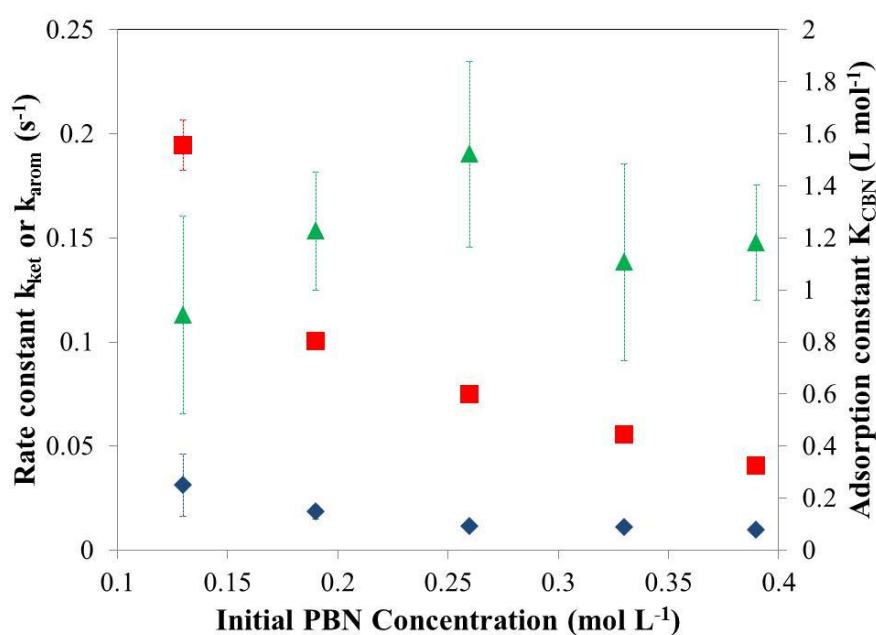


**Figure 3.11: Estimated parameter values for (◆)  $k_{ket}$ , (■)  $k_{arom}$  and (▲)  $K_{CBN}$  using the surface reaction r.d.s model with product desorption for experimental data using different starting concentrations of PBN at 343 K**

The adsorption fitting parameter  $K_{CBN}$  appears to be similar for all estimates, within error. The latter observation adds a degree of confidence to the model as the adsorption constant value should not change with surface coverage, assuming a Langmuir-type adsorption model. The trend shown for  $k_{ket}$  and  $k_{arom}$  suggests that both values are lumped terms which could not be deconvoluted in the temperature varied experiments. A PBN

inhibition term should therefore be considered for these data. To demonstrate, the following equation was used to fit the estimated rate constant vs. initial PBN concentration data:

$$k_{ket/arom} = \frac{k_0}{(1 + K_{PBN} [PBN_0])^n} \quad (3.13)$$

Fitting using  $n = 1$  was unsuccessful and gave indeterminate parameters. Using  $n = 2$  was considerably more successful. Table 3.10 confirms that rate constant values,  $k_0$ , are an order of magnitude in difference but also shows that adsorption of PBN is considerably stronger for the aromatic ring pathway. This confirms the experimental observation of higher selectivity towards CBN and subsequently the preferred mode of adsorption in the hexane solvent. A second order fit to this equation is a strong indicator that PBN competitively adsorbs with hydrogen on the catalyst surface, as a square term is seen in kinetic expressions with such a basis. Parameters associated with hydrogen adsorption are simply not seen in the hexane solvent study due to invariance of concentration and small changes in solubility across the dataset.

**Table 3.10: Estimated parameters for Eq. (3.13) using  $n = 2$**

Pathway	$k_0$ ( $\text{min}^{-1}$ )	$K_{PBN}$ ( $\text{L mol}^{-1}$ )
<b>Ketone</b>	0.11	2.4
<b>Aromatic Ring</b>	1.2	13.2

### 3.4.3 Kinetic model application to a range of solvents

The five parameter surface reaction r.d.s. with product desorption model was then applied to isothermal data tested with different solvents. The data for each experiment were fitted using  $k_{ket}$  and  $k_{arom}$  as lumped rate terms (due to temperature invariance) thus reducing parameters in the model to 3.

Figure 3.12 shows that there is a direct correlation between dominant adsorption constant,  $K_{CBN}$  and selectivity towards CBN in the reaction system. Meanwhile, the summated rate constant ( $k_{ket} + k_{arom}$ ) follows the same trend as observed PBN conversion with respect to  $k_H$  for  $\text{H}_2$  solubility. This correlates with the PBN conversion vs. Henry's Constant graph shown in Figure 3.6. The final model can therefore describe both selectivity

(via correlation with dominant adsorption constant) and link turnover rate to H<sub>2</sub> solubility as a function of solvent choice.

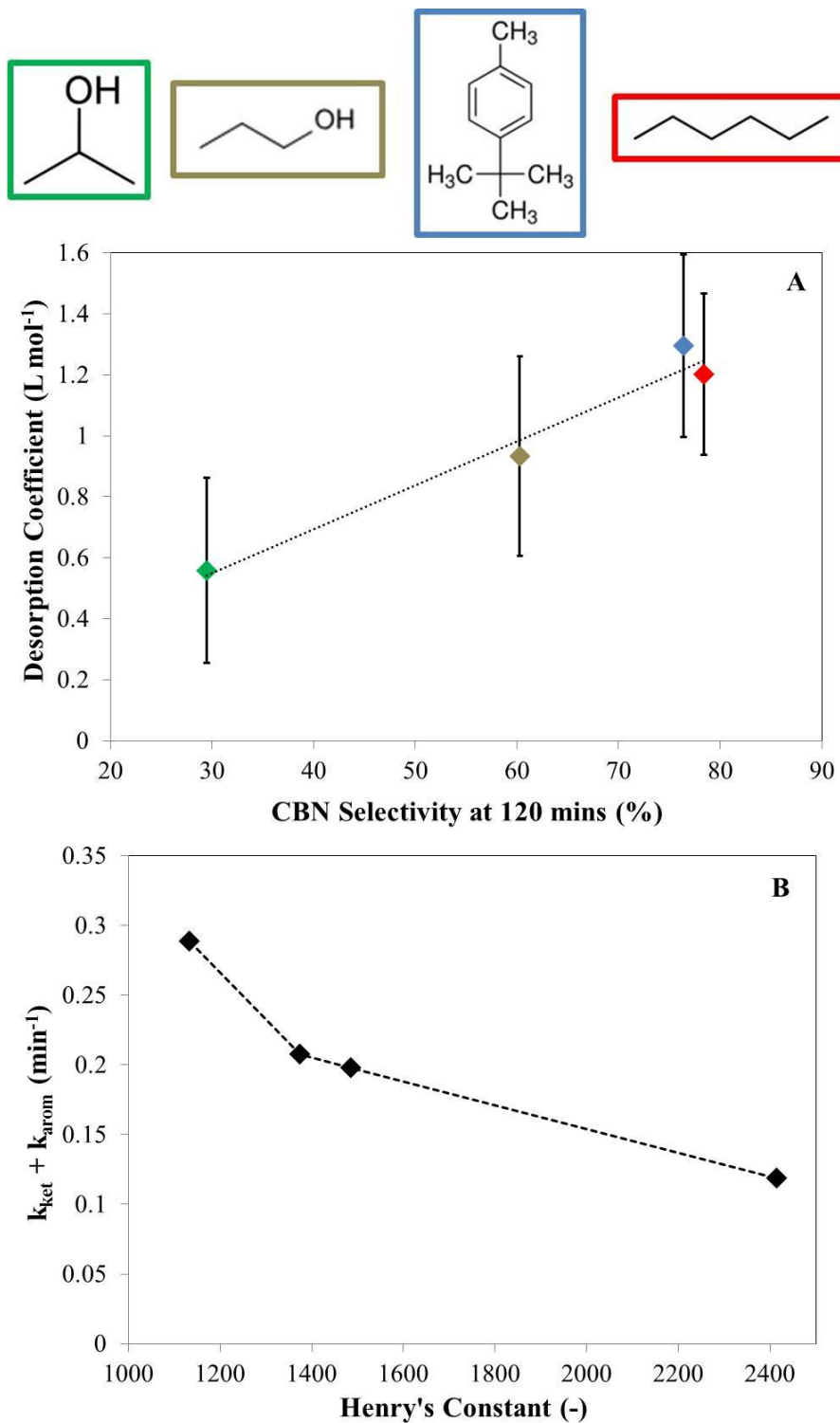


**Figure 3.12: A) Magnitude of CBN adsorption constant against selectivity for PBN hydrogenation in different solvents and B) Summated rate constant  $k_{\text{arom}} + k_{\text{ket}}$  plotted against  $k_H$  for H<sub>2</sub> solubility at 5 bar, 343 K in various solvents**

### 3.5 Discussion

In section 3.1, it was stressed that the pursuit of elucidating solvent effects in liquid-phase reactions via kinetic modelling should incorporate a strong statistical and mechanistic basis. The approach demonstrated in this work is discussed in reference to these critical requirements.

The critical pre-determining step in any kinetic study is the number of proposed models to which data are subsequently fitted. Use of a range of models that include different rate determining steps in their mechanism (Bertero *et al.*, 2008; Mounzer *et al.*, 2010; Chang *et al.*, 2000), assumptions of non-competitive and competitive reactant adsorption (Mukherjee and Vannice, 2006a; Bergault *et al.*, 1998), dissociative or associative molecular adsorption (Mathew *et al.*, 1999; Bergault *et al.*, 1998) and inhibition effects (Mounzer *et al.*, 2010; Mukherjee and Vannice, 2006a) all define this scope. At a maximum of these possibilities, model comparison without a systematic statistical analysis is likely impossible. In the current work, such a range of steps were condensed into four ‘over-parameterised’, starting models with different rate determining steps. From here, parameter reduction via sensitivity, condition number and *F*-test analysis takes each model to a defined stop point; ergo, the bi-directional problem of over-simplification/complication of kinetic models can be avoided.

In the work of Bergault *et al.*, (1998), the batch-time acetophenone hydrogenation behaviour draws comparison with the current study, particularly with initial rate behaviour at different acetophenone start concentrations. All possible adsorption effects (including inhibition) were considered and led to indeterminacy in their estimation when the data were fitted, as is seen in the current study. This was circumvented by normalising adsorption constant values, however the authors do not comment on the statistical significance of the newly estimated parameters. Similarly, their proposed model does not link parameters in identical reaction pathways, of which the estimated parameters in the work would suggest to be a viable move. A similar process is seen in Mathew *et al.*, (1999); in this work two  $E_a$  values for aromatic ring hydrogenation are estimated at 47 and 44 kJ mol<sup>-1</sup> respectively but are left unpaired. A parameter pairing approach in the current work was found to have little impact on residuals and freed up extra degrees of freedom to aid in the parameter estimation process.

A parallel can be drawn between the current study and the mixed ketone hydrogenation study of Chang *et al.*, (2000). The latter eliminated parameters based on insignificant *t*-values and wide 95% confidence intervals. A product desorption term was found to be a significant parameter for the dominant ketone hydrogenation pathway but not the other reaction pathways. Instead, this desorption term appears as an inhibition factor for the other pathways, again as reported in this study. The study also demonstrated that all ketone hydrogenation routes could be adequately lumped together into one expression, which echoes the linking of reaction pathways demonstrated in this work.

The importance of a product desorption term is also in line with the work of Mounzer *et al.*, (2010), whereby desorption of product P from active sites was driven by solvent composition. In the current work, the ring hydrogenated product CBN has a lower polarity than that of the ketone hydrogenated product PBL. The former has a greater likelihood of removal from the catalyst surface by apolar aprotic solvents such as hexane rather than protic alcohols. The correlation between solvent selectivity towards CBN and  $K_{CBN}$  may be a reflection of this. Specific CBN and PBL desorption studies may mark interesting future work on this topic to further test the modelling results experimentally.

Variation of PBN initial concentration in this study further demonstrates dominant pathways;  $K_{arom}$  out-stripping  $K_{ket}$  by a factor of 6 in a hexane solvent. Multiple adsorption modes of a single species are rarely fitted as different adsorption constants as parameter cross-correlation is often induced. Indeed,  $K_{PBN}$  was found to be highly cross-correlated in the temperature varied study of this work. The methodology presented in section 3.4.3 which fits ‘lumped’ reaction pathways as a function of adsorption mode goes some way to decoupling these effects presenting logical results in light of the product selectivities observed. Such results can be compared to DFT studies of aromatic ketone adsorption modes (Vargas *et al.*, 2008).

### 3.6 Conclusions

The role of the solvent can be critical in many catalytic liquid phase reactions; in particular influencing adsorption/desorption of reactants and products as well as influencing overall catalytic turnover rates and gas phase solubility. Data from an experimental study of 4-phenyl-2-butanone hydrogenation over a Pt/TiO<sub>2</sub> catalyst have been used to develop a

kinetic analysis methodology to elucidate solvent effects and unify solvation, dominant adsorption constant and product selectivity.

The methodology has successfully drawn upon previous mechanistic descriptions proposed in literature (Mathew *et al.*, 1999; Mounzer *et al.*, 2010; Bergault *et al.*, 1998). The fitting of data to these models has been combined with a rigorous statistical analysis procedure to eliminate non-influential parameters in their descriptions (Quiney and Schuurman, 2007). During this procedure, the physical and chemical meaning of estimated parameters was considered and this led to pairing of similar reaction pathways (e.g. initial reactant and intermediate ketone hydrogenation). The final model assumed the surface reaction of the organic species with hydrogen to be the rate determining step and included a selective product, 4-cyclohexyl-2-butanone, desorption term.

Based on the outcomes from the kinetic modelling, solvents can be recommended based on the required reaction products. The use of alkanes as solvent would be preferable if you wished to achieve good aromatic ring hydrogenation selectivity and activity. Meanwhile, a secondary alcohol (such as 2-propanol) is preferable to achieve good ketone hydrogenation selectivity and activity. Use of this particular solvent suppresses aromatic ring hydrogenation by inhibiting desorption of the CBN intermediate product.

The role of the solvent in determining catalytic turnover frequency and specific selectivity towards products is varied in literature and this study shows a further, different, example. A good correlation was seen both experimentally and via modelling relating hydrogen solubility in the solvent and overall reaction rate in this study. The modelling process further showed an adsorption constant  $K_{CBN}$  which is directly linked to product selectivity. Meanwhile, a previous study using a Ni/SiO<sub>2</sub> catalyst in a range of solvents for acetophenone hydrogenation results in a strong selectivity towards ketone hydrogenation due to strong C=O group binding on the nickel surface (Bertero *et al.*, 2011). In a different system, citral hydrogenation (Mukherjee and Vannice, 2006b), no link with hydrogen solubility of solvent is seen due to a negligible dependence on hydrogen partial pressure. This re-iterates the complexity of these systems when catalyst metal/support, reactants and solvents are all considered. The kinetic analysis methodology proposed however can quickly elucidate a fundamentally and statistically sound kinetic model for a chosen system with limited experimental data. This can subsequently be used to understand the link between

solvent, dominant mode of adsorption and selectivity as well as predict catalytic turnover rates.

### 3.7 Appendices - Experimental and *a priori* checks for mass transport limitations

#### 3.7.1 Experimental checks for mass transport limitations

Experiments were carried out using different stirrer speeds (Figure 3.13) and catalyst mass (Figure 3.14) to assess the impact of gas-liquid and liquid-solid mass transport limitations respectively. It is seen that for stirrer speed values of 800 rpm or greater, rate of reaction with respect to PBN conversion is roughly constant. This led to a choice of 1400 rpm for the bulk of the experimental programme (see section 3.2.1). A reasonably linear trend was seen between initial PBN conversion rate and catalyst mass suggesting that liquid-solid mass transport effects are negligible within the reactor setup. A similar, linear observation is made if different starting PBN concentrations are used. This further verifies the absence of liquid-solid mass transport limitations and consolidates the kinetic findings in Figure 3.4, which demonstrated that product desorption effects have an impact on reaction performance.

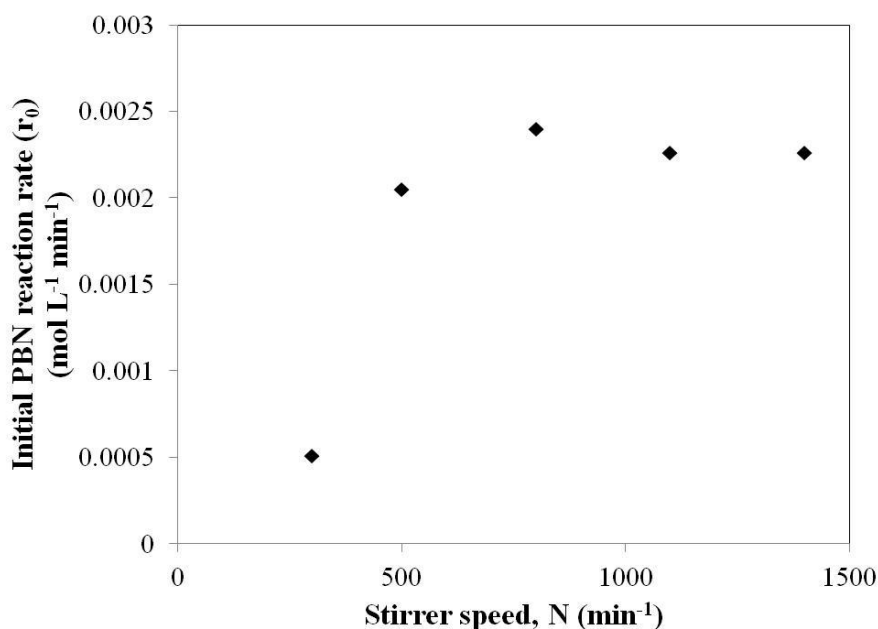


**Figure 3.13: Effect of stirrer speed on initial reaction rate of PBN (100 mg catalyst, 5 bar H<sub>2</sub> pressure, 343 K, 0.26 mol L<sup>-1</sup> initial PBN concentration)**

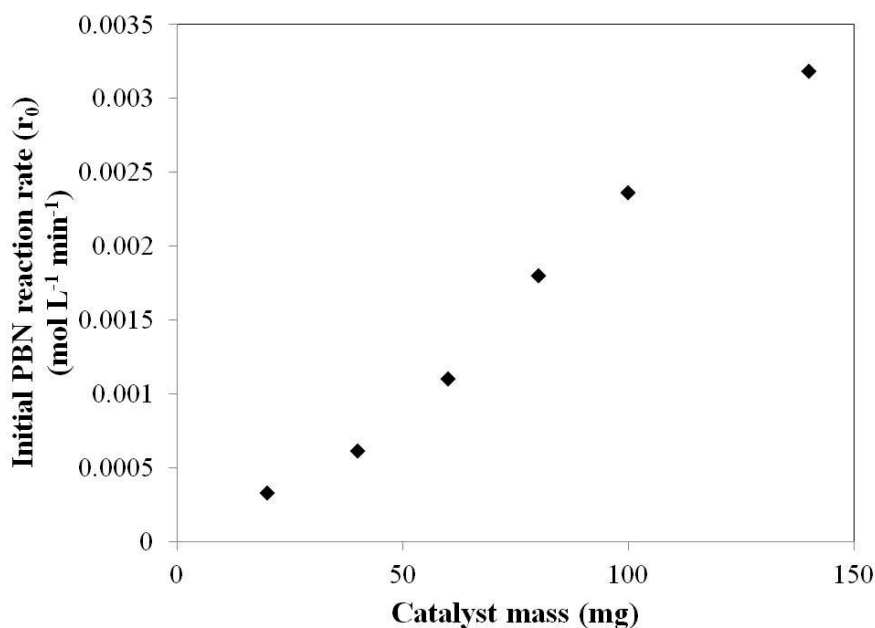


**Figure 3.14: Effect of catalyst mass on initial reaction rate of PBN (1400 rpm stirrer speed, 5 bar H<sub>2</sub> pressure, 343 K, 0.26 mol L<sup>-1</sup> initial PBN concentration)**

### 3.8 References

- Akpa B.S., D'Agostino C., Gladden L.F., Hindle H., Manyar H., McGregor J., Li R., Neurock M., Sinha N., Stitt E.H., Weber D., Zeitler J.A., Rooney D.W., (2012), 'Solvent effects in the hydrogenation of 2-butanone', *J. Catal.*, 289, 30-41
- Bergault I., Fouilloux P., Joly-Vuillemin C., Delmas H., (1998), 'Kinetics and intraparticle diffusion modelling of a complex multistep reaction: Hydrogenation of acetophenone over a rhodium catalyst', *J. Catal.*, 175, 328-337
- Bertero N.M., Apesteguia C.R., Marchi A.J., (2008), 'Catalytic and kinetic study of the liquid-phase hydrogenation of acetophenone over Cu/SiO<sub>2</sub> catalyst', *App. Cat. A: Gen.*, 349, 100-109
- Bertero N.M., Trasarti A.F., Apesteguia C.R., Marchi A.J., (2011), 'Solvent effects in the liquid-phase hydrogenation of acetophenone over Ni/SiO<sub>2</sub>: A comprehensive study of the phenomenon', *App. Cat. A: Gen.*, 394, 228-338
- Boudart M., Cheng W-C., (1987), 'Catalytic hydrogenation of cyclohexene: Part VII. Liquid phase reaction on supported nickel', *J. Catal.*, 106, 134-143

- Carey F.A., Sundberg R.J., (1990), '*Advanced organic chemistry*', Plenum Press, New York, Ch. 6
- Caracotsios M., Stewart W.A.E., (1985), '*Sensitivity analysis of initial value problems with mixed ODEs and algebraic equations*', *Comp. and Chem. Eng.*, 9, 4, 359-365
- Chang M-Y., Eiras J.G., Morsi B.I., (1991), '*Mass transfer characteristics of gases in n-hexane at elevated pressures and temperatures in agitated reactors*', *Chem. Eng. Proc.*, 29, 49-60
- Chang N-S., Aldrett S., Holtzapple M.T., Davison R.R., (2000), '*Kinetic studies of ketone hydrogenation over Raney nickel catalyst*', *Chem. Eng. Sci.*, 53, 5721-5732
- Dumesic J.A., Trevino A.A., '*Kinetic simulation of ammonia synthesis catalysis*', *J.Catal*, (1989), 116, 119-129
- Gamez A., Köhler J., Bradley J., (1998), '*Solvent effects in the kinetics of the enantioselective hydrogenation of ethyl pyruvate*', *Catal. Lett.*, 55, 73-77
- Gonzo E.E., Boudart M., (1978), '*Catalytic hydrogenation of cyclohexene: Part III. Gas phase and liquid phase reaction on supported palladium*', *J. Catal.*, 52, 462-471
- Hu B., Fishwick R.P., Pacek A.W., Winterbottom J.M., Wood J., Stitt E.H., Nienow A.W., (2007), '*Simultaneous measurement of in situ bubble size and reaction rates with a heterogeneous catalytic hydrogenation reaction*', *Chem. Eng. Sci.*, 62, 5392-5396
- Jansson J., '*Studies of catalytic low-temperature CO oxidation over cobalt oxide and related transition metal oxides*', (2002), Ph.D. Thesis. Chalmers University of Technology, Sweden,
- Katayama T., Nitta T., (1978), '*Solubilities of hydrogen and nitrogen in alcohols and n-hexane*', *J. Chem. Eng. Data*, 21, 2, 194-197
- Kishida S., Teranishi S., (1968), '*Kinetics of liquid-phase hydrogenation of acetone over Raney nickel catalyst*', *J. Catal.*, 12, 90-96
- Lemcoff N.O., (1977), '*Liquid phase catalytic hydrogenation of acetone*', *J. Catal.*, 46, 356-364

- Madon R.J., O'Connell J.P., Boudart M., (1978), '*Catalytic hydrogenation of cyclohexene: Part II. Liquid phase reaction on supported platinum in a gradientless slurry reactor*', *AIChE J.*, 24, 904-911
- Marquardt D., '*An algorithm for least-squares estimation of nonlinear parameters*', (1963), *S.I.A.M. K. App. Math.*, 11, 143
- Mathew S.P., Rajeseckharam M.V., Chaudhari R.V., (1999), '*Hydrogenation of p-isobutyl acetophenone using a Ru/Al<sub>2</sub>O<sub>3</sub> catalyst: reaction kinetics and modelling of a semi-batch slurry reactor*', *Catal. Today.*, 49, 49-56
- Menshutkin N., (1890), '*Regarding the question on the influence of chemically indifferent solutions on reaction speed*', *Z. Phys. Chem.*, 6, 589-600
- Mounzer H.N., Wood J., Stitt E.H., (2010), '*Heterogeneous oxidation of 2-octanol on 5wt%Pt-1wt%Bi/Carbon catalyst*', *Chem Eng. Sci.*, 65, 179-185
- Mukherjee S., Vannice M.A., (2006a), '*Solvent effects in liquid-phase reactions II. Kinetic modelling for citral hydrogenation*', *J. Catal.*, 243, 131-148
- Mukherjee S., Vannice M.A., (2006b), '*Solvent effects in liquid phase reactions I. Activity and selectivity during citral hydrogenation on Pt/SiO<sub>2</sub> and evaluation of mass transfer effects*', *J. Catal.*, 243, 108-130
- Quiney A.S., Schuurman Y., (2007), '*Kinetic modelling of CO conversion over a Cu/ceria catalyst*', *Chem. Eng. Sci.*, 62, 5026-5032
- Singh U.K., Vannice M.A., (2001), '*Kinetics of liquid-phase hydrogenation over supported metal catalysts – A review*', *App. Cat. A: Gen.*, 213, 1-24
- Sinha N.K., Neurock M., (2012), '*A first principles analysis of the hydrogenation of C<sub>1</sub> to C<sub>4</sub> aldehydes and ketones over Ru(0 0 0 1)*', *J. Catal.*, 295, 31-44
- Tsuji T., Shinya Y., Haiki T., Itoh N., (2005), '*Hydrogen solubility in a chemical hydrogen storage medium, aromatic hydrocarbon, cyclic hydrocarbon, and their mixture for fuel cell systems*', *Fluid Phase Equ.*, 228-229, 499-503

Vargas A., Reimann S., Diezi S., Mallat T., Baiker A., (2008), '*Adsorption modes of aromatic ketones on platinum and their reactivity towards hydrogenation*', J. Mol. Cat. A, 282, 1-8

Weisz P.B., Prater C.D., (1954), Adv. Cat. Rel. Subj., 6, 143

Weisz P.B., (1957), Z. Phys. Chem. (Frankfurt Am Main), 11, 1

## Chapter 4:

### **A novel approach to understanding and modelling the performance evolution of catalysts during their initial operation under reaction conditions –**

#### **Case study of vanadium phosphorus oxides for *n*-butane selective oxidation**

*In heterogeneous catalysis, catalyst precursor activation and subsequent initial operation ('conditioning') under reaction conditions are often highly dynamic steps which are important in delivering effective catalyst performance over time scales of years. In many cases however, the phenomena occurring in both steps are often poorly understood. A novel approach to assess the conditioning step, comprising advanced catalyst testing methods in micro-reactors, catalyst characterisation and detailed kinetic and activity modelling techniques is demonstrated for a model system: the selective oxidation of *n*-butane to maleic anhydride (MA) using a pre-activated vanadium phosphorus oxide (VPO) catalyst. A transient kinetic model for the conditioning step is presented which describes the decline of population of active sites for three reaction pathways on the catalyst surface over time. Two reaction pathways, *n*-butane  $\rightarrow$  MA and *n*-butane  $\rightarrow$  CO<sub>x</sub> decay similarly with time whilst a third, MA  $\rightarrow$  CO<sub>x</sub> declines very sharply. The approach used provides important mechanistic information on catalyst reaction kinetics whilst also providing understanding the impact of reaction conditions on the catalyst during conditioning.<sup>8</sup>*

---

<sup>8</sup> Material presented in this chapter has been published: Wilkinson S.K., Simmons M.J.H., Stitt E.H., Baucherel X., Watson M.J., *Journal of Catalysis*, (2013), 299, 249-260

#### **4. Introduction: ‘Catalyst conditioning – The final stage of catalyst activation?’**

Solid catalysts are structured products which are invaluable in assisting a wide range of chemical processes on an industrial scale. As discussed in chapter 1 of this thesis, critical performance features of a ‘good’ catalyst often comprise high activity, high selectivity towards desired reaction products and stability during long-term operation. The pursuit of understanding and subsequently controlling the development of such features for different catalyst systems requires knowledge of a number of stages of catalyst production, which chiefly includes, but is not limited to:

- Catalyst precursor preparation.
- Activation of the precursor.
- Initial, unsteady state, ‘conditioning’ of the catalyst under reaction conditions. This can also be referred to as ‘equilibration’.

For the last step, catalytic performance can change significantly over time and may or may not tend towards a quasi-steady-state (QSS) performance. For many reaction systems, precursor preparation and performance of the catalyst under QSS reaction conditions are often studied. Less explored are the activation and conditioning steps, which are often highly dynamic in nature. With the conditioning step in particular, there is very little mechanistic understanding of why the catalyst performance changes. Hence, there is considerable scope to develop techniques for a range of systems to de-convolute and describe phenomena occurring during both steps. The conditioning period may also provide valuable information around the fundamental reaction kinetics of catalyst systems, such as an understanding of which active sites are being generated and lost on the catalyst surface over time.

In this chapter, a novel approach will be used which combines advanced reactor testing methods to track catalyst evolution (chiefly, parallel difference testing (Birtill, 2003)) with kinetic/activity modelling and supporting characterisation methods during the conditioning period. Using a model system, evolution of active sites will be demonstrated and linked through to fundamental physical and chemical changes occurring to the catalyst itself. Investigation into the effect of reaction conditions during conditioning will aid in developing mechanistic models for catalyst evolution.

## 4.1 Vanadium phosphorus oxide catalysts for *n*-butane selective oxidation

Vanadium phosphorus oxides (VPOs), which carry out the selective oxidation of *n*-butane to maleic anhydride (MA), are a model example of catalysts whose final QSS performance is strongly dependent on prior preparation, activation and conditioning methods (Burnett *et al.*, 1987) and have been selected for investigation in this work. Whilst the effect of the preparation method of the VPO precursor, vanadyl phosphohemihydrate ( $\text{VOHPO}_4 \cdot 0.5\text{H}_2\text{O}$ ) on QSS performance has been extensively explored and understood (Hodnett, 1985; Lombardo *et al.*, 1992; Guliants *et al.* 1996), the same cannot be said for the activation and conditioning stages. It is accepted that both stages are critical in the generation and loss of desired (MA forming) and undesired (carbon oxide ( $\text{CO}_x$ ) forming) active sites on the catalyst (Centi *et al.*, 2001; Lombardo *et al.*, 1992); however, there is a strong disconnect between previous literature efforts on the topic.

The existing confusion around the phenomena taking place during VPO activation and conditioning is dependent upon two key issues:

Firstly, the fundamental catalytic reaction mechanisms taking place under *n*-butane/air conditions are still not fully understood, particularly regarding the precise roles of the catalyst surface and bulk phases in the MA and  $\text{CO}_x$  producing reactions. Whilst there is substantial evidence that the presence of a vanadyl pyrophosphate ( $(\text{VO})_2\text{P}_2\text{O}_7$ ) phase (in particular the (100) face) is an important feature to an active and selective VPO catalyst (Centi *et al.*, 2001; Ziółkowski *et al.*, 1990), conflicting evidence exists around the role of  $\text{V}^{5+}$  phases (such as  $\alpha$ - $\text{VOPO}_4$ ) in the reaction mechanisms (Guliants *et al.*, 1996; Zhang-Lin *et al.*, 1994a; Zhang-Lin *et al.* 1994b; Cavani *et al.*, 2010). Ultimately, the ‘end-product’ bulk and surface requirements for an active and selective VPO catalyst at QSS performance are not fully defined, and hence, the actual purposes of the activation and conditioning processes are somewhat unclear.

The second issue arises due to the vast number of possible strategies that can be employed for these activation and conditioning processes, resulting in contradictory results and conclusions in literature. In general, the available strategies fall into two categories (Albonetti *et al.*, 1996):

- *Ex situ* activation and conditioning. Activation is performed in a controlled gas atmosphere (typically air or nitrogen) at temperatures up to 873 K. During this step, the  $\text{VOHPO}_4 \cdot 0.5\text{H}_2\text{O}$  is transformed into a mixture of  $\text{V}^{4+}$  and  $\text{V}^{5+}$  phases. The activated VPO catalyst is then exposed to n-butane/air reaction conditions and undergoes the conditioning step.
- *In situ* activation and conditioning. The VPO precursor is exposed to n-butane/air reaction conditions without prior treatment, undergoing both processes in tandem.

Firstly, considering the *ex situ* methodologies, the activations employed by (Bergeret *et al.*, 1987; Guliants *et al.*, 1995) resulted in a VPO catalyst dominated by poorly crystalline  $(\text{VO})_2\text{P}_2\text{O}_7$ , whilst the air activation in Albonetti *et al.*, (1996) resulted in a catalyst containing  $\text{V}^{5+}$  and some remaining precursor as well as  $(\text{VO})_2\text{P}_2\text{O}_7$ . The final QSS performance developed with respect to bulk composition was largely crystalline  $(\text{VO})_2\text{P}_2\text{O}_7$  in each case. Catalyst performances are not comparable due to the differences in reaction conditions employed. Analysis of the catalyst surface is only attempted in (Albonetti *et al.*, 1996), which compares surface evolution between fresh, non-QSS and QSS VPO catalysts using x-ray photoelectron spectroscopy (XPS). Surface evolution was comparable to that of the bulk catalyst, which featured a gradual phase transformation to a largely crystalline  $(\text{VO})_2\text{P}_2\text{O}_7$  phase ( $V_{\text{ox}}$  of +4.0) over 1000 h on stream.

Lombardo *et al.*, (1992) investigated a variety of activation strategies comprising n-butane in air. It was found that n-butane content and gas flow rate of the feed had a significant effect on catalyst activity and selectivity towards MA at QSS performance. The final bulk composition of the catalysts tested was very similar (mostly crystalline  $(\text{VO})_2\text{P}_2\text{O}_7$  phases) suggesting that there is little correlation between bulk phase and VPO catalyst performance.

The conclusions of Lombardo *et al.*, (1992) were largely based around QSS performance observations, whilst other studies (Abon *et al.*, 1995; Waugh and Taufiq-Yap, 2003) systematically tracked VPO evolution over time. In Abon *et al.*, (1995), the findings revealed a shift in bulk phase structure from an initial  $\text{V}^{4+}/\text{V}^{5+}$  mixture to a more crystalline  $\text{V}^{4+}$  phase over time on stream. The ratio of  $\text{V}^{4+}/\text{V}^{5+}$  at the surface was measured by XPS and increased with time on stream, as did n-butane conversion and MA selectivity. Although the catalyst was activated *in situ*, the findings are in agreement with Albonetti *et al.*, (1996).

Meanwhile, in Waugh and Taufiq-Yap, (2003), temperature programmed desorption (TPD) and temperature programmed reduction (TPR) served as useful analytical techniques to measure the number of monolayers of oxygen removed from the VPO catalyst. Monolayers of oxygen were progressively removed with time due to surface and bulk morphology changes.

Some insights may be afforded via forced unsteady-state experiments using a temporal analysis of products (TAPs) reactor system. Schuurman and Gleaves, (1994, 1997) applied both steady-flow and transient-response experiments on a fully conditioned VPO catalyst. They found that the apparent activation energy for n-butane oxidation could be reduced following exposure of the catalyst to oxygen pulses over a short period of time. They proposed a two site model comprising high and low activation energy sites associated with  $V^{4+}$  and  $V^{5+}$  VPO phases, respectively, with the number of both types of site being a strong function of the overall oxidation state of the catalyst.

Transient analysis of VPO catalysts has also been carried out using a tapered element oscillating microbalance (TEOM) (Wang *et al.*, 2000; Wang and Barteau, 2001). The TEOM assessed rates of reduction and oxidation of a VPO catalyst under a variety of conditions by observing changes in catalyst mass. This technique produced detailed kinetic models; however, the reduction and oxidation steps of the catalyst were considered separately rather than under n-butane/air conditions.

Further transient kinetic investigations include decoupling oxidation and reduction steps of  $VOPO_4$  in a TAP reactor system (Mills *et al.*, 1999) and kinetic investigations under separate reduction and oxidation steps (Lorences *et al.*, 2004).

It is clear from these studies that a lack of a common and systematic methodology has prevented full understanding of the evolution of VPO catalysts during activation and conditioning. This relates to the analysis and catalyst testing techniques used but also the large differences in catalyst preparation, activation and conditioning methods between different research works. A critical missing element is a kinetic and activity modelling study which could be utilised to explain the generation and loss of active sites on the catalyst under reaction conditions during this period of operation.

### 4.1.1 Chapter Objectives

Selective oxidation of *n*-butane using a VPO catalyst has been identified as a model candidate system to develop experimental and modelling techniques to understand catalyst evolution during activation and conditioning. The conditioning step of an *ex situ* activated VPO catalyst will be examined in detail in an integral mode reactor under a range of conditions. The objectives for the work presented in this chapter are therefore as follows:

- Develop and demonstrate a methodology to understand the performance evolution that catalysts, using VPO as a model system, undergo during conditioning, which will include the following:
  - Experimental catalyst reaction testing methods.
  - Kinetic and activity modelling application to data.
  - Supporting evidence from catalyst characterisation methods.

## 4.2 Materials and methods

### 4.2.1 Sample preparation and properties

The VPO precursor was synthesized using an organic preparation method as described in US patent 4,567,158 (Wrobelski *et al.*, 1986). This methodology comprises introducing V<sub>2</sub>O<sub>5</sub> into an alcohol medium to reduce the average vanadium valence state to less than +5. This forms a slurry which is then contacted with an alcohol modifying agent, further reducing some of the vanadium in the mixture to +4. A pentavalent phosphorus compound is then added to the mixture to form a phosphorus–vanadium mixed oxide catalyst precursor. This is subsequently recovered, dried and formed into pellets. The P:V ratio of the catalyst was 1.0.

The pellet batch was subsequently activated using a methodology based on US patent 5,137,860 (Ebner and Andrews, 1992). This comprises heating the formed catalyst precursor in an atmosphere comprising air, steam and nitrogen to a temperature not exceeding 573 K. It is subsequently maintained at this temperature for a nominal time. The temperature is then ramped at a rate between 2 and 12 °C per minute to eliminate water of hydration from the precursor. The temperature is then held at a value in the 623 – 823 K range, still under air and

steam to provide a vanadium oxidation state between +4.0 and +4.5. The gas atmosphere is subsequently switched to a non-oxidising nitrogen–steam atmosphere, at the same temperature for a defined time to complete the activation process.

#### 4.2.2 Micro-reactor test rig

Selective oxidation of *n*-butane was carried out in a fixed-bed, down-flow, steel micro-reactor at atmospheric pressure. Five parallel tubes were used with inner diameter of 3 mm and length of ~20 cm.

Parallel difference testing, a methodology described in detail by Birtill, (2003) (see Section 2.1.2.2 for background detail), is used to investigate the performance evolution of VPO catalysts operating in integral mode reactors. The simple setup for this study comprises four tubes in parallel containing 0.165, 0.33, 0.495 and 0.66 g, respectively. Flow rate ( $30 \text{ ml min}^{-1}$ ), inlet reactant concentration and temperature are the same for each tube throughout the test. The use of the four tubes allows subtraction between the exit concentrations of each catalyst bed at discrete times on stream. This enables performance to be broken down into four sectors of equal length down the bed. Experimental repeats were carried out as a check for reproducibility.

Parallel difference tests were carried out for up to 100 h on stream. At certain times on stream, the flow rate through the reactors was reduced, so that *n*-butane conversion across the 0.66 g ‘full’ bed was restored to its initial level from the start of the test. Relative performances of each sector of the catalyst bed (via product yields) could therefore be compared to their initial values. This provides information on the influence of axial concentration gradients on the evolution of catalyst performance. Selectivity evolution of separate reaction pathways can also be investigated by this test which can be linked to fundamental changes to the catalyst.

VPO catalysts were also tested in a differential mode setup; 50 mg catalyst was used to ensure *n*-butane conversions which were <10% in  $30 \text{ ml min}^{-1}$  (standard temperature and pressure) flow conditions.

Experiments were designed to ensure the presence of plug-flow conditions and the absence of heat and mass transport limitations allowing for the measurement of intrinsic rates. Full details of reactor setup and catalyst properties are shown in Table 4.1. This was

confirmed by use of key calculations set out in literature (Perez Ramirez *et al.*, 2000) including calculation of intraparticle mass transport limitations (Wheeler Weisz Modulus), Mears' criterion for intraparticle heat transport limitations and radial temperature gradients. A  $180 < d_p < 250 \mu\text{m}$  sieve fraction of VPO powder was chosen for testing to minimise wall effects in the reactor (Chu and Ng, 1989) and prevent large pressure drops (Ergun, 1952).

**Table 4.1: List of properties of catalyst and experimental setup conditions.**

<b>Experimental property</b>	<b>Value</b>
<b>Catalyst Mass (g)</b>	0.165 – 0.66
<b>Catalyst Pore Volume (<math>\text{cm}^3 \text{g}^{-1}</math>)</b>	0.13
<b>Catalyst Pore Size (<math>\text{\AA}</math>)</b>	610
<b>Catalyst BET surface area (<math>\text{m}^2 \text{g}^{-1}</math>)</b>	20
<b>Catalyst particle size (<math>\mu\text{m}</math>)</b>	180 – 250
<b>Reactor diameter (mm)</b>	3
<b>Temperature range (K)</b>	623 – 683
<b>Feedstock (v/v% <i>n</i>-butane – air)</b>	2 / 98
<b>Flow Rate (<math>\text{ml min}^{-1}</math>)</b>	30

Transport limitations were checked at the extreme of the test programme operation, namely the 1st sector of a VPO catalyst bed operating at 683 K at  $t = 0$  h on stream. Apparent *n*-butane conversion rate was  $1.08 \text{ mmol kg cat}^{-1} \text{ s}^{-1}$ . Under these conditions, the radial heat transport gradient was 2.2 K, and both internal and external mass transfer efficiencies were >99%. These values satisfy threshold criteria.

Each reactor was packed, firstly with silicon carbide ( $180 < d_p < 250 \mu\text{m}$ ), then VPO catalyst (up to 0.66 g), then the remainder with silicon carbide. This ensured that pressure drops, although negligible, were constant across all reactor tubes. Thermocouples were positioned in the tube before this process, so that one registers the temperature at the catalyst bed inlet and the other at the catalyst bed outlet. A West 6400 temperature controller was used to control the temperature of the furnace block to within  $\pm 2$  K of the set point value. A Grant Remote Squirrel (1250 Series) was used to log temperature data from each

thermocouple periodically. Throughout the test programme, inter- and intra- tube axial temperature differences were within 2 K of each other.

Gases (air or helium) with/without *n*-butane were fed to each micro-reactor tube using a Brookes PID mass flow controller. Maximum v/v% concentration of *n*-butane within the feed was 2%. Flow through each reactor tube was up to 30 ml min<sup>-1</sup> (standard temperature and pressure, STP) during the test programme.

Reactor outlet gases were analysed by gas chromatography (Varian CP-3800); a thermal conductivity detector analysed carbon oxides, nitrogen and oxygen. The carrier gas used was helium. The setup comprised a Hayesep Q (flow through: 25 ml min<sup>-1</sup> at 1.7 bar gauge) with molecular sieve column (flow through: 27 ml min<sup>-1</sup> at 2 bar gauge) in series; the carrier gas was helium. Typical retention times were 0.7 min for CO<sub>2</sub>, 1.6 min for O<sub>2</sub>, 2.1 min for N<sub>2</sub> and 3.1 min for CO. A flame ionisation detector analysed *n*-butane, MA and trace acrylic and acetic acid. The carrier gases used were air and hydrogen. A capillary column was used (flow through: 10 ml min<sup>-1</sup> at 0.45 bar gauge). Typical retention times were 1.2 min for *n*-butane, 5.5 min for MA, and trace acrylic and acetic acid were eluted in the 2–3 min range.

The calculated carbon balance was between 99% and 101% for all experiments. As the amount of acrylic and acetic acid formed was negligible (yields of < 0.5% (combined) throughout the dataset), the molar carbon balance across the reactor simplifies to:

$$\text{Moles } n\text{-butane (In)} = \text{Moles } n\text{-butane (Out)} + \text{Moles MA (Out)} + 0.25 * \text{Moles CO}_x \text{ (Out)} \quad (4.1)$$

Reaction testing was carried out in the range of 623 – 683 K, chosen to encompass typical operating temperatures of an industrial VPO catalyst. For each test run, the catalyst beds were heated to set point temperature under a helium flow. At the set point, this was switched to 2% *n*-butane in air for all experiments. After each experimental run, catalysts were cooled down in a helium environment, to minimise changes to the VPO catalyst during the shutdown step. After testing, VPO catalyst samples were retained for future characterisation studies.

One micro-reactor tube filled with silicon carbide acted as a blank experiment. 2% *n*-butane in air was fed under reaction conditions to ensure no homogenous reaction contributed to the overall reaction.

### 4.2.3 Catalyst characterisation

Fresh and post-reactor used VPO samples were characterised by the following *ex situ* techniques:

- *X-ray diffraction*: Samples were tested using a Siemens D5000 diffractometer using Cu Ka X-rays at wavelength 1.5406 Å.
- *Raman spectroscopy*: Samples were tested using a JY Horiba Infinity Spectrometer.
- *X-ray photoelectron spectroscopy*: Samples were tested using a Thermo Escalab 250. The exciting radiation used was monochromatised aluminium Ka radiation, 200 W, 650 µm spot size.
- *V<sub>ox</sub> determination via titration*: Samples were tested using a Metrohm 809 Titrando auto-titration device using a methodology previously described in literature (Busca *et al.*, 1986). Dissolved samples were first titrated using 0.1 N KMnO<sub>4</sub> to fully oxidise the VPO compounds into a V<sup>5+</sup> state. A second titration using 0.1 N Mohr's Salt was then carried out to fully reduce the VPO compounds into a V<sup>4+</sup> state. The following equation was then used to determine the bulk V<sub>ox</sub> of the VPO catalyst:

$$V_{ox} = 5 - \frac{(\text{vol. KMnO}_4 \text{ added})}{(\text{vol. Mohr's salt added})} \quad (4.2)$$

### 4.2.4 Kinetic modelling

For kinetic modelling purposes, parametric estimation within the kinetic models was carried out using Athena Visual Studio<sup>9</sup> software. A plug-flow reactor model was used. A Bayesian estimation routine was used for fitting of model parameters with the objective function being minimised using a forward difference method. To minimise cross-correlation between activation energy ( $E_a$ ) and pre-exponential factor ( $A_i$ ) parameters, a re-parameterised Arrhenius equation was used:

$$k_i = A_{i,613} \cdot \exp\left(\left(\frac{E_a}{T_{base} \cdot R}\right) \cdot \left(1 - \frac{T_{base}}{T}\right)\right) \quad (4.3)$$

---

<sup>9</sup> Athena Visual Studio 14.2, Stewart & Associates Engineering Software, Inc.

Where base temperature,  $T_{base}$ , is 613 K, and  $A_{i,613}$  is the value of the rate constant,  $k_i$  at 613 K. Kinetic model fitting was carried out at nine discrete time on stream points between 0.4 and 11.4 h. At each time on stream, the data set comprised 28 independent observations (seven temperatures each with four sector profiles).

## 4.3 Results

### 4.3.1 Parallel difference testing

Parallel difference tests were carried out over a temperature range of 623 – 683 K. Figure 4.1 shows an example of raw VPO catalytic performance evolution with time on stream. Values are reported on an intrinsic rate basis for each sector, calculated as the change in a reactant or product concentration over a sector divided by the residence time of the gas within that sector. As each sector contains the same mass, these values are directly representable on a mass basis also. In this example, carried out at 653 K, total *n*-butane conversion across the entire bed was 74% at the start and 61% after 60 h on stream. It is important to note that CO and CO<sub>2</sub> formation was considered as a lumped CO<sub>x</sub> term across the study. This was due to the fact that CO:CO<sub>2</sub> ratio across all sectors, temperatures and times on stream remained roughly steady in the range of 1.5–1.7.

There are some key differences in the approach to QSS performance for each sector. A sharp initial decline is seen in the 1<sup>st</sup> sector for both MA and CO<sub>x</sub> formation rates over the first 5 h which is followed by a much slower rate of change over the rest of the test period. The 2<sup>nd</sup>–4<sup>th</sup> sectors show a very different behaviour to the 1<sup>st</sup> sector with respect to MA formation rates. The 2<sup>nd</sup> sector shows a very slow decline, whilst the 3<sup>rd</sup>/4<sup>th</sup> sectors actually improve slightly at the start of the test. Meanwhile, for CO<sub>x</sub> formation rates, a similar decline pattern is seen in each sector of the catalyst bed although the 1<sup>st</sup> sector shows the greatest losses. On inspection, evolution of *n*-butane consumption appears much the same as that for MA formation, owing to the high selectivity of the catalyst (>70%) towards MA under these conditions. It is important to note that these changes are happening on a very short (order of hours) time scale in context to a VPO catalyst's working life, which is in the order of years.

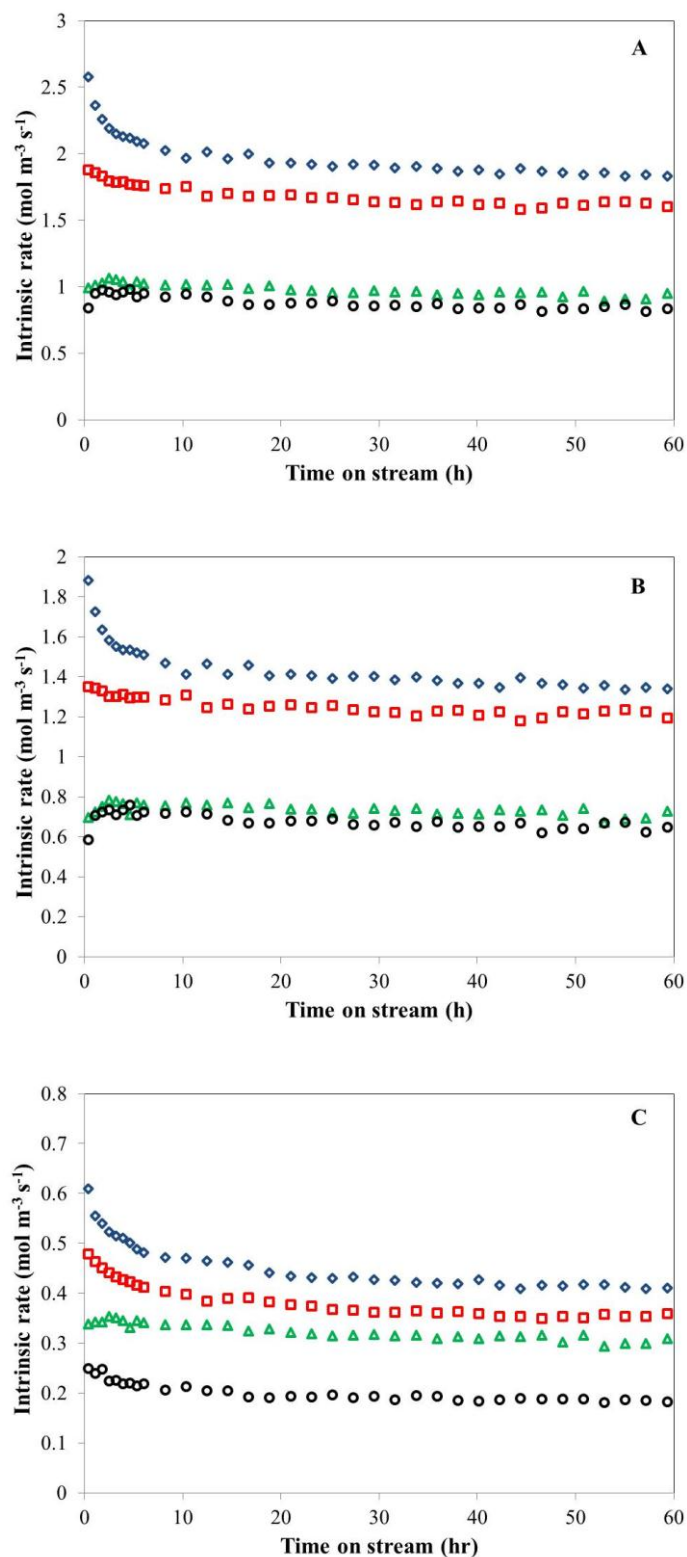


**Figure 4.1: Time on stream intrinsic rate evolution for individual sectors of an example run for (A) *n*-butane consumption, (B) MA formation, (C) CO<sub>x</sub> formation over a VPO catalyst. Conditions: 30 ml min<sup>-1</sup> flow, 2% v/v *n*-butane/air reactor inlet concentration and 653 K. Symbols denote: (◇) 1<sup>st</sup> sector, (□) 2<sup>nd</sup> sector, (△) 3<sup>rd</sup> sector, (○) 4<sup>th</sup> sector.**

A comparison of full bed (sectors 1–4 combined) *n*-butane conversions in the 623 – 683 K temperature range is shown in Figure 4.2. For each temperature, *n*-butane conversion drops between the initial reading and 17 h on stream. At 17 h, the flow rate through the reactors was adjusted to restore initial *n*-butane conversion across the full bed. In Figure 4., the reduced flow rates required to achieve this are very similar at all temperature points, with all values in the 23–24 ml min<sup>-1</sup> range. The level of flow rate reduction required to restore initial conversion is a good indicator of the extent of activity loss in a catalyst bed. This suggests that the rate of activity evolution during conditioning may be temperature independent (for the tested inlet conditions of 2% *n*-butane in air; further investigation would be needed for other reactor inlet feeds).

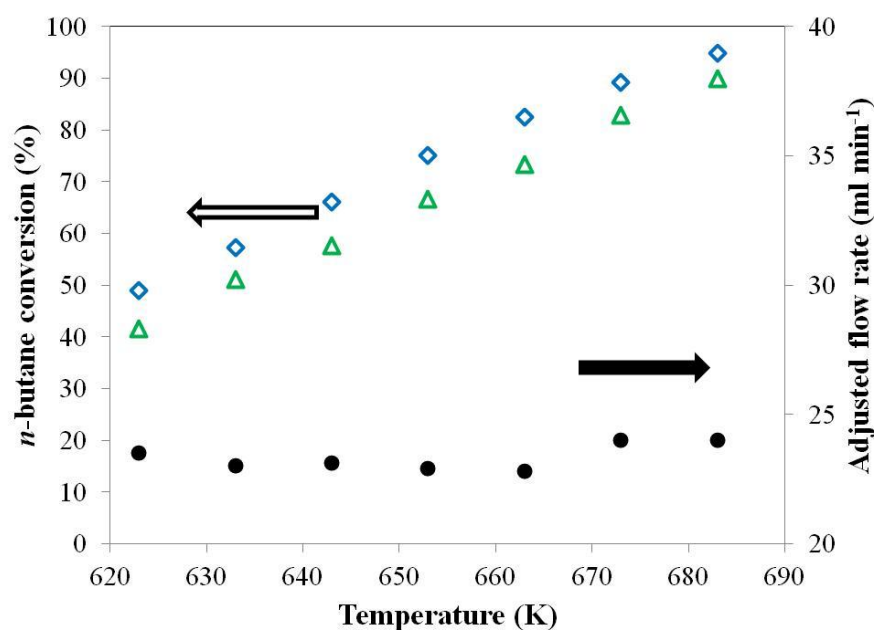


**Figure 4.2: Evolution of *n*-butane conversion over the full catalyst bed between initial reading (t = 0.4 h) (◇) and 17 h on stream (△) for different reaction temperatures. (●) represents the adjusted reactor inlet flow rates required at 17 h on stream to achieve initial *n*-butane conversion over the full catalyst bed.**

Figure 4.3 makes a comparison of the sector contributions to overall catalyst bed performance at the initial and restored initial conversion readings. Sector MA and CO<sub>x</sub> yields were calculated using (Eqs. (4.4a) and (4.4b)) and were subsequently normalised. It is important to note that in these equations, the term ‘reactor inlet feed’ refers to 2% *n*-butane/air.

$$\text{Yield MA} = \frac{\% \text{ MA formed over sector(s)}}{\% \text{ n-butane in reactor inlet feed}} \quad (4.4a)$$

$$\text{Yield CO}_x = \frac{\% \text{ CO}_x \text{ formed over sector(s)}}{\% \text{ n-butane in reactor inlet feed}} \quad (4.4b)$$

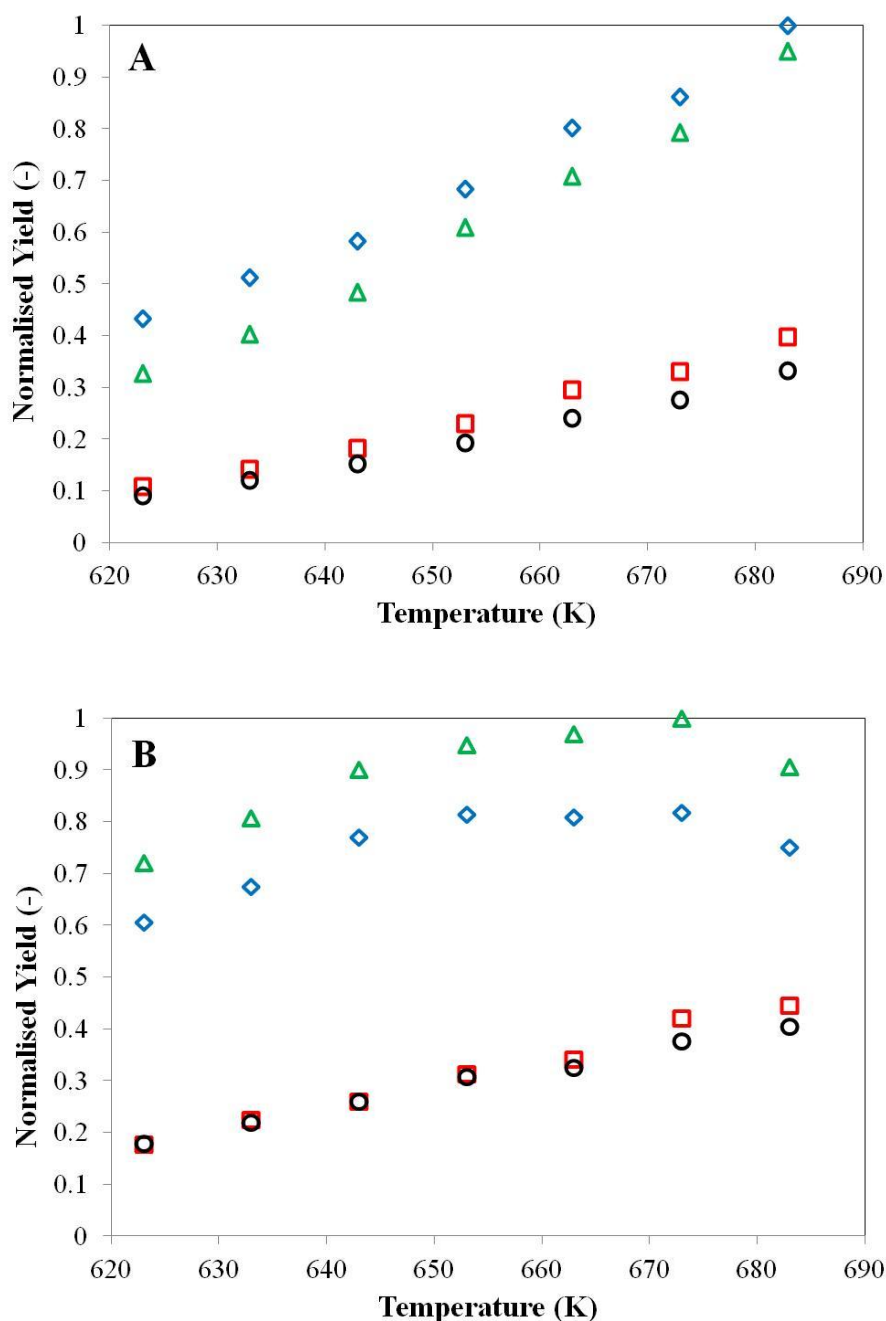


**Figure 4.3: Performance evolution over A) Sector 1, B) Sectors 2-4 combined. (◇) and (□) denotes initial MA and CO<sub>x</sub> yields respectively, (△) and (○) MA and CO<sub>x</sub> yields respectively under adjusted inlet flows at 17 h on stream.**

In sector 1 (Figure 4.3A), a loss of yield for both MA and CO<sub>x</sub> formation is seen at restored initial conversion. Meanwhile, sectors 2–4 (Figure 4.3B) evolve quite differently over the first 17 h. Relative yields with respect to MA formation have increased, whilst for CO<sub>x</sub> formation, the yields remain roughly unchanged.

Yields of MA and CO<sub>x</sub> also change very differently with temperature in sectors 2–4. Whilst CO<sub>x</sub> yields systematically increase with temperature, this does not happen to the MA yields which appear to decline at the highest temperatures. The latter observation suggests that MA may either be re-oxidised to CO<sub>x</sub> or inhibited by its own formation at high *n*-butane conversions.

The observations in Figure 4.3 firstly suggest that the mechanism behind the evolution of catalyst performance is driven by concentration of reactants (*n*-butane and/or oxygen). The 1<sup>st</sup> sector of the reactor sees the greatest apparent loss in catalyst performance, and it is in this sector that reactant concentrations are highest.

The problem is, however, clearly more complex than this as there are differences in performance evolution for the MA and CO<sub>x</sub> formation routes in sectors 2–4. Furthermore, an Arrhenius Plot analysis of the 1<sup>st</sup> sector (Table 4.2) reveals differences in the two product formation routes. The apparent activation energy ( $E_a$ ) for MA formation is ~15–20 kJ mol<sup>-1</sup> lower at the initial reading compared to 17 h on stream. This ‘drift’ is a similar observation to that made by Schuurman and Gleaves, (1997) under forced unsteady-state testing. Meanwhile, there are no changes in apparent  $E_a$  observed for CO<sub>x</sub> formation during the conditioning period.

**Table 4.11: Apparent activation energies for MA and CO<sub>x</sub> product formation in the 1<sup>st</sup> sector obtained via Arrhenius Plot ( $R^2 > 0.99$  in all cases).**

<b>Product</b>	<b><math>E_a</math> (initial)</b> <b>(kJ mol<sup>-1</sup>)</b>	<b><math>E_a</math> (17 h)</b> <b>(kJ mol<sup>-1</sup>)</b>	<b><math>E_a</math> (17 h, restored)</b> <b>(kJ mol<sup>-1</sup>)</b>
<b>MA</b>	49.1	67.2	62.6
<b>CO<sub>x</sub></b>	77.3	80.3	76.6

Figure 4.4 shows the evolution of MA intrinsic selectivity, which is seen to systematically improve over the first 17 h at all reaction temperatures. This shows that the

relative proportion of MA and CO<sub>x</sub> producing sites on the VPO catalyst have changed over time. Hence, there must be a minimum of two different active sites on the catalyst which are both:

- Evolving at different rates.
- Declining in population to different extent over the testing period.

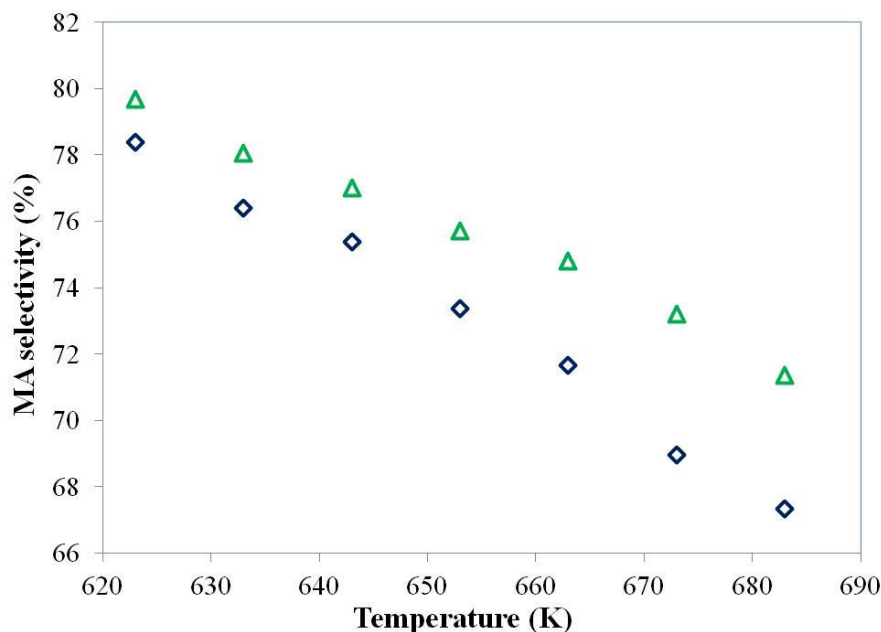


**Figure 4.4: Evolution of MA intrinsic selectivity of a VPO catalyst across a full catalyst bed for different reaction temperatures. (◇) denotes initial MA selectivity, (△) MA selectivity under adjusted inlet flows at 17 h on stream.**

### 4.3.2 Characterisation

XRD analysis of fresh and post-reactor use samples revealed very little change to the bulk structure during the conditioning period. All catalysts were found to contain significant amounts of (VO)<sub>2</sub>P<sub>2</sub>O<sub>7</sub> via the technique (Gulians *et al.*, 1996), with reflections at 18.5°, 23°, 28.5°, 30° and 33.7°. Graphite peaks were also observed at 26.7° and ~34.5° in some cases. A shoulder between 28.5° and 30° is observed. Reflections in this region could be characteristic of  $\gamma$ -VOPO<sub>4</sub> or  $\alpha$ <sub>I</sub>-VOPO<sub>4</sub>. Degree of crystallinity afforded by the sharpness of observed peaks (full width at half maximum) changes minimally with time, reactor axial position of the catalyst or reaction temperature. An example of this is shown in Figure 4.5 for time on stream evolution of the 1<sup>st</sup> sector of the catalyst bed.

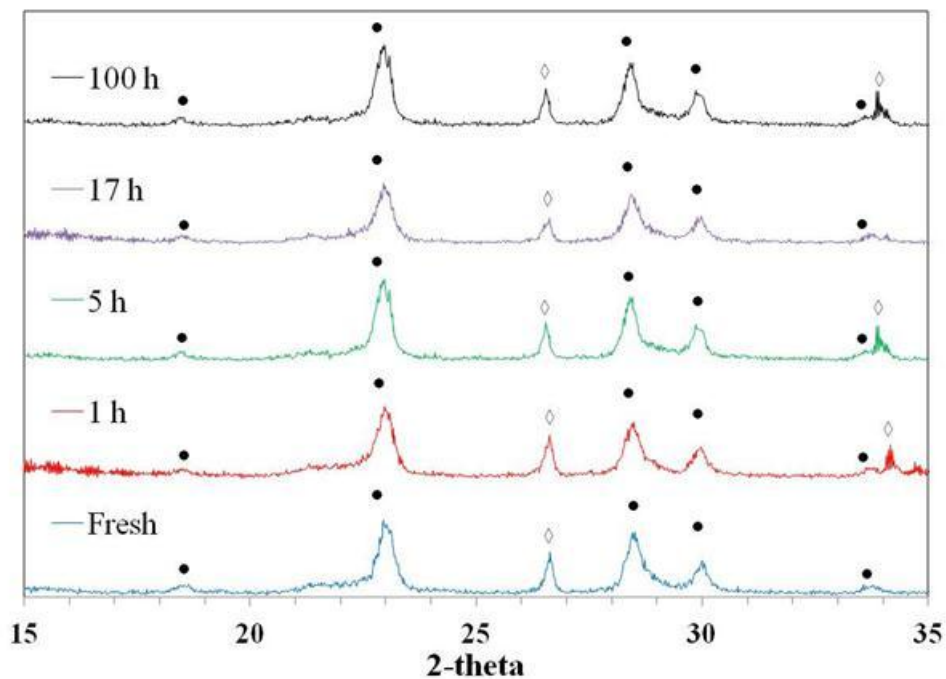


**Figure 4.5: XRD analysis of VPO catalyst from the 1<sup>st</sup> sector of the catalyst bed, before and after testing at 653 K, 2% *n*-butane in air reactor inlet conditions, 30 ml min<sup>-1</sup> flow.**

**(●) denotes (VO)<sub>2</sub>P<sub>2</sub>O<sub>7</sub> phase (◇) denotes graphite.**

Raman spectra for all samples, regardless of time on stream, reaction temperature or axial position, appear to be similar, with only small variations. Spectra plotted as a function of time on stream are shown in Figure 4.6. Again, the in depth work of Gulians *et al.*, (1996) has been used for interpretation. In all cases, a sharp peak is detected around 920 cm<sup>-1</sup>, which is characteristic of (VO)<sub>2</sub>P<sub>2</sub>O<sub>7</sub>. A weakly intense response is also seen at 1180–1190 cm<sup>-1</sup>, again characteristic of (VO)<sub>2</sub>P<sub>2</sub>O<sub>7</sub>. A mixture of peaks is also seen in the 1015–1045 cm<sup>-1</sup> range. The presence of a doublet in the fresh sample at c.a. 1020 and 1035 cm<sup>-1</sup> is characteristic of  $\gamma$ -VOPO<sub>4</sub>. The intensities in this region for the used samples are less clear and could constitute either  $\gamma$ -VOPO<sub>4</sub> or  $\alpha_1$ -VOPO<sub>4</sub>. A mixture of low intensity responses is seen c.a. 940 and 980 cm<sup>-1</sup> at fresh and all times on stream which could again relate to either  $\gamma$ -VOPO<sub>4</sub> or  $\alpha_1$ -VOPO<sub>4</sub>.

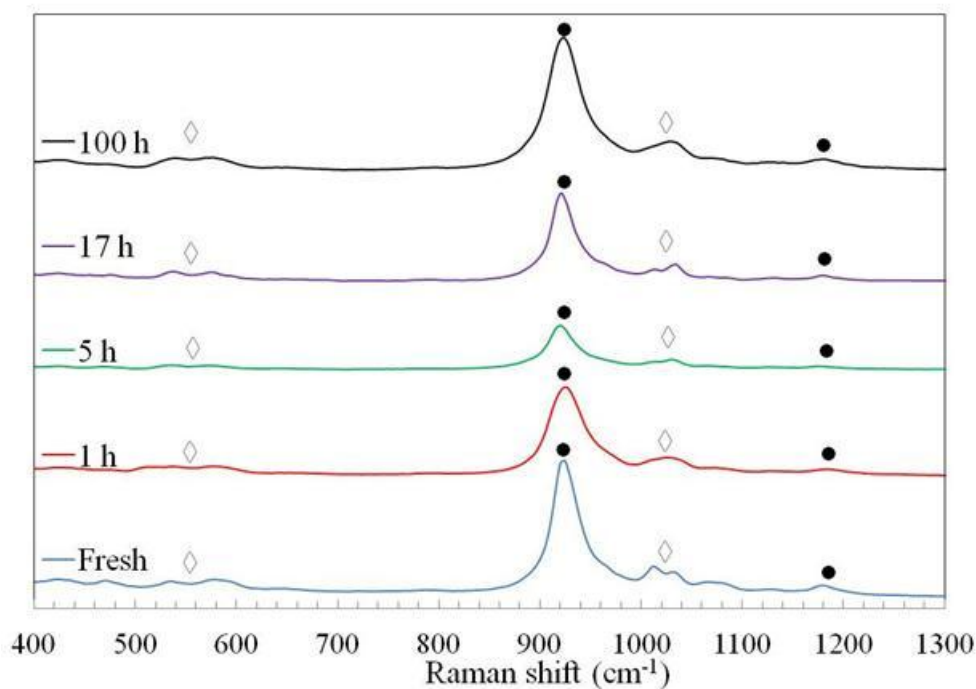


**Figure 4.6: Raman analysis of VPO catalyst from the 1<sup>st</sup> sector of the catalyst bed, before and after testing at 653 K, 2% *n*-butane / air reactor inlet conditions, 30 ml min<sup>-1</sup> flow. (●) denotes peaks assigned to (VO)<sub>2</sub>P<sub>2</sub>O<sub>7</sub> and (◇) denotes peaks assigned to VOPO<sub>4</sub> phases.**

The measured average bulk  $V_{ox}$  of the VPO catalyst is seen to decrease slowly with time on stream. The majority of changes to catalyst performance in all parallel difference tests were seen during the first 10 h of operation; however, Figure 4.7 shows that the bulk  $V_{ox}$  of the catalyst changes very little during this time, regardless of sector position. By 100 h on stream, the average bulk  $V_{ox}$  of the catalyst bed is seen to decline to +4.10–4.15. It has previously been noted in the literature that VPO catalysts tend towards a bulk  $V_{ox}$  of +4.0 with a few weeks on stream, such as in (Albonetti *et al.*, 1996). This is being approached with this particular catalyst, but the changes do not correlate with catalyst performance evolution observed during the first few hours on stream.

Bulk  $V_{ox}$  measurements were also made after 17 h on stream for VPO catalysts conditioned at 623 K and 683 K. Their  $V_{ox}$  values were +4.25 and +4.30, respectively; very similar within measurement error. This suggests conditioning temperature has little influence upon transitions within the catalyst bulk in the range 623 – 683 K.

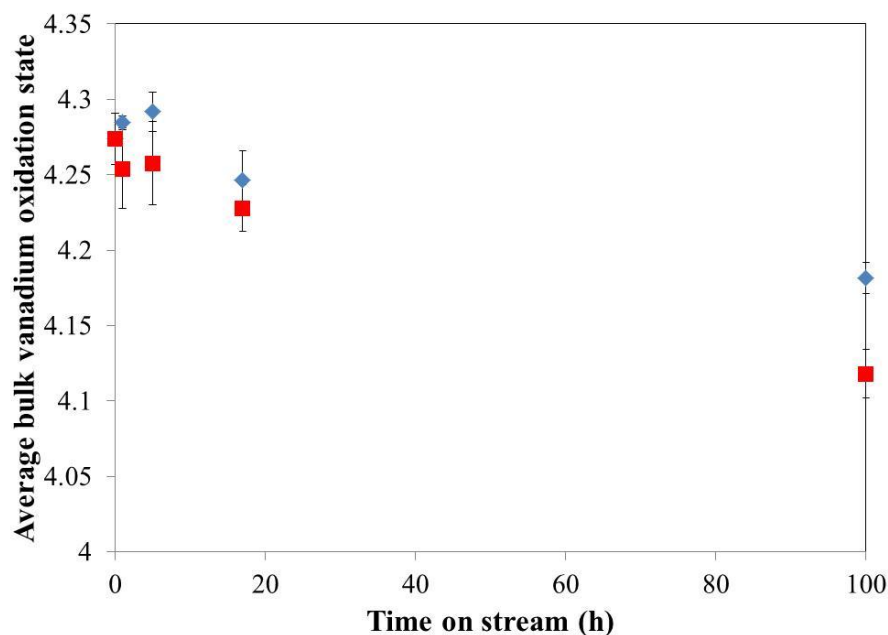


**Figure 4.7: Measured bulk  $V_{ox}$  via auto-titration of VPO catalyst before and after testing at 653 K, 2%  $n$ -butane in air reactor inlet conditions, 30 ml min<sup>-1</sup> flow. (◆) denotes 1<sup>st</sup> sector, (■) 4<sup>th</sup> sector. Error bars denote standard deviation over three samples measured.**

The evolution of the catalyst surface as a function of treatment/time on stream was studied using XPS. Figure 4.8 shows that the peak binding energies for both the V2p<sub>3/2</sub> and O1s signals shift during the initial first 5 h of operation. Using a calculation method in Coulston *et al.*, (1996), evolution of surface  $V_{ox}$  with time on stream could be ascertained. For the fresh and 1 h conditioned catalyst, surface  $V_{ox}$  was calculated to be +4.2. For observations at 5, 17 and 100 h, this dropped to +4.1. Also, there appears to be some shifts in the shape of the V2p<sub>3/2</sub> signal, particularly during the first 5 h. This may suggest that the phases present at the VPO surface are changing to a certain extent. This may be in line with Raman observations which suggest the presence of either  $\gamma$ -VOPO<sub>4</sub> or  $\alpha_1$ -VOPO<sub>4</sub>, the former of which appears to be more predominant in the fresh sample.

Phosphorus–Vanadium (P:V) ratio was also calculated and was found to be fairly consistent at ~1.9 regardless of time on stream, temperature or axial position. The values observed agree with literature that the surface of a working VPO catalyst is phosphorus enriched compared to the bulk (Hodnett *et al.*, 1983).

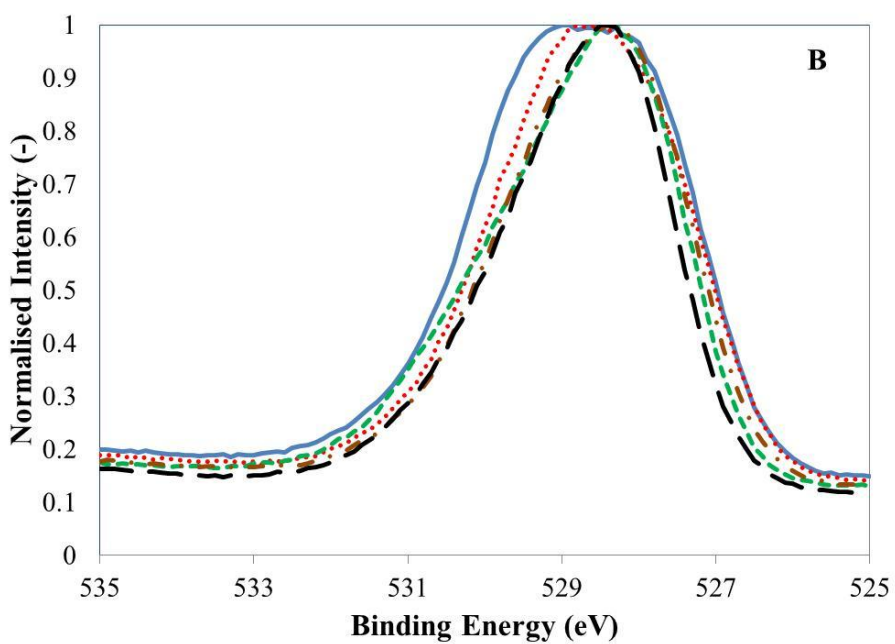
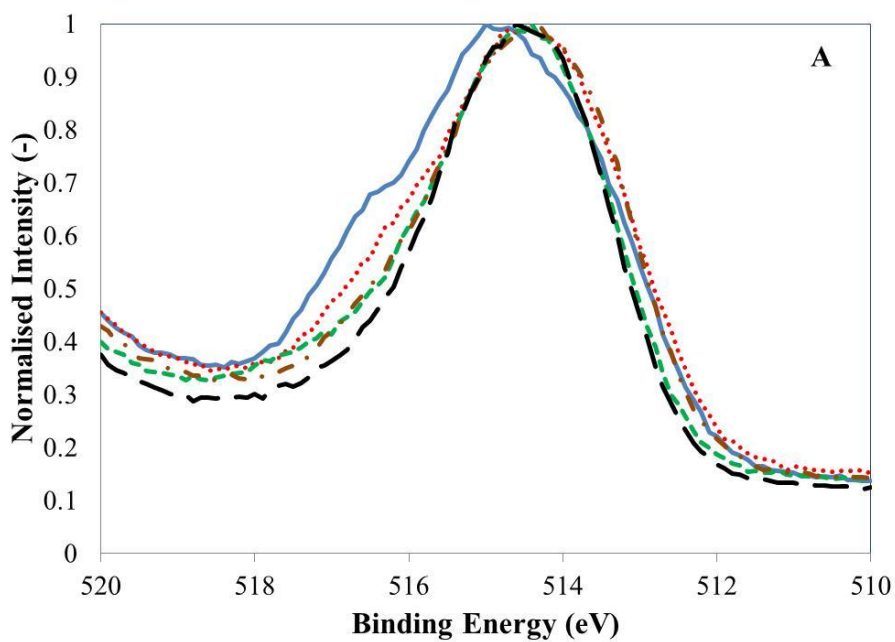


**Figure 4.8: XPS analysis of VPO catalyst from the 1<sup>st</sup> sector of the catalyst bed, before and after testing at 653 K, 2% *n*-butane in air reactor inlet conditions, 30 ml min<sup>-1</sup> flow. a) denotes V2p<sub>3/2</sub> signal, b) O1s signal. (—) Fresh VPO, (···) 1 h, (- - -) 5 h, (- · - · -) 17 h, (- - - -) 100 h.**

### 4.3.3 Testing in differential mode

In separate experiments, 50 mg of VPO catalyst was conditioned at either 623 or 683 K in a flow of 2% v/v *n*-butane in air. After 48 h on stream, VPO performance with respect to *n*-butane consumption, MA formation and CO<sub>x</sub> formation had reached a QSS performance level. Following this, the catalyst was exposed to a series of temperature ramps. These are shown in graphs A–C in Figure 4. (noting that *t* = 0 h in this case follows an initial 48 h of conditioning).

Inspection of the graphs in Figure 4.9 shows that the QSS performance developed under temperatures of either 623 K or 683 K is almost identical. This suggests that conditioning temperature employed has little effect on the final catalyst surface developed, within the scope of this study. The extent that this is true in the >683 K range would need to be ascertained by further study. This confirms the initial observations made in Figure 4.2. The specific rates for *n*-butane conversion measured at 623 and 683 K were  $\sim 1.5 \times 10^{-8}$  and  $5.5 \times 10^{-8}$  mol m<sup>2</sup> s<sup>-1</sup>. These rates are comparable with differential rates measured previously in literature (Zhang-Lin *et al.*, 1994a; Wang and Barteau, 2001; Hodnett *et al.*, 1983).

Figure 4.9 also shows that when the VPO catalyst undergoes an imposed temperature step change, a new QSS performance is immediately observed. In effect, changing reaction temperature on a QSS operation VPO catalyst does not appear to impose a further transient period of performance on the catalyst (i.e. further conditioning). This suggests that the surface is not inherently modified (e.g. progressively reduced or oxidised) as a result of changing reaction temperature over the range of test conditions employed.

When the VPO catalyst is returned to its reference ‘conditioning’ temperature (623 or 683 K) following a temperature step change, the catalyst also returns to its original QSS reference performance. This shows that altering reaction temperature at QSS performance does not invoke any irreversible effects on the catalyst which would result in a generation or loss of active sites.

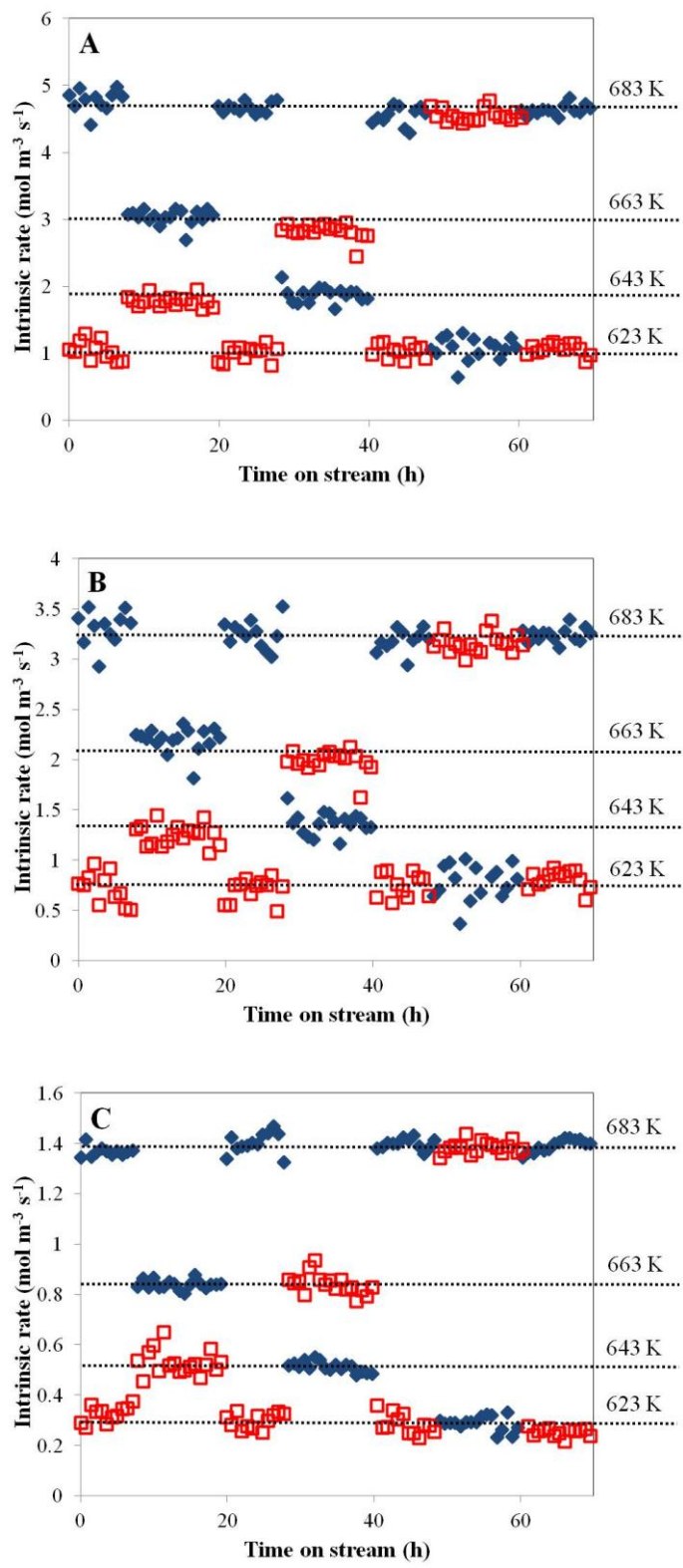


**Figure 4.9: Differential mode testing of VPO catalyst under steady state performance following 48 hours conditioning. Inlet feed 2% v/v *n*-butane in air, (♦) denotes catalyst conditioned at 623 K, (□) at 683 K. Graph a) *n*-butane consumption, b) MA formation, c) CO<sub>x</sub> formation.**

## 4.4 Kinetic modelling

### 4.4.1 Apparent kinetics

The parallel difference test provides an axial concentration profile of each reactant and product along the catalyst bed at each discrete time on stream measurement. Simple power law-type relationships for a parallel reaction network can be applied to the data (Eqs. (4.5a) and (4.5b)). A concentration dependence on *n*-butane has been chosen for the both MA and CO<sub>x</sub> forming reactions, based on differential mode observations. Furthermore, it is the limiting reactant in the feed (at 2% v/v compared to 21% O<sub>2</sub>) and is also unanimously cited as part of unsteady-state (Schuurman and Gleaves, 1997; Mills *et al.*, 1999) and steady state (Escardino *et al.*, 1973; Buchanan and Sundaresan, 1985; Schneider *et al.*, 1987; Bej and Rao, 1991; Sharma and Cresswell, 1991; Golbig and Werther, 1997) kinetic models in literature.

$$r_{MA} = k_1[C_4H_{10}]^{n_1} \quad (4.5a)$$

$$r_{CO_x} = k_2[C_4H_{10}]^{n_2} \quad (4.5b)$$

Log–log plots of (*r<sub>i</sub>*) against [C<sub>4</sub>H<sub>10</sub>] were generated to determine apparent order in *n*-butane (*n<sub>i</sub>*) and apparent rate constant (*k<sub>i</sub>*) via gradient and y-intercept, respectively. *R*<sup>2</sup> values from this fitting process were >0.9 across the data sets. Figure 4.10A shows how *n<sub>i</sub>* systematically changes with time towards apparent 1<sup>st</sup> order for the MA formation reaction at different temperatures. In Figure 4.10B, *n<sub>i</sub>* for CO<sub>x</sub> formation changes with both time and temperature.

This result instantly shows that the assumption of a simple parallel reaction network is wrong; therefore, reaction orders in a correct model should not change with time or temperature. More complex models are therefore needed to describe the selectivity evolution discussed earlier.

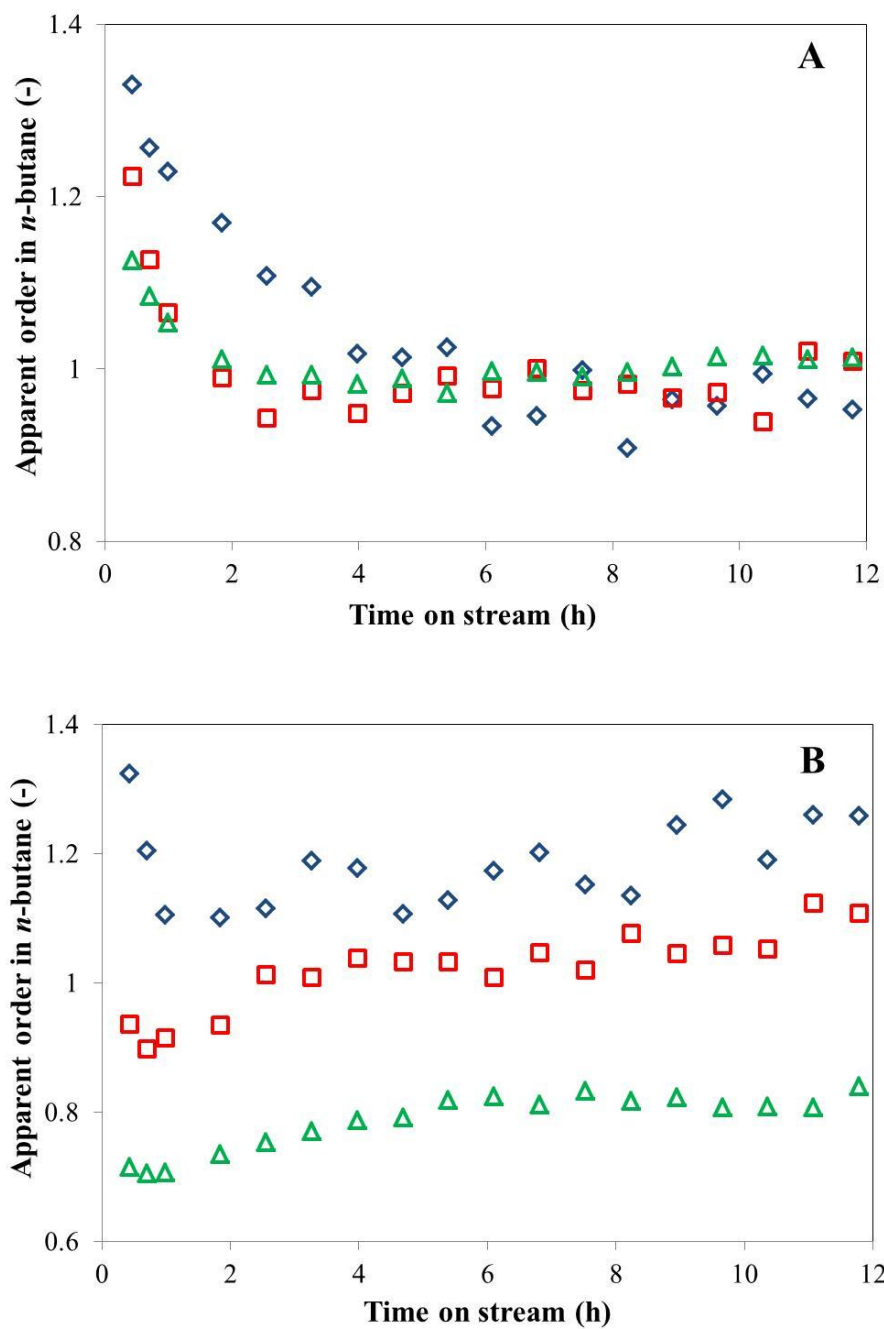


**Figure 4.10: Evolution in apparent reaction order in *n*-butane with time on stream for A) MA formation, B) CO<sub>x</sub> formation. (◇) 633 K, (□) 653 K, (△) 683 K.**

#### 4.4.2 Triangular networks

Triangular network models are the main focus as there is strong evidence in the aforementioned results that MA re-oxidation is playing a role in the reaction network during reactor start-up. The transient kinetic model in Schuurman and Gleaves, (1997) has also been selected for comparison purposes. Figure 4.11 shows a diagram of the triangular network, and Table 4.12 shows the kinetic models which were tested based on this network.

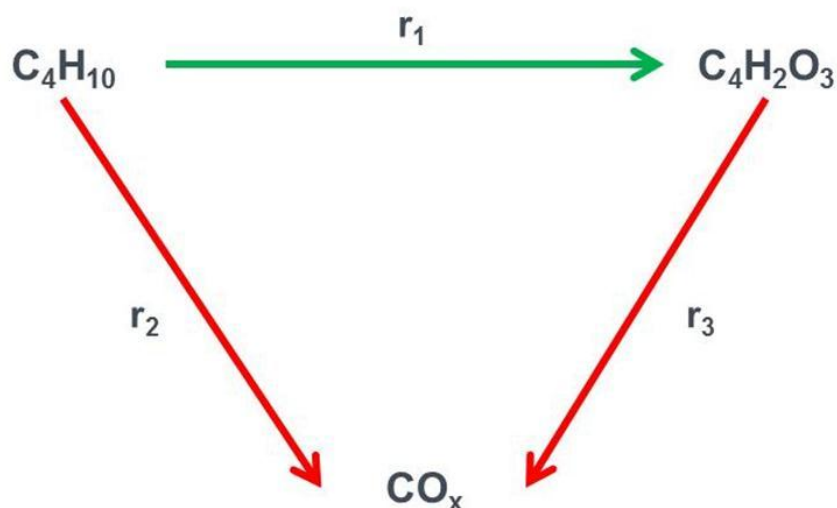


**Figure 4.11: Schematic of triangular reaction network.**

The aim of this section of the study is to isolate a kinetic model, which can describe the entire data set, as the VPO catalyst is not fundamentally changing in structure during the conditioning period. Hence, for a correct model, the fundamental nature of the active site should not change with time on stream (reflected in fitted  $E_a$  values), and instead, a decay of active site populations should be observed (via fitted pre-exponential factor,  $A_i$ , values).

The triangular networks in Table 4.12 are representative of three levels of model. The model of Escardino *et al.*, (1973) uses a set of simple pseudo-first-order reactions, thus providing a pragmatic base case for describing the system. The model of Buchanan and Sundaresan, (1986) will assess if a Mars–van Krevelen (MvK) type description is necessary: an important consideration as VPO catalysts fundamentally function via a redox mechanism (Centi *et al.*, 2001; Schiott and Jorgensen, 1993). Finally, the model of Sharma and Cresswell, (1991) considered product inhibition factors in an integral mode reactor and so is applicable to this study.

**Table 4.12: Selected kinetic models from literature applied in this study.**

Study	Network type	Rate expressions*	Activation energies (kJ mol <sup>-1</sup> )	Reaction conditions and mode of operation
<b>Escardino <i>et al.</i> (1973)</b>	Triangular (6 param.)	$r_1 = k_1[C_4H_{10}]$ $r_2 = k_2[C_4H_{10}]$ $r_3 = k_3[C_4H_2O_3]$		<ul style="list-style-type: none"> <li>• 673 – 753 K</li> <li>• &lt;0.95% <i>n</i>-butane in air</li> <li>• QSS operation</li> </ul>
<b>Buchanan and Sundaresan (1986)</b>	Triangular (8 param.)	$r_1 = \frac{k_1[C_4H_{10}]}{N}$ $r_2 = \frac{k_2[C_4H_{10}]}{N}$ $r_3 = \frac{k_3[C_4H_2O_3]}{N}$ $N = 1 + \frac{K_{Bu}[C_4H_{10}]}{[O_2]} + \frac{K_{MA}[C_4H_2O_3]}{[O_2]}$	$E_{a1} = 125.0$ $E_{a2} = 145.0$ $E_{a3} = 180.0$	<ul style="list-style-type: none"> <li>• 663 – 703 K</li> <li>• 0.62 – 1.55% <i>n</i>-butane in air</li> <li>• Up to 100% <i>n</i>-butane conversion</li> <li>• QSS operation</li> </ul>
<b>Sharma and Cresswell (1991)</b>	Triangular (8 param.)	$r_1 = \frac{k_1[C_4H_{10}]^n}{(1 + K_{MA}[C_4H_2O_3])}$ $r_2 = k_2[C_4H_{10}]^n$ $r_3 = \frac{k_3[C_4H_2O_3]}{(1 + K_{MA}[C_4H_2O_3])^2}$	$E_{a1} = 93.0$ $E_{a2} = 93.0$ $E_{a3} = 155.0$	<ul style="list-style-type: none"> <li>• 573 – 673 K</li> <li>• Up to 3% <i>n</i>-butane in air</li> <li>• Up to 90% conversion</li> <li>• QSS operation</li> </ul>
<b>Schuurman and Gleaves (1997)</b>	<i>n</i> -butane → products only (4 param.)	$r = k_B[C_4H_{10}]$ $k_B = k_{B1} + k_{B2}$	$E_{aB1} = 50.2$ $E_{aB2} = 96.3$	<ul style="list-style-type: none"> <li>• 533 – 698 K</li> <li>• TAP reactor</li> <li>• QSS and unsteady state operation</li> </ul>

\* =  $r_1 = n$ -butane → MA,  $r_2 = n$ -butane → CO<sub>x</sub>,  $r_3 = MA$  → CO<sub>x</sub>.  $k_{B1}$  and  $k_{B2}$  refer to high and low energy site reaction pathways respectively.

#### 4.4.2.1 6-parameter model of Escardino *et al.*, (1973)

Examples of results returned using a 6-parameter pseudo-first order model are shown in Table 4.13. At each time on stream point (illustrated here by  $t = 0.4$  and  $11.4$  h), the quality of fit ( $R^2$ ) is excellent. Values of  $E_{a1}$  and  $E_{a2}$  stay roughly constant at different times with

acceptable confidence intervals. The value of  $E_{a1}$  is also lower than  $E_{a2}$  which is observed in a number of the aforementioned literature models. This suggests that the rate-determining steps within the mechanisms for  $n$ -butane  $\rightarrow$  MA and  $n$ -butane  $\rightarrow$  CO<sub>x</sub> are different. For both  $n$ -butane oxidation routes, the parameters which change with time on stream are the pre-exponential factors.

**Table 4.13: 6-parameter model of Escardino *et al.* at 0.4 and 11.4 h.**

<b>Time on stream (h)</b>	<b>Ln [<math>A_{1,613}</math>] (s<sup>-1</sup>)</b>	<b>Ln [<math>A_{2,613}</math>] (s<sup>-1</sup>)</b>	<b>Ln [<math>A_{3,613}</math>] (s<sup>-1</sup>)</b>	<b><math>E_{a1}</math> (kJ mol<sup>-1</sup>)</b>	<b><math>E_{a2}</math> (kJ mol<sup>-1</sup>)</b>	<b><math>E_{a3}</math> (kJ mol<sup>-1</sup>)</b>	<b><math>R^2</math></b>	<b>Obj. func.</b>
0.4	0.4 ± 0.1	-1.1 ± 0.2	-2.8 ± 1.2	71.3 ± 7.0	95.8 ± 9.4	81.5 ± 64.8	0.99	-435
11.4	0.1 ± 0.1	-1.4 ± 0.1	-7.4 ± 5.1	74.7 ± 7.23	93.5 ± 8.1	268.5 ± 258.9	0.99	-462

The main shortcoming of the 6-parameter model is the clear cross-correlation between the  $A_{3,613}$  and  $E_{a3}$  parameters in the MA  $\rightarrow$  CO<sub>x</sub> route. In most cases, the 95% confidence intervals for these parameters are large. Similarly,  $E_{a3}$  is seen to drift significantly with time on stream which is not feasible in a correct model.

A logical step to overcome the observed cross-correlation was to reduce the number of parameters in the model to 5. This was achieved by assuming that  $E_a$  for both  $n$ -butane  $\rightarrow$  CO<sub>x</sub> and MA  $\rightarrow$  CO<sub>x</sub> are the same. It is important to note that equating these  $E_a$  is an approximation; both reaction routes involve C-C bond breakage as a rate determining step but would be expected to have different reactant adsorption energies on the active site. The conclusion here is that these differences in adsorption energy are negligible statistically.

Fitting a five parameter model resulted in only a negligible reduction in  $R^2$  and objective function values and, as Figure 4.12 attests, improves the quality of the parameter estimations. In Figure 4.12B, the estimations for  $E_{a1}$  and  $E_{a2}$  remain roughly the same when plotted against time on stream. Meanwhile, in Figure 4.12B, each pre-exponential factor value decays with time. The 95% confidence interval for  $A_{3,613}$  is significantly improved.

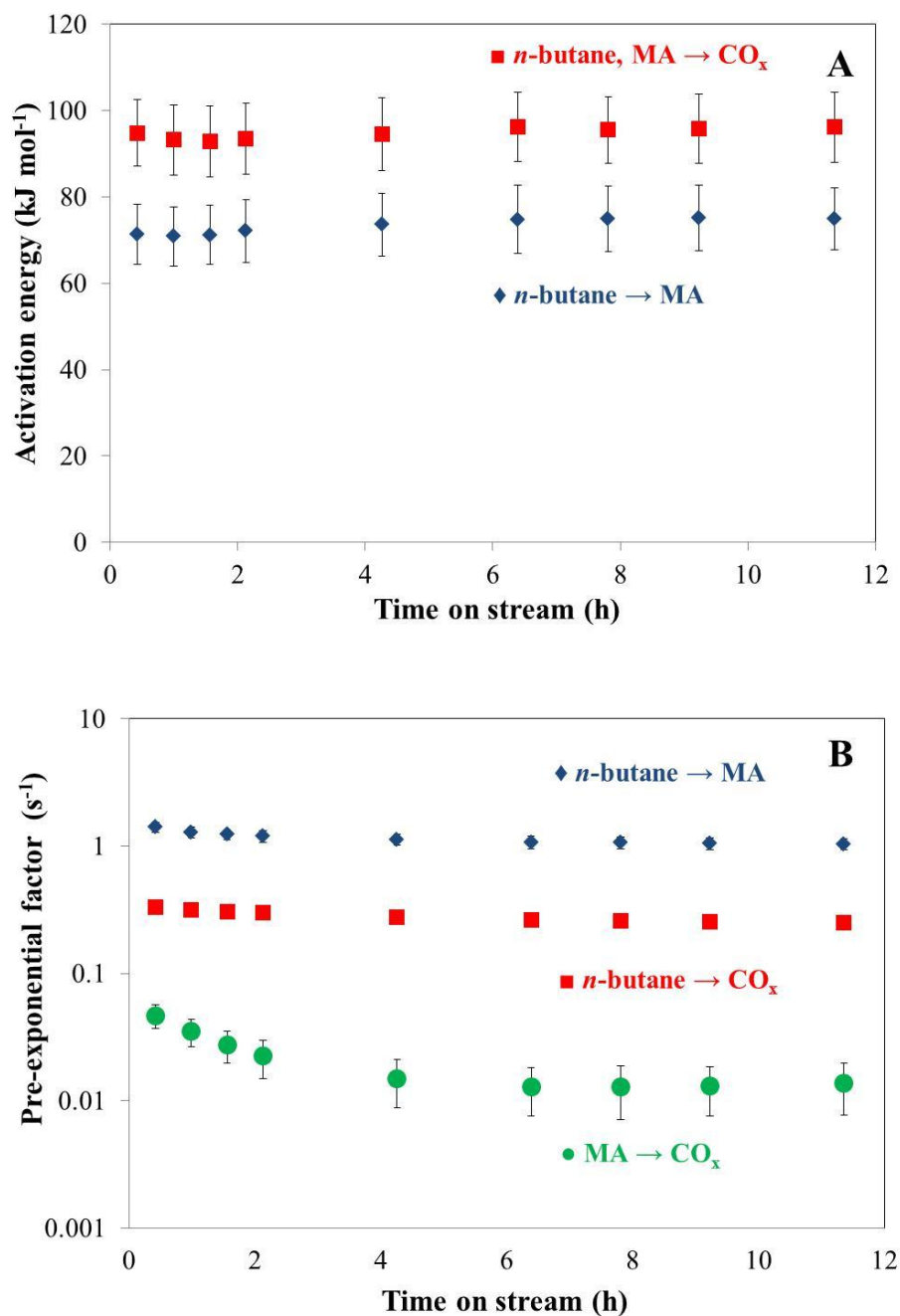


**Figure 4.12: Fitted parameters against time on stream for 5-parameter model using pseudo-first order relationships. A) Activation energies B) Re-parameterised pre-exponential factors Error bars denote 95% confidence intervals.**

Parity plots for prediction of *n*-butane, MA and CO<sub>x</sub> concentrations suggest that a simple pseudo-first-order model predicts VPO performance during the conditioning period extremely well. These are shown in Figure 4.13. Measured residuals within the model for *n*-butane, MA and CO<sub>x</sub> prediction are small and do not follow a systematic pattern, such as increasing with temperature or axial reactor position.

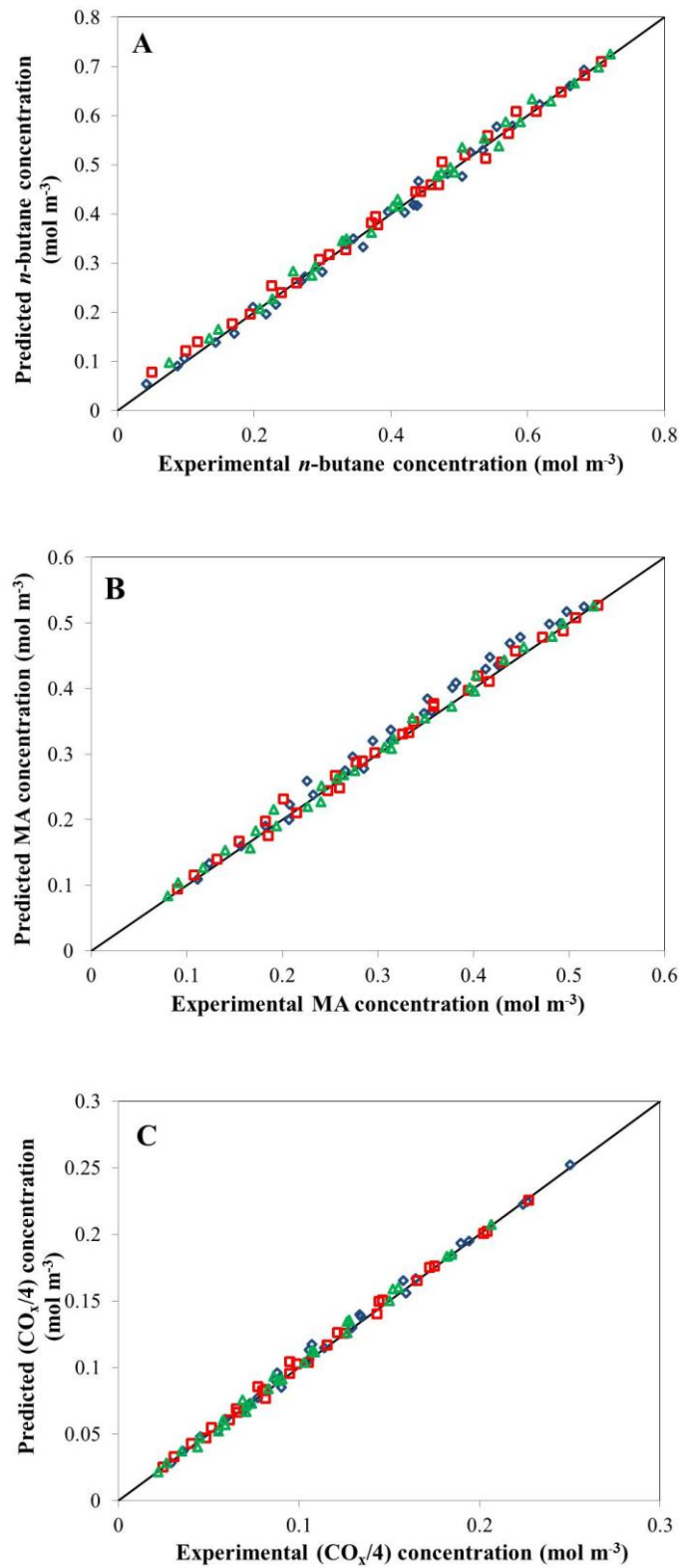


**Figure 4.13: Parity plots of predicted concentrations (from 5-parameter model) against experimental concentrations of A) *n*-butane, B) MA, C) CO<sub>x</sub>/4. Data from 3 different time on stream points are shown: 0.4 h (◇), 2.1 h (□), 11.4 h (△).**

The models of Buchanan and Sundaresan, (1986) and Sharma and Cresswell, (1991) were also tested and found to be over-parameterised. In both cases, the models could be reduced down to a pseudo-first-order network. The model of Schuurman and Gleaves, (1997) resulted in poor quality of fit and wide confidence intervals for the estimated parameter. Detailed discussion of all three of these models can be found in Section 4.7.1 (Appendix).

#### 4.4.3 Activity-time modelling

The 5-parameter kinetic model accurately describes catalyst behaviour for the entire data set (all temperatures, concentration profiles and times on stream). This has allowed evolution of VPO performance to be described by changes in  $A_i$  for each of the reaction pathways, with time on stream.

The evolution of  $A_i$  can now be defined via activity–time models. Firstly, the principle of separability is invoked (Levenspiel, 1972):

$$r_i(t) = f_1(C, T) \cdot f_2(t) \quad (4.6)$$

Eq. (4.6) makes the assumption that the fundamental reaction kinetics ( $f_1$ ) on the catalyst are time-independent and can therefore be separated from catalyst activity ( $f_2$ ), which describes current activity relative to a reference activity and is time-dependent. This is a valid approach as VPO behaviour across the entire data set is described by the same kinetic model. Activity evolution of VPO can be ascribed to changes in the pre-exponential factors of each reaction pathway. Hence, VPO evolution can be modelled using the following, normalised activity measure,  $a_i(t)$ , and will represent the  $f_2(t)$  term in Eq. (4.6):

$$a_i(t) = \frac{A_i(t)}{A_i(t=0)} \quad (4.7)$$

Figure 4.14 plots activity evolution for each of the three reaction pathways, based on pre-exponential factor values generated from kinetic modelling. For each pathway, activity is lost over time; however, there are clear differences between the *n*-butane oxidation pathways and the MA oxidation pathway. A large amount of MA oxidation activity is quickly lost in comparison with the *n*-butane oxidation pathways. This finding validates the intrinsic selectivity evolution of the VPO catalyst described in Section 4.3.1. Intrinsic selectivity towards MA has improved due to a sharp loss of MA oxidation sites on the catalyst.

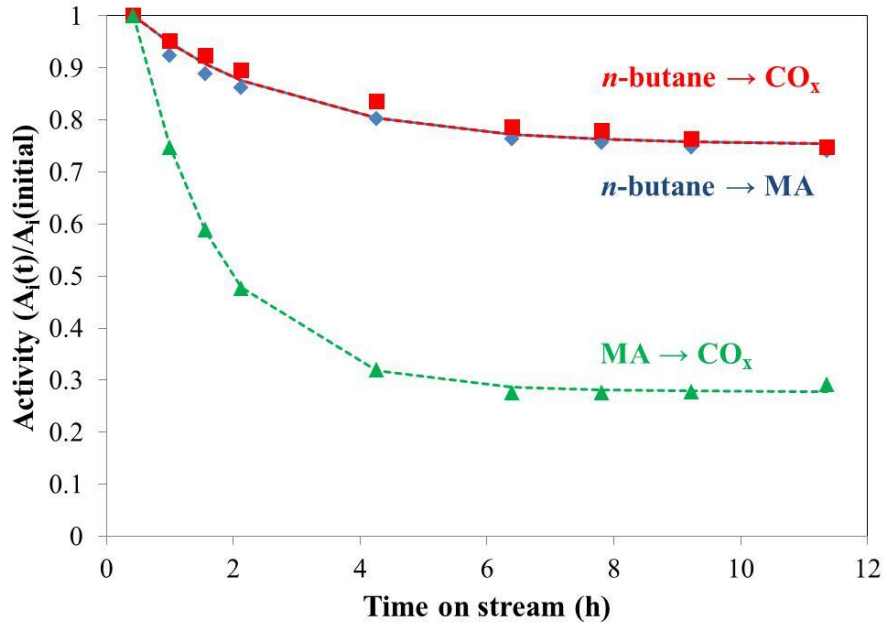


**Figure 4.14: Evolution of normalised pre-exponential factors ('activity') with time on stream for the 5 parameter kinetic model. Lines denote fitted 1<sup>st</sup> order activity-time models.**

Both *n*-butane oxidation pathways have a strikingly similar evolution pattern, suggesting that both reactions are taking place at the same active site.

A number of activity–time models exist in literature to describe evolution of catalyst performance. The most appropriate model for each reaction pathway was a simple first-order activity–time relationship with residual activity (Fuentes, 1985):

$$a_i(t) = a_{i,QSS} + (1 - a_{i,QSS}) \cdot \exp^{-\psi t} \quad (4.8)$$

In Eq. (4.8),  $a_{QSS}$  describes the residual catalyst activity at QSS operation, and  $\psi$  is a rate constant of activity evolution. The initial model for activity evolution of reaction pathways in the system contained six parameters (three  $a_{QSS}$  and three  $\psi$  values, respectively). A methodology described by Quiney and Schuurman, (2007) which assesses the statistical significance of parameters within a system was used to scrutinise this model. Jacobian norm analysis was carried out on each activity response dataset using the following equation:

$$norm(J_k)_m = \sqrt{\sum_i \left( \beta_j \frac{dy_i}{d\beta_j} \right)^2} \quad (4.9)$$

Where  $norm(J_k)_m$  is the norm of the Jacobian Matrix across  $m$  experiments,  $i$  and  $j$  denote correspondence to experiment  $i$  and parameter  $j$  respectively.  $y$  denotes a response variable and  $\beta$  a model parameter. This norm gives relative information on the influence of model parameters within the system (Quiney and Schuurman, 2007). By comparing these ‘lumped’ sensitivities, non-influential parameters can be removed systematically from the model.

The use of Eq. (4.9) revealed that the  $\psi$  parameters for the  $n$ -butane  $\rightarrow$  MA and  $n$ -butane  $\rightarrow$  CO<sub>x</sub> pathways had a relatively low influence on the quality of fit compared to the  $a_{QSS}$  parameters (Figure 4.15). Furthermore, the fitted  $a_{QSS}$  values for both of these pathways were found to be the same, within their 95% confidence intervals. As a result, both  $\psi$  and  $a_{QSS}$  values for both  $n$ -butane oxidation pathways were equated, reducing the parameters in the model to 4. Use of the global  $F$ -test, which considers the statistical significance of parameter reduction (within 95% confidence), showed this to be an acceptable move. The MA  $\rightarrow$  CO<sub>x</sub> pathway is distinct from the  $n$ -butane oxidation pathways exhibiting higher  $\psi$  and lower  $a_{QSS}$  values than the latter. Both parameters in the MA  $\rightarrow$  CO<sub>x</sub> pathway are have similar norm of the Jacobean matrix values, showing that both are significant to the model fit and cannot be reduced further, unlike the  $n$ -butane pathways.

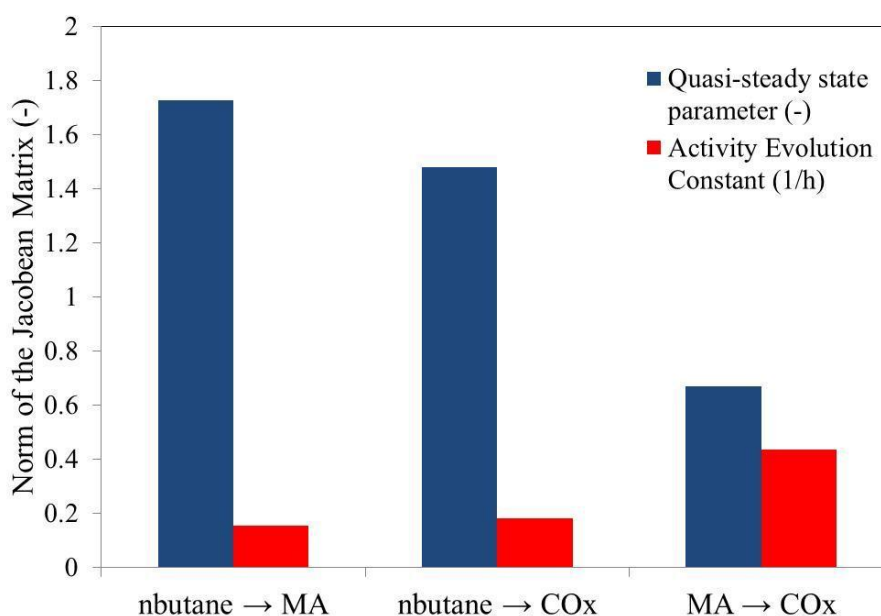


**Figure 4.15: Calculated norms of the Jacobian matrix for each parameter in the activity evolution model network.**

Modelling results are shown in Table 4.5 and graphically represented in Figure 4.14. The fitting process for each reaction yielded a high quality of fit ( $R^2 > 0.99$ ) and small 95% confidence intervals for the fitting parameters. From the parameter reduction process, the active site evolution network is reduced to two pathways, one for *n*-butane oxidation and the other for MA oxidation. The values of  $\psi$  suggest that activity evolution of the  $\text{MA} \rightarrow \text{CO}_x$  pathway is the fastest, whilst the *n*-butane oxidation pathway evolves more slowly.

**Table 4.5: 1<sup>st</sup> order activity-time model parameters for each reaction pathway.**

Reaction	$a_{QSS}$ (-)	$\psi$ ( $\text{h}^{-1}$ )	$R^2$
<i>n</i> -butane $\rightarrow$ MA	$0.75 \pm 0.02$	$0.41 \pm 0.09$	0.99
<i>n</i> -butane $\rightarrow$ $\text{CO}_x$			0.99
MA $\rightarrow$ $\text{CO}_x$	$0.28 \pm 0.02$	$0.75 \pm 0.07$	0.99

A comprehensive kinetic and activity model fit across the data set shows that the evolution of active sites for each reaction pathway on the VPO catalyst is insensitive to both temperature and axial concentration gradients during the conditioning period (i.e.  $a_{QSS}$  and  $\psi$  do not change as a function of process conditions). Hence, a VPO catalyst conditioned at 623 K under 2% *n*-butane/air reactor inlet conditions will lose the same proportion of active sites at the same rate as a VPO conditioned at 683 K. This supports the observations made in differential mode operation.

## 4.5 Discussion

In the spirit of the introduction, the findings are discussed with reference to the current barriers in furthering understanding of the effect of activation and conditioning methods on the structure and intrinsic performance of solid catalysts, with a focus on VPO for this model study:

### 4.5.1 Methodology development

Whilst previous work using TAP reactors (Schuurman and Gleaves, 1997) and TEOM setups (Wang *et al.*, 2000; Wang and Barteau, 2001) has provided good insight into transient behaviour of VPO catalysts under differential conditions, there was a clear gap in the understanding of integral reactors displaying transient behaviour. The parallel difference test

has demonstrated itself as an effective methodology for recording a full performance history of a VPO catalyst during conditioning, providing a wealth of data for kinetic modelling purposes. Extra investigations, such as restoring initial *n*-butane conversion after a set time on stream in a parallel difference test, provide many insights into the drivers behind the performance evolution of the VPO catalyst.

Investigating transient kinetics of a VPO catalyst during conditioning has shown considerable advantages over the traditional steady-state kinetic modelling approach. An evolution of active sites for different reaction pathways can be investigated, and this can be linked back to fundamental mechanisms. For example, the almost identical evolution of both *n*-butane oxidation pathways, suggesting both reactions occur at the same active surface, would be simply missed in a steady-state investigation.

#### **4.5.2 Critically assessment of the impact of activation and conditioning periods**

In this work, the systematic investigation of a pre-activated VPO catalyst under *n*-butane/air reaction conditions has allowed catalyst conditioning effects to be understood. During conditioning, it is seen that a pre-activated VPO catalyst undergoes a subtle surface rearrangement which impacts on the activity of three reaction pathways. The loss of catalyst activity is largely temperature and concentration gradient independent. Meanwhile, the catalyst bulk remains largely unchanged in structure during the key periods of performance evolution. This suggests that the catalyst surface developed during prior activation is critical to the catalyst's eventual QSS performance. The catalyst bulk should not be ignored however as the phases developed within it during activation, and their degree of crystallinity may provide indications of the nature of the surface developed.

Returning to previous literature investigations of *ex situ* activated catalysts (Albonetti *et al.*, 1996; Bergeret *et al.*, 1987; Guliants *et al.*, 1995), each study used a different activation method and ended up with different QSS performance levels. In each case, however, the catalyst bulk chiefly comprised  $(VO)_2P_2O_7$  at QSS performance after many hours on stream, as was found in this study. This suggests that  $(VO)_2P_2O_7$  is a key component of QSS performance but not necessarily a marker of an effective working catalyst surface. This confirms some of the findings in Lombardo *et al.*, (1992).

### 4.5.3 Insight into reaction mechanisms

Evolution of active sites, summarised in Figure 4.14, provides new insight into the nature of the working surface of a VPO catalyst. Both  $n$ -butane  $\rightarrow$  MA and  $n$ -butane  $\rightarrow$  CO<sub>x</sub> pathways decline at the same rate and to the same extent suggesting that they are associated with the same active site; meanwhile, the MA  $\rightarrow$  CO<sub>x</sub> pathway declines faster and more sharply suggesting it is associated with a different active site. This two-site model differs in basis to the one proposed by Schuurman and Gleaves, (1997), which proposed that  $n$ -butane oxidation occurs at either a low  $E_a$  (V<sup>5+</sup> dominated) or high  $E_a$  (V<sup>4+</sup> dominated) site. Interestingly, the apparent  $E_a$  drift which was observed in transient operation in a differential TAP reactor is echoed in the 1<sup>st</sup> sector apparent  $E_a$  observations in this work. This work, however, considered the full profile of an integral mode reactor allowing clearer observations of an MA oxidation route to be made and fitted to a triangular kinetic model.

Direct comparison with works which utilise separate oxidation and reduction steps can also be afforded. In Lorences *et al.*, (2004), a three site model is proposed: two different V<sup>5+</sup> sites for  $n$ -butane  $\rightarrow$  MA and MA  $\rightarrow$  CO<sub>x</sub>, respectively, and a V<sup>C4</sup> site, a carbon metal complex which interacts with gas-phase oxygen to form CO<sub>x</sub>. In the current work, activity–time models observe a 25% loss in  $n$ -butane oxidation sites and 75% loss in MA oxidation sites between  $t = 0$  h and QSS operation. Also in Lorences *et al.*, (2004), pre exponentials for the  $n$ -butane  $\rightarrow$  MA and  $n$ -butane  $\rightarrow$  CO<sub>x</sub> pathways decline by 64% and 62%, respectively, between transient and QSS observations, whilst MA  $\rightarrow$  CO<sub>x</sub> is more significant (85% loss). Whilst the active site basis of the current work is different, as well as the mode of reactor operation, common ground can be drawn between the nature of site evolution for each reaction pathway, even though in Lorences *et al.*, (2004), the extent of active site loss is greater.

A number of density functional theory (DFT) works have discussed the importance of surface morphology and adsorbate configuration on the reactions taking place at the catalyst surface (Courtine and Bordes, 1997; Thompson *et al.*, 2003; Thompson *et al.*, 2004). A key conclusion reached in all these works is that the (100) face of the (VO)<sub>2</sub>P<sub>2</sub>O<sub>7</sub> phase is the active-selective surface for the  $n$ -butane  $\rightarrow$  MA reaction.  $n$ -butane  $\rightarrow$  CO<sub>x</sub> is less well understood and has been attributed to other faces of (VO)<sub>2</sub>P<sub>2</sub>O<sub>7</sub> such as (001), (010), (021) and (010) (Courtine and Bordes, 1997). As both  $n$ -butane oxidation pathways are declining at the same rate from the kinetic analysis of the current work, this questions the argument that

alternative faces are responsible for the total oxidation pathways. An alternative argument may be that selectivity of *n*-butane  $\rightarrow$  MA versus *n*-butane  $\rightarrow$  CO<sub>x</sub> may be a function of the configuration in which the *n*-butane adsorbs to the (VO)<sub>2</sub>P<sub>2</sub>O<sub>7</sub> surface. A less favourable mode of adsorption in this case may lead to C-C breakage (via attack from electrophilic oxygen species (Centi *et al.*, 2001)) and subsequent formation of CO<sub>x</sub>.

Further works which support the single *n*-butane oxidation site include that of Herrmann *et al.*, (1997), who investigated links between VPO activity and its p-type semiconducting properties. The *n*-butane activation step (C–H cleavage) is hypothesised to occur at a V<sup>5+</sup>–O<sup>2-</sup> site (in equilibrium with V<sup>4+</sup>–O<sup>-</sup>). Such a coupling will polarise an *n*-butane molecule leading to C–H cleavage. However, the presence of electrophilic oxygen, O<sup>-</sup>, can also lead to CO<sub>x</sub> formation and could occur at the same site. It may be that the V<sup>5+</sup>–O<sup>2-</sup> site is stabilised by the (100) face of (VO)<sub>2</sub>P<sub>2</sub>O<sub>7</sub> (Duvauchelle and Bordes, 1999).

XPS results suggest that there are some significant changes to the phases present at the surface occurring during the first 5 h of operation, and that the surface V<sub>ox</sub> state drops from +4.2 to +4.1 during this time. Whilst tentative, some correlation could be afforded with the decline of the MA  $\rightarrow$  CO<sub>x</sub> pathway, which loses a majority of its active sites during this time. Previous works have proposed that whilst (VO)<sub>2</sub>P<sub>2</sub>O<sub>7</sub> is the key active phase, nearby V<sup>5+</sup> phases at stacking fault boundaries (surface defects) are critical to supplying the oxygen needed to transform *n*-butane  $\rightarrow$  MA (Nguyen *et al.*, 1996; Haras *et al.*, 2003). Similarly, other works have suggested that specific V<sup>5+</sup> phases present at the VPO surface before reaction condition exposure are replaced by different V<sup>5+</sup> phases upon re-oxidation (Bordes *et al.*, 1984; Ebner and Thompson, 1991). The loss in VPO activity observed may be attributed to healing of surface defects or replacement of more active V<sup>5+</sup> phases with less active ones during re-oxidation steps. An understanding of the relative quantities and evolution of different V<sup>5+</sup> phases in the catalyst could constitute useful further work, such as carrying out <sup>31</sup>P NMR spectroscopy akin to the work of Abon *et al.*, (1995). This may show if particular phases are correlated with the MA  $\rightarrow$  CO<sub>x</sub> reaction. Such work could eventually be compared to previous reference phase kinetics studies (Zhang-Lin *et al.*, 1994a).

## 4.6 Conclusions

The impact of activation and conditioning methods on many catalyst systems is a largely unresolved topic. In this work, a novel combination of catalyst testing methods

(particularly parallel difference testing), kinetic modelling and supporting characterisation has allowed a systematic investigation to be carried out upon the conditioning period. This methodology has demonstrated, using a model catalyst system, how phenomena occurring during conditioning can be understood. In a wider sense, the techniques employed could be applied to the conditioning step of a wider range of differently activated catalysts. This could shed light on the impact of different activation strategies behind forming different types of active sites.

This work has demonstrated that a VPO catalyst bed operating in integral mode under industrially relevant conditions (2% *n*-butane/air) undergoes a time-dependent transition during conditioning. The changes involved are shown, via kinetic modelling to involve a sharp loss in active sites attributed to MA  $\rightarrow$  CO<sub>x</sub> oxidation. Meanwhile, a separate active site, attributed to the oxidation of *n*-butane to both MA and CO<sub>x</sub>, is seen to decay in activity much less severely. The physical and/or chemical changes driving these active site decays appear to be subtle. XPS suggests a decline in surface  $V_{ox}$  and a change in the nature of the surface phases present, in particular during the first 5 h on stream. This may relate to the sharp decay in MA  $\rightarrow$  CO<sub>x</sub> sites observed over this time frame. The result is an intrinsically less active catalyst surface at QSS performance in comparison with initial performance, but it is also intrinsically more selective to *n*-butane oxidation rather than MA oxidation.

The evolution of VPO performance towards QSS performance during conditioning is described by a single set of activity–time models. Within the bounds of the study, this evolution is independent of temperature and reactor axial position (concentration gradient effects). This suggests that the final working surface of the VPO catalyst at QSS performance is largely dictated by catalyst precursor preparation and activation methods, rather than the nature of the reaction conditions exposed to it during conditioning. From an optimisation perspective, this would suggest that the prior catalyst preparation and *ex situ* activation methods are the more significant areas to consider during catalyst development for a VPO subsequently operated under 2% *n*-butane/air conditions.

## 4.7 Appendices

### 4.7.1 Other kinetic models tested in section 4.4

*8-parameter model of Buchanan and Sundaresan (1986):*

Fitting all the parameters of this model was unsuccessful. Values for  $K_{MA}$  were indeterminate suggesting there are no kinetic inhibition effects due to MA. Similarly, the values for  $K_{bu}$  were small ( $< 5$ ) at all times on stream and returned large 95% confidence intervals suggesting that kinetic inhibition effects due to *n*-butane were also negligible.  $E_a$  values changed significantly with time on stream for each reaction pathway (particularly MA  $\rightarrow$  CO<sub>x</sub>). Similarly  $A_{i,613}$  values for each pathway changed inconsistently over time and again returned large 95% confidence intervals.

The results from fitting this model suggest that redox-type expressions are not required. In the original work, Buchanan and Sundaresan note that this model is chosen to represent the oxidation state of the catalyst surface. In this work however, it is shown that re-oxidation of the catalyst is not a rate determining step and also surface and bulk oxidation states change very slowly with time on stream. Buchanan and Sundaresan also used three different inlet *n*-butane concentrations in their experiments whilst only one is used in this study. This suggests that the reactor inlet O<sub>2</sub>:*n*-butane molar ratio may be important in defining the redox behaviour of the VPO catalyst.

*8-parameter model of Sharma and Cresswell (1991):*

Fitting of the 8 parameters in this model was successful across the testing period, however evidence of over-parameterisation in the model was seen in the  $E_{a3}$ ,  $A_{3,613}$  and  $K_{MA}$  parameters (see Table 4.14). Large 95% confidence intervals were seen in each of them again confirming cross-correlation in describing the MA re-oxidation reaction. In the original work, the  $K_{MA}$  term was significantly larger however the value fitted for  $E_{a3}$  was similar to our findings. The apparent *n*-butane reaction order term,  $n$ , was found to be 0.8 – 0.95 for all times on stream, with smaller confidence intervals. This gives further confidence to the pseudo-1<sup>st</sup> order model described earlier.

**Table 4.14: 8-parameter model of Sharma and Cresswell at 0.4 and 11.4 h.**

<b>Time on str. (h)</b>	$Ln A_{1,613}$ (s <sup>-1</sup> )	$Ln A_{2,613}$ (s <sup>-1</sup> )	$Ln A_{3,613}$ (s <sup>-1</sup> )	$E_{a1}$ (kJ mol <sup>-1</sup> )	$E_{a2}$ (kJ mol <sup>-1</sup> )	$E_{a3}$ (kJ mol <sup>-1</sup> )	$n$	$K_{MA}$ (mol <sup>-1</sup> m <sup>3</sup> )	$R^2$	<b>Obj. func.</b>
0.4	0.32 ± 0.1	-1.12 ± 0.12	-5.17 ± 3.6	70.0 ± 6.3	90.9 ± 7.6	206 ± 181	0.84 ± 0.1	0.64 ± 0.41	0.99	-460
11.4	0 ± 0.1	-1.38 ± 0.13	-5.25 ± 5.0	72.3 ± 6.7	92.5 ± 8.2	159 ± 251	0.94 ± 0.1	-0.22 ± 0.36	0.99	-468

*4-parameter model of Schuurman and Gleaves (1997):*

The fitting process did not return 4 parameter fits for this model. This was circumvented by fixing the two  $E_a$  values reducing the problem to a 2-parameter model. The  $E_a$  values used were the same as those in the original work based on the similar  $E_a$  ‘drift’ seen in the 1<sup>st</sup> sector of the VPO catalyst bed earlier in the study. The results from this suggest that the pre-exponential factor for the ‘low’ energy sites decayed to a greater extent than that for the ‘high’ energy sites. Whilst this is consistent with the aforementioned work, the 95% confidence intervals were broad for both parameters. The low confidence in the estimations and the need to ‘force-fit’ two of the parameters shows this specific model is not a good descriptor for the testing conditions in this study, again confirming the requirement for an MA re-oxidation route in the reaction network.

## 4.8 References

Abon M., Bere K.E., Tuel A., Delichere P., (1995), ‘*Evolution of a VPO catalyst in n-butane oxidation reaction during the activation time*’, J. Catal., 156, 28-36

Albonetti S., Cavani F., Trifiro F., Venturoli P., Calestani G., López-Granados M., Fierro J.L.G., (1996), ‘*A comparison of the reactivity of ‘non-equilibrated’ and ‘equilibrated’ V-P-O catalysts: Structural evolution, surface characterisation, and reactivity in the selective oxidation of n-butane and n-pentane*’, J. Catal., 160, 52-64

Bej S.K., Rao M.S., (1991), ‘*Selective oxidation of n-butane to maleic anhydride (3 parts)*’, Ind. Eng. Chem. Res., 30, 1819-1832

Bergeret G., David M., Broyer J.P., Volta J.C., (1987), '*A contribution to the knowledge of the active sites of VPO catalysts for butane oxidation to maleic anhydride*', Catal. Today, 1, 37-47

Birtill J.J., (2003), '*But will it last until the shutdown? Deciphering catalyst decay!*', Catal. Today, 81, 531-545

Bordes E., Johnson J.W., Courtine P., (1984), '*On the topotactic dehydration of VOHPO<sub>4</sub>.0.5H<sub>2</sub>O into vanadyl pyrophosphate*', J. Solid State Chem., 55, 3, 270-279

Buchanan J.S., Sundaresan S., (1986), '*Kinetics and redox properties of vanadium phosphate catalysts for butane oxidation*', App. Cat., 26, 211-226

Burnett J.C., Keppel R.A., Robinson W.D., (1987), '*Commercial production of maleic anhydride by catalytic processes using fixed bed reactors*', Catal. Today, 1, 537-586

Busca G., Cavani F., Centi G., Trifiro F., (1986), '*Nature and mechanism of formation of vanadyl pyrophosphate: Active phase in n-butane selective oxidation*', J. Catal., 99, 400-414

Cavani F., De Santi D., Luciani S., Löfberg A., Bordes-Richard E., Cortelli C., Leanza R., (2010), '*Transient reactivity of vanadyl pyrophosphate, the catalyst for n-butane oxidation to maleic anhydride, in response to in-situ treatments*', App. Cat. A: Gen, 376, 66-75

Centi G., Cavani F., Trifiro F., (2001), '*Selective oxidation by heterogeneous catalysis*', Kluwer Academic/Plenum

Chu C.F. and Ng K.M., (1989), '*Flow in packed tubes with a small tube to particle diameter ration*' AIChE Jnl. 35, 148

Coulston G.W., Thompson E.A., Herron N., (1996), '*Characterisation of VPO catalysts by x-ray photoelectron spectroscopy*', J. Catal., 163, 122-129

Courtine P., Bordes E., (1997), '*Mode of arrangement of components in mixed vanadia catalyst and its bearing for oxidation catalysts*', App. Cat. A: Gen., 157, 46-65

Duvauchelle N., Bordes E., (1999), '*Influence of the nanostructure and morphology of (VO)<sub>2</sub>P<sub>2</sub>O<sub>7</sub> on its catalytic reactivity*', Catal. Letters, 57, 81-88

J.R. Ebner, M.R. Thompson, in: R.K. Grasselli, A.W. Sleight (Eds.), (1991), *Stud. Surf. Sci. Catal.*, 67, 31

Ebner J.R., Andrews W.J., (1992), (to Monsanto Company), U.S. Patent 5,137,860

Ergun S., (1952) '*Fluid flow through packed columns*' *Chem. Eng. Prog.* 49, 89-94

Escardino A., Sola C., Ruiz F., (1973), *An. Quim.*, 69, 1157

Fuentes G.A., (1985) '*Catalyst deactivation and steady-state activity: A generalised power-law equation model*', *App. Cat.*, 15, 33-40

Golbig K.G., Werther J., (1997), '*Selective synthesis of maleic anhydride by spatial separation of n-butane oxidation and catalyst reoxidation*', *Chem. Eng. Sci.*, 52, 4, 583-595

Gulians V.V., Benziger J.B., Sundaresan S., Yao N., Wachs I.E., (1995), '*Evolution of the active surface of the vanadyl pyrophosphate catalysts*', *Catal. Lett.*, 32, 379-386

Gulians V.V., Benziger J.B., Sundaresan S., Wachs I.E., Jehng J.-M., Roberts J.E., (1996), '*The effect of the phase composition of model VPO catalysts for partial oxidation of n-butane*', *Catal. Today*, 28, 275-295

Haras A., Witko M., Salahub D.R., (2003), '*Chemical nature of point defects at the (VO)<sub>2</sub>P<sub>2</sub>O<sub>7</sub> (1 0 0) surface*', *Surf. Sci.*, 538, 160-170

Herrmann J.-M., Vernoux P., Bere K.E., Abon M., (1997), '*In situ study of redox and of p-type semiconducting properties of vanadyl pyrophosphate and of V-P-O catalyst during the partial oxidation of n-butane to maleic anhydride*', *J. Catal.*, 167, 106-117

Hodnett B.K., Permanne P., Delmon B., (1983), '*Influence of the P/V ratio on the phase composition and catalytic activity of vanadium phosphate based catalysts*', *App. Cat.*, 6, 231-244

Hodnett B.K., (1985), '*Vanadium-phosphorus oxide catalysts for the selective oxidation of C<sub>4</sub> hydrocarbons to maleic anhydride*', *Catal. Rev. Sci. Eng.*, 27, 3, 373-424

Levenspiel O., (1972) '*Chemical reaction engineering, 2<sup>nd</sup> edition*', Wiley, New York, Chapter 15

Lombardo E.A., Sánchez C.A., Cornaglia L.M., (1992), 'The effect of preparation methods and activation strategies upon the catalytic behaviour of the vanadium-phosphorus oxides', *Catal. Today*, 15, 407-418

Lorences M.J., Patience G.S., Diez F.V., Coca J., (2004), 'Transient *n*-butane partial oxidation kinetics over VPO', *App. Cat. A: Gen*, 263, 193-202

Mills P.L., Randall H.T., McCracken J.S., (1999), 'Redox kinetics of VOPO<sub>4</sub> with butane and oxygen using the TAP reactor system', *Chem. Eng. Sci.*, 54, 3709-3721

Nguyen P.T., Sleight A.W., Roberts N., Warren W.W., (1996), 'Modelling the extended defects in the vanadium phosphate catalyst for butane oxidation, (VO)<sub>2</sub>P<sub>2</sub>O<sub>7</sub>', *J. Solid State Chem.*, 122, 2, 259-265

Perez-Ramirez J., Berger R.J., Mul G., Kapteijn F., Moulijn J.A., (2000) 'The six-flow reactor technology: A review on fast catalyst screening and kinetic studies' *Catalysis Today* 60, 93-109

Quiney A.S., Schuurman Y., (2007), 'Kinetic modelling of CO conversion over a Cu/ceria catalyst', *Chem. Eng. Sci.*, 62, 5026-5032

Schiøtt B., Jørgensen K.A., (1993), 'The oxidative species on a vanadyl pyrophosphate surface. A model for some steps in the maleic anhydride synthesis', *Catal. Today*, 16, 79-90

Schneider P., Emig G., Hofmann H., (1987), 'Kinetic investigation and reactor simulation for the catalytic gas-phase oxidation of *n*-butane to maleic anhydride', *Ind. Eng. Chem. Res.*, 26, 2236-2241

Schuurman Y., Gleaves J.T., (1994), 'Activation of vanadium phosphorus oxide catalysts for alkane oxidation. The influence of the oxidation state on catalyst selectivity', *Ind. Eng. Chem. Res.*, 33, 2935-2941

Schuurman Y., Gleaves J.T., (1997), 'A comparison of steady-state and unsteady-state reaction kinetics of *n*-butane oxidation over VPO catalysts using a TAP-2 reactor system', *Catal. Today*, 33, 25-37

Sharma R.K., Cresswell D.L., Newson E.J., (1991), 'Kinetics and fixed-bed reactor modelling of butane oxidation to maleic anhydride', *AIChE Jnl.*, 37, 1, 39

Thompson D.J., Fanning M.O., Hodnett B.K., (2003), '*Modelling the active sites in vanadyl pyrophosphate*', J. Mol. Cat. A: Chem., 198, 125-137

Thompson D.J., Ciobica I.M., Hodnett B.K., van Santen R.A., Fanning M.O., '*Electronic structure of the extended vanadyl pyrophosphate (1 0 0) surface*', Catal. Today, 91-92, 177-180

Wang D., Kung H.H., Barteau M.A., (2000), '*Identification of vanadium species involved in sequential redox operation of VPO catalysts*', App. Cat. A: Gen., 201, 203-213

Wang D., Barteau M.A., (2001), '*Kinetics of butane oxidation by a vanadyl pyrophosphate catalyst*', J Catal., 197, 17-25

Waugh K.C., Taufiq-Yap Y.-H., (2003), '*The effect of varying the duration of the butane/air pretreatment on the morphology and reactivity of (VO)<sub>2</sub>P<sub>2</sub>O<sub>7</sub> catalysts*', Catal. Today, 81, 215-225

Wrobelski J.T., Edwards J.W., Graham C.R., Keppel R.A., Raffelson H., (1986), (to Monsanto Company), U.S. patent 4,567,158

Zhang-Lin Y., Forissier M., Sneed R.P., Védrine J.C., Volta J.C., (1994a), '*On the mechanism of n-butane oxidation to maleic anhydride on VPO catalysts – I. A kinetics study on a VPO catalyst as compared to VPO reference phases*', J. Catal., 145, 256-266

Zhang-Lin Y., Forissier M., Védrine J.C., Volta J.C., (1994b), '*On the mechanism of n-butane oxidation to maleic anhydride on VPO catalysts – II. Study of the evolution of the VPO catalysts under n-butane, butadiene and furan oxidation conditions*', J. Catal., 145, 267-275

Ziółkowski J., Bordes E., Courtine P., (1990), '*Oxidation of butane and butene on the (100) face of (VO)<sub>2</sub>P<sub>2</sub>O<sub>7</sub>: A dynamic view in terms of the crystallochemical model of active sites*', J. Catal., 122, 126-150

## Chapter 5:

### **A combinatorial study using steady state performance kinetics and temperature programmed desorption studies to elucidate active site populations on $V_2O_5$ - $WO_3$ / $TiO_2$ catalyst formulations for ammonia selective catalytic reduction of nitric oxides**

*$V_2O_5$ - $WO_3$ / $TiO_2$  catalyst formulations have seen increasing use in the past 30 years in stationary de- $NO_x$  emissions control applications by ammonia selective catalytic reduction (SCR). In this study, two formulations of this catalyst are assessed; one catalyst had undergone higher temperature calcination than the other and showed greater de- $NO_x$  performance across a 453 – 673 K temperature sweep. Following extensive thermal ageing however, both catalyst formulations showed essentially the same performance.*

*Performance data of both catalysts were modelled at different stages of ageing using steady-state ammonia SCR kinetic models from literature. A simplified version of the micro-kinetic model of Dumesic et al., 1996 was found to be the best candidate. This model identified populations of two distinct active sites on the catalyst surface, one for ammonia adsorption and the other for ammonia activation (the immediate precursor to the de- $NO_x$  step of the SCR reaction). The two fresh catalysts were distinctly different in their populations; the better performing formulation showing a greater population of activation sites but a lower population of adsorption sites than the other.*

*Ex-situ characterisation methods such as XRD and Raman Spectroscopy were largely ineffective at discerning differences in these catalyst formulations which could be linked to performance. Ammonia adsorption and temperature programmed desorption (TPD) methods were more fruitful. The two catalyst formulations showed very different fresh TPD profiles but similar ones in their aged state. The use of single-site adsorption models was found to be poor at describing the TPD profiles. The presence of two or more sites was postulated from this. Further analysis to discern these active site populations marks future work to add quantitative conclusions to the assessment of these profiles.*

## 5. Introduction: ‘Stability, storage and reaction’

In both stationary and mobile applications, nitrogen oxides (NO<sub>x</sub>) are unavoidably formed from fuel combustion processes by the oxidation of atmospheric nitrogen at high temperature. Such emissions can cause serious ecological problems such as acid rain if not treated prior to atmospheric release. In terms of stationary applications, such as power plants, significant efforts have been made to control these emissions over the past few decades (Forzatti, 2001).

Whilst the dissociation of NO<sub>x</sub> into N<sub>2</sub> and O<sub>2</sub> is thermodynamically favoured at low temperatures, this reaction is slow and catalytic advances in this area are limited (Busca *et al.*, 1998). In stationary emissions control, catalytic technologies using a reducing agent have seen significant development (Nakajima and Hamada, 1996). Chief among these is the selective catalytic reduction (SCR) of NO<sub>x</sub> by ammonia (NH<sub>3</sub>) over a supported vanadia (V<sub>2</sub>O<sub>5</sub>) catalyst which was first commercially applied in Japan in the 1970’s (Forzatti, 2001). The catalyst is typically operated within a 473 – 673 K operating window and carries out the following reactions:



In commercial applications, V<sub>2</sub>O<sub>5</sub> is almost always exclusively supported on an anatase titania (TiO<sub>2</sub>) support (Busca *et al.*, 1998). Anatase TiO<sub>2</sub> is critical to formulating an effective catalyst in stationary applications for three key reasons:

- Enhancing V<sub>2</sub>O<sub>5</sub> surface dispersion to provide isolated vanadyl centres and polyvanadate species giving rise to a very active SCR catalyst (Chen and Yang, 1992).
- In real industrial feed streams, provide good resistance to SO<sub>2</sub> poisons which are only weakly and/or reversibly sulphated on TiO<sub>2</sub>, protecting the V<sub>2</sub>O<sub>5</sub> centres (Went *et al.*, 1992a, 1992b).
- NH<sub>3</sub> can adsorb and be subsequently stored on TiO<sub>2</sub>, creating a reserve which is available for reaction through fast desorption and re-adsorption over active V<sub>2</sub>O<sub>5</sub>-based sites, which carry out the NH<sub>3</sub> SCR reaction (Lietti *et al.*, 1998).

Anatase  $\text{TiO}_2$  is a metastable  $\text{TiO}_2$  polymorph and transformation into undesired rutile is favoured in all conditions (Barin, 1989); the addition of  $\text{V}_2\text{O}_5$  also promotes this transformation. Tungsten trioxide ( $\text{WO}_3$ ) (or sometimes molybdenum trioxide ( $\text{MoO}_3$ )) is included in the formulation as a promoter in order to counteract this effect and prevent anatase sintering, as well as promote the redox properties of  $\text{V}_2\text{O}_5$  during reaction (Busca *et al.*, 1998).

In stationary industrial applications,  $\text{V}_2\text{O}_5\text{-WO}_3/\text{TiO}_2$  catalysts are utilised in a flow-through monolithic form. In formulating these catalysts, the three active components can either be wash-coated onto a cordierite monolith support or be extruded into monolith form (Kleeman *et al.*, 2000). Examples can be seen in Figure 5.1:



**Figure 5.1: Examples of commercial  $\text{V}_2\text{O}_5\text{-WO}_3/\text{TiO}_2$  catalysts<sup>10</sup>**

$\text{NO}_x$  emission limits are ever tightening globally<sup>11</sup> and there is a constant drive to improve the effectiveness of these catalysts, particularly upon initial use and for stability over the longer (years) time scale. During catalyst development, it is common to subject formulations to accelerated thermal ageing procedures (typically 823 – 923 K) and subsequently characterise and analyse aged performance. An example is seen in Madia *et al.*, (2002) where SCR activity, catalyst surface area and anatase particle dimension were tracked. A  $\text{V}_2\text{O}_5$  loading above 2 w/w% resulted in significant  $\text{TiO}_2$ -anatase sintering and surface area loss.

Whilst a more exhaustive list of references and discussion on supported  $\text{V}_2\text{O}_5$  SCR systems can be found elsewhere (Busca *et al.*, 1998), the subsequent section summarises points of agreement and conflict, particularly where different formulations and modes of operation are concerned.

<sup>10</sup> Images supplied courtesy of Dr. Jörg Münch of Johnson Matthey Catalysts, Redwitz,

<sup>11</sup> [http://ec.europa.eu/environment/air/index\\_en.htm](http://ec.europa.eu/environment/air/index_en.htm)

## 5.1 Kinetics and mechanism

### 5.1.1 Steady state kinetic studies in literature for NH<sub>3</sub> SCR of NO

Steady state behaviour of supported V<sub>2</sub>O<sub>5</sub> ammonia SCR catalysts have been extensively explored in literature (Busca *et al.*, 1998). As expected, the scope of these studies is wide, particularly with reference to the gas phase conditions tested (NH<sub>3</sub>, NO: 100 – 2500 ppm; O<sub>2</sub>, H<sub>2</sub>O: 0 – 10%) but also with respect to tested catalyst formulations (e.g. variation in vanadia loadings) and mode of operation (integral vs. differential).

Many empirical kinetic studies suggest that NO has an order of ~1 and NH<sub>3</sub> of ~0 for the standard SCR reaction, the latter indicating a strong NH<sub>3</sub> adsorption process as part of the overall reaction; examples of this include the early work of Inomata *et al.* (1980) on V<sub>2</sub>O<sub>5</sub> and Orlik *et al.* (1995) on V<sub>2</sub>O<sub>5</sub>/TiO<sub>2</sub>. In the latter, a dependency on NH<sub>3</sub> concentration was reported at low NH<sub>3</sub>:NO ratios and elsewhere in Efstathiou and Flitoura (1995), a dependency on NH<sub>3</sub> of 0.4 – 0.5 was reported in the 453 – 493 K range. Regarding NO, some works have measured orders of less than 1 which increase with reaction temperature (Lintz and Turek, 1992; Odenbrand *et al.*, 1991). The opposite was measured in the work of Efstathiou and Flitoura (1995) where an order in NO of 1.1 was measured at 453 K and 0.85 at 543 K. The latter paper did not contain water in the feed and it is feasible that evolution of product water, particularly under higher temperature conversions may impact this parameter. In contrast, the effect of water was decoupled in the work of Lintz and Turek (1992). Based upon this, the general consensus is that NO weakly interacts with the catalyst surface or not at all; evidenced by the use of Eley-Rideal type expressions for this step in many of the these studies.

Contrast is also seen in the estimated apparent  $E_a$  values for the NO reduction reaction, with a range of 40 – 93 kJ mol<sup>-1</sup> reported (Efstathiou and Flitoura, 1992; Inomata *et al.*, 1980; Tronconi *et al.*, 1992; Beekman and Hegedus, 1991). The effect of V<sub>2</sub>O<sub>5</sub> loading on apparent  $E_a$  for NO reduction can contribute to this as demonstrated by Amiridis and Solar, (1996), observing a decrease from 65.9 to 37 kJ mol<sup>-1</sup> over a 1 – 15.9 w/w% V<sub>2</sub>O<sub>5</sub> range, with particular sensitivity in the 0 – 3 w/w% loading range.

The work of Dumesic *et al.*, (1996) affords a description of NO reduction via NH<sub>3</sub> over a V<sub>2</sub>O<sub>5</sub>/TiO<sub>2</sub> with a strong mechanistic basis. The work also supplied confidence

intervals for the estimated parameters. A culmination of a series of prior work (Dumesic *et al.*, 1993; Topsøe *et al.*, 1995), the authors proposed 6 distinct mechanistic steps (Figure 5.2), in particular:

- Adsorption of  $\text{NH}_3$  on a Brønsted acid site (Step 1,  $\text{V}^{5+}\text{-OH}$ ).
- Ammonia activation (Step 2, via redox  $\text{V}=\text{O}$  sites). This is cited as a slow step and is supported by Busca and Ramis, (1994) as a reason for observed NO reaction orders of less than 1 in previous empirical kinetics studies. The  $\text{VONH}_4\text{OV}$  ‘activated ammonia’ complex must form via 2-site (Brønsted acid and redox site) interaction to allow subsequent NO reduction to take place.
- NO reduction step proceeding via an Eley-Rideal type mechanism.

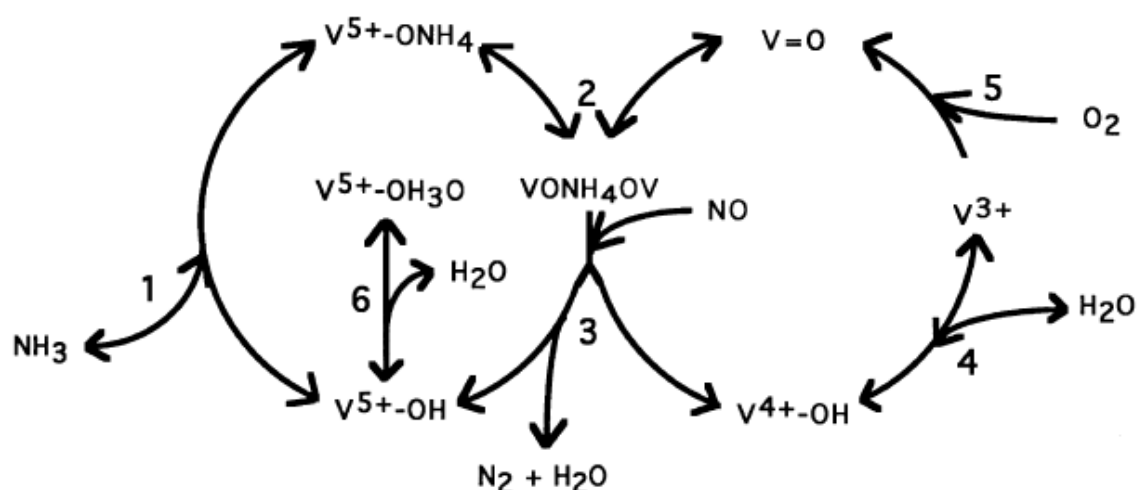


**Figure 5.2: Schematic for the  $\text{NH}_3$  SCR of NO over a  $\text{V}_2\text{O}_5/\text{TiO}_2$  catalyst (taken from Dumesic *et al.*, 1996)**

The roles of water and oxygen (Steps 4-6) could also be suitably incorporated depending on conditions employed. Importantly, the initial model utilised a 6%  $\text{V}_2\text{O}_5/\text{TiO}_2$  catalyst under water-free differential conditions and was validated against both industrially relevant conditions (5%  $\text{H}_2\text{O}$ , 4%  $\text{O}_2$ ) and the dataset of Lintz and Turek, (1992). In the latter, the higher  $\text{V}_2\text{O}_5$  loading of 20% was reflected in a higher pre-exponential factor for Step 3, rather than a significant change in apparent activation energy for the overall reaction, as seen in empirical studies.

### 5.1.2 Adsorption-desorption kinetic studies using NH<sub>3</sub> and/or NO

Adsorption and desorption studies using NO and NH<sub>3</sub>, typically comprising spectroscopic and/or desorption techniques, represent an alternative route to extract detailed mechanistic information on supported V<sub>2</sub>O<sub>5</sub> systems. Whilst extrapolation of predictive models from these systems to real working conditions is cautioned due to the clean conditions of operation (Busca *et al.*, 1998), they provide an excellent complement to steady state model findings.

Transient response methods have been developed in great detail by the group of Tronconi, Forzatti and co-workers at Politecnico di Milano, Italy (Lietti *et al.*, 1997); their work is based upon an approach originally described by Kobayashi and Kobayashi (1972) and Kobayashi (1982). Such methods, typically using a micro-reactor flow rig with mass spectrometer analysis, utilise abrupt step changes in gas composition and observe the response in catalyst behaviour. Figure 5.3 shows the evolution of V<sub>2</sub>O<sub>5</sub>-WO<sub>3</sub>/TiO<sub>2</sub> catalyst behaviour when exposed to either a NH<sub>3</sub> or NO step change. In the case of NH<sub>3</sub> there is a clear uptake by the catalyst (*A*<sub>1</sub>) showing a strong surface adsorption effect. When the NH<sub>3</sub> is cut from the feed, some of the adsorbed NH<sub>3</sub> desorbs (*A*<sub>2</sub>) although a strongly bound proportion remains which can be removed via temperature programme desorption (TPD) (Srnak *et al.*, 1992; Lietti and Forzatti, 1994). In Figure 5.3B, there is very little adsorption of NO which would support steady state kinetics findings.

The experimental approach in Figure 5.3 can be further applied to mixed gases (e.g. NH<sub>3</sub> + NO + O<sub>2</sub>) and targeted feed step changes can provide further response information (Nova *et al.*, 2000). Also a step change response can be substituted for a ramped concentration response (concentration programmed reaction (CPR)) (Nova *et al.*, 2001).

Data generated from these experiments can lead to the development of adsorption, desorption and reaction models for these catalysts. It has been suggested from these models that NH<sub>3</sub> adsorbs on V<sub>2</sub>O<sub>5</sub>/TiO<sub>2</sub> by a non-activated process ( $E_a = 0 \text{ kJ mol}^{-1}$ ) (Lietti *et al.*, 1997). Regarding the desorption step, Temkin-type kinetics have provided better descriptions of data than their Langmuir-type counterpart, suggesting there are a range of adsorption sites on the catalyst surface (Tronconi *et al.*, 1996; Lietti *et al.*, 1997).  $E_d^0$  values of  $\sim 100 \text{ kJ mol}^{-1}$  are typically estimated (Srnak *et al.*, 1992; Lietti *et al.*, 1998).

In some cases, a dual site modelling approach has been successful, particularly for  $\text{NH}_3$  adsorption on Fe-Zeolite catalysts at low temperatures (Colombo *et al.*, 2012). Such models utilised a Temkin description for weak acid sites and a Langmuir description for strong acid sites. Similarly, an NO reaction step has been incorporated (Lietti *et al.*, 1998), typically yielding an  $E_a$  of  $\sim 60 \text{ kJ mol}^{-1}$ . A modified  $\theta$  kinetics approach (an Eley-Rideal description utilising a critical ( $\theta_{\text{NH}_3}^*$ ) coverage value) provided the most successful description in these cases, suggesting that the NO reduction rate is independent of surface coverage above this value.  $\theta_{\text{NH}_3}^*$  was estimated to be similar to surface  $\text{V}_2\text{O}_5$  coverage for both  $\text{V}_2\text{O}_5\text{-WO}_3/\text{TiO}_2$  and  $\text{V}_2\text{O}_5/\text{TiO}_2$  formulations.

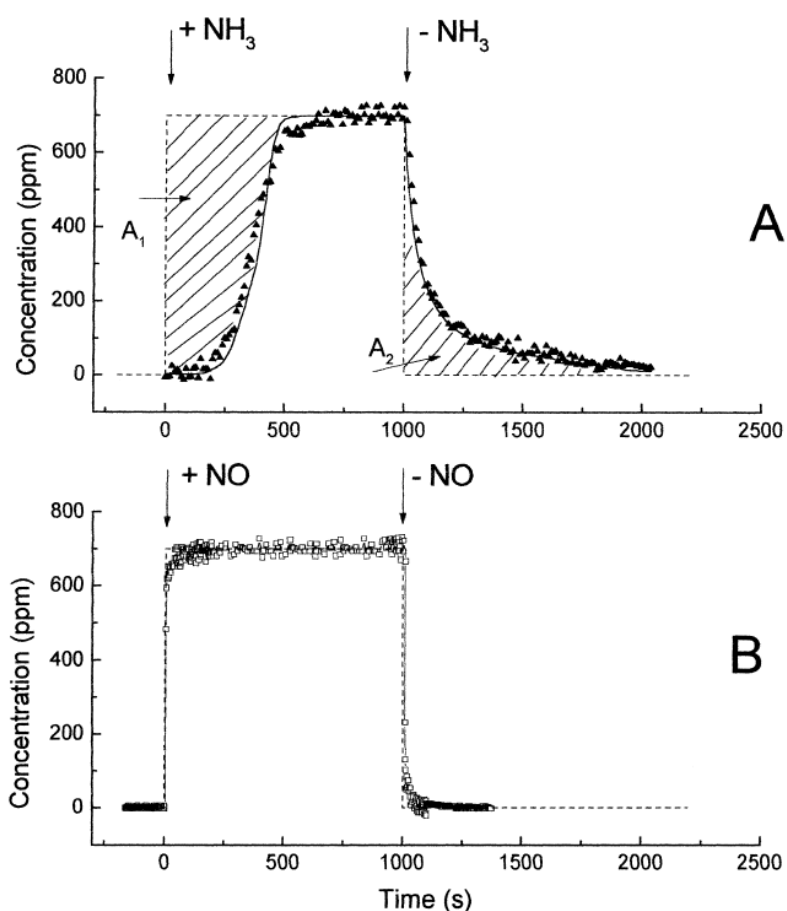


**Figure 5.3: Dynamic adsorption-desorption of  $\text{NH}_3$  (Graph A) and NO (Graph B) on a model  $\text{V}_2\text{O}_5\text{-WO}_3/\text{TiO}_2$  catalyst at 493 K (carrier gas: 1%  $\text{O}_2$  / He at  $120 \text{ ml min}^{-1}$  (STP)).**

**Dashed line: ideal step, Dotted Line: model fit (taken from Lietti *et al.*, 1998)**

Fourier transform infra-red (FTIR), TPD and combined FTIR-TPD techniques have also been employed to understand the interaction of  $\text{NH}_3$  and NO with supported  $\text{V}_2\text{O}_5$

catalysts. Topsøe *et al.*, (1995) analysed FTIR spectra of TiO<sub>2</sub> and 0.6 – 6 % V<sub>2</sub>O<sub>5</sub>/TiO<sub>2</sub> under NH<sub>3</sub> + O<sub>2</sub> and NH<sub>3</sub> + NO + O<sub>2</sub> conditions. No spectra peaks were found which related to NO adsorption whilst clear adsorbed NH<sub>3</sub> species were identified. For V<sub>2</sub>O<sub>5</sub>/TiO<sub>2</sub>, a number of sites were identified, namely OH groups, Lewis acid and Brønsted acid. V<sup>5+</sup>-OH sites were strongly linked to the NH<sub>3</sub> SCR reaction. These findings were further developed in a study of reduced V<sub>2</sub>O<sub>5</sub>-WO<sub>3</sub>/TiO<sub>2</sub> and WO<sub>3</sub>/TiO<sub>2</sub> catalysts for the standard and fast SCR reactions to explain importance of V species (Tronconi *et al.*, 2007).

In general, Lewis-bonded ammonia and ammonium ions bonded at Brønsted acid sites have been seen to prevail on V<sub>2</sub>O<sub>5</sub>/TiO<sub>2</sub> in many further studies via FTIR (Lietti *et al.*, 1996; Went *et al.*, 1992a,b) and are shown in Figure 5.4. Differentiation of Ti<sup>4+</sup> and vanadyl Lewis-acid sites is not possible using this method. To circumvent this, kinetic analysis of NH<sub>3</sub> adsorption and desorption methods can provide further direction to FTIR findings. Further characterisation using x-ray photoelectron spectroscopy (XPS), temperature programme reduction (TPR) and solid state <sup>51</sup>V nuclear magnetic resonance (NMR) can also be employed (Bond and Tahir, 1991).

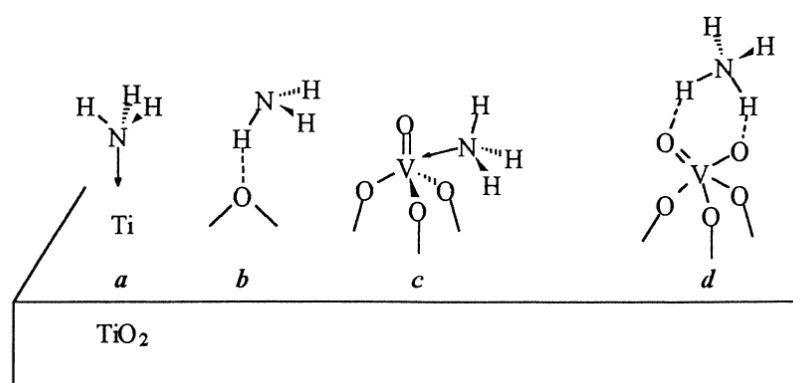


**Figure 5.4: Proposed structures for ammonia adsorbed on V<sub>2</sub>O<sub>5</sub>/TiO<sub>2</sub>:**  
**a) Lewis-bonded NH<sub>3</sub> at Ti sites; b) H-bonded NH<sub>3</sub> at oxide sites; c) Lewis-bonded NH<sub>3</sub> at vanadyl sites; d) ammonium ions bonded at V Brønsted acid sites (taken from Busca *et al.*, 1998)**

### 5.1.3 Chapter Objectives

In this chapter, a challenge is presented to understand the fundamental differences in reactor performance between two commercial  $V_2O_5$ - $WO_3$ / $TiO_2$  catalysts, which have undergone different calcination procedures prior to reactor use and show different de- $NO_x$  performance in their fresh form. The three aims to achieve this and in the process develop new methodologies to further understand  $V_2O_5$ - $WO_3$ / $TiO_2$  catalyst behaviour are thus:

- Combine an ‘apparent kinetics’ approach, based on integral operation commercial catalyst testing data, with a focused  $NH_3$  and  $NO$  adsorption-desorption type study to examine and understand the fundamental differences in two different  $V_2O_5$ - $WO_3$ / $TiO_2$  catalyst formulations.
- Understand the extent at which predominantly differential mode kinetic models from literature can be successfully applied to integral operation commercial catalyst testing data to elucidate the nature and magnitude of surface sites on the catalysts under scrutiny.
- Utilise methodologies to elucidate the nature and magnitude of storage and reaction sites on  $V_2O_5$ - $WO_3$ / $TiO_2$  catalysts and allow comparison between different formulations.

## 5.2 Materials and methods

### 5.2.1 Sample preparation and properties

A  $V_2O_5$ - $WO_3$ / $TiO_2$  catalyst ( $V_2O_5 = 1.7\%$  w/w,  $WO_3 = 9\%$  w/w,  $TiO_2$  anatase form) was employed exclusively in this study and was supplied by Johnson Matthey Catalysts<sup>12</sup>. Samples of this catalyst were received in extruded monolithic form with a cell density of 300 cells / in<sup>2</sup> and a specific surface area of 2200 m<sup>2</sup>/m<sup>3</sup>. Two distinct fresh versions of this catalyst are utilised in this study, SCR1 and SCR, which differ based on their final calcination procedure before use. SCR 2 underwent a calcination procedure in air at a temperature 30 K higher than SCR1 and for 50% longer time.

---

<sup>12</sup> All catalysts tested in this study supplied courtesy of Dr. Jörg Münch of Johnson Matthey Catalysts, Redwitz, Germany.

SCR1 and SCR2 catalysts were tested in both fresh and aged form. The ageing procedure for both catalysts was carried out in an oven with no flow at either 823 or 873 K for up to 1000 h. SCR1 and SCR 2 had BET surface areas of 69 and 56 m<sup>2</sup> g<sup>-1</sup> respectively when fresh and 39 and 38 m<sup>2</sup> g<sup>-1</sup> following 200 h thermal ageing at 873 K<sup>13</sup>.

All V<sub>2</sub>O<sub>5</sub>-WO<sub>3</sub>/TiO<sub>2</sub> catalysts tested for steady state reaction studies (section 5.2.2) were retained in monolithic form ( $d = 1 \text{ in}^2$ ,  $l = 140 \text{ mm}$ ) and for adsorption-desorption-titration studies (section 5.2.3) were ground and sieved into powder form (<106, 106 – 180, 180 – 250, 250 – 355  $\mu\text{m}$  sieve fractions).

### 5.2.2 Catalyst characterisation

- *X-ray diffraction*: Samples were tested using a Siemens D5000 diffractometer using Cu K $\alpha$  X-rays at wavelength 1.5406 Å.
- *Raman spectroscopy*: Samples were tested using a JY Horiba Infinity Spectrometer.

### 5.2.3 Steady-state reaction studies

Steady state catalyst testing data for fresh and aged SCR1 and SCR2 catalysts were provided by Johnson Matthey Catalysts<sup>14</sup>. Monolithic samples were tested in a flow rig under the following conditions (Table 5.1):

**Table 5.1: Feed conditions used for collection of steady-state data in this study**

Condition	Value
Space time	60000 h <sup>-1</sup>
Temperature	453 – 773 K
v/v NH <sub>3</sub>	100 ppm
v/v NO	100 ppm
v/v H <sub>2</sub> O	7.0%
v/v O <sub>2</sub>	9.3%

<sup>13</sup> BET surface area experiments and analysis were carried out by Dr. Iain Hitchcock of Johnson Matthey Technology Centre, Sonning, UK

<sup>14</sup> Catalyst testing data supplied courtesy of Dr. Jörg Münch of Johnson Matthey Catalysts, Redwitz, Germany.

Inlet and outlet stream analysis was carried out using FTIR. At all temperature points tested during a typical run the performance of the catalyst was allowed to equilibrate before noting steady state values. This typically took up to 1 h.

*A priori* checks were made for these operational conditions to check for the presence of heat and mass transport limitations, chiefly using correlations for gas-solid mass transport (Carberry, 1987), gas-solid heat transport (Mears, 1971), intra-particle diffusion (Weisz, 1957) and intraparticle heat transport (Mears, 1971); the equations for which are given in Chapter 2 (p. 58–60). Calculations were made based on test cases at 453 and 673 K operation at 10, 50 and 90% NO conversion (assuming a 1:1 conversion ratio with NH<sub>3</sub>). Heat transport limitations were negligible in all cases (< 0.1 K gradients), however mass transport limitations were noted, as shown in Table 5.2:

**Table 5.2: Estimated mass transport criteria and efficiency values for a flow through monolith V<sub>2</sub>O<sub>5</sub>-WO<sub>3</sub>/TiO<sub>2</sub> catalyst under operating conditions in Table 5.1**

% NO Conversion	Temperature (K)	Damkohler	Estimated gas-solid efficiency at channel exit ( $n_{g-s}$ ) <sup>b</sup>	Wheeler-Weisz Criterion (-) [ $\Phi_{crit} = 0.16$ ]	Estimated reactor wall efficiency ( $n_{diff}$ )
		Number (Da) <sup>a</sup> For both NO (1 <sup>st</sup> order) and NH <sub>3</sub> (zero order)			
10	453	0.1	0.97	0.21	0.93
50	453	0.5	0.86	1.06	0.75
90	453	0.9	0.77	1.91	0.64
10	773	0.1	0.97	0.25	0.92
50	773	0.5	0.86	1.25	0.72
90	773	0.9	0.77	2.26	0.61

<sup>a</sup>  $Da = k_{app} \cdot C_a^{n-1} \cdot t$

<sup>b</sup>  $n_{g-s} = \Gamma_p / \Gamma_m$ , calculated via Eqs. (5.4-5.5)

Table 5.2 shows gas-solid mass transport efficiencies at both temperature extremes for monolith testing in this chapter. These values were calculated using calculations from the work of Tronconi and Forzatti, (1992) which are applicable to square shape channel monoliths:

$$\frac{d\Gamma_m}{dz} = -4 \cdot \frac{Da \cdot Sh}{Da + Sh} \Gamma_m \quad (5.4)$$

$$\Gamma_p = \frac{Sh \cdot \Gamma_m}{Da + Sh} \quad (5.5)$$

Where  $Sh$  denotes Sherwood Number,  $Da$  denotes Damköhler Number,  $\Gamma_m$  denotes dimensionless average concentration of gas phase species in the monolith channel cross section,  $\Gamma_p$  denotes dimensionless concentration of gas phase species at the channel wall and  $z$  is axial co-ordinate (m). The same work demonstrated  $Sh$  to be approximately 3 for square channels and was utilised in this analysis. For  $Da$  calculations, the dependency of NO and NH<sub>3</sub> on the SCR reaction was taken to be 1 and 0 respectively. It can be seen that gas-solid transport efficiency drops with conversion, which will add a degree of extrinsic influence on the SCR kinetics for monolith operation in this chapter.

Coupled with the above, diffusional transport limitations in the monolith wall are evident and estimated efficiencies decrease with higher NO conversions. Intraporous diffusivities were calculated using the Weisz criterion given in Eq. (2.9) on p.60, Chapter 2. Diffusional transport efficiencies are similar across the temperature range, however. The results of the kinetic modelling described in section 5.3.2 are therefore likely to contain some lumped transport effects. It is important to note however that two SCR catalysts are under comparison in this study and are operating at similar levels of conversion across the temperature range. Any lumped mass transport effects are unlikely to significantly bias observed kinetic differences between the catalysts on a comparative level. The presence of diffusion limitations does however further promote the need to carry out further studies on powders, in order that the crux of the investigation is carried out free of transport limitations.

#### 5.2.4 NH<sub>3</sub> temperature programmed desorption (TPD) studies

NH<sub>3</sub> TPD studies were performed in a flow U-tube micro-reactor setup (Altimira Instruments). The methodology employed in this section is based on previous approaches by

Lietti and co-workers (Lietti *et al.*, 1997; Lietti *et al.*, 1998). The feed gases supplied to the micro-reactor comprised 200 ppm NH<sub>3</sub> / He, 5 % O<sub>2</sub> / He and He (BOC Beta Standard). Flow rates of chosen feed gases were measured and controlled by two mass-flow controllers with 50 and 100 ml min<sup>-1</sup> flow rate limits respectively. Gas flows through the two mass-flow controllers were then mixed into a single stream prior to the reactor at a tube T-junction of the two feed gases.

The reactor comprised a U-shaped quartz tube (3 mm ID) which was filled with 1.5 cm height quartz wool, 100 mg V<sub>2</sub>O<sub>5</sub>-WO<sub>3</sub>/TiO<sub>2</sub> catalyst and 1.5 cm height quartz wool on the up-flow side of the tube. During operation, the U-tube was contained within an electric furnace driven by a proportional-integral-derivative (PID) controller. A *K*-type thermocouple was directly positioned in the catalyst bed during operation to act as a temperature control. The temperature of the furnace was also measured during operation.

Reactor exit stream analysis was carried out using a mass spectrometer (Ametek Process Instruments: Proline-Dycor) which was directly connected downstream of the U-tube reactor. During operation, eight different mass-to-charge (*m/e*) ratios were used to monitor the gas phase components, namely: 4 (He), 17 (NH<sub>3</sub>), 18 (H<sub>2</sub>O), 28 (N<sub>2</sub>), 30 (NO), 32 (O<sub>2</sub>), 44 (N<sub>2</sub>O) and 46 (NO<sub>2</sub>). Quantitative analysis was enabled using response factors measured experimentally from blank tube experiments with the supplied gases, which carried an analysis certification from BOC. Further blank checks were carried out to elucidate the interference of H<sub>2</sub>O on *m/e* 17. Relevant interference factors were applied to the data to reconcile gas-phase compositions.

Table 5.3 shows the typical reactor feed conditions employed in the process of obtaining the TPD profiles. It is noted that these experiments were carried out as a final step of a longer experiment which also comprises isothermal ammonia adsorption and desorption steps. Unfortunately, unlike in some literature setups (Lietti *et al.*, 1997), the gas composition changes between each step involve a slower, non-stepped response owing to the distance between the reactor and inlet feed valve. Analysis of these steps (and incorporation into kinetic models) is currently in progress due to the additional non-linearity encountered and is not incorporated into this chapter. In future work this will assist in firstly, closing the NH<sub>3</sub> balance in the experiment and secondly, providing a physically consistent initial condition for simulation of the subsequent NH<sub>3</sub> TPD.

To achieve the required space time and gas compositions, the flow of O<sub>2</sub> / He was set to 25 ml min<sup>-1</sup> and 200 ppm NH<sub>3</sub> / He to 100 ml min<sup>-1</sup>. Space time under these conditions was 48000 h<sup>-1</sup>. In this chapter, the program described in Table 5.3 involved isothermal ammonia adsorption and desorption steps at 523 K, for all catalysts employed. Blank (no catalyst) versions of this program were also employed and a calibration for NH<sub>3</sub> response on the mass spectrometer was also produced. The calibration response was tested at a number of different temperatures. An inert tracer (such as Ar) was not used in this chapter, but should be incorporated in future studies as an internal standard during transient response steps.

**Table 5.3: Typical experimental program used in NH<sub>3</sub> adsorption-desorption experiments in this study**

<b>Prog. Stage</b>	<b>Total Flow Rate (ml min<sup>-1</sup>)</b>	<b>Overall gas composition</b>	<b>Notes</b>
1	125	1% O <sub>2</sub> / He	Ramp to 523 K from room temp. (15 K min <sup>-1</sup> ), Hold for 120 min
2	125	160 ppm NH <sub>3</sub> / 1% O <sub>2</sub> / He	Maintain 523 K, Hold for 90 min
3	125	1% O <sub>2</sub> / He	Maintain 523 K, Hold for 90 min
4	125	He	Cool to 323 K, Hold for 5 min
5	125	He	Ramp to 1273 K (15 K min <sup>-1</sup> )

Transport criteria were checked at a temperature of 1023 K for these experiments with two distinct particle sizes in Table 5.4. This temperature marks the high-end of ammonia evolution during the TPD step. Calculations were made assuming 250 ppm ammonia desorbs, which was the maximum amount observed during the experiments. In common with the monolith experiments, gas-solid mass transport efficiencies approached unity. When assessing diffusion limitations, particle size was found to be important: mass transport efficiencies were compromised with larger particles (250 – 355 μm) under conditions where higher amounts of NH<sub>3</sub> are desorbed. To ensure such transport effects are avoided, a 106 –

180  $\mu\text{m}$  size fraction was selected to maintain a >99% transport efficiency throughout the TPD experiments.

**Table 5.4: Estimated mass transport criteria and efficiency values for a 0.1 g  $\text{V}_2\text{O}_5\text{-WO}_3/\text{TiO}_2$  catalyst powder fixed bed during step 5 in Table 5.3 at 1023 K**

ppm $\text{NH}_3$ desorbed	Particle Size Range ( $\mu\text{m}$ )	Carberry Number (-) [ $Ca_{crit} = 0.05$ ]	Estimated gas-solid efficiency ( $n_{g-s}$ )	Wheeler-Weisz Criterion (-) [ $\Phi_{crit} = 0.16$ ]	Estimated particle efficiency ( $n_{diff}$ )
25	106 – 180	0.001	0.99	0.004	0.99
125	106 – 180	0.001	0.99	0.023	0.99
250	106 – 180	0.001	0.99	0.047	0.97
25	250 – 355	0.001	0.99	0.025	0.98
125	250 – 355	0.002	0.99	0.13	0.93
250	250 – 355	0.003	0.99	0.26	0.87

### 5.2.5 Kinetic modelling procedure

Parameter estimation was carried out using Athena Visual Studio © software<sup>15</sup>. The kinetic models tested within this work contain multiple parameters including some which are non-linear (e.g. activation energies in the Arrhenius equation). The Levenberg-Marquardt procedure, an indirect method for constrained optimisation of parameters, is appropriate for this problem (Marquardt, 1963). For the steady state study described in section 5.3.2 and 5.3.3, reaction rates connecting the values of the input and response variables are linked by a single reaction (Eq. (5.1)), hence parameter estimation can be carried out explicitly:

$$y_u = f_u(\xi_u; \theta_j) + \varepsilon_u \quad (5.6)$$

<sup>15</sup> Athena Visual Studio 14.2, Stewart & Associates Engineering Inc.

Where  $y_u$  is a model response,  $\xi_u$  are the process settings (input variables),  $\theta_j$  are model parameters and  $\varepsilon_u$  is error, the latter of which comprises model and experimental error. Sensitivities of model parameters can subsequently be derived as followed:

$$B(t) = [F(\beta^+) - F(\beta^-)] / (2\Delta\beta) \quad (5.7)$$

Where  $B(t)$  is the sensitivity function and  $\beta^+$ ,  $\beta^-$  are perturbation thresholds for the model parameters under estimation (van der Waal, 2000).

For the temperature programmed desorption modelling described in section 5.3.4, gas phase concentration and surface coverage response variables were solved implicitly using a set of differential equations:

$$\frac{dy}{dt} = f(y, \beta) \quad (5.8)$$

Subsequently, a direct decoupled method is used to estimate parametric sensitivities (Caracotsios and Stewart, 1985):

$$B(t) = \frac{\partial y(t)}{\partial \beta} \quad (5.9)$$

$$\frac{\partial}{\partial \beta} \left( \frac{dy}{dt} \right) = \frac{d}{dt} B(t) = \frac{df}{dy} \cdot B(t) + \frac{df}{d\beta} \quad (5.10)$$

In Eq. (5.8) it can be seen that defining sensitivities as a function of time allows them to be solved alongside the main system differential equations, improving solver efficiency and performance.

To minimise cross-correlation between activation energy ( $E_a$ ) and pre-exponential factor ( $A_i$ ) parameters, a re-parameterised Arrhenius equation was used:

$$k_i = A_i \cdot \exp \left( \left( \frac{E_a}{T_{base} \cdot R} \right) \cdot \left( 1 - \frac{T_{base}}{T} \right) \right) \quad (5.11)$$

Where base temperature is  $T_{base}$  (K) and  $A_i$  is the value of the rate constant  $k_i$  at  $T_{base}$ . The fitting process can be further improved by solving  $A_i$  as an exponential term and lumping fitted value,  $E_a$  with constants  $T_{base}$  and ideal gas constant,  $R$  ( $\text{J K}^{-1} \text{mol}^{-1}$ ) to give fitting parameter  $E_{a,lump}$ . This brings the values of  $A_i$  and  $E_{a,lump}$  into the same order of magnitude (typically 1 – 10) further reducing cross-correlation in this expression:

$$k_i = \exp\left(A_i + \left(E_{a,lump} \cdot \left(1 - \frac{T_{base}}{T}\right)\right)\right) \quad (5.12)$$

The above procedure was also applied to Van't Hoff adsorption terms ( $K_i$ ) featuring a heat of adsorption term ( $\Delta H_{ads}$ ) and associated  $A_i$  value.

For the TPD studies, data were modelled using a heterogeneous, one-dimensional plug-flow dynamic reactor model, with the assumptions of a catalyst bed that is isothermal and isobaric (as checked in Section 5.2.4). The model is derived following an unsteady-state differential mass balance for gaseous and adsorbed ammonia and is based on a number of previous works (Kobayashi and Kobayashi, 1972, Lietti *et al.*, 1997, Colombo *et al.*, 2012):

$$\frac{\partial \theta_{NH_3}}{\partial t} = r_a - r_d \quad (5.13)$$

$$\frac{\partial C_{NH_3}}{\partial t} = -v \cdot \frac{\partial C_{NH_3}}{\partial z} + \Omega(r_d - r_a) \quad (5.14)$$

In Eqs (5.11-12),  $\theta_{NH_3}$  denotes the fractional coverage of ammonia on the catalyst surface (assuming ammonia has a molecular diameter of 3.6 Å),  $r_a$  and  $r_d$  denote the rates of ammonia adsorption and desorption respectively,  $C_{NH_3}$  denotes the gas phase concentration of ammonia,  $v$  denotes the interstitial gas velocity through the catalyst bed and  $\Omega$  denotes catalyst ammonia storage capacity.

## 5.3 Results and discussion

### 5.3.1 Catalyst characterisation

XRD analysis of fresh and aged samples revealed only small structural differences, showing predominantly TiO<sub>2</sub>-anatase phase in all cases (Figure 5.5). The strong reflection at 25.2° (a characteristic TiO<sub>2</sub>-anatase peak (Shi *et al.*, 2011, Madia *et al.*, 2002)), shows differences in height and peak area across the four samples, suggesting some variation in crystallite size.

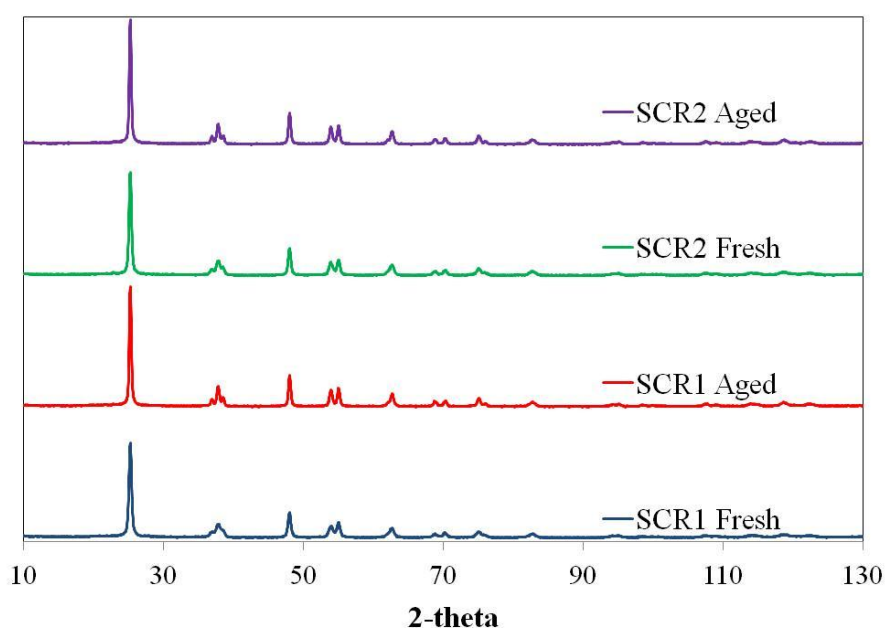


**Figure 5.5: XRD analysis of fresh and aged SCR1 and SCR 2 catalyst powders. All reflections are assigned to TiO<sub>2</sub>-anatase**

The full-width at half maximum (FWHM) for the fresh samples is broader than that of the two aged samples. As a result, calculation of the TiO<sub>2</sub>-anatase average crystallite size in each sample was carried out using the Scherrer Equation (Klug and Alexander, 1974):

$$\tau = \frac{K_{shape} \lambda}{\beta \cos \theta_B} \quad (5.15)$$

Where  $\tau$  is the mean size of ordered crystal domains (nm),  $K_{shape}$  is a shape factor (-),  $\lambda$  is the X-ray wave-length (nm),  $\beta$  is the line broadening at FWHM (-) and  $\theta_B$  is the Bragg angle (-). Use of Eq. (5.13) shows a crystallite size of 24.1 and 27 nm for the fresh SCR1 and

SCR2 catalysts respectively, whilst the aged samples are 34.3 and 34.7 nm respectively. The greater crystallite size in both aged samples is expected, given their extensive thermal ageing. Such effects have been shown in previous ageing studies (Madia *et al.*, 2002). The crystallite size of SCR2 is also greater than SCR1 in the fresh form, which may be driven by the higher calcinations temperature employed.

On initial inspection of Figure 5.6A, Raman spectroscopy shows the presence of TiO<sub>2</sub>-anatase, with spectrum exhibited bands at 397, 516 and 639 cm<sup>-1</sup> respectively (Madia *et al.*, 2002). However, it is important to scrutinise each spectrum between 750 and 1050 cm<sup>-1</sup> (see Figure 5.6B. In all samples, a shouldered peak is observed at 980 cm<sup>-1</sup> and a weakly intense region is observed at ~800 cm<sup>-1</sup>. The latter could not be confidently assigned to SCR1 (fresh).

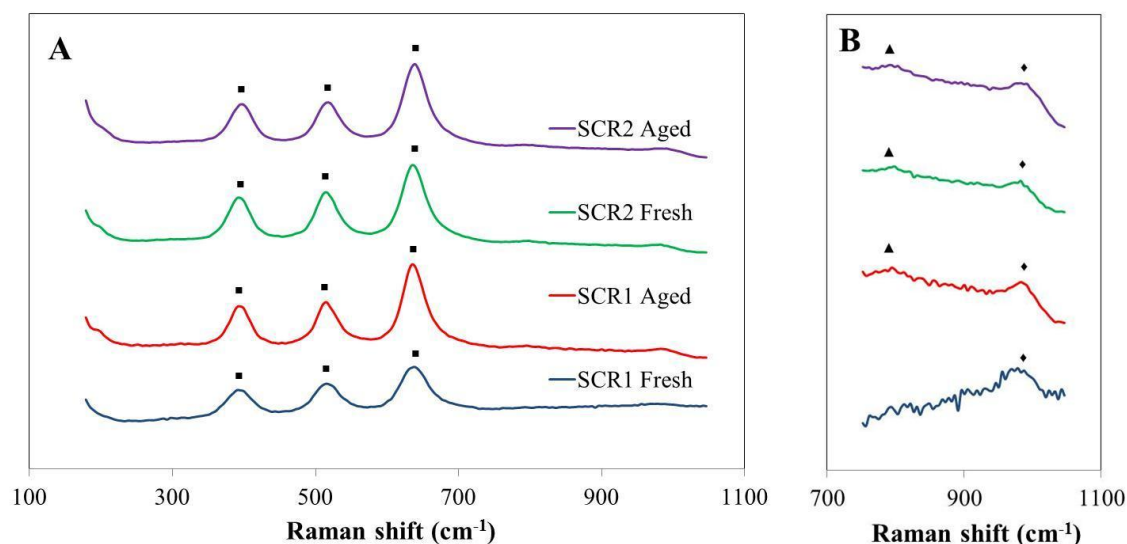


**Figure 5.6: Raman spectroscopy analysis of fresh and aged SCR1 and SCR2 catalyst powders. A) Overall spectra, B) Zoomed spectra between 750 and 1050 cm<sup>-1</sup>. (■) denotes TiO<sub>2</sub>-anatase, (▲) W-O-W stretching vibration, (◆) M=O stretching vibration, where M denotes metal.**

Previous literature has attributed the ~800 cm<sup>-1</sup> band as an overlapping of second-order anatase features with the W-O-W stretching of octahedrally co-ordinated W units in a similar environment to that of bulk WO<sub>3</sub> (Madia *et al.*, 2002, Alemany *et al.*, 1995). Such works have suggested the presence of this band is consistent with ageing. This would support the lack of such a band on the SCR1 (fresh) spectrum, however the presence of this peak in SCR2 (fresh) suggests only a short, higher temperature exposure may be needed to generate it.

Went *et al.*, (1992) assign the  $\sim 800\text{ cm}^{-1}$  band to polyvanadate species, albeit in  $\text{V}_2\text{O}_5/\text{TiO}_2$  catalysts. In such works it is observed with  $\text{V}_2\text{O}_5$  loadings between 1.3 and 9.8% and is exacerbated by increased reduction of the catalyst in  $\text{H}_2$  at higher temperatures. An alternative argument may therefore suggest that this band relates to  $\text{V}^{3+}=\text{O}$  groups.

It has previously been suggested that the small peaks at  $980\text{ cm}^{-1}$  relate to the growth of metavanadate and/or metatungstate chains by polymerisation of  $\text{VO}_x$  and  $\text{WO}_x$  groups (Madia *et al.*, 2002). These may be apparent in all samples as a function of the higher temperature calcination and/or ageing procedures. Overall it appears the Raman spectra for all samples are relatively similar barring some small differences in SCR1 (fresh).

### 5.3.2 Steady state results

Figure 5.7 shows an example in the differences in  $\text{NO}_x$  removal performance seen with both catalysts and ageing time:

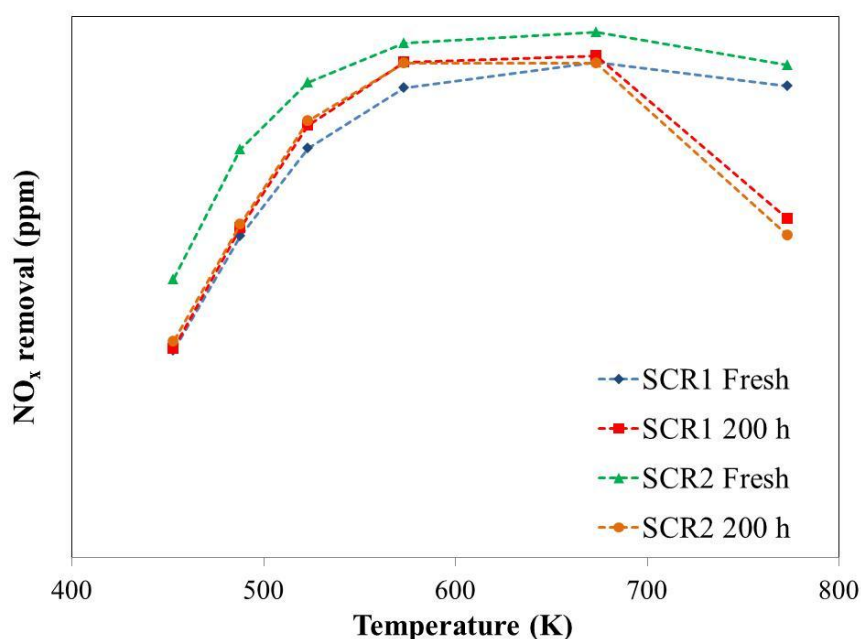


**Figure 5.7:  $\text{NO}_x$  removal performance of fresh and 200 hours 873 K aged for SCR1 and SCR2 catalysts in the 453 – 773 K temperature range (Inlet: 100 ppm  $\text{NH}_3$ , 100 ppm  $\text{NO}$ , 9.3%  $\text{O}_2$ , 7.0  $\text{H}_2\text{O}$ )**

The fresh catalysts are very different in performance, with SCR2 achieving greater  $\text{NO}_x$  removal than SCR 1 at all tested temperatures. After 200 hours of 873 K thermal ageing however, performance of both catalysts is largely the same. A striking change is seen for

both catalysts at 773 K reaction conditions with ageing time; a large drop in NO<sub>x</sub> removal is observed. A significant drop in NH<sub>3</sub> conversion at the same points does not occur in parallel to this. This will be discussed later in Figure 5.8 of this section.

Across the datasets available, inlet and outlet levels of NO<sub>2</sub> always made a negligible contribution to NO<sub>x</sub> content (< 2% of total). Thus, returning to the key NH<sub>3</sub> SCR equations discussed in introduction Section 5, the NO<sub>2</sub> featured reactions (Eq. (5.2-3)) can be disregarded, leaving the ‘standard’ SCR reaction for NO (Eq. (5.1)) which involves equimolar amounts of NH<sub>3</sub> and NO.

Figure 5.8 charts the ratios of NO<sub>x</sub>:NH<sub>3</sub> consumed across both catalysts at different stages of ageing, calculated as follows:

$$Ratio(NO : NH_3) = \frac{(Inlet - Outlet) ppmNO}{(Inlet - Outlet) ppmNH_3} \quad (5.16)$$

It can be seen that at all temperatures, except 773 K, ratio of consumption is ~1, within 95% confidence. At 773 K this is not the case and the ratio decreases with ageing time, suggesting other reaction pathways are prevalent here (e.g. NH<sub>3</sub> oxidation).

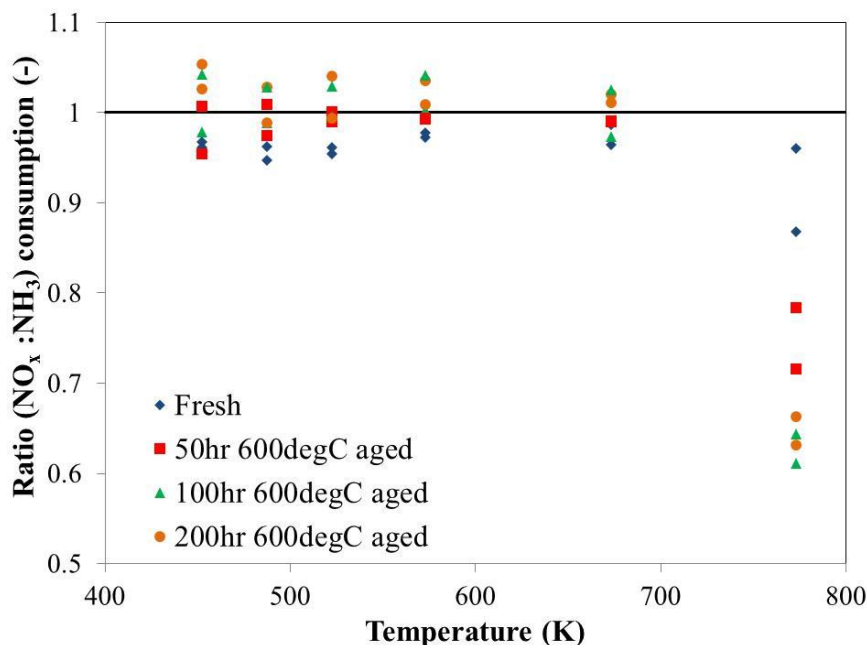


**Figure 5.8: Ratio of NO<sub>x</sub> to NH<sub>3</sub> consumption at different temperatures and aged state of catalysts (N.B.: SCR1 and SCR2 data are lumped together in this instance).**

In this steady state kinetic study, a single  $\text{NO}_x \rightarrow \text{N}_2$  reaction will be modelled explicitly using the 453 – 673 K temperature range. For each catalyst and ageing time, only 5 experimental data points are therefore available. When these data are fitted to models, there should be a maximum of 4 parameters (total observations minus 1) to retain a degree of freedom for residual analysis. SCR1 and SCR2 catalysts aged at 823 K will also be investigated in this manner, having shown similar NO and  $\text{NH}_3$  consumption trends at different ageing times.

### 5.3.3 Steady state kinetic modelling

#### 5.3.3.1 Kinetic analysis using the model of Lintz and Turek

The model of Lintz and Turek, (1992) modelled a single  $\text{NO} \rightarrow \text{N}_2$  reaction following a series of experiments under intrinsic conditions. Key parameters varied in the original work were NO,  $\text{NH}_3$  (both 250 – 1000 ppm),  $\text{H}_2\text{O}$  (up to 10 mol%) and, to a limited extent, temperature (523 and 623 K). Their final expression (Eq. (5.15)) utilised an Eley-Rideal type expression with  $\text{NH}_3$  adsorption and  $\text{H}_2\text{O}$  inhibition:

$$r_{\text{NO}} = k_3 P_{\text{NO}}^n \bullet \frac{P_{\text{NH}_3}}{1 + K_{\text{NH}_3} P_{\text{NH}_3}} \bullet \frac{1}{1 + K_{\text{H}_2\text{O}} P_{\text{H}_2\text{O}}} \quad (5.17)$$

In the current work  $\text{H}_2\text{O}$  concentration is not varied across the dataset. The  $\text{H}_2\text{O}$  inhibition term was thus disregarded. Similarly, NO inlet concentrations were always 100 ppm, so the concentration order,  $n$ , was set to 1. This left a 4 parameter model containing a NO reduction ( $k_3$ ) and ammonia adsorption ( $K_{\text{NH}_3}$ ) Arrhenius terms. As a result, the model was re-parameterised as follows:

$$r_{\text{NO}} = \frac{P_{\text{NO}} P_{\text{NH}_3}}{\frac{1}{k_3} + \frac{K_{\text{NH}_3}}{k_3} P_{\text{NH}_3}} \quad (5.18)$$

Whilst not explicitly quoted in their work, the  $\Delta H_{\text{ads}}$  for  $K_{\text{NH}_3}$  and  $E_a$  for  $k_3$  can be calculated to be -65.6 and 13.8  $\text{kJ mol}^{-1}$  respectively from their data by taking an Arrhenius plot of individual rate constant terms at the temperatures they tested. The datasets for fresh and 873 K aged SCR1 and SCR2 catalysts were initially tested with both values fixed. However the quality of fit was poor in all cases ( $R^2 < 0.85$ ) and the 95% confidence intervals

for the two pre-exponential parameters were greater than their estimated values. The model was subsequently re-tested without fixing the energy values (Figure 5.9):

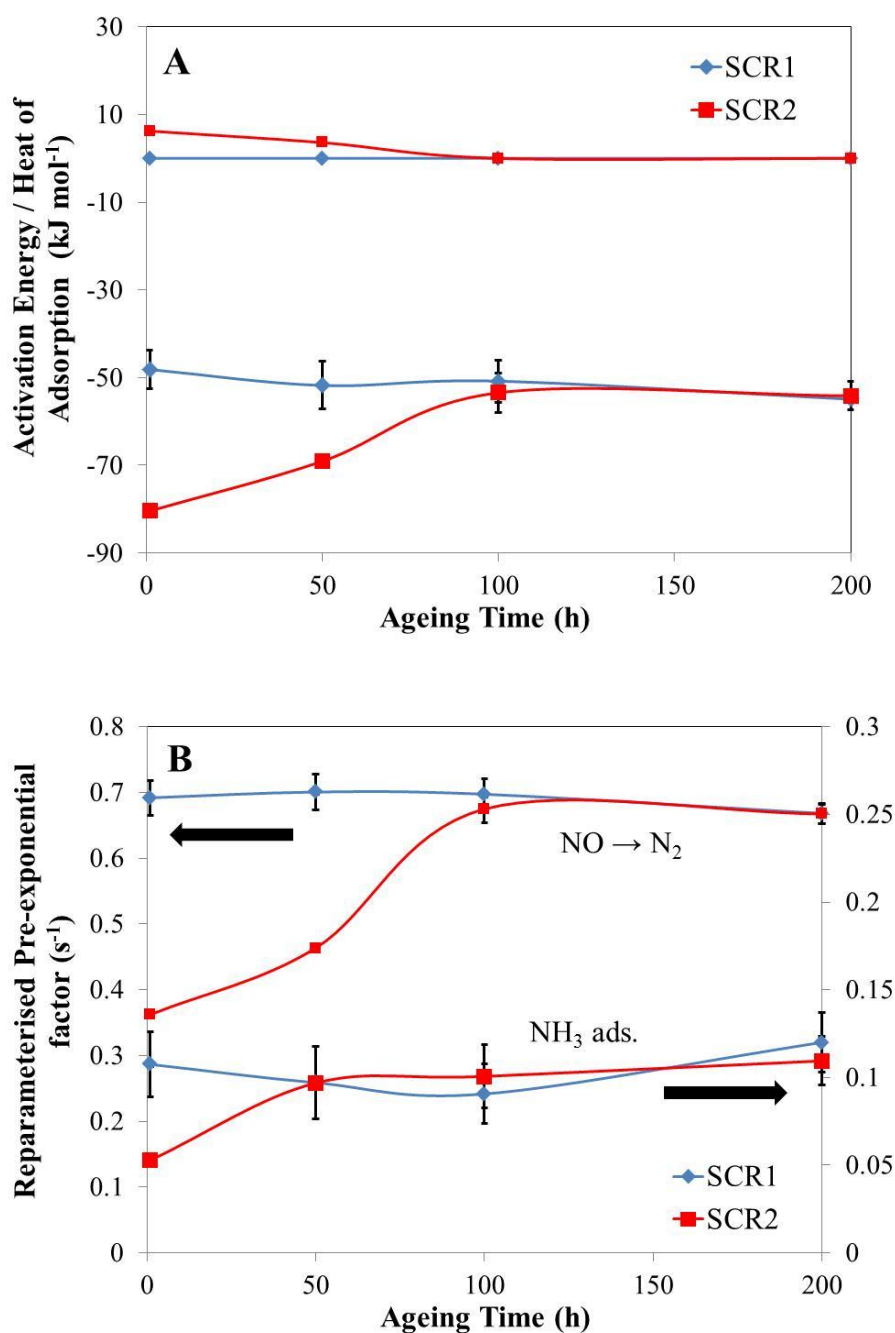


**Figure 5.9: Parameter estimates for energies of model reaction steps (A) and their re-parameterised pre-exponential factors (B). Ageing conditions were 873 K and  $T_{base} = 423\text{K}$  for re-parameterisation.**

In all cases, quality of fit was greatly improved ( $R^2 > 0.99$ ) and as Figure 5.9 shows, parametric 95% confidence intervals are acceptable. Inspection of the parametric estimates in

Figure 5.9 suggests that SCR2 in particular is quite dynamic in its kinetic evolution over the first 100 h of ageing. Indeed the value of  $\Delta H_{ads}$  for SCR2 changes with time before reaching the value of SCR1 (after 100 h ageing) suggesting development/loss of different adsorption sites. These observations aside however, questions are raised around the suitability of this model:

- Both pre-exponential factors measured for SCR2 increase with time. These values should relate to populations of active sites, which suggest that their population is increasing with time. This is counter intuitive as  $\text{NO}_x$  conversion performance of SCR2 decreases with time in the 453 – 673 K range.
- $E_a$  values for the  $\text{NO} \rightarrow \text{N}_2$  step are very small (or set to zero). This agrees to some extent with the low value presented by Lintz and Turek, (1992) although it is of concern that the value is tending towards insignificance.

Whilst the model of Lintz and Turek, (1992) suggests that catalyst SCR2 possesses different site populations in comparison to SCR1 initially, there are a number of inconsistencies with the parameters measured and so further models should be tested.

### 5.3.3.2 Kinetic analysis using the model of Dumesic *et al.*

The model of Dumesic *et al.*, (1996) used a rigorous approach and in its complete form features 6 reaction steps to cover both the acid and redox cycles in  $\text{V}_2\text{O}_5\text{-WO}_3/\text{TiO}_2$  catalyst behaviour for ammonia SCR. Model parameters in this work were ascertained from an intrinsic kinetic study but were validated against industrial operating conditions, not too dissimilar to the feed and temperature conditions used in the current work.

Three of these steps, which involve product water removal, water inhibition and redox site re-oxidation ( $\text{V}^{3+} \rightarrow \text{V}=\text{O}$ ) are omitted from this analysis. This is due to high feed concentrations of water and oxygen the current work, which are relatively unchanged at the reactor exit. The 3 remaining reactions considered are shown below (Eq. (5.15-17)):



Eq. (5.17) describes ammonia adsorption onto an acid site (M) and is a fast, equilibrated term ( $K_{NH3}$ ). Eq. (5.18) describes ammonia activation via a reactive site (S) and is slow and reversible (rate terms:  $k_2$  and  $k_{-2}$ ). Eq. (5.19) describes the interaction of NO with activated ammonia to produce products such as  $N_2$ . The above sequence is mathematically described below (Topsøe *et al.*, 1995):

$$r_{NO} = P_{NO} \frac{K_3 \frac{P_{NH3}}{P_{NO}}}{1 + K_1 \frac{P_{NH3}}{P_{NO}} + \frac{K_2}{P_{NO}} + K_{NH3} P_{NH3}} \quad (5.22)$$

Where,  $K_1 = k_2 K_{NH3} / k_3$ ,  $K_2 = k_{-2} / k_3$  and  $K_3 = k_2 K_{NH3}$ . For each of these terms, a lumped activation energy was employed, based on the values presented in Dumesic *et al.*, (1996) for an  $V_2O_5$ - $WO_3$ / $TiO_2$  catalyst operating under industrially relevant conditions. These values and confidence intervals are shown in Table 5.5 below:

**Table 5.5: Kinetic parameters quoted in Dumesic *et al.*, (1996) used in this study.**

Parameter	$\Delta H_{ads}$ or $E_a$ (kJ mol <sup>-1</sup> )	
$K_{NH3}$	-83.6	-
$k_2$	90.3	± 9.2
$k_{-2}$	134.2	± 22.2
$k_3$	23.0	± 0.4
$K_1$	-16.3	± 31.8
$K_2$	111.2	± 22.6
$K_3$	6.7	± 9.2

When fitting these data, the  $\Delta H_{ads}$  and  $E_a$  values for each of the parameters were fixed, initially using the centre points in Table 5.5. This left 4 fitting parameters, the pre-exponential factors for each of the  $K_i$  terms, which were re-parameterised using a  $T_{base}$  of 348 K. Initial model testing over all data sets provided a good fit ( $R^2 > 0.99$ ) but in all cases the model was over parameterised. Using the parameter reduction method described in Chapter 3, terms  $K_1$  and  $K_2$  yielded insignificant contributions and were removed from the expression. This is not surprising, due to the wide confidence intervals on the lumped energy values on

these parameters. Ultimately, this reduced the kinetic expression to the following equation which was used for the rest of the fitting process:

$$r_{NO} = \frac{P_{NH_3}}{\frac{1}{K_{NH_3}k_2} + \frac{1}{k_2}P_{NH_3}} \quad (5.23)$$

The two parameter model therefore describes two steps, ammonia adsorption ( $K_{NH_3}$ ) and the forwards term for ammonia activation ( $k_2$ ). It is noted that these parameters can also be estimated separately, without the use of lumped terms. No NO reduction term ( $k_3$ ) is present, which agrees with the low  $E_a$  values estimated using the model of Lintz and Turek (1992). Previous apparent kinetics analysis revealed the apparent reaction order in  $NH_3$  to be approximately zero, suggesting that  $NH_3$  strongly binds to the catalyst surface. The prevalence of the  $K_{NH_3}$  and  $k_2$  in the final kinetic model support this as both pertain to chemisorbed  $NH_3$  (in two different conformations).

The activation energies used in Eq. (5.21) required only minor changes to the values quoted by Dumesic *et al.*, (1996) to optimise the fitting procedure. The adjustments carried out on  $k_2$  were less than  $1 \text{ kJ mol}^{-1}$  for both catalysts. This is well within the confidence range quoted in Table 5.5.  $R^2$  values for all fits were  $> 0.99$ .

Parameter estimation results using Eq. (5.21) are shown in Figure 5.10. SCR1 and SCR2 are distinctly different from one another in their fresh form. SCR1 has a significantly higher  $K_{NH_3}$  pre-exponential factor than SCR2 suggesting that it has a greater population of active sites for ammonia adsorption. Meanwhile, for  $k_2$ , the reverse is true where SCR2 has a much greater population of sites for ammonia activation than SCR1. Given that ammonia activation has previously been cited as a slow step in the catalytic cycle, particularly in comparison to ammonia adsorption (Lintz and Turek, 1992; Dumesic *et al.*, 1996; Efstatiou and Fliatoura, 1995; Forzatti, 2001) this may explain the better performance of SCR2 initially.

For 873 K ageing times of 50, 100 and 200 hr, both catalysts have largely similar  $k_2$  values within parameter confidence intervals. Evolution of the  $K_{NH_3}$  differs for both catalysts. The population of ammonia adsorption sites for SCR2 quickly equilibrates over the initial 50 hours ageing and then remains roughly constant. Meanwhile,  $K_{NH_3}$  site populations for SCR1

decrease over 50 – 100 hours ageing before increasing again towards a similar value to SCR2 at 200 hours ageing.

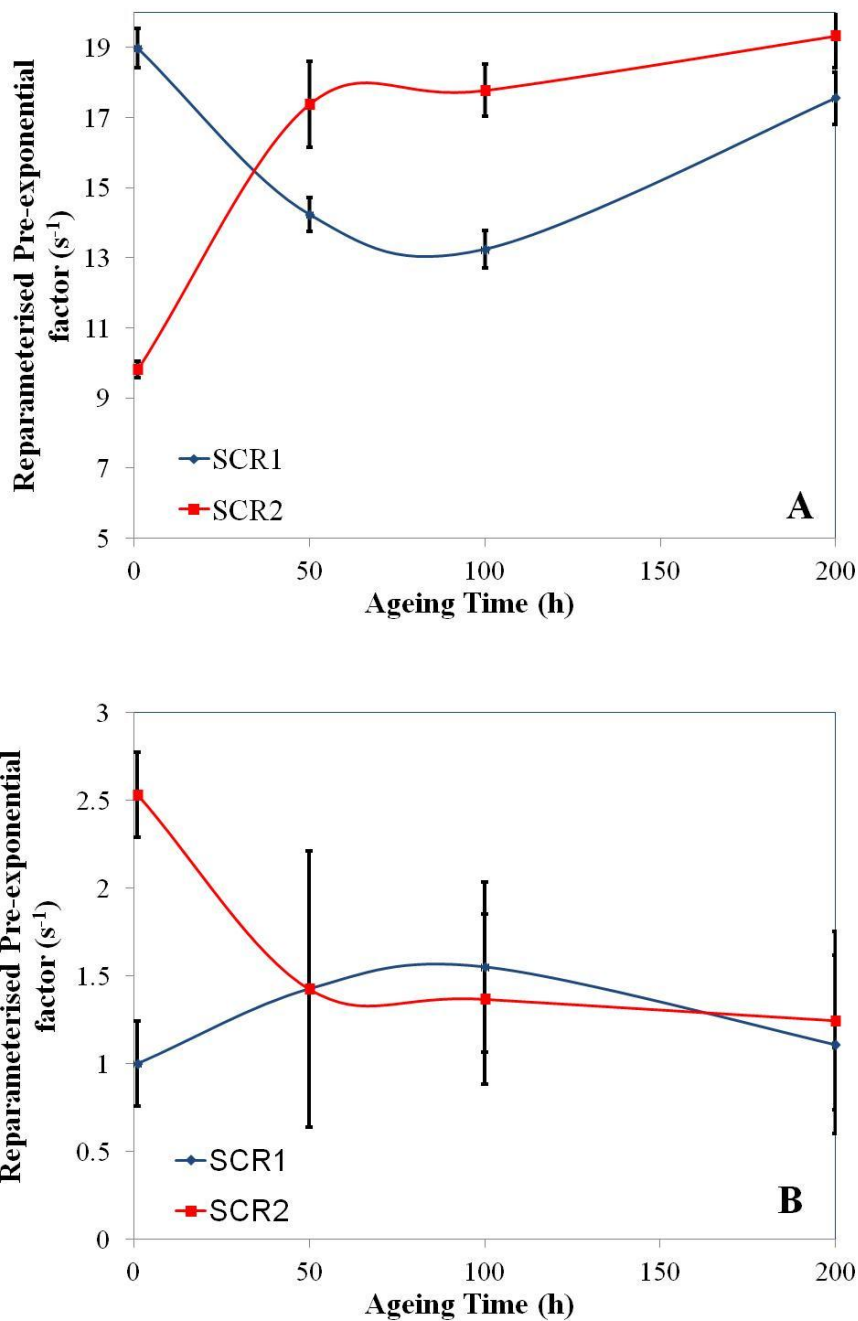


**Figure 5.10: Parameter estimates for re-parameterised pre-exponential factors ( $T_{base} = 348K$ ) of  $K_{NH3}$  (Graph A) and  $k_2$  (Graph B) for SCR1 and SCR2 catalysts. Ageing conditions were 873 K. N.B.: Lines are to guide the eye.**

Further analysis was carried out using 823 K ageing data for comparison (Figure 5.11). There are some important similarities and differences to 873 K garnered from this:

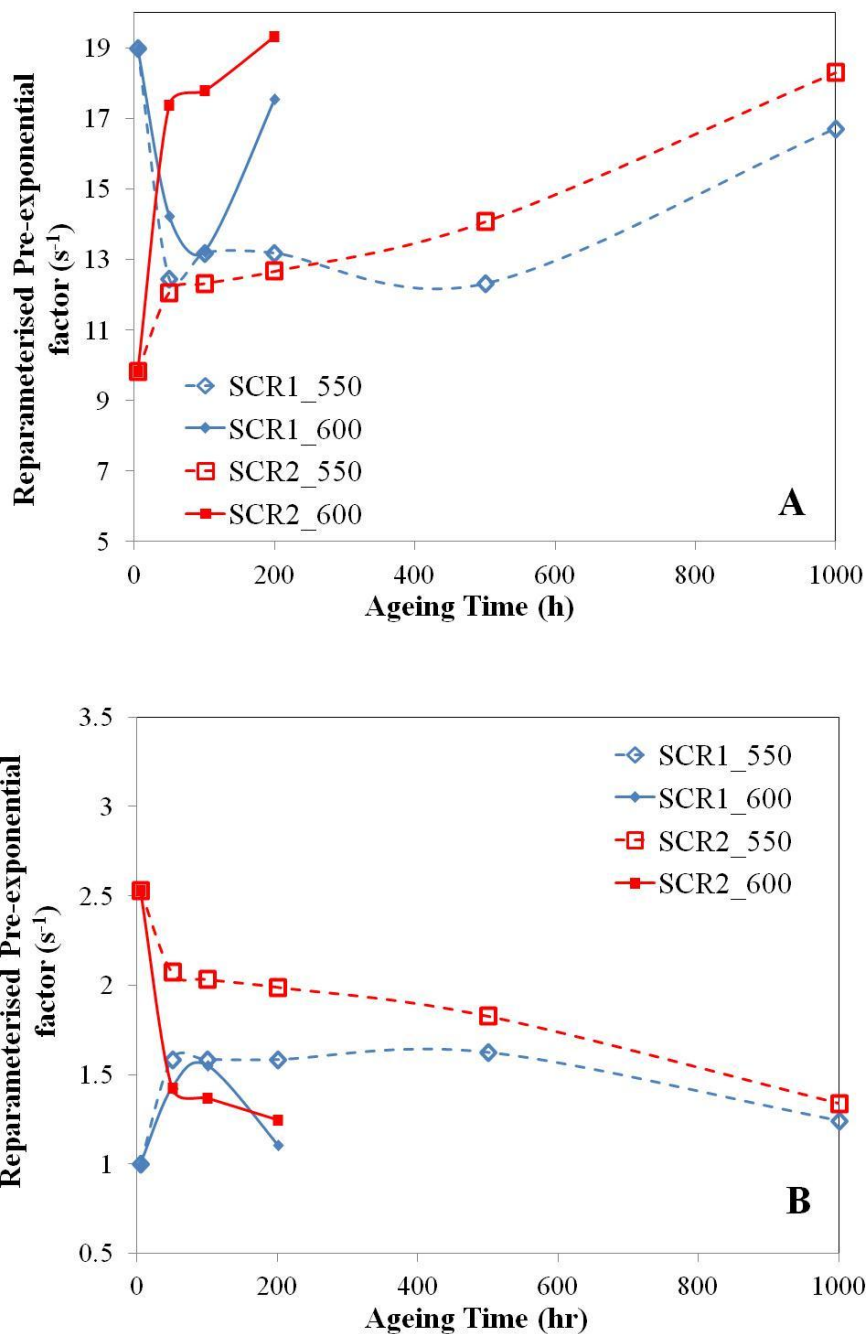


**Figure 5.11: Comparison of parametric evolution ( $T_{\text{base}} = 348\text{K}$ ) of  $A_{\text{NH}_3}$  (graph A) and  $A_2$  (graph B) for SCR1 and SCR2 at different ageing temperatures against ageing time (open symbols: 823 K, closed symbols 873 K). N.B.: Lines are to guide the eye; error bars are omitted for clarity.**

- Initial evolution of both  $K_{NH_3}$  and  $k_2$  for SCR2 over the first 50 hours is ageing temperature dependent; both parameters evolve more significantly under 873 K ageing.
- A SCR1 catalyst aged for 1000 hours at 823 K has very similar kinetic parameters to one aged for 200 hours at 873 K. Evolution of the catalyst is similar for both temperatures of the first 50 hours but appears to be a function of temperature over the longer periods of ageing.
- Similarly, SCR2 catalysts after 200 hours 873 K ageing or 1000 hours 823 K ageing have similar kinetic parameters. Longer term evolution of this catalyst appears to be ageing temperature dependent.
- Pre-exponential factors for  $K_{NH_3}$  were also checked for thermodynamic consistency. In this term, the pre-exponential represents  $e^{\Delta S_{ads}/R}$ .  $(-\Delta S_{ads})$  must remain positive and not exceed the entropy of the gas,  $S^0$  at a given temperature and pressure. For the estimated parameters,  $(-\Delta S_{ads})$  was found to range between 46.2 and 52.4 J mol<sup>-1</sup> K<sup>-1</sup> which is lower than the entropy of ammonia at 100 ppm in the tested temperature range (222 and 242 J mol<sup>-1</sup> K<sup>-1</sup> for 453 and 773 K respectively (Barin, 1989).

Overall, the model of Dumesic *et al.*, (1996) suggests that a fresh SCR2 catalyst has a high population of ammonia activation sites. These decay with ageing time whilst ammonia adsorption site population increases, thus NO<sub>x</sub> conversion decreases as a result. Meanwhile SCR1 undergoes an initial ‘activation’ period whereby ammonia adsorption site population increases, as does NO<sub>x</sub> conversion. Following this, SCR1 undergoes long term performance decay in a similar manner to SCR2.

The literature has discussed the importance of the ammonia activation step in context of the V<sub>2</sub>O<sub>5</sub>-WO<sub>3</sub>/TiO<sub>2</sub> de-NO<sub>x</sub> mechanism. Some works discuss this as involving interaction between an acid site (V<sup>5+</sup>-ONH<sub>4</sub>) with a redox site (V=O) (Topsøe *et al.*, 1995; Dumesic *et al.*, 1996) and others discuss NH<sub>3</sub> adsorption (and storage) taking place on Ti sites with subsequent activation by reactive V sites (again such as V=O) (Lietti *et al.*, 1998; Nova *et al.*, 2001).

Based on these arguments, it is possible that an improved calcination procedure (SCR2) can generate an increased quantity of reactive V sites, or indeed an improved surface

distribution between  $\text{NH}_3$  adsorption/storage sites and reactive sites. Performance of SCR2 does decay with ageing time which may be a function of a shift in distribution of these sites or perhaps a change in physical-chemical structure of the reactive V sites. Interestingly, initial thermal ageing of SCR1 increases its quantity of reactive sites for ammonia activation and suggests that a certain level of thermal effects alone can develop a more active catalyst, as has been developed to a greater extent with the calcinations process for SCR2. The product performance data applied in this section has provided a working model for study, which will be probed in the subsequent section using TPD techniques. As the steady state kinetic model has suggested two different populations of chemisorbed  $\text{NH}_3$  (adsorption and ‘activated’ sites), TPD will act as an initial approach to probe quantities of these adsorbed states.

The de- $\text{NO}_x$  performance sensitivities seen as a function of calcination and ageing time and temperature are in line with observations from a previous work (Kompio, 2010). A formulation comprising 5 wt. %  $\text{WO}_3$  and 1.5 wt. %  $\text{V}_2\text{O}_5$  showed a non-linear progression of de- $\text{NO}_x$  performance as a function of calcination temperature (873 or 1023 K) and time (5 – 10000 min). de- $\text{NO}_x$  performance maxima were seen following a 15 min or 4 h calcination at 1023 K or a week or 4 weeks for a 873 K calcination.

#### 5.3.4 TPD studies

TPD studies were carried out using the methodology described in section 5.2.4. In this section, four TPD profiles are analysed for the fresh and 200 h, 873 K aged SCR1 and SCR2 catalysts respectively. In each case the catalysts had undergone isothermal adsorption and desorption of ammonia at 523 K. The raw TPD profiles are shown in Figure 5.12 (overleaf).

Inspection of Figure 5.12 reveals that the magnitude of ammonia adsorbed is very different on each of the SCR catalysts. The general trend is that the molar amount of ammonia desorbed during the TPD increases with age and extent of thermal treatment (SCR1-Fresh < SCR2- Fresh < SCR1-Aged < SCR2-Aged). These values are quoted below in Table 5.6 with accompanying surface coverage and storage capacity values.

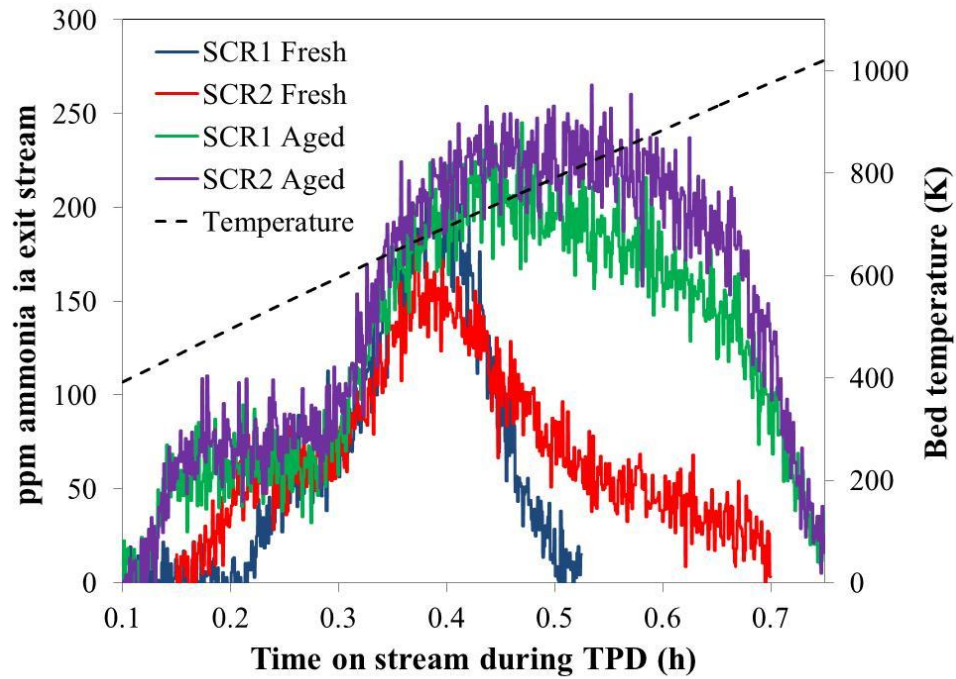


**Figure 5.12: Raw exit stream ammonia response during TPD for all four SCR catalysts tested. In all cases 0.1 g catalyst had undergone isothermal adsorption and desorption of ammonia at 523 K.**

The changing shape of the TPD profiles with age is also distinct. An increased amount of adsorbed ammonia with age is seen both in the lower temperature range (shoulder between 423 and ~600 K) and higher temperature range (700 – 1000 K). Such observations provide initial clues that multiple adsorption sites may be prevalent on the catalyst surface, which vary in number with age.

In order to model ammonia desorption during the TPD step, the non-steady state models described in Eq. (5.11-12) were utilised. The fractional surface  $\text{NH}_3$  coverage values prior to TPD, shown in Table 5.6, were utilised as the input conditions for the desorption models. As the inlet flow conditions always comprised 0 ppm of ammonia, only the ammonia desorption step was modelled and  $r_a$  was set to zero by virtue of the inlet concentration.

**Table 5.6: Ammonia desorbed during TPD and calculated ammonia surface coverage and catalyst storage capacity prior to TPD step (N.B.: basis for surface coverage is an ammonia molecule has a diameter of 0.36 nm)**

<b>Catalyst</b>	<b>NH<sub>3</sub> desorbed from surface during TPD (μmol)</b>	<b>Calculated surface coverage of NH<sub>3</sub> prior to TPD (-)</b>	<b>Catalyst NH<sub>3</sub> storage capacity; based on NH<sub>3</sub> adsorbed prior to TPD (mol m<sup>-3</sup>)</b>
<b>SCR1 Fresh</b>	9.5	0.08	151
<b>SCR2 Fresh</b>	13.0	0.14	208
<b>SCR1 Aged</b>	27.0	0.42	433
<b>SCR2 Aged</b>	31.8	0.51	509

In order to model the results in Table 5.6 and Figure 5.12, an activated desorption step was utilised and is described as follows:

$$r_d = k_d^0 \exp\left(\frac{-E_d}{RT} \cdot \theta_{NH_3}\right) \quad (5.24)$$

In Eq. (5.22),  $k_d^0$  and  $E_d$  denote the pre-exponential factor and activation energy of desorption. It has been noted in previous literature that V<sub>2</sub>O<sub>5</sub>-WO<sub>3</sub>/TiO<sub>2</sub> catalysts can feature a degree of surface heterogeneity which can impact on the value of  $E_d$  as a function of surface coverage of ammonia (Lietti *et al.*, 1998). Four different models to describe the spread of  $E_d$  values over a single type of adsorption site were considered:

$$E_d = \text{constant} \quad (5.25)$$

$$E_d = E_d^0(1 - \alpha \cdot \theta_{NH_3}) \quad (5.26)$$

$$E_d = E_d^0(1 - \alpha \cdot \theta_{NH_3}^\sigma) \quad (5.27)$$

$$E_d = E_d^0 \exp(\alpha \cdot \theta_{NH_3}) \quad (5.28)$$

Eq. (5.23) describes a Langmuir-type assumption whereby  $E_d$  does not change with coverage. Eq. (5.24-25) describes a Temkin-type and modified Temkin-type assumption respectively whereby  $E_d$  shows a linear decrease with surface coverage. Eq. (5.26) describes a Freundlich-type description whereby  $E_d$  shows a logarithmic decrease with surface coverage.  $\alpha$  and  $\sigma$  are fitting constants.

When solving the non-steady state concentration balance in Eq. (5.12), catalyst storage capacity,  $\Omega$ , was originally included in the fitting procedure. The value of this constant however was always found to tend to a value similar to the amount of ammonia stored on catalyst prior to the TPD step. Hence capacity was fixed based on the initial stored amount. An added benefit of this decision was the removal of cross-correlation between  $\Omega$  and estimated values of  $k_d^0$ .

During the parameter estimation process for all four SCR catalysts it was found that the use of modified Temkin and Freundlich-type descriptions did not enhance the data fitting process and led to poor confidence intervals of estimated parameters. Ultimately, a Langmuir-type model was found to be best for both fresh SCR catalysts and a Temkin-type model was best for the aged ones. Temkin models are good indicators of the presence of more than one adsorption site without the need to utilise specific site coverage values on the surface. This therefore suggests that a second site adsorption site may have been developed as a function of ageing.

The results, showing experimental data and model predictions are shown in Figure 5.13. It is clearly seen on these plots that the assumption of a single type of adsorption site ( $\theta_{NH_3}$ ) becomes less effective with age of the catalyst. The data fit for SCR1-Fresh is largely good, barring the small ‘shoulder’ below 600 K. For SCR2-Fresh and the aged catalysts however, a single site assumption becomes an increasingly poorer prediction, even with the use of a Temkin-type assumption.

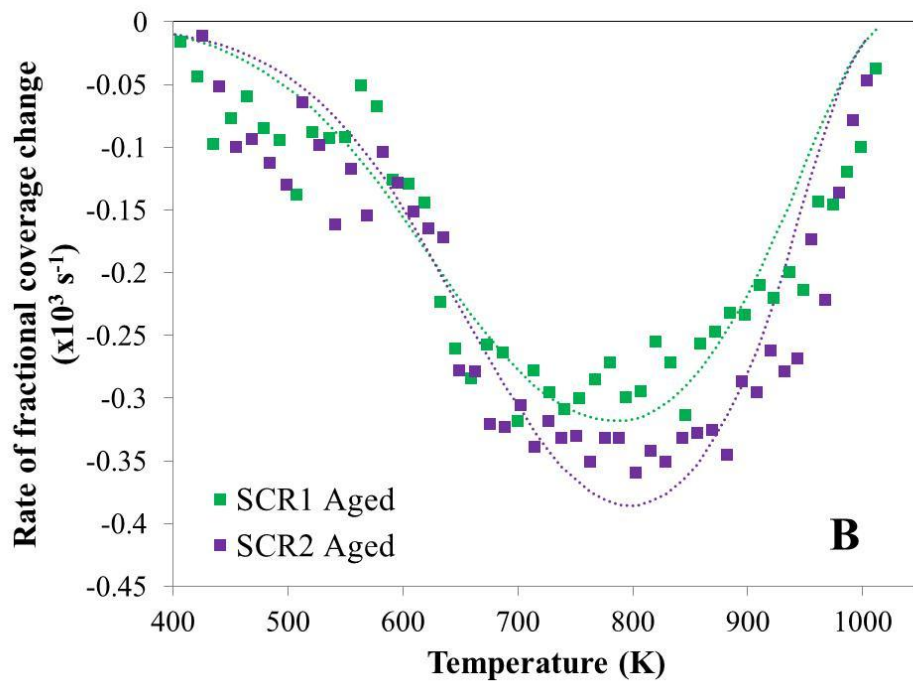
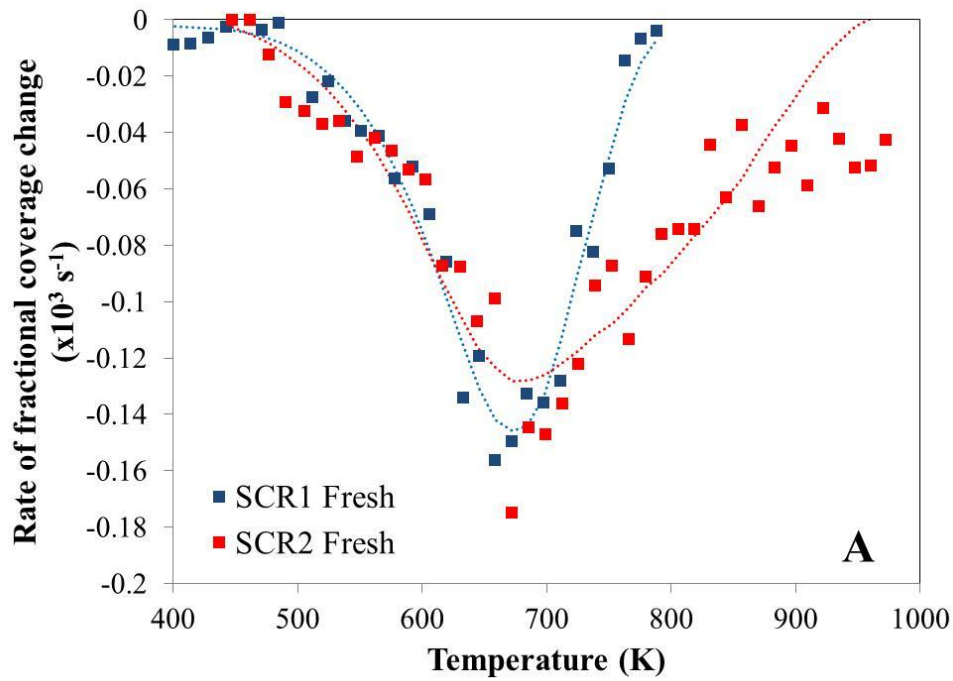


**Figure 5.13: Ammonia TPD over 0.1 g of A) Fresh SCR1 and SCR2 and B) 200 h 873 K aged SCR1 and SCR2 using a temperature ramp rate of  $15 \text{ K min}^{-1}$ . Solid squares denote experimental data, dotted lines denote final single site model (Eq. 5.23 for fresh catalysts in A), Eq. 5.24 for aged catalysts in B)**

Table 5.7 shows the final estimated parameters for all four catalysts. Whilst the confidence intervals for all estimated parameters are good, key concerns centre around the drastically changing  $E_d^0$  values between the catalysts; for example SCR1-Fresh and SCR2-Fresh both utilise a Langmuir assumption but have very different  $E_d^0$  values. If a single site model was fully correct, fundamentally both of these catalysts should estimate a similar  $E_d^0$  value. Coupled with a poorer data fit, this suggests that at least two distinct sites may be prevalent on the catalyst surface for SCR2-Fresh. For the two aged catalysts, the need for a Temkin-type model, although still inadequate, again suggests multiple distinct adsorption sites may be required.

**Table 5.7: Final  $E_d$  models and estimated parameters to describe TPD profiles for the four SCR catalysts tested (N.B.: error bars are 95% confidence intervals generated in the parameter estimation process)**

Catalyst	$E_d$ model used	$k_d^0$ (mol m <sup>-3</sup> s <sup>-1</sup> ) (repar. at $T_{base}$ = 625 K) (x 10 <sup>3</sup> )	$E_d^0$ (kJ mol <sup>-1</sup> )	$\alpha$ (-)
SCR1 Fresh	Langmuir	24.8 ± 1.4	59.9 ± 3.7	-
SCR2 Fresh	Langmuir	7.5 ± 0.5	25.6 ± 2.2	-
SCR1 Aged	Temkin	1.4 ± 0.1	33.2 ± 3.0	0.91 ± 0.28
SCR2 Aged	Temkin	1.0 ± 0.1	37.1 ± 2.5	0.91 ± 0.17

In context to the steady-state kinetic modelling carried out in Section 5.3.3, the TPD profiles provide good but qualitative evidence that two or more distinct ammonia adsorption sites are prevalent on these SCR catalysts. Previous literature, using model V<sub>2</sub>O<sub>5</sub>/TiO<sub>2</sub> and V<sub>2</sub>O<sub>5</sub>-WO<sub>3</sub>/TiO<sub>2</sub> has typically utilised Temkin-type models over a single type of ammonia adsorption site with  $E_d^0$  values estimated in the range of 100 – 110 kJ mol<sup>-1</sup> (Lietti *et al.*, 1997). In this work, the catalysts tested were calcined at 823 K, lower than any of the materials in the current study. A postulation for the presence of at least two distinct ammonia adsorption sites in the current work could therefore be driven by the use of higher calcination temperatures, and subsequent ageing.

The catalysts in the current study show significantly lower  $E_d^0$  values than in Lietti *et al.* (1997); indeed for the aged catalysts strongly bound ammonia desorbed at 800 – 1000 K is unlikely to feature an energy of  $\sim 30$  kJ mol<sup>-1</sup>. This is a further indication that the current model is inadequate as the estimated values should be much higher than this. Dual/multiple site approaches such as those discussed in Colombo *et al.* (2012) should be applied as future work if an understanding of specific adsorption site coverage fractions can be ascertained.

## 5.4 Conclusions

A study of V<sub>2</sub>O<sub>5</sub>-WO<sub>3</sub>/TiO<sub>2</sub> ammonia SCR catalyst formulations, differing in state as a function of initial calcination and extent of thermal ageing was investigated. This topic was identified as an excellent case study to utilise a combination of steady and non-steady state kinetic analysis methods to elucidate fundamental differences in surface populations of adsorption sites. Central to this study were two SCR catalysts which showed different de-NO<sub>x</sub> performance (SCR2 > SCR1) in their post calcination, ‘fresh’, form but were essentially the same in performance following extensive thermal ageing.

Steady state de-NO<sub>x</sub> performance data of the two differently calcined SCR catalysts were modelled at different stages of catalyst ageing (Fresh → 200 h 873 K thermal aged). A simplified version of the mechanistic literature model of Dumesic *et al.* (1996) was found to be most appropriate at describing all datasets. The model chiefly comprised two terms to describe ammonia adsorption and activation respectively, the latter a precursor to NO<sub>x</sub> reduction. In fresh form, catalyst SCR1 was found to contain a higher population of ammonia adsorption sites and a lower population of ammonia activation sites than SCR2 (calcined at a temperature 30 K higher). Estimated parameters were very similar for both catalysts following 200 h 873 K ageing, which agrees with the similar de-NO<sub>x</sub> behaviour they exhibit during testing.

In line with the aims, a detailed mechanistic model from the literature was found to be highly suitable at describing performance evolution of both SCR catalysts, even with the limited datasets employed (5 data points in each case). This led to a model for SCR catalyst performance that is linked to populations of two active sites, namely ammonia adsorption and activation. This is consistent with previous SCR literature, which has shown that both acidic and redox sites are needed to carry out the overall NO reduction reaction by NH<sub>3</sub>, the latter of which is achieved by the addition of V<sub>2</sub>O<sub>5</sub> (Lietti *et al.*, 1997).

Various catalyst characterisation and TPD methods were employed to further understand fundamental differences between SCR1 and SCR2. Characterisation methods such as XRD and Raman were not effective in this. A link with ageing and anatase crystallite size was observed however this is non-linear with de-NO<sub>x</sub> performance of the catalysts tested.

TPD methods were more effective in discerning the nature of the catalyst surface for both SCR1 and SCR2. Both catalysts were assessed in their fresh and 200 h, 873 K thermally aged form. Fresh SCR2 showed a greater amount of adsorbed ammonia removed than fresh SCR1 during the TPD, the additional amount of which was found in both the lower and higher temperature stages of the temperature ramp. Both aged catalysts showed significantly more adsorbed ammonia removed during the TPD, in particular in the high temperature region (> 700 K).

Non-steady state kinetic modelling of the TPD steps has led to qualitative conclusions at this stage. A single site coverage model was found to be reasonably effective at describing the TPD of the SCR1-Fresh catalyst but not with SCR2-Fresh or the aged materials. This suggests that at least a second distinct ammonia adsorption site has developed in these materials. It is important to note that the findings from the TPDs imply a multiplicity of NH<sub>3</sub> adsorption sites but these are not currently proven to relate to the active sites in the postulated steady state kinetic model.

On reflection of the aims, this study has seen success, albeit qualitative, in combining steady and non-steady state kinetics methods to discern differences in site populations of different catalyst formulations. Further work is needed to understand the nature of distinct active site surface coverages for these materials to provide quantitative conclusions from these methods. Finally, and more importantly, methods such as reactive titrations using NO should be applied to the catalysts prior to the TPD step. The aim here will be to look at the reactivity of the adsorbed NH<sub>3</sub> and subsequently assess the remaining unreacted NH<sub>3</sub> by TPD. This will provide support as to which of the postulated NH<sub>3</sub> adsorption sites relate to the active site for the NO reduction reaction, an elucidate their quantities for each catalyst formulation.

## 5.5 References

- Amiridis M.D., Solar J.P., (1996), '*Selective catalytic reduction of nitric oxide by ammonia over  $V_2O_5/TiO_2$ ,  $V_2O_5/TiO_2/SiO_2$  and  $V_2O_5-WO_3/TiO_2$  catalysts: Effect of vanadia content on the activation energy*', Ind. Eng. Chem. Res., 35, 978-981
- Barin I., (1989), '*Thermochemical data of pure substances*', Verlag Chemie, Berlin
- Bond G.C., Tahir S.F., (1991), '*Vanadium oxide monolayer catalysts: Preparation, characterisation and catalytic activity*', App. Cat., 71, 1-31
- Busca G., Ramis G., (1994), in '*Proceedings of the Italian conference on chemical and process engineering, Firenze, 1993*', AIDIC, Milan, p 91
- Busca G., Lietti L., Ramis G., Berti F., (1998), '*Chemical and mechanistic aspects of the selective catalytic reduction of  $NO_x$  by ammonia over oxide catalysts: A review*', App. Cat. B: Env., 18, 1-36
- Caracotsios M., Stewart W.A.E., (1985), '*Sensitivity analysis of initial value problems with mixed ODEs and algebraic equations*', Comp. and Chem. Eng., 9, 4, 359-365
- Carberry J.J., in: Anderson J.R., Boudart M., (eds), (1987) '*Catalysis: Science and Technology, Vol. 8*' Springer, Berlin, p. 131
- Chen J.P., Yang R.T., (1992), '*Selective catalytic reduction of NO with  $NH_3$  on  $SO_4^{2-}/TiO_2$  superacid catalyst*', J. Catal., 139, 277-288
- Colombo M., Kolsakis G., Nova I., Tronconi E., (2012), '*Modelling the ammonia adsorption-desorption process over a Fe-zeolite catalyst for SCR automotive applications*', Catal. Today, 188, 42-52
- Dumesic J.A., Topsøe N-Y., Slabiak T., Morsing P., Clausen B.S., Törnqvist E., Topsøe H., (1993), '*Proceedings of the 10<sup>th</sup> international congress on catalysis, Budapest*', p. 1325
- Dumesic J.A., Topsøe N-Y., Topsøe H., Chen Y., Slabiak T., (1996), '*Kinetics of selective catalytic reduction of nitric oxide by ammonia over vanadia/titania*', J. Catal, 163, 409-417

- Efstathiou A.M., Fliatoura K., (1995), '*Selective catalytic reduction of nitric oxide with ammonia over  $V_2O_5/TiO_2$  catalyst: A steady-state and transient kinetic study*', App. Cat. B: Env., 6, 35-59
- Forzatti P., (2001), '*Present status and perspectives in de- $NO_x$  SCR catalysis*', App. Cat. A: Gen, 222, 221-236
- Hegedus L.L., Beekman J.W., Pan W.-H., Solar J.P., (1990), '*Catalysts for selective catalytic reduction denox technology*', U.S. Patent 4,929,586
- Ingemar Odenbrand C.U., Gabriellson P.L.T., Brandin J.G.M., Andersson L.A.H., (1991), '*Effect of water vapour on the selectivity in the reduction of nitric oxide with ammonia over vanadia supported on silica-titania*', App. Cat., 78, 109-123
- Inomata M., Miyamoto A., Murakami Y., (1980), '*Mechanism of the reaction of NO and  $NH_3$  on vanadium oxide catalyst in the presence of oxygen under dilute gas condition*', J. Catal., 62, 140-148
- Kleemann M., Elsener M., Koebel M., Wokaun A., (2000), '*Investigation of the ammonia adsorption on monolithic SCR catalysts by transient response analysis*', App. Cat. B: Env, 27, 231-242
- Klug H.P., Alexander L.E., (1974), '*X-ray diffraction procedures*', Wiley Interscience, New York
- Kobayashi M., Kobayashi H., (1972), '*Application of transient response method to the study of heterogeneous catalysis – 3 parts*', J. Catal., 27, 100-119
- Kobayashi M., (1982), '*Characterisation of transient response curves in heterogeneous catalysis – 2 parts*', Chem. Eng. Sci., 37, 3, 393-409
- Kompio P.G.W.A. (2010), '*Der einfluss von Hocktempertaurbehandlungen auf  $V_2O_5-WO_3/TiO_2$ -Katalysatoren für die Selektive Katalytische Reduktion von Stickoxiden mit Ammoniak*', PhD thesis, Ruhr-Universität Bochum
- Lietti L. and Forzatti P., (1994), '*Temperature programmed desorption/reaction of ammonia over  $V_2O_5/TiO_2$  de- $NO_x$ -ing catalysts*', J. Catal., 147, 241-249

- Lietti L., Alemany J.L., Forzatti P., Busca G., Ramis G., Giamello E., Bregani F., (1996), '*Reactivity of  $V_2O_5$ - $WO_3$ / $TiO_2$  catalysts in the selective catalytic reduction of nitric oxide by ammonia*', Catal. Today, 29, 143,148
- Lietti L, Nova I, Camurri S., Tronconi E., Forzatti P., (1997), '*Dynamics of the SCR- $DeNO_x$  reaction by the transient response method*', AIChE Jnl., 43, 10, 2259
- Lietti L., Nova I., Tronconi E., Forzatti P., (1998), '*Transient kinetic study of the SCR- $DeNO_x$  reaction*', Catal. Today, 45, 85-92
- Lintz H.-G., Turek T., (1992), '*Intrinsic kinetics of nitric oxide reduction by ammonia on a vanadia-titania catalyst*', App. Cat. A: Gen, 85, 13-25
- Madia G., Elsener M., Koebel M., Raimondi F., Wokaun A., (2002), '*Thermal stability of vanadia-tungsta-titania catalysts in the SCR process*', App. Cat. B: Env, 39, 181-190
- Marquardt D., '*An algorithm for least-squares estimation of nonlinear parameters*', (1963), S.I.A.M. K. App. Math., 11, 143
- Mears D.E., (1971) '*The role of axial dispersion in trickle-flow laboratory reactors*' Chem. Eng. Sci. 26, 1361
- Nakajima F., Hamada I., (1996), '*The state-of-the-art technology of  $NO_x$  control*', Catal. Today, 29, 109-115
- Nova I., Lietti L., Tronconi E., Forzatti P., (2000), '*Dynamics of SCR reaction over a  $TiO_2$  supported vanadia-tungsta commercial catalyst*', Catal. Today, 60, 73-82
- Nova I., Lietti L., Tronconi E., Forzatti P., (2001), '*Transient response method applied to the kinetic analysis of the  $DeNO_x$ -SCR reactions*', Chem. Eng. Sci., 56, 1229-1237
- Orlik S.N., Ostapyuk V.A., Martsenyuk-Kurkharuk M.G., (1995), Kinetic Katal., 36, 284
- Shi A., Wang X., Yu T., Shen M., (2011), '*The effect of zirconia additive on the activity and structure stability of  $V_2O_5$ / $WO_3$ - $TiO_2$  ammonia SCR catalysts*', App. Cat. B: Env, 106, 359-269

Srnak T.Z., Dumesic J.A., Clausen B.S., Törnqvist E., Topsøe N.-Y., (1992), '*Temperature-programmed desorption/reaction and in situ spectroscopic studies of vanadia/titania for catalytic reduction of nitric oxide*', J. Catal., 135, 246-262

Topsøe N.-Y., Dumesic J.A., Topsøe H., (1995), '*Vanadia/titania catalysts for selective catalytic reduction of nitric oxide by ammonia*', J. Catal., 151, 241-252

Tronconi E., Forzatti P., (1992), '*Adequacy of lumped parameter models for SCR reactors with monolith structure*', AIChE Journal, 38, 2, 201

Tronconi E., Forzatti P., Gomez Martin J.P., Malloggi S., (1992), '*Selective catalytic removal of NO<sub>x</sub>: A mathematical model for design of catalyst and reactor*', Chem. Eng. Sci., 47, 2401-2406

Tronconi E., Lietti L., Forzatti P., Malloggi S., (1996), '*Experimental and theoretical investigation of the dynamics of the SCR-DeNO<sub>x</sub> reaction*', Chem. Eng. Sci., 51, 11, 2965

Tronconi E., Nova I., Ciardelli C., Chatterjee D., Weibel M., (2007), '*Redox features in the catalytic mechanism of the 'standard' and 'fast' NH<sub>3</sub>-SCR of NO<sub>x</sub> over a V-based catalyst investigated by dynamic methods*', J. Catal., 245, 1-10

Van de Waal S.W.A., (2000), '*Methods in parameter estimation*', EUROKIN consortium internal document

Weisz P.B., (1957), Z. Phys. Chem. (Frankfurt Am Main), 11, 1

Went G.T., Leu L.-J, Bell A.T., (1992a), '*Quantitative structural analysis of dispersed vanadia species in TiO<sub>2</sub>(anatase)-supported V<sub>2</sub>O<sub>5</sub>*', 134, 479-491

Went G.T., Leu L.-J, Rosin R.R., Bell A.T., (1992b), '*The effects of structure on the catalytic activity and selectivity of V<sub>2</sub>O<sub>5</sub>/TiO<sub>2</sub> for the reduction of NO by NH<sub>3</sub>*', 134, 492-505

## Chapter 6:

### Functionality and formulation of copper-based methanol synthesis catalysts –

#### Part I: Kinetic model development using steady and non-steady state operation under CO/CO<sub>2</sub>/H<sub>2</sub> feeds

*Methanol is a key industrial chemical, with a world production level placed at 45 million tonnes in 2010. Central to this high level of capacity is the low pressure methanol synthesis process, which produces methanol from mixtures of CO/CO<sub>2</sub>/H<sub>2</sub> over a Cu/ZnO/Al<sub>2</sub>O<sub>3</sub> catalyst. Understanding the mechanism for methanol synthesis and the water gas shift reaction over this catalyst and the aspects of its formulation which deliver catalytic activity continues to this day to be a critical area of investigation for these catalysts. In this work, steady and non-steady state experimental and kinetic modelling methods are presented to demonstrate changes in functionality of a Cu/ZnO/Al<sub>2</sub>O<sub>3</sub> catalyst based on gas composition.*

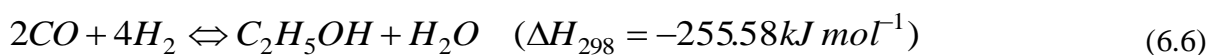
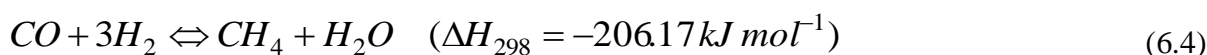
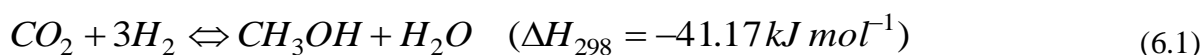
*Steady-state testing of a Cu/ZnO/Al<sub>2</sub>O<sub>3</sub> catalyst, utilising a parallel difference testing methodology, generated performance data over a range of P<sub>CO</sub> to P<sub>CO2</sub> ratios (1 – 10). Using a mechanistically sound literature kinetic model (Vanden Bussche and Froment, 1996), a three reaction network described the functionality of the catalyst. Importantly, the third reaction, a combined forward water gas shift and methanol synthesis reaction, was found to be important with increasing axial distance along the reactor and at high P<sub>CO</sub> to P<sub>CO2</sub> ratios.*

*Non-steady state, ‘reactor start-up’, testing of a Cu/ZnO/Al<sub>2</sub>O<sub>3</sub> catalyst marked a novel approach to further understanding the functionality of the catalyst. Initial changes in surface carbon and oxygen populations were quantified and linked to subsequent dynamic changes in methanol synthesis and water gas shift activity. Cu/ZnO and Cu/Al<sub>2</sub>O<sub>3</sub> formulations were also evaluated and tested using kinetic models, permitting a structural and compositional comparison with Cu/ZnO/Al<sub>2</sub>O<sub>3</sub>.*

## 6. Introduction: ‘Functionality, feed and formulation’

Methanol (CH<sub>3</sub>OH) has a long history as a key industrial chemical, chiefly serving as an intermediate in the production of other chemicals such as formaldehyde and methyl-tert-butyl ether (MTBE). Methanol has also recently found increased use in alternative fuel applications such as fuel cells (Rasmussen *et al.*, 2012). The world production of methanol was 45 million metric tonnes in 2010, a figure which is increasing annually (Rasmussen *et al.*, 2012). The industrial production of methanol via catalytic technologies has a 90 year history, following the original commercialisation of a process by BASF in 1923. This process synthesised methanol from carbon monoxide (CO) and hydrogen (H<sub>2</sub>) mixtures at high temperature (> 673 K) and pressure (100 – 300 bar) over a ZnO/Cr<sub>2</sub>O<sub>3</sub> catalyst (Twigg, 1989). Since then, the production of methanol has seen significant developments on a practical level (in terms of catalyst and process improvements) but also on a scientific level, to understand the fundamentals of how this catalytic process actually works.

The catalytic synthesis of methanol from mixtures of CO/CO<sub>2</sub>/H<sub>2</sub> (termed ‘syngas’) was the second major industrial application of catalysis, following that of ammonia synthesis (Twigg, 1989). Unlike ammonia synthesis however, it is critical to deliver a catalyst that is both *active* and *selective* to the methanol synthesis reaction as unwanted reactions may occur. Under CO/CO<sub>2</sub>/H<sub>2</sub> conditions the following catalytic reactions may be prevalent:



Eq. (6.1) and (6.3) describe methanol synthesis via hydrogenation of CO<sub>2</sub> and CO respectively and are both mildly exothermic. Eq. (6.2) is the reverse water gas shift (RWGS) reaction and is mildly endothermic. Eq. (6.4-6) describes methanation, dimethyl ether synthesis and ethanol synthesis reactions respectively and are considerably more exothermic

than Eq. (6.1) and Eq. (6.3). In a standard methanol synthesis process it is desirable to avoid these latter three reactions. Whilst the initial ZnO/Cr<sub>2</sub>O<sub>3</sub> catalyst met these selectivity requirements, its overall methanol synthesis activity was poor and it was eventually replaced by a Cu/ZnO/Al<sub>2</sub>O<sub>3</sub> catalyst which was pioneered by ICI in the 1960's. This catalyst formulation showed much higher activity and could operate at lower pressures and temperatures (50 – 100 bar, < 573 K), therefore increasing plant efficiency and greatly reducing operating costs.

The methanol synthesis process over a Cu/ZnO/Al<sub>2</sub>O<sub>3</sub> catalyst has attracted great research interest and debate over the past 40 years. Central to this have been the pursuit of the nature of the active site(s) for the methanol synthesis and RWGS reactions and also the reaction mechanisms by which these reactions proceed. Early kinetic studies for this system, such as Leonov *et al.*, (1973) assumed that CO was the source of carbon in the synthesis of methanol. Subsequent works such as Andrew, (1980) and Klier *et al.*, (1982) noticed discrepancies in catalyst performance based on the CO<sub>2</sub> content of the syngas feeds, leading to a maximum in the methanol production rate over integral operation reactors at P<sub>CO</sub>/P<sub>CO<sub>2</sub></sub> ratios between 5 – 10 (see for example Figure 6.1). The key argument placed at the time was that CO<sub>2</sub> could help maintain a degree of oxidised copper sites on the catalyst surface and hence a redox-type mechanism for methanol synthesis could be optimised under certain conditions.

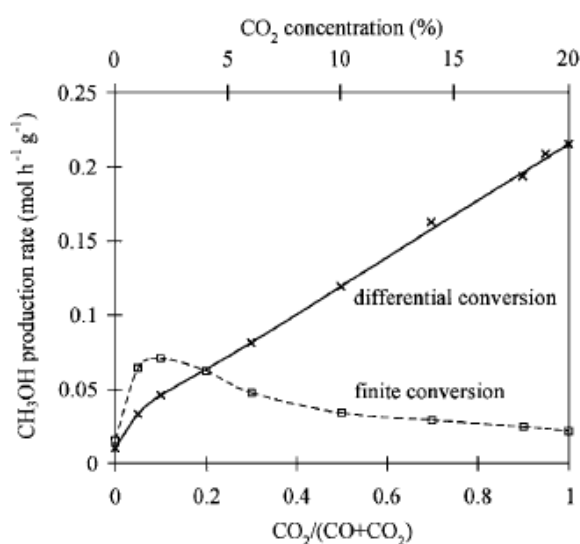


**Figure 6.1: Methanol production rates from CO/CO<sub>2</sub>/H<sub>2</sub> gas mixtures under differential and finite conversion over Cu/ZnO/Al<sub>2</sub>O<sub>3</sub> at 523 K (Sahibzada *et al.*, (1998))**

The works of Liu *et al.*, (1985) and Chinchin *et al.*, (1986) greatly altered the views on the reaction pathway for methanol synthesis over Cu/ZnO/Al<sub>2</sub>O<sub>3</sub> catalysts. In the former, an isotope labelling study using <sup>18</sup>O CO<sub>2</sub> found that the source of carbon in methanol under CO/CO<sub>2</sub>/H<sub>2</sub> conditions was in fact CO<sub>2</sub> not CO. In the latter, a linear trend between copper metal surface areas and CO<sub>2</sub> hydrogenation activity of a wide range of copper-based formulations was found. Linking to this, CO<sub>2</sub> partial pressure is directly related to methanol production rate under differential conditions (see Figure 6.1).

From this understanding of copper metal surface area and the CO<sub>2</sub> hydrogenation pathway being critical in determining methanol synthesis activity, the rest of this literature review will examine kinetics and mechanistic developments in the understanding of copper-based catalysts in recent years. The main focus will be to identify gaps in understanding of the linkage between catalyst formulation, functionality and feed content under reaction conditions.

## **6.1 Kinetics and reaction mechanisms for copper-based catalysts in literature**

### **6.1.1 CO/CO<sub>2</sub>/H<sub>2</sub> conditions**

Table 6.1 shows a selection of key kinetic models proposed in literature based on operation under CO/CO<sub>2</sub>/H<sub>2</sub> conditions. The model of Mochalin *et al.*, (1984) was unique at the time of writing as it completely disregarded the CO hydrogenation to methanol route, owing to the fact the authors were never able to synthesise methanol over a Cu/ZnO/Al<sub>2</sub>O<sub>3</sub> catalyst under CO/H<sub>2</sub> conditions. Water inhibition is apparent in both the methanol synthesis (from CO<sub>2</sub>) and RWGS routes described but the work expanded no further on this or the physical basis of the overall model.

The model of Graaf *et al.*, (1988) was proposed based on a statistical discrimination approach whereby experimental data from a spinning basket reactor were fitted to 48 different kinetic models. The final, most successful model proposed comprised both CO and CO<sub>2</sub> hydrogenation routes as well as the RWGS reaction and was based on a dual site mechanism, one for CO and CO<sub>2</sub> adsorption and the other for H<sub>2</sub> and H<sub>2</sub>O adsorption.

**Table 6.1: Selected kinetic models for methanol synthesis under CO/CO<sub>2</sub>/H<sub>2</sub> conditions taken from literature**

Model	Rate expressions:	Exp. conditions tested	Fitted activation energies or heat of adsorption (kJ mol <sup>-1</sup> )
	$r_1 = \text{CO}_2 \rightarrow \text{CH}_3\text{OH}$ $r_2 = \text{CO}_2 \rightarrow \text{CO}$ $r_3 = \text{CO} \rightarrow \text{CH}_3\text{OH}$		
<b>Mochalin et al., (1984)</b> (6.7)	$r_1 = \frac{k_1 P_{\text{CO}_2} P_{\text{H}_2} (1 - K_1^* (P_{\text{MeOH}} P_{\text{H}_2\text{O}}) / (P_{\text{CO}_2} P_{\text{H}_2}^3))}{(P_{\text{CO}_2} + K_{\text{H}_2\text{O}} P_{\text{CO}_2} P_{\text{H}_2\text{O}} + K'' P_{\text{H}_2\text{O}})}$ $r_2 = \frac{k_1 P_{\text{CO}_2} P_{\text{H}_2} (1 - K_2^* (P_{\text{CO}} P_{\text{H}_2\text{O}}) / (P_{\text{CO}_2} P_{\text{H}_2}))}{(P_{\text{CO}_2} + K_{\text{H}_2\text{O}} P_{\text{CO}_2} P_{\text{H}_2\text{O}} + K'' P_{\text{H}_2\text{O}})}$	> 0 % CO <sub>2</sub>	Not quoted
<b>Graaf et al., (1988)</b> (6.8)	$r_1 = \frac{k_1 K_{\text{CO}_2} (P_{\text{CO}_2} P_{\text{H}_2}^{3/2} - P_{\text{MeOH}} P_{\text{H}_2\text{O}} / (P_{\text{H}_2}^{3/2} K_1^*))}{(1 + K_{\text{CO}} P_{\text{CO}} + K_{\text{CO}_2} P_{\text{CO}_2}) \left( P_{\text{H}_2}^{1/2} + \frac{K_{\text{H}_2\text{O}} P_{\text{H}_2\text{O}}}{K_{\text{H}_2}^{1/2}} \right)}$ $r_2 = \frac{k_2 K_{\text{CO}_2} (P_{\text{CO}_2} P_{\text{H}_2} - P_{\text{CO}} P_{\text{H}_2\text{O}} K_2^*)}{(1 + K_{\text{CO}} P_{\text{CO}} + K_{\text{CO}_2} P_{\text{CO}_2}) \left( P_{\text{H}_2}^{1/2} + \frac{K_{\text{H}_2\text{O}} P_{\text{H}_2\text{O}}}{K_{\text{H}_2}^{1/2}} \right)}$ $r_3 = \frac{k_3 K_{\text{CO}} (P_{\text{CO}} P_{\text{H}_2}^{3/2} - P_{\text{MeOH}} / (P_{\text{H}_2}^{1/2} K_3^*))}{(1 + K_{\text{CO}} P_{\text{CO}} + K_{\text{CO}_2} P_{\text{CO}_2}) \left( P_{\text{H}_2}^{1/2} + \frac{K_{\text{H}_2\text{O}} P_{\text{H}_2\text{O}}}{K_{\text{H}_2}^{1/2}} \right)}$	15 – 50 bar 483 – 518 K 0 – 22 % CO 2 – 26 % CO <sub>2</sub> in H <sub>2</sub> Spinning basket reactor	$E_{a,1} = 65.2$ $E_{a,2} = 123.4$ $E_{a,3} = 109.9$ $\Delta H_{\text{ads,CO}_2} = -67.4$ $\Delta H_{\text{ads,CO}} = -58.1$ $\Delta H_{\text{ads,H}_2\text{O}/\text{H}_2} = -104.5$
<b>Coteron and Hayhurst, (1994)</b> (6.9)	$r_1 = \frac{k_1 K_{\text{CO}_2} K_{\text{H}_2} K_{\text{HCO}_2}}{1 + K_{\text{CO}_2} P_{\text{CO}_2} + K_{\text{CO}_2} K_{\text{H}_2}^{1/2} K_{\text{HCO}_2} P_{\text{CO}_2} P_{\text{H}_2}^{1/2} + \frac{K_{\text{CO}_2} P_{\text{CO}_2}}{K_{\text{CO}} P_{\text{CO}}}}$	10 bar 473 – 523 K 10 – 20 % CO 10 – 20% CO <sub>2</sub> in H <sub>2</sub> Differential operation	$E_{a,1} = 47.0$ $\Delta H_{\text{ads,CO}_2} = 0$ $\Delta H_{\text{ads,H}_2} = -6.3$

<b>Vanden Bussche and Froment, (1996) (6.10)</b>	$r_1 = \frac{k'_{MeOH} P_{CO_2} P_{H_2} (1 - K_1^* (P_{MeOH} P_{H_2O}) / (P_{CO_2} P_{H_2}^3))}{\left(1 + \left(\frac{K_{H_2O}}{K_8 K_9 K_{H_2}}\right) \frac{P_{H_2O}}{P_{H_2}} + \sqrt{K_{H_2} P_{H_2}} + K_{H_2O} P_{H_2O}\right)^3}$	15 – 51 bar	$E_{a,MeOH} = -36.7$
		453 – 553 K	$E_{a,2} = 94.8$
		$P_{CO}/P_{CO_2} = 0$	$\Delta H_{ads,H_2} = -17.2$
		- 4.1	
		Integral operation	$\Delta H_{ads,H_2O} = -124.1$
	$r_2 = \frac{k_2 P_{CO_2} (1 - K_2^* (P_{CO} P_{H_2O}) / (P_{CO_2} P_{H_2}))}{\left(1 + \left(\frac{K_{H_2O}}{K_8 K_9 K_{H_2}}\right) \frac{P_{H_2O}}{P_{H_2}} + \sqrt{K_{H_2} P_{H_2}} + K_{H_2O} P_{H_2O}\right)}$		

The confidence intervals in the 12 estimated parameters of the final model in Graaf *et al.*, (1988) were excellent barring the pre-exponential factor for RWGS. The concerns with this model lie in the physical basis of the model which does not acknowledge that certain surface intermediates can feature in more than one overall reaction (Vanden Bussche and Froment, 1996). Instead all reactions are assumed to proceed via individual routes.

In Graaf *et al.*, (1988), the magnitude of the estimated value of  $\Delta H_{ads,CO}$  is close to a number of estimations in literature for the adsorption of CO on a Cu<sup>0</sup> surface which are in the range of 42 – 53 kJ mol<sup>-1</sup> (Parris and Klier, 1986; Ovesen *et al.*, 1992). CO coverage under methanol synthesis conditions was shown to be low in these works however which brings the significance of this parameter into question. The value is also similar to the reaction of CO with surface oxygen on a Cu/ZnO/Al<sub>2</sub>O<sub>3</sub> surface to form CO<sub>2</sub>(ads)<sup>-</sup> in the range of 64 – 80 kJ mol<sup>-1</sup> (Ovesen *et al.*, 1992; Waugh, 1999). Many works support a redox mechanism for the WGS reaction, of which the formation of CO<sub>2</sub>(ads)<sup>-</sup> occurs in the forwards direction (Nakamura *et al.*, 1990; Vanden Bussche and Froment, 1996). It is therefore plausible that  $r_3$  in this network is a lumped descriptor of forward water gas shift (FWGS) and CO<sub>2</sub> hydrogenation to methanol activity, rather than a separate mechanistic route for methanol synthesis from adsorbed CO. This may also explain the error in the fitted RWGS pre-exponential factor if the reaction network is over-determined.

The work of Coteron and Hayhurst, (1994) refuted the existence of a CO hydrogenation route under CO/CO<sub>2</sub>/H<sub>2</sub> conditions and instead left the role of CO purely to the removal of oxygen from the catalyst surface. This term is ‘lumped’ into their CO<sub>2</sub> hydrogenation to methanol model, rather than being incorporated into a WGS term which is

not considered. The authors did not include a thermodynamic driving force term in their model.

The model of Vanden Bussche and Froment, (1996) is perhaps the unifying work for methanol synthesis and WGS reaction under CO/CO<sub>2</sub>/H<sub>2</sub> conditions. The strength of this work lies in a sound mechanistic basis for both reactions (see Figure 6.2). The active site for both reactions was assumed to occur over the copper component of the catalyst, which was assumed to be partially oxidised and contain surface oxygen, denoted *O.s*. The hydrogenation of surface formate (*HCO<sub>2</sub>.2s*) was assumed to be the rate determining step for methanol synthesis from CO<sub>2</sub> based on previous temperature programmed desorption (TPD) studies (Bowker *et al.*, 1988; Vanden Bussche and Froment, 1994). The RWGS reaction, proceeding via a redox mechanism, is rate determined by the dissociative adsorption of CO<sub>2</sub>. The model considers all possible surface intermediates in the reaction network. This enables application to a wide range of CO/CO<sub>2</sub>/H<sub>2</sub> conditions, under which the populations of these individual species may vary and can therefore be accounted for.

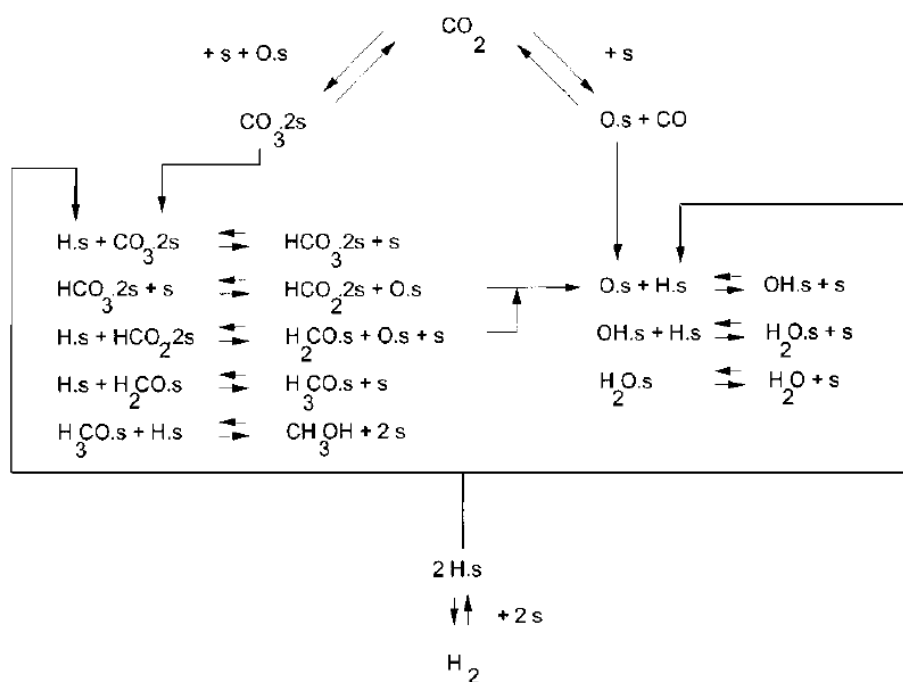


**Figure 6.2: Reaction scheme for the synthesis of methanol and WGS reaction (Vanden Bussche and Froment, 1996)**

Other kinetic studies under CO/CO<sub>2</sub>/H<sub>2</sub> conditions in the literature which link with catalyst formulation include the micro-kinetic models from Topsøe (Ovesen *et al.*, 1997). In

these works the authors place great emphasis on oxygen vacancies at Zn-O-Cu interfaces, the proportion of which are believed to change as a function of the redox potential of the syngas (ratio of ‘reducing’ CO and H<sub>2</sub> gas to ‘oxidising’ CO<sub>2</sub> and H<sub>2</sub>O). A change in the number of oxygen vacancies (Zn-[ ]-Cu) has been shown to impact on copper surface morphology and particle surface area, directly impacting methanol synthesis activity. They suggest that methanol synthesis from CO<sub>2</sub> is therefore a structure sensitive reaction. The opposite is suggested in Chinchén and Spencer, (1991) who state that Cu surface area is critical to methanol synthesis activity but other parameters such as shape and size distribution of metal crystallites are not.

A recent work by Peter *et al.*, (2012) examined power law, Langmuir-Hinshelwood (LH) (Vanden Bussche and Froment, 1996) and dynamic micro-kinetic (Ovesen *et al.*, 1997) models using experimental data under CO/CO<sub>2</sub>/H<sub>2</sub> conditions and found all levels of model to be very similar in their predictions. This could suggest that the dynamic nuances of the micro-kinetic models based on feed composition may not be critical to accurately predicting methanol synthesis performance of Cu/ZnO/Al<sub>2</sub>O<sub>3</sub> formulations under CO/CO<sub>2</sub>/H<sub>2</sub> although the extent of conditions for which this is true would require further scrutiny.

### 6.1.2 Chapter Objectives

From an examination of the literature to date, there are a number of kinetic studies which investigate the mechanisms behind the methanol synthesis reaction under CO/CO<sub>2</sub>/H<sub>2</sub>. Whilst there is considerable agreement as to the mechanism of CO<sub>2</sub> hydrogenation to methanol over copper-based catalysts, there is still scope to increase understanding around the generation of catalytic activity under these conditions. This is particularly true at high P<sub>CO</sub> to P<sub>CO<sub>2</sub></sub> ratios, as evidenced in Figure 6.1 whereby large shifts are seen in differential and integral methanol productivity.

In keeping with the key themes of this thesis, no studies exist in the literature which analyse the reactor start-up (both H<sub>2</sub>/N<sub>2</sub> reduction step and onset of CO/CO<sub>2</sub>/H<sub>2</sub> conditions) at realistic pressures in an experimental rig. Furthermore, few studies exist in the literature, which combine a kinetic study with a strong link to catalyst formulation requirements. In light of this, the aims for this study are thus:

- Develop experimental methods to probe steady and non-steady state behaviour of copper-based catalyst formulations under industrially relevant conditions.

- Develop mechanistically sound steady state kinetic models to describe behaviour of a model ternary Cu/ZnO/Al<sub>2</sub>O<sub>3</sub> catalyst under CO/CO<sub>2</sub>/H<sub>2</sub> conditions (P<sub>CO</sub>/P<sub>CO2</sub> ratios of 1 – 10 whereby the most dynamic changes in methanol production rate are observed).
- Analyse non-steady state behaviour of a Cu/ZnO/Al<sub>2</sub>O<sub>3</sub> catalyst during initial exposure to CO/CO<sub>2</sub>/H<sub>2</sub> conditions to understand physical and/or chemical transformations which the catalyst may undergo during this period of operation and link this to generation/loss of active sites for methanol synthesis.
- Apply models to experimental performance data of binary catalyst formulations (Cu/ZnO and Cu/Al<sub>2</sub>O<sub>3</sub>). Compare observations with the ternary catalyst formulation and link catalyst functionality, formulation and impact of feed gas.

## 6.2 Materials and methods

### 6.2.1 Sample preparation and properties

Three catalysts were chosen for this study, which were all ground into powder form (particle size range  $180 < d_p < 355 \mu\text{m}$ ). Key structural details of the respective precursor formulations are described in Table 6.2:

**Table 6.2: Compositional and structural data of catalyst precursor formulations used in this study<sup>16</sup>**

Catalyst precursor	Precursor composition (weight %)	BET surface area ‘as received’ (m <sup>2</sup> g <sup>-1</sup> )	Cu surface area ‘as received’ (m <sup>2</sup> g <sup>-1</sup> )	Cu surface area following reduction step (m <sup>2</sup> g <sup>-1</sup> )
CuO/ZnO/Al <sub>2</sub> O <sub>3</sub>	60/30/10	97.9	32.4	41.1
CuO/ZnO	34/66	31.8	16.0	17.1
CuO/Al <sub>2</sub> O <sub>3</sub>	25/75	205.1	6.4	7.4

Copper surface areas were measured using reactive frontal chromatography (Chinchen *et al.*, 1987). This technique is based on the decomposition of nitrous oxide (N<sub>2</sub>O)

<sup>16</sup> Data supplied by C. Ranson and R.Fletcher (both of Johnson Matthey)

molecules over a reduced copper surface yielding chemisorbed oxygen atoms and N<sub>2</sub>, the latter of which is released into the gas phase:



In this equation *s* denotes a surface atom. The copper surface areas supplied were measured at 333 K. In these conditions it has been shown that oxidation of copper by N<sub>2</sub>O is mild and only oxidises surface copper atoms to a Cu<sup>+</sup> state (Narita *et al.*, 1982).

### 6.2.2 Micro-reactor test rig

Reaction studies using the catalyst precursor formulations described in Section 6.2.1 were carried out in fixed-bed, down-flow, steel micro-reactors. Six parallel tubes were used with inner diameter of 3 mm and length of ~20 cm. The use of a 180 < *d<sub>p</sub>* < 355 μm powder sieve fraction ensured a reactor internal diameter (*d<sub>r</sub>*) to *d<sub>p</sub>* ratio of at least 10 in order to minimise wall effects (Chu and Ng, 1989) and prevent large pressure drops (Ergun, 1952).

During operation, thermocouples were placed in the jacket walls of all micro-reactors, 10 cm below the reactor inlet. Throughout the experimental program, wall temperature variation between the tubes never exceeded ±1 K and deviation from the oven set point never exceeded ±2 K. The micro-reactors were themselves housed in a nitrogen-purged oven.

Experiments were performed in the absence of heat and mass transport limitations allowing for the measurement of intrinsic rates. Full details of reactor setup and catalyst properties are shown in Table 6.3. This was confirmed by use of key calculations set out in literature (Perez-Ramirez *et al.*, 2000) and described in Chapter 2, including calculation of intraparticle mass transport limitations (Wheeler Weisz Modulus), Mears' criterion for intraparticle heat transport limitations and radial temperature gradients.

To illustrate, transport limitations were calculated a priori at the extreme of the test programme operation, namely a 500 mg Cu/ZnO/Al<sub>2</sub>O<sub>3</sub> catalyst bed operating at 493 K, 35 bar under a 3% CO / 3% CO<sub>2</sub> / 67% H<sub>2</sub> / 27% N<sub>2</sub> gas mix at steady state. The apparent methanol formation rate was 0.95 μmol g cat<sup>-1</sup> s<sup>-1</sup> over this integral bed. Under these conditions, the radial heat transport gradient was 0.01 K, and both internal and external mass transfer efficiencies were >99%. These values satisfy threshold criteria.

In Table 6.3, CO<sub>x</sub> containing gases contain CO:CO<sub>2</sub> ratios between 10 and 1. The explored total pressure range is lower than typical industrial operation of ~50 bar; this owed to limitations of the pressure relief valves on the rig. The temperature range of 453 – 493 K was deliberately chosen so that the catalyst could be operated under conditions that keep catalyst deactivation through sintering to a minimum (such a phenomena is not directly under investigation in this study).

**Table 6.3: List of properties of catalyst and experimental setup conditions.**

Experimental property	Value			
Catalyst Mass (g)	0.125 – 0.5			
Catalyst and SiC diluent particle size (µm)	180 – 355			
Reactor diameter (mm)	3			
Temperature range (K)	453 – 493			
Operating pressure range (bar)	10 – 35			
Flow Rate (L h <sup>-1</sup> ) (STP)	7.5			
Feed-stocks used (vol. %)	CO	CO <sub>2</sub>	H <sub>2</sub>	N <sub>2</sub>
	0	0	2	98
	3	0.3	67	29.7
	3	1	67	29
	3	3	67	27

An assessment can be made using the Hüttig and Tammann approximations, which estimate temperatures for which atoms and bulk respectively become mobile (Kung, 1992):

$$T > T_{Hüttig} = 0.3T_{melting} \quad (6.12)$$

$$T > T_{Tammann} = 0.5T_{melting} \quad (6.13)$$

Cu<sup>0</sup>, ZnO and Al<sub>2</sub>O<sub>3</sub> have melting points of 1358, 2250 and 2350 K respectively. At the operational extreme (493 K), ZnO and Al<sub>2</sub>O<sub>3</sub> are below  $T_{Hüttig}$  at 0.22 and 0.21 ( $T_{melting}$ )

respectively whilst  $\text{Cu}^0$  is above at 0.36 ( $T_{\text{melting}}$ ). To further predict catalyst thermal stability, sintering models for  $\text{Cu}/\text{ZnO}/\text{Al}_2\text{O}_3$  catalysts were applied over the temperature range (Hanken, 1995; Løvik *et al.*, 2001). Application of these models revealed that activity loss from sintering over the maximum 50 hours of operation in this would be at most 5% of the starting activity. These prior calculations will be checked experimentally in Section 6.3.2.

Parallel difference testing, a methodology described in detail by Birtill, (2003), was utilised in both steady and non-steady state experiments in this study. The simple setup (see Figure 6.3) comprises four tubes in parallel containing 0.125, 0.25, 0.375 and 0.5 g of catalyst respectively. Flow rate ( $7.5 \text{ L h}^{-1}$ ), inlet reactant concentration and temperature are the same for each tube throughout the test. Subtraction between the exit concentrations of each catalyst bed at discrete times on stream allows performance to be broken down into four sectors of equal length down the bed. Experimental repeats were carried out as a check for reproducibility. Parallel difference tests were carried out for up to 50 h on stream during the experimental program.

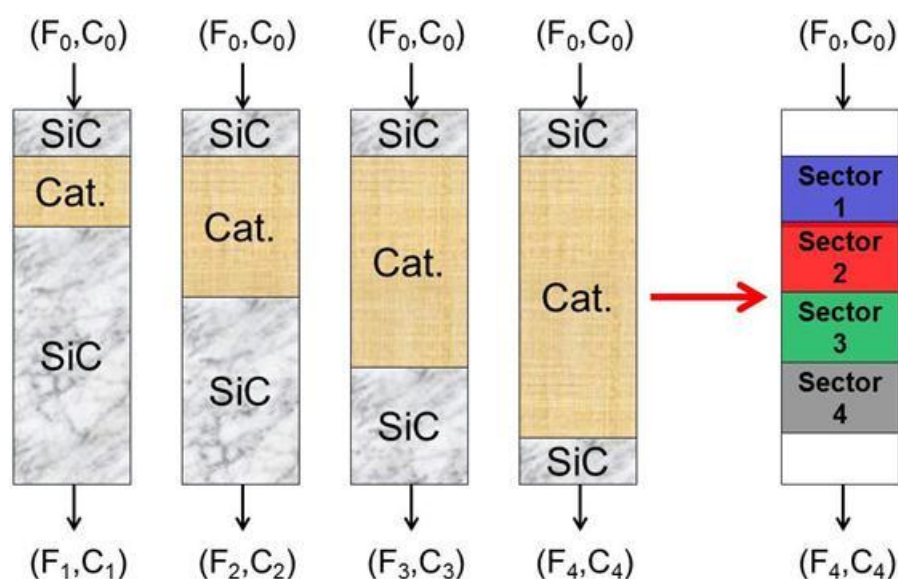


**Figure 6.3: Parallel difference setup for testing copper-based catalysts**

As seen in Figure 6.3, each reactor was packed, firstly with SiC ( $180 < d_p < 355 \mu\text{m}$ ), then catalyst (up to 0.5 g), then the remainder with SiC. This ensured that pressure drops, although negligible, were constant across all reactor tubes. The remaining two parallel micro-reactor tubes remained empty during testing and served two purposes:

- To quantify ‘blank’ activity and show that no homogeneous reaction had occurred.
- To act as a catalyst bed ‘bypass’ route when new gas feeds were introduced into the experimental rig. This enabled the new gas feeds to fully equilibrate at their true concentration, prior to the individual reactor mass flow controllers, before being fed over the catalysts under testing.

Gases (see Table 6.3) were fed to each micro-reactor tube using 6 PID mass flow controllers (MFCs); one for each reactor. The maximum set point for each MFC was  $7.5 \text{ L h}^{-1}$  (standard temperature and pressure, STP). The true flow through each MFC relative to respective set point was measured using a rotary gas meter, positioned downstream of the reactors. A 5-point calibration was obtained for all 6 MFCs and was applied to the computer software controlling the rig.

A 6-port valve was positioned downstream of the micro-reactors. Gases from the selected reactor tube were diverted at this valve to an infra-red (IR) analyser. Volume % values of CO, CO<sub>2</sub>, CH<sub>3</sub>OH and H<sub>2</sub>O in the reactor effluent were all measured using this analyser. The IR analyser was calibrated periodically during the experimental program using 6% CO / 9.2% CO<sub>2</sub> / 67% H<sub>2</sub> / Balance N<sub>2</sub> (for CO and CO<sub>2</sub> response) and propylene (for CH<sub>3</sub>OH and H<sub>2</sub>O). The IR analyser provided real time measurements with outputs on a second timescale.

A carbon and oxygen balance was calculated across all reactors at all stages of experimental testing. At steady state, the balances take the following formulae:

**Carbon:**  $\text{Moles CO (In)} + \text{Moles CO}_2 \text{ (In)} =$

$$\text{Moles CO (Out)} + \text{Moles CO}_2 \text{ (Out)} + \text{Moles CH}_3\text{OH (Out)} \quad (6.14)$$

**Oxygen:**  $\text{Moles CO (In)} + 2 \times \text{Moles CO}_2 \text{ (In)} =$

$$\text{Moles CO (Out)} + 2 \times \text{Moles CO}_2 \text{ (Out)} + \text{Moles CH}_3\text{OH (Out)} + \text{Moles H}_2\text{O (Out)} \quad (6.15)$$

In this study, carbon and oxygen balances were calculated between 99% and 101% under all steady state tests in this study. Balances under non-steady state conditions are discussed in Section 6.3. Measurement and population balance of hydrogen is the only omission in the analysis. Later sections of this study focus on surface population dynamics of

carbon and oxygen species, which act as indicators for reaction intermediates and spectator species. Understanding the surface population of hydrogen would strengthen this analysis but is not a critical component.

All non-steady state behaviour experiments in this study were triggered by a change in feed conditions over the catalyst beds. These were nominally a switch from 2% H<sub>2</sub> / N<sub>2</sub> to CO / CO<sub>2</sub> / H<sub>2</sub> feeds. A detailed set of blank measurements were carried out for these changes in feed conditions, including:

- Checking all 6 reactors individually.
- Checking the effect of reactor packing.
- Examining the effect of temperature and pressure on the measured feed break-through profile.

A study of the above ensured carbon and oxygen could be fully tracked during non-steady state operation during catalyst reaction testing. Relevant blank feed change profiles will be included in the results presentation in Section 6.3.

### 6.2.3 Kinetic modelling

Parameter estimation within the kinetic models was carried out using Athena Visual Studio<sup>©</sup> software<sup>17</sup>. The kinetic models tested within this work contain multiple parameters including some which are non-linear (e.g. activation energies in the Arrhenius equation). The Levenberg-Marquardt procedure, an indirect method for constrained optimisation of parameters, is appropriate for this problem (Marquardt, 1963). All response variables in the methanol synthesis reaction network are dependent on multiple reactions and so the models must be solved implicitly using a set of differential equations:

$$\frac{dy}{dt} = f(y, \beta) \quad (6.16)$$

In Eq. (6.16),  $y$  denotes model responses,  $t$  denotes time and  $\beta$  denotes the model parameters. A direct decoupled method is used to estimate parametric sensitivities (Caracotsios and Stewart, 1985):

---

<sup>17</sup> Athena Visual Studio 14.2, Stewart & Associates Engineering Software, Inc.

$$B(t) = \frac{\partial y(t)}{\partial \beta} \quad (6.17)$$

$$\frac{\partial}{\partial \beta} \left( \frac{dy}{dt} \right) = \frac{d}{dt} B(t) = \frac{df}{dy} \cdot B(t) + \frac{df}{d\beta} \quad (6.18)$$

In Eq. (6.17),  $B(t)$  defines the sensitivity function for each model response with respect to each model parameter. In Eq. (6.18) it can be seen that defining sensitivities as a function of time allows them to be solved alongside the main system differential equations, improving solver efficiency and performance.

To minimise cross-correlation between activation energy ( $E_a$ ) and pre-exponential factor ( $A_i$ ) parameters, a re-parameterised Arrhenius equation was used:

$$k_i = A_{i,473.15} \cdot \exp \left( \left( \frac{E_a}{T_{ave} \cdot R} \right) \cdot \left( 1 - \frac{T_{ave}}{T} \right) \right) \quad (6.19)$$

Where average temperature,  $T_{ave} = 473.15$  K and  $A_{i,473.15}$  is the value of the rate constant  $k_i$  at 473.15 K. The fitting process can be further improved by solving  $A_{i,473.15}$  as an exponential term and lumping fitted value,  $E_a$  with constants  $T_{ave}$  and the ideal gas constant,  $R$  ( $\text{J K}^{-1} \text{mol}^{-1}$ ) to give fitting parameter  $E_{a,lump}$ . This typically brings the values of  $A_{i,473.15}$  and  $E_{a,lump}$  into the same order of magnitude (typically 1 – 10) further reducing cross-correlation in this expression:

$$k_i = \exp \left( A_{i,473.15} + \left( E_{a,lump} \cdot \left( 1 - \frac{T_{ave}}{T} \right) \right) \right) \quad (6.20)$$

The above procedure was also applied to Van't Hoff adsorption terms ( $K_i$ ) featuring a heat of adsorption term ( $\Delta H_{ads}$ ) and associated  $A_i$  value.

Equilibrium constants, taken from Graaf *et al.*, (1986), were utilised in all kinetic equations to account for thermodynamic limitations. The values for these are calculated as follows:

$$CO_2 + 3H_2 \xrightleftharpoons[k_{-1}]{k_1} CH_3OH + H_2O = \log_{10} K_1^* = \frac{-3066}{T} + 10.592 \quad (6.21)$$

$$CO_2 + H_2 \xrightleftharpoons[k_{-2}]{k_2} CO + H_2O = \log_{10} K_2^* = \frac{2073}{T} - 2.029 \quad (6.22)$$

$$CO + 2H_2 \xrightleftharpoons[k_{-3}]{k_3} CH_3OH = \log_{10} K_3^* = \frac{-5139}{T} + 12.621 \quad (6.23)$$

Gaseous components were also checked for non-ideal behaviour. This was achieved by using the Soave-Redlich-Kwong (Soave, 1972) equation of state, which takes the following form:

$$Z = Pv/RT = \frac{v_m}{v_m - b} - \frac{a(T)}{RT(v+b)} \quad (6.24)$$

Where  $Z$  is compressibility factor,  $P$  is total pressure (bar),  $v_m$  is molar volume ( $m^3 mol^{-1}$ ),  $R$  is gas constant ( $J mol^{-1} K^{-1}$ ),  $a$  (-) and  $b$  ( $m^3 mol^{-1}$ ) are constants taken from literature (Graaf *et al.*, (1986)). Across all data generated in the experimental programme,  $Z$  never exceeded the bounds of  $0.99 < Z < 1.01$ . Hence the use of partial pressures, rather than fugacities, is acceptable for this kinetic study.

### 6.3 Results and discussion

In order to tackle the objectives given in Section 6.1.2, the results and discussion for this study are divided into four sections. In the first three, attention is given to understanding the kinetics and functionality of a Cu/ZnO/Al<sub>2</sub>O<sub>3</sub> catalyst. Using Figure 6.4 as a guide, the initial precursor reduction step will be firstly examined. Following this, steady and non-steady state kinetics under CO/CO<sub>2</sub>/H<sub>2</sub> conditions will be explored. The understanding of catalyst functionality under each of these feeds will then be applied to binary formulations. It is noted in Figure 6.4 that catalyst formulations performance can be explored under CO/H<sub>2</sub> conditions, leading to very different behaviour compared to under CO/CO<sub>2</sub>/H<sub>2</sub>. These conditions, as well as the impact of switching between CO/CO<sub>2</sub>/H<sub>2</sub> and CO/H<sub>2</sub> feeds will be explored in depth in Chapter 7.

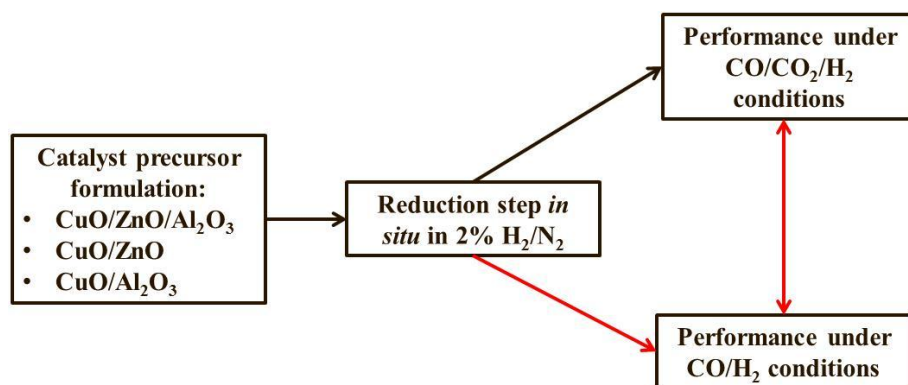


**Figure 6.4: Transitions of gas-phase conditions over copper-based catalysts explored in Chapter 6 (→) and Chapter 7 (→)**

### 6.3.1 Initial reduction of CuO/ZnO/Al<sub>2</sub>O<sub>3</sub> in H<sub>2</sub>/N<sub>2</sub>

In all experiments carried out in this study, the catalyst precursors were initially reduced under a flow of 2% H<sub>2</sub>/N<sub>2</sub>. Table 6.4 shows the standard procedure which was applied to all catalyst beds during the reduction step:

**Table 6.4: Standard catalyst precursor reduction procedure employed in this study**

Step	Gas	Set Point (K)	Ramp Rate (K h <sup>-1</sup> )	Flow rate (L h <sup>-1</sup> )	Pressure (bar)	Dwell (h)
1.	2% H <sub>2</sub> /N <sub>2</sub>	363	120	7.5	10	0
2.	2% H <sub>2</sub> /N <sub>2</sub>	408	60	7.5	10	0
3.	2% H <sub>2</sub> /N <sub>2</sub>	498	30	7.5	10	1
4.	2% H <sub>2</sub> /N <sub>2</sub>	473	60	7.5	25	6

It is important to analyse the gaseous products from this reduction step in order to understand the transformations that the catalyst precursor undergoes in delivering a catalyst in the ‘active’ state for methanol synthesis. This will also provide a reference state for the catalyst prior to exposure to CO/CO<sub>2</sub>/H<sub>2</sub> and CO/H<sub>2</sub> gases in this and the following chapter.

Figure 6.5A and B show the product H<sub>2</sub>O and CO<sub>2</sub> evolved, respectively, during the reduction step across CuO/ZnO/Al<sub>2</sub>O<sub>3</sub> catalyst beds of different mass using the parallel difference test configuration. It can be seen that both H<sub>2</sub>O and CO<sub>2</sub> are evolved in a ‘wave-

like' fashion along the catalyst bed. It is well known in literature that the evolution of H<sub>2</sub>O during this reduction step is largely due to the reduction of copper(II) oxide (CuO) to copper metal (Cu<sup>0</sup>) (Bart and Sneed, 1987), which occurs under mild temperatures and reducing conditions. At temperatures below 373 K, H<sub>2</sub>O evolution may also be attributed to physisorbed moisture in the sample. The CO<sub>2</sub> evolved can be attributed to decomposition of metal hydroxy-carbonates (e.g. Cu<sub>2</sub>(OH)<sub>2</sub>CO<sub>3</sub>) which were not removed in prior catalyst precursor formulation steps (e.g. calcination) (Himelfarb *et al.*, 1985). It is worthy of note that whilst ZnO is a reducible component, it is highly unlikely that it is reduced under the applied reduction conditions. This has been demonstrated previously in literature (Bart and Sneed, 1987).

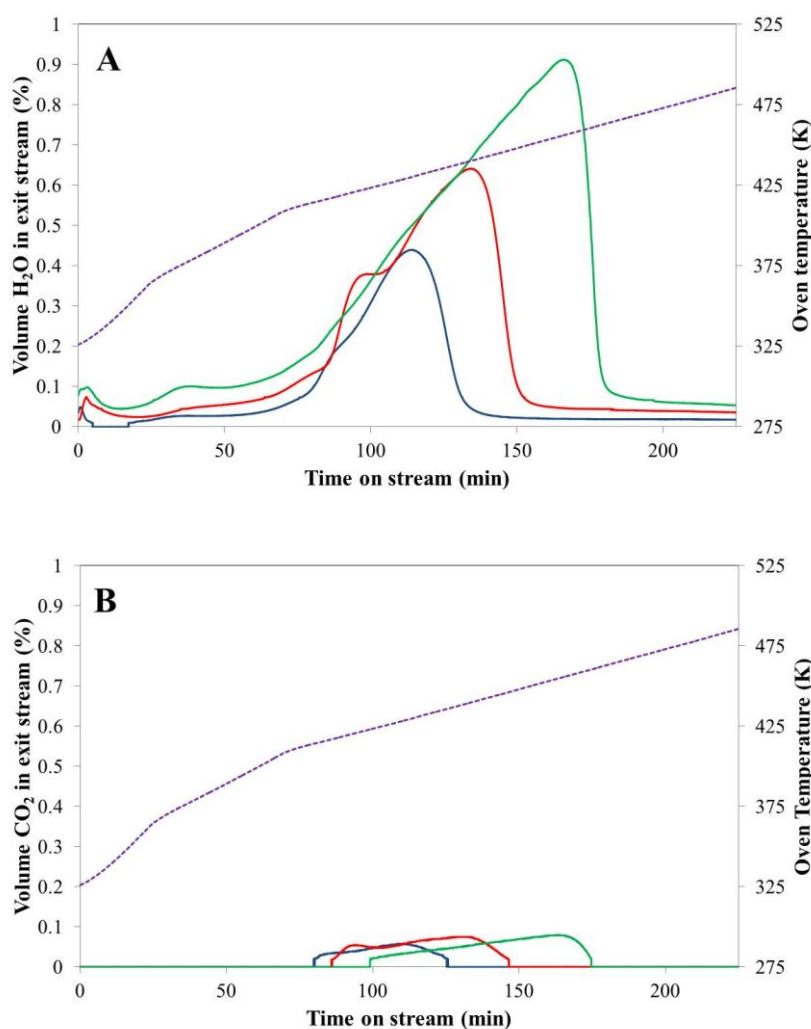


**Figure 6.5: Evolution of A) H<sub>2</sub>O and B) CO<sub>2</sub> during the initial CuO/ZnO/Al<sub>2</sub>O<sub>3</sub> reduction step under 2% H<sub>2</sub>/N<sub>2</sub> at 10 bar. (—) denotes 125 mg bed, (—) 250mg bed, (—) 500 mg bed and (---) oven temperature (K).**

Based on structural compositions of the initial CuO/ZnO/Al<sub>2</sub>O<sub>3</sub> sample, the volumes of H<sub>2</sub>O and CO<sub>2</sub> observed can be linked to specific mass losses in the sample. In Table 6.5, the measured oxygen mass loss calculated from product H<sub>2</sub>O is very similar to the calculated mass of oxygen in the CuO component of the catalyst precursor. This suggests that this component is almost entirely reduced to Cu<sup>0</sup> by the end of the reduction step.

**Table 6.5: Comparison of measured mass losses of CuO/ZnO/Al<sub>2</sub>O<sub>3</sub> during reduction with calculated values**

	Initial mass of catalyst		
	125 mg	250 mg	500 mg
Measured mass of oxygen lost from catalyst (based on H <sub>2</sub> O eluted) (mg)	17	33	60
Calculated mass of oxygen in CuO component of initial precursor sample (mg)	15	30	60
% overall mass loss of catalyst during reduction (based on CO <sub>2</sub> and H <sub>2</sub> O evolution)	17.2	16.5	15.9

## 6.3.2 Kinetic analysis of Cu/ZnO/Al<sub>2</sub>O<sub>3</sub> under CO/CO<sub>2</sub>/H<sub>2</sub> feeds

### 6.3.2.1 Steady state experimental

Following the reduction step described in Section 6.3.1, Cu/ZnO/Al<sub>2</sub>O<sub>3</sub> catalysts were tested under steady state conditions. The testing was carried out in parallel difference mode (bed masses: 125, 250, 375 and 500 mg). All catalyst beds were initially exposed to 3% CO / 3% CO<sub>2</sub> / 67% H<sub>2</sub> / 27% N<sub>2</sub> gas at 25 bar and 473 K for 10 h, during which time steady state behaviour was observed. Subsequently, all catalyst beds were cycled through a variety of conditions:

- 3 different feed gases (CO/CO<sub>2</sub> % varied: 3:3, 3:1, 3:0.3)
- 5 temperatures (453, 463, 473, 483, 493 K)
- 3 pressures (15, 25, 35 bar)

In total 33 distinct set point observations were made for each of the four catalyst beds and blank reference reactor. These observations were made in a randomised order with periodic checks made at the reference condition in order to confirm that the catalyst had not intrinsically changed in activity. Each catalyst bed was exposed to each set point for a minimum 3 h allowing multiple readings and confirmation of stability to be obtained. An example of such a procedure is shown in Figure 6.6. Intrinsic activity losses, as checked by the reference conditions, never exceeded 5% throughout the steady state testing program, confirming earlier calculations.

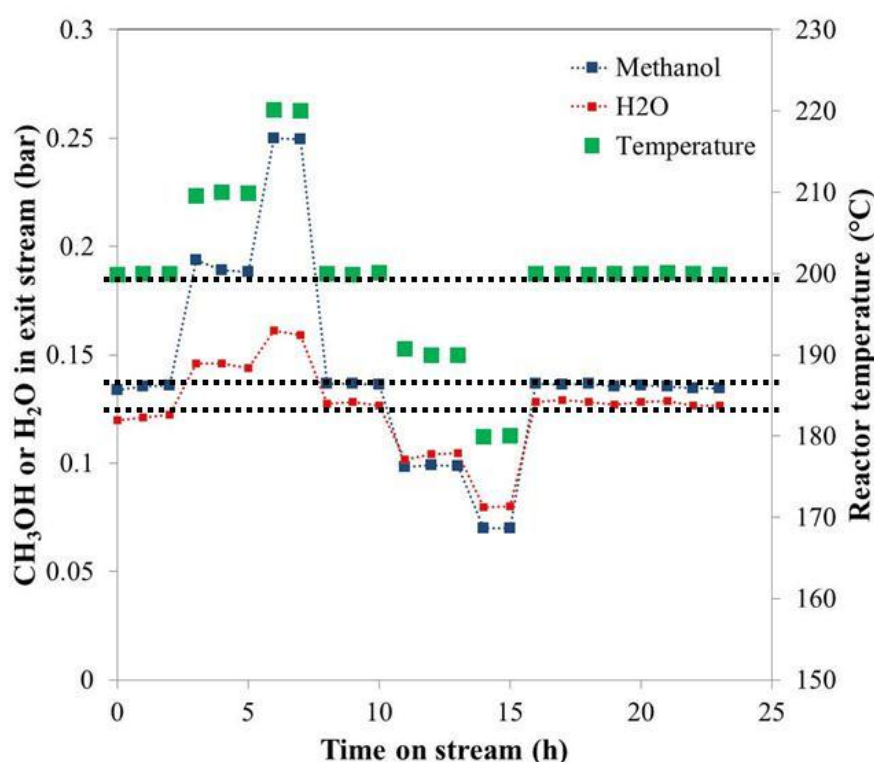


**Figure 6.6: Catalyst stability example during steady state testing. Conditions: Feed CO/CO<sub>2</sub>/H<sub>2</sub>/N<sub>2</sub> (3/3/67/27), flow rate 7.5 L h<sup>-1</sup>, 500 mg Cu/ZnO/Al<sub>2</sub>O<sub>3</sub> catalyst**

The final dataset of 165 distinct observations, each containing four responses (CO, CO<sub>2</sub>, CH<sub>3</sub>OH, H<sub>2</sub>O) is too extensive to incorporate into this text, however examples of catalyst steady state performance are shown in Figure 6.7. In these three graphs the Cu/ZnO/Al<sub>2</sub>O<sub>3</sub> catalyst is exposed to 25 bar, 473 K conditions under the three different feed gases. By using the outlet responses from all four catalyst beds, a set of axial concentration profiles are observed:

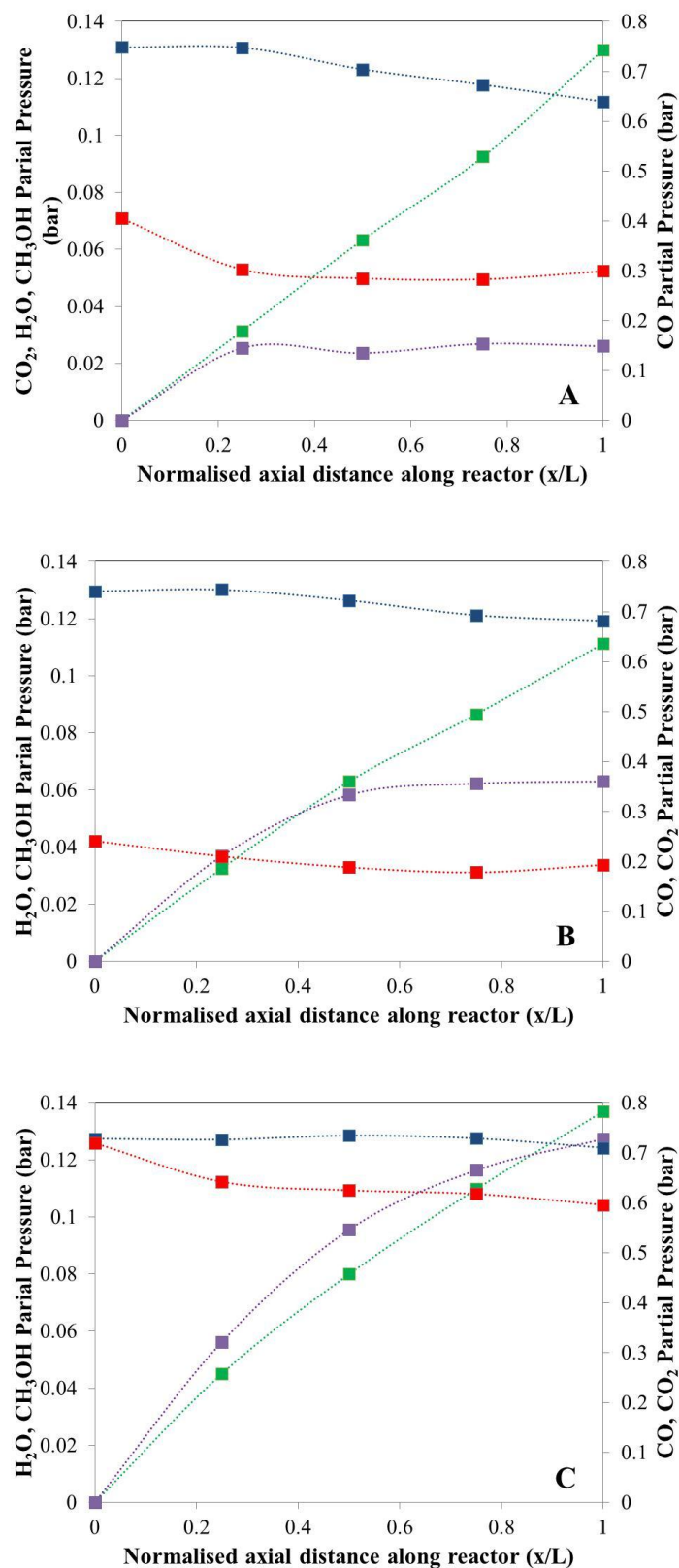


**Figure 6.7: Steady-state axial concentration plots for a Cu/ZnO/Al<sub>2</sub>O<sub>3</sub> catalyst operating under 473 K, 7.5 L h<sup>-1</sup> conditions with CO/CO<sub>2</sub> inlet ratios of A) 10:1, B) 3:1 and C) 1:1. Symbols denote: (■) CO, (■) CO<sub>2</sub>, (■) CH<sub>3</sub>OH and (■) H<sub>2</sub>O. Lines are to guide the eye.**

In Figure 6.7A, apparent CO<sub>2</sub> consumption occurs in the first sector of the catalyst bed but reaches a steady value thereafter. CO behaves in the exact opposite manner and is consumed in sectors 2-4. H<sub>2</sub>O is only produced in the first sector and also reaches a steady level in the subsequent sectors. Use of Eq. (6.22) reveals that the equilibrium composition for the RWGS is reached under these conditions and explains the steady levels of CO<sub>2</sub> and H<sub>2</sub>O in sectors 2-4. CH<sub>3</sub>OH production increases with axial distance along the reactor (0.93 and 1.12 μmol s<sup>-1</sup> g<sup>-1</sup> in the 1<sup>st</sup> and 4<sup>th</sup> sectors respectively). These values are consistent with the observations of Sahibzada *et al.*, (1998) who found that CH<sub>3</sub>OH production rates were greater under integral ‘finite’ conversion compared to differential conversion in CO<sub>2</sub>/(CO+CO<sub>2</sub>) feed inlet values of less than 0.2 (in this example, 0.09).

In Figure 6.7B, a higher CO<sub>2</sub> content in the inlet feed results in CO<sub>2</sub> consumption being observed in the 1<sup>st</sup> and 2<sup>nd</sup> sectors before reaching a steady level. This is again mirrored by H<sub>2</sub>O production. The levelling off of both gas phase species can again be attributed to the equilibrium composition of the RWGS reaction being reached. Again CO consumption appears to replace CO<sub>2</sub> consumption in the back sectors of the catalyst bed. CH<sub>3</sub>OH production rates are greatest in the 1<sup>st</sup> sector of the reactor and slowly retard along the reactor (0.97 and 0.73 μmol h<sup>-1</sup> g<sup>-1</sup> in the 1<sup>st</sup> and 4<sup>th</sup> sectors respectively). This again agrees with Sahibzada *et al.*, (1998) for a CO<sub>2</sub>/(CO+CO<sub>2</sub>) feed inlet values of 0.25.

In Figure 6.7C, CO<sub>2</sub> consumption is observed along the complete axial length of the reactor. The equilibrium composition for the RWGS reaction is approached but is not reached, owing to the shift in this value from the increased CO<sub>2</sub> content in the inlet feed. CH<sub>3</sub>OH production rates are considerably higher at the front of the reactor compared to the back (1.34 and 0.81 μmol h<sup>-1</sup> g<sup>-1</sup> in the 1<sup>st</sup> and 4<sup>th</sup> sectors respectively). This again agrees with Sahibzada *et al.*, (1998) for a CO<sub>2</sub>/(CO+CO<sub>2</sub>) feed inlet values of 0.5.

The observations in Figure 6.7 are indicative of the general trends seen in the wider dataset. In general, it appears that CO<sub>2</sub> consumption is gradually replaced by CO consumption along the reactor as the RWGS equilibrium compositions are reached. This replacement does not lead to a sharp loss in CH<sub>3</sub>OH productivity. On face value, this would suggest CO becomes the source of carbon in CH<sub>3</sub>OH production along the reactor; a route which was supported by earlier works (Andrew, 1980; Klier *et al.*, 1982; Villa *et al.*, 1985; Graaf *et al.*, 1988). However it was earlier discussed that the CO<sub>2</sub> → CH<sub>3</sub>OH route has been demonstrated to be considerably faster than the CO route over Cu/ZnO/Al<sub>2</sub>O<sub>3</sub> and is key to

maintaining CH<sub>3</sub>OH activity over this catalyst (Mochalin *et al.*, (1984); Liu *et al.*, (1985); Chinchin *et al.*, (1986); Vanden Bussche and Froment, (1996)). Hence a more detailed steady state model may be required to describe this behaviour.

In the discussion of Figures 6.7A-C, it was noted that the equilibrium mixture for the RWGS reaction is reached at different stages along the axial length of the reactor, depending on feed, temperature and pressure. Indeed, for all three reactions described in Eq. (6.1-3), proximity to equilibrium mixtures should be analysed and utilised in the subsequent kinetic model. To illustrate, an overall ‘equilibrium term’,  $\beta_i^*$ , which comprises both a thermodynamic constant,  $K_i^*$  (based on Graaf *et al.*, 1986) and driving force (partial pressures) of the gases in the forwards and backwards direction of each reaction of interest can be calculated:

$$\text{For } CO_2 \rightarrow CH_3OH: \beta_1^* = K_1^* \frac{P_{CH_3OH} P_{H_2O}}{P_{CO_2} P_{H_2}^3} \quad (6.25)$$

$$\text{For } CO_2 \rightarrow CO: \beta_2^* = K_2^* \frac{P_{CO} P_{H_2O}}{P_{CO_2} P_{H_2}} \quad (6.26)$$

$$\text{For } CO \rightarrow CH_3OH: \beta_3^* = K_3^* \frac{P_{CH_3OH}}{P_{CO} P_{H_2}^2} \quad (6.27)$$

Figure 6.8A and 6.8B illustrates the overall magnitude of the ‘equilibrium term’ at axial sector outlets for both the CO<sub>2</sub> → CH<sub>3</sub>OH and CO<sub>2</sub> → CO (RWGS) reaction respectively, for all steady state conditions tested. A  $\beta_i^*$  value of exactly 1 implies a particular reaction is at equilibrium. For the CO<sub>2</sub> → CH<sub>3</sub>OH reaction in Figure 6.8A, all conditions tested favour the forward reaction to methanol. The largest value of  $\beta_1^*$  across the entire dataset is 0.5 at the 4<sup>th</sup> sector outlet under 15 bar, 493 K conditions. Hence thermodynamic limitations should be considered when testing kinetic models for this reaction but a full mechanism to describe the back reaction, CH<sub>3</sub>OH → CO<sub>2</sub> is not necessary.

In Figure 6.8B, describing the equilibrium term for the CO<sub>2</sub> → CO reaction, a distinct trend is seen. The outlet equilibrium terms in the 1<sup>st</sup> sector are predominantly on the side of favouring RWGS ( $\beta_2^* < 1$ ) whilst the 2<sup>nd</sup> – 4<sup>th</sup> sectors are predominantly on the other side of the equilibrium term ( $\beta_2^* > 1$ ), favouring the FWGS reaction. Hence across the steady state

dataset it may not be sufficient to describe WGS catalysis by one reaction with an equilibrium term. A kinetic expression for both the FWGS and RWGS reactions may be needed.

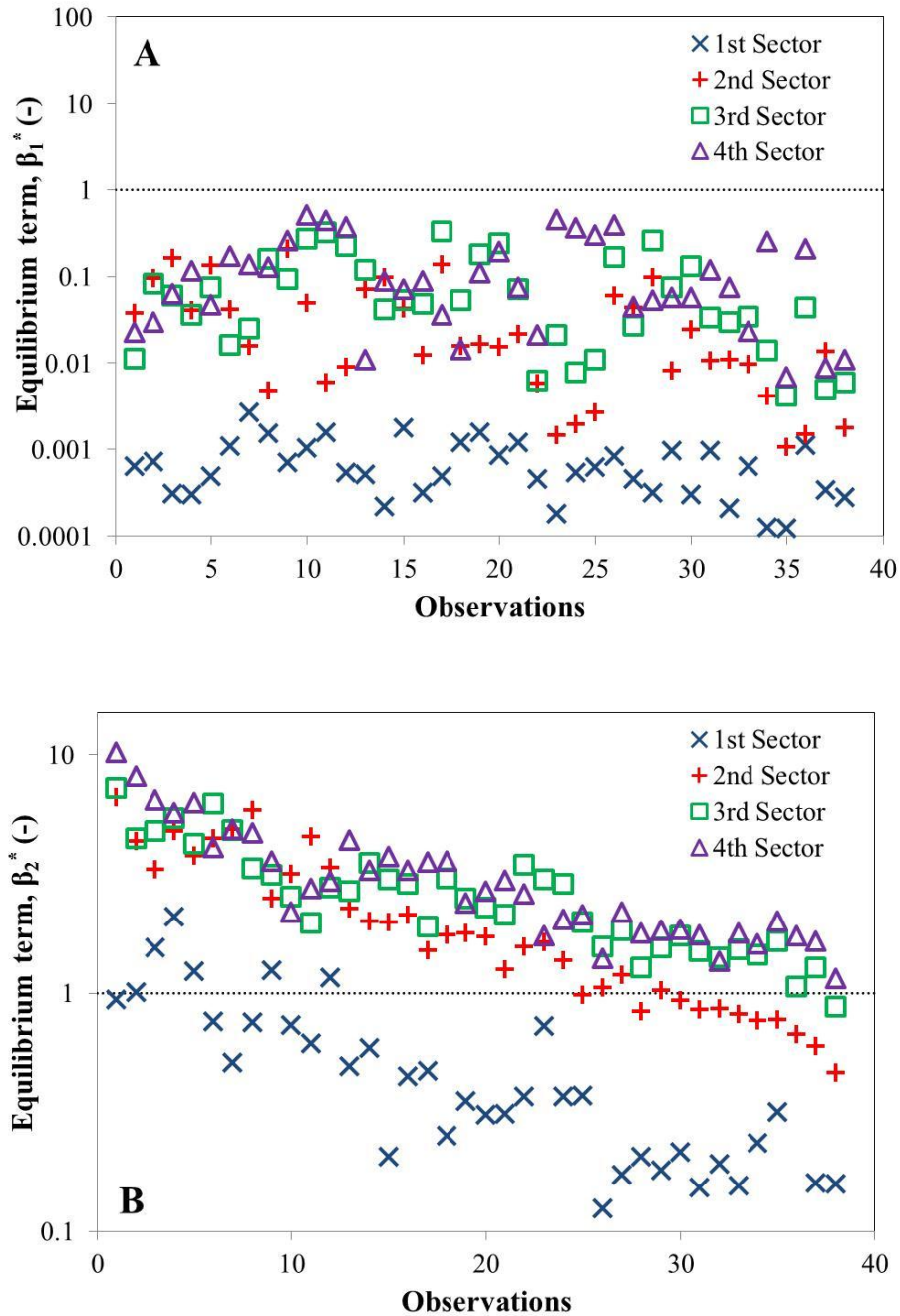


**Figure 6.8: Values of equilibrium terms A)  $\beta_1^*$  and B)  $\beta_2^*$  at individual sector outlets for all experimental steady state data points (temperature/pressure/feed conditions inclusive) in the kinetic study.**

### 6.3.2.2 Steady state kinetic modelling

The kinetic models for CO/CO<sub>2</sub>/H<sub>2</sub> feeds discussed in Table 6.1 acted as a start point for building a suitable description for the data discussion in Section 6.3.2.1. The model of Graaf *et al.*, (1988), comprising 3 reactions and 12 parameters was tested first. This is notable for its two-site basis, one for the adsorption of CO and CO<sub>2</sub> and the other for H<sub>2</sub> and H<sub>2</sub>O. Whilst an initial fit of this model provided a high quality of fit, both the  $A_{i,473.15}$  and  $\Delta H_{ads}$  values pertaining to the lumped parameter  $K_{H_2O/H_2}^{0.5}$  were found to be insignificant in their statistical contribution, as shown via the *F*-test. Hence the model was reduced to a 1 site basis.

The model of Graaf *et al.*, (1988) was ultimately reduced to a 9 parameter model (Table 6.6) however the subsequent removal of the  $A_{i,473.15}$  term in  $K_{CO_2}$  resulted in a significant shift in the methanol response residual, again demonstrated by the *F*-test. This suggests that the CO<sub>2</sub> adsorption term, whilst poorly estimated, is of importance in this description. On wider inspection of the parameters in Table 6.6, parameter estimation confidence is poor, particularly for the energy values.

**Table 6.6: 9 parameter model of Graaf *et al.*, (1988) (overall  $R^2 = 0.995$ )**

Parameter	Pre-exponential factor, $A_{i,473.15}$ (s <sup>-1</sup> )	Activation energy or heat of adsorption, $E_a$ or $\Delta H_{ads}$ (kJ mol <sup>-1</sup> )
$k_1$	$3.25 \times 10^2$ (Indeterminate 95% confidence interval)	$102 \pm 43$
$k_2$	$(7.65 \pm 2.42) \times 10^2$	$123 \pm 33$
$k_3$	$(1.64 \pm 0.45) \times 10^2$	$104 \pm 59$
$K_{CO}$	$(6.37 \pm 0.80) \times 10^3$	$80 \pm 48$
$K_{CO_2}$	$(2.59 \pm 3.04) \times 10^{18}$	-

Estimated  $A_{i,473.15}$  and  $E_a$  values for  $k_1$  and  $k_3$  are very similar in magnitude and absolute value respectively, suggesting that they may in fact contribute to the same reaction

rather than prevail as separate  $\text{CO}_2 \rightarrow \text{CH}_3\text{OH}$  and  $\text{CO} \rightarrow \text{CH}_3\text{OH}$  routes respectively, thus agreeing with an observation made in Vanden Bussche and Froment, (1996). Similarly, both of these  $E_a$  values showed fairly strong normalised cross correlation values with  $\Delta H_{ads}$  for  $K_{CO}$  of 0.88 and 0.95 respectively. As the estimated value of  $\Delta H_{ads}$  for  $K_{CO}$  is within the range of previous literature values for CO oxidation over a partially oxidised copper surface (Ovesen *et al.*, 1992; Waugh, 1999), this may suggest that the methanol synthesis and FWGS pathways may be interrelated within  $k_1$  and  $k_3$ , as discussed earlier. Whilst these findings show that the model of Graaf *et al.*, (1988) is not suitable to describe the CO/CO<sub>2</sub>/H<sub>2</sub> dataset over Cu/ZnO/Al<sub>2</sub>O<sub>3</sub> in this work, it does further demonstrate that kinetic descriptions for both directions of WGS are required.

The 2 reaction model of Mochalin *et al.*, (1984) was unable to improve on the findings above. Both denominator terms, linked with the adsorption of water were found to be statistically insignificant in their contribution, following that of Graaf *et al.*, (1988). The final 4 parameter model measured  $E_a$  values for  $k_1$  and  $k_2$  which were indiscriminate from zero, owing to their low fitted values and wide 95% confidence intervals. With respect to  $k_2$ , this again suggests that a model that does not account for the kinetic descriptions of both RWGS and FWGS leads to either lumped or meaningless parameters. Similar findings were made with the model of Coteron and Hayhurst, (1994) although the confidence in estimated parameters and overall residuals were even further reduced due to the complete omission of either WGS reaction term in the reaction network.

The use of the model of Vanden Bussche and Froment, (1996) afforded a broader approach due to the strong mechanistic basis designated in Figure 6.2. The start point for using the model in this study was to consider the initial overall site population balance within the model. This is assumed to occur over the copper phase of the catalyst:

$$1 = \frac{c_s}{c_t} + \frac{c_{O.s}}{c_t} + \frac{c_{H_2O.s}}{c_t} + \frac{c_{HCO_2.2s}}{c_t} + \frac{c_{CO_3.2s}}{c_t} + \frac{c_{H.s}}{c_t} \quad (6.28)$$

In Eq. (6.28),  $c_t$  denotes the total number of sites (-) and  $c_s$  is a vacant site (-). It is noted that this balance contains a mixture of mono-dentate and bi-dentate species leading to the following simplified description:

$$1 = b \left( \frac{c_s}{c_t} \right) + a \left( \frac{c_s}{c_t} \right)^2 \quad (6.29)$$

In Eq. (6.29),  $a$  denotes the bi-dentate adsorbed species (formate ( $\text{HCO}_2.2s$ ) and carbonate ( $\text{CO}_3.2s$ )) and  $b$  denotes the mono-dentate adsorbed species (hydrogen ( $\text{H}.s$ ), water ( $\text{H}_2\text{O}.s$ ) and surface oxygen ( $\text{O}.s$ )). In the original work, the bi-dentate species were found to yield a negligible contribution in describing the dataset and the final equations (Eq. (6.10)) only featured the mono-dentate species. In the current work, all mono-dentate species and (bi-dentate) formate parameters were found to be negligible via the statistical analysis methods described in Chapter 3, leading to a description for methanol synthesis and RWGS only featuring a carbonate adsorption ( $K_{\text{Carb}}$ ) term:

$$r_1 = \frac{k'_{\text{MeOH}} P_{\text{CO}_2} P_{\text{H}_2} (1 - K_1^* (P_{\text{MeOH}} P_{\text{H}_2\text{O}}) / (P_{\text{CO}_2} P_{\text{H}_2}^3))}{(1 + K_{\text{Carb}} P_{\text{CO}_2} P_{\text{H}_2})^3} \quad (6.30)$$

$$r_2 = \frac{k_2 P_{\text{CO}_2} (1 - K_2^* (P_{\text{CO}} P_{\text{H}_2\text{O}}) / (P_{\text{CO}_2} P_{\text{H}_2}))}{(1 + K_{\text{Carb}} P_{\text{CO}_2} P_{\text{H}_2})} \quad (6.31)$$

The overall description shown in Eq. (6.30-31) therefore comprised 6 fitting parameters. Owing to the earlier discussion that a kinetic description for FWGS may also be required, an extended reaction network was proposed (Figure 6.9):

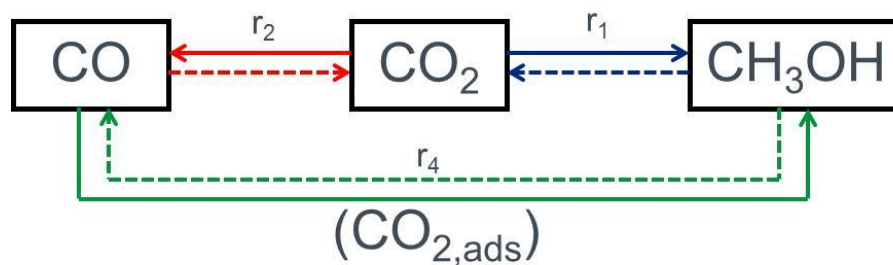


**Figure 6.9: Extended reaction network for methanol synthesis and WGS catalysis over a Cu/ZnO/Al<sub>2</sub>O<sub>3</sub> catalyst. Solid lines denote direction of reaction dictated by kinetics and dashed lines denote backwards reaction dictated by thermodynamic limitations**

In Figure 6.9 it is of critical importance to stress that  $r_4$  is a lumped reaction term, comprising FWGS leading to adsorbed  $\text{CO}_{2,ads}$  which is subsequently hydrogenated to methanol via the same mechanism described in  $r_1$ . The rate model for  $r_4$  is thus:

$$r_4 = \frac{k_{MeOH}' k_4 P_{CO} P_{H_2} (1 - K_3^* P_{MeOH} / (P_{CO} P_{H_2}^2))}{(1 + K_{Carb} P_{CO} P_{H_2})^3} \quad (6.32)$$

$k_4$  denotes the kinetic rate constant for FWGS ( $s^{-1}$ ). Parameter estimation results for both models (i.e. including and excluding  $r_4$ ) are shown in Table 6.7. In both cases  $\Delta H_{ads}$  for  $K_{Carb}$  was set to zero due to a statistically insignificant contribution, reducing the models to 5 and 7 parameters respectively:

**Table 6.7: Parameter estimation results using a 5 and 7 parameter model based on the model of Vanden Bussche and Froment, (1996)**

Parameter	Pre-exponential factor, $A_{i,473.15}$ ( $10^3 s^{-1}$ )		Energy value (kJ mol $^{-1}$ )	
	5 parameter	7 parameter	5 parameter	7 parameter
$k_{MeOH}'$	$33 \pm 8$	$13 \pm 4$	$-35 \pm 5$	$-36 \pm 5$
$k_2$	$173 \pm 35$	$66 \pm 22$	$85 \pm 10$	$76 \pm 15$
$k_4$	-	$4.2 \pm 0.6$	-	$60 \pm 8$
$K_{Carb}$	$240 \pm 53$	$127 \pm 40$	-	-

High  $R^2$  values of 0.994 and 0.995 were returned for the 5- and 7-parameter models respectively. The estimated parameters for  $k_{MeOH}'$  were similar for both models; the estimated energies are similar to those reported by Vanden Bussche and Froment, (1996) and the negative sign is acceptable as this parameter is a lumped  $E_a$  and  $\Delta H_{ads}$  term. The pre-exponential for  $k_{MeOH}'$  is higher in the 5-parameter model, owing to the omission of the  $r_4$  pathway in the network. The  $E_a$  for RWGS in  $k_2$  was found to be lower than the 95 kJ mol $^{-1}$  measured in the initial work in both cases however within confidence intervals, not significantly so. In the 7-parameter model, the estimated  $E_a$  for FWGS of 60 kJ mol $^{-1}$  is very close to the value calculated by Ovesen et al., (1992) for CO oxidation over an O.s site on copper. This step features in the FWGS mechanism and therefore adds validity to the presence of this parameter. In  $r_4$ , the dependence of H $_2$ O (a reactant in FWGS) was omitted.

In  $r_4$ , the dependence of  $H_2O$  (a reactant in FWGS) was omitted, owing to the redox nature of the overall  $r_4$  reaction. Here the product  $H_2O$  produced from the methanol synthesis stage of the reaction does not desorb (owing to thermodynamic limitations) and therefore supplies the FWGS step. A gas phase  $H_2O$  driving force is therefore not necessary.

Model discrimination was carried out using the global F-test as described thoroughly in Chapter 3. As Table 6.8 shows, the reduction of the 7 parameter model to 5 parameters by complete elimination of  $k_4$  results in an  $F$ -value for all 4 model responses that is significantly greater than  $F_{crit}$ . This therefore shows the statistical importance of the  $r_4$  route in this network. Parity plots for the 4 model responses for the 7-parameter model can be found in the appendices in section 6.5.

**Table 6.8:  $F$ -test analysis to verify significance of extra parameters in the 7-parameter model**

Model response	Sum of square of residuals ( $\times 10^2$ )		$F$ -test	
	5 parameter	7 parameter	$F$ -value when reducing from 7 to 5 parameters	$F_{crit}$
$CO$	12.5	9.8	19.7	3.91
$CO_2$	5.3	5.0	4.1	
$CH_3OH$	12.9	9.3	27.0	
$H_2O$	3.8	2.9	22.9	

In contrast with the dataset fitted in Vanden Bussche *et al.*, (1996), the current work is carried out at higher  $P_{CO}$  to  $P_{CO_2}$  ratios (between 1 – 10 as opposed to 0 – 2.5 in the former) and lower temperatures, which has led to the prevalence of a kinetically driven FWGS reaction in the back sectors of the catalyst bed under many of the conditions tested. The lack of a redox term in the current model (denoted as  $K_{H_2O}/K_8K_9K_{H_2}$  in the original) suggests that

the surface oxidation state, assuming copper as the active site, is largely invariant across the dataset used in this study under steady state conditions.

### 6.3.2.3 Start-up in CO/CO<sub>2</sub>/H<sub>2</sub> feeds

In addition to developing a steady state kinetic model under CO/CO<sub>2</sub>/H<sub>2</sub> conditions, understanding the approach to steady state performance of a Cu/ZnO/Al<sub>2</sub>O<sub>3</sub> catalyst during start-up can have value in further understanding the generation of methanol synthesis and WGS activity on the catalyst surface. Start-up under CO/CO<sub>2</sub>/H<sub>2</sub> is shown in Figure 6.10:

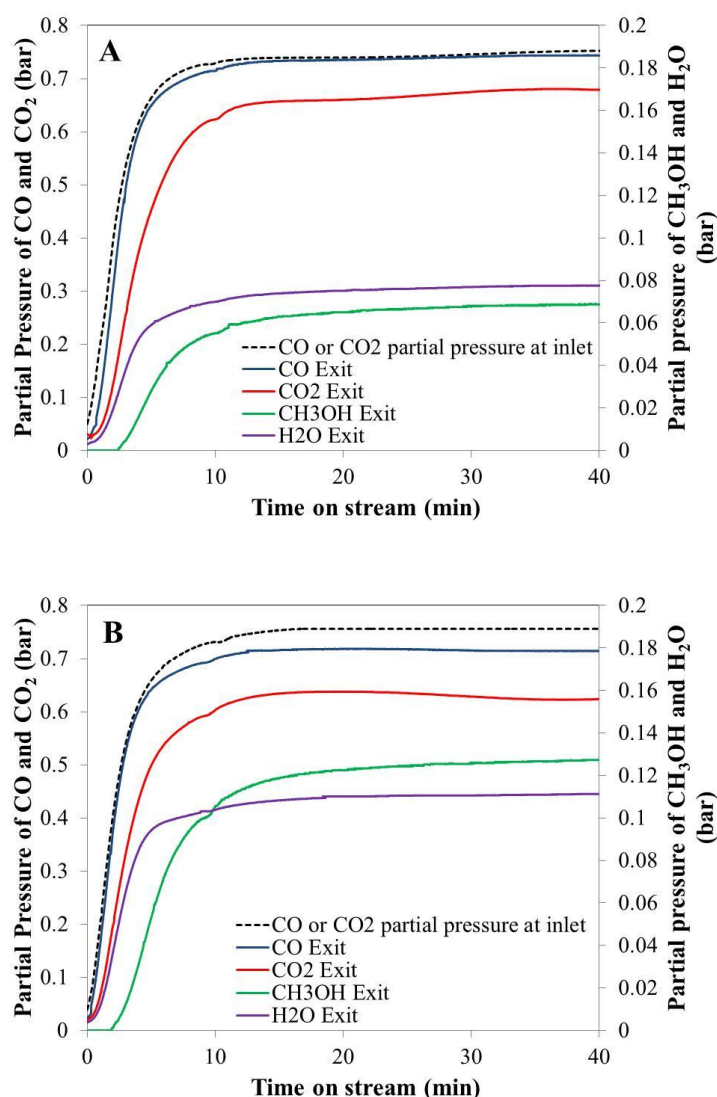


**Figure 6.10: Reaction performance of A) 250 mg, B) 500 mg of Cu/ZnO/Al<sub>2</sub>O<sub>3</sub> catalyst upon feeding CO/CO<sub>2</sub>/H<sub>2</sub>/N<sub>2</sub> (3:3:67:27) at 7.5 L h<sup>-1</sup> (STP) at 25 bar, 473 K. The catalyst had undergone reduction in 2% H<sub>2</sub>/N<sub>2</sub> as shown in Section 6.3.1 prior to this exposure.**

Both profiles in Figure 6.10 show an immediate consumption of CO<sub>2</sub> upon breakthrough of the CO/CO<sub>2</sub>/H<sub>2</sub> gas at t=0 min. The majority of this consumption is in the front 250 mg of the catalyst bed. Consumption of CO is not observed initially, and only in notable levels across the 500 mg bed from t=5 min onwards. Water production is increasingly observed from t=0 min, whilst methanol production is not seen until t=2.5 min in both beds.

This suggests that RWGS takes place from t=0 min whilst the methanol synthesis reaction is delayed. It is important to note that the initial copper surface under these conditions is assumed to be a completely reduced one, based on calculations in Section 6.3.1. In the kinetic model proposed in Section 6.3.2.2, the following initial steps are prevalent for methanol synthesis and RWGS respectively:



Hence, on an initially reduced copper surface it is feasible to assume that the methanol synthesis initiation step in Eq. (6.33) is not possible until a population of O.s sites has built up via Eq. (6.34). To further explore, the carbon and oxygen balances over both catalyst beds were explored and were found to be significantly less than 100% initially.

Figure 6.11A shows a cumulative plot for missing moles of ‘C’ and ‘O’ over the first 30 min time on stream for both catalyst beds. Further small increases in missing carbon and oxygen were seen after this time but cannot be reasonably discriminated due to experimental error in the rig.

In Figure 6.11A, missing oxygen is always greater than carbon in both the 250 and 500 mg beds. It is very clear however, that the majority of the missing species are located in the front 250 mg of the catalyst bed. After 30 min operation,  $260 \pm 21$   $\mu\text{mol}$  of carbon species are present on the front 250 mg of the catalyst bed compared to  $100 \pm 36$   $\mu\text{mol}$  in the back 250 mg (error bars assuming 5% error in all experimental measurements). Assuming these species are a similar molecular size to that of CO<sub>2</sub> (3.9 Å), this leads to a surface coverage of 57 and 23 m<sup>2</sup> g<sup>-1</sup> (based on as received weight) for each 250 mg sector respectively. Both of these estimated values are within range of the copper surface area of the catalyst (32.4 m<sup>2</sup> g<sup>-1</sup> based on ‘as received’ weight).

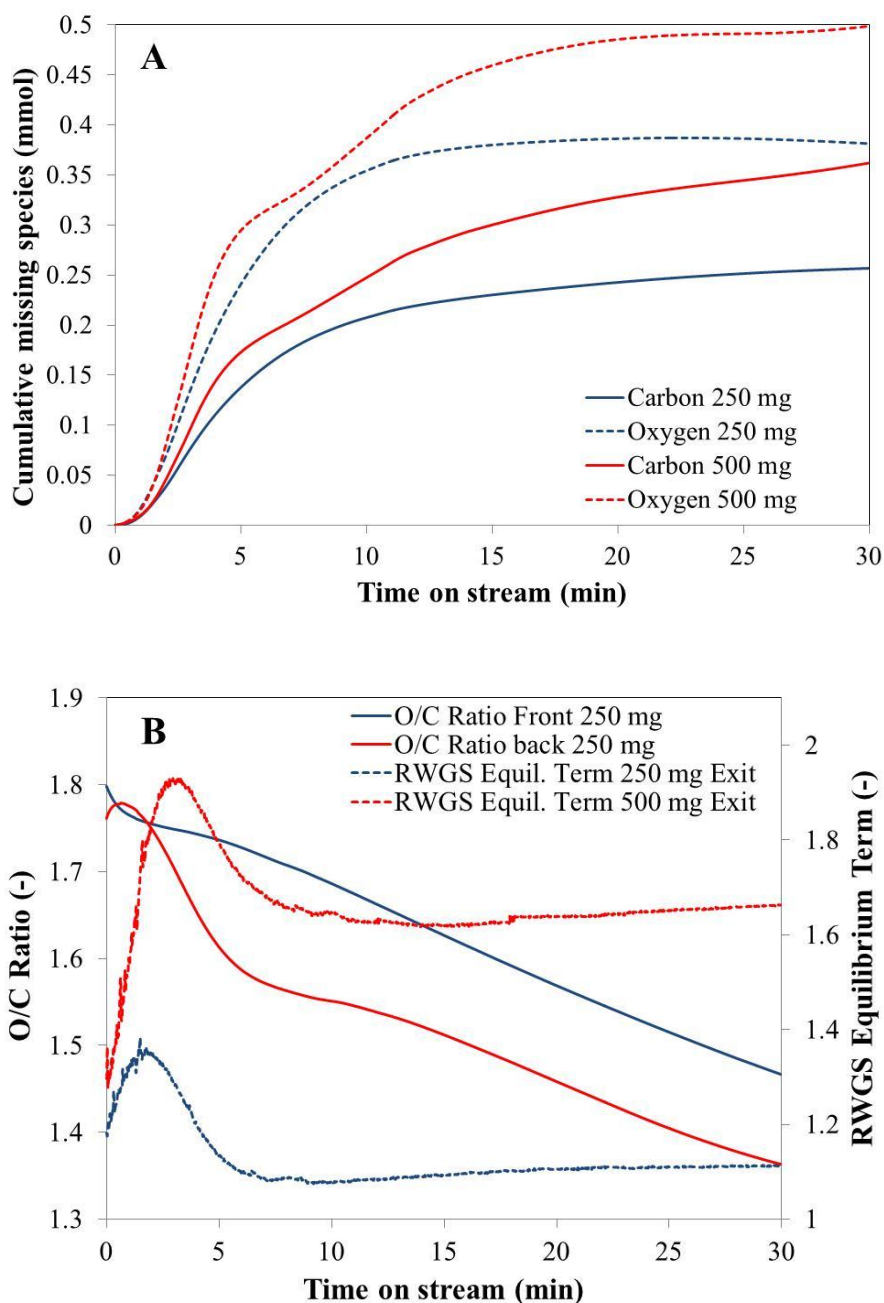


**Figure 6.11: A) Cumulative missing carbon and oxygen over a Cu/ZnO/Al<sub>2</sub>O<sub>3</sub> catalyst during the first 30 min operation under CO/CO<sub>2</sub>/H<sub>2</sub>/N<sub>2</sub> (3:3:67:27) at 7.5 L h<sup>-1</sup> (STP) at 25 bar, 473 K. B) Calculated O/C ratio and RWGS equilibrium term at bed exits**

Corresponding methanol productivity over each sector after 30 minutes was 1.05 and 0.89  $\mu\text{mol s}^{-1} \text{g}^{-1}$  which would correspond to less than 0.4 and 0.9% of the carbon surface population respectively. Hence there appears to be no direct link between overall carbon coverage and methanol productivity. The significant carbon coverage observed does however provide indirect support for the presence of the  $K_{carb}$  term in the steady state model.

The overall missing oxygen to carbon (O/C) ratio is also shown for the first 30 min on stream in Figure 6.11B. Initially, this ratio is ~1.8 in both 250 mg sections of the bed suggesting that the majority of adsorbed species likely originate from CO<sub>2</sub>. This ratio subsequently declines slowly in the front 250 mg and much more quickly in the back 250 mg to values of 1.45 and 1.36 respectively after 30 min. The dynamic changes in this ratio appear to coincide with changes in the position of the RWGS equilibrium term. The term, shown in Eq. (6.26), rapidly increases between 0 and 4 min, particularly at the 500 mg exit. This suggests that the direction of WGS has reversed leading to the back reaction in Eq. (6.34) resulting in a loss of oxygen from the catalyst surface in relative terms.

A further analysis can be made on the front 250 mg of the catalyst bed by examining the rate of water production from RWGS, using the following assumption:

$$\text{Mol } H_2O \text{ from RWGS} = \text{Mol } H_2O \text{ at 250 mg bed exit} - \text{Mol } CH_3OH \text{ at 250 mg bed exit} \quad (6.35)$$

In Eq. (6.35), moles of methanol observed at the bed exit acts as a representation of the number of moles of water formed as a result of methanol synthesis from CO<sub>2</sub>. The results for this over the first 15 min of operation are shown in Figure 6.12:

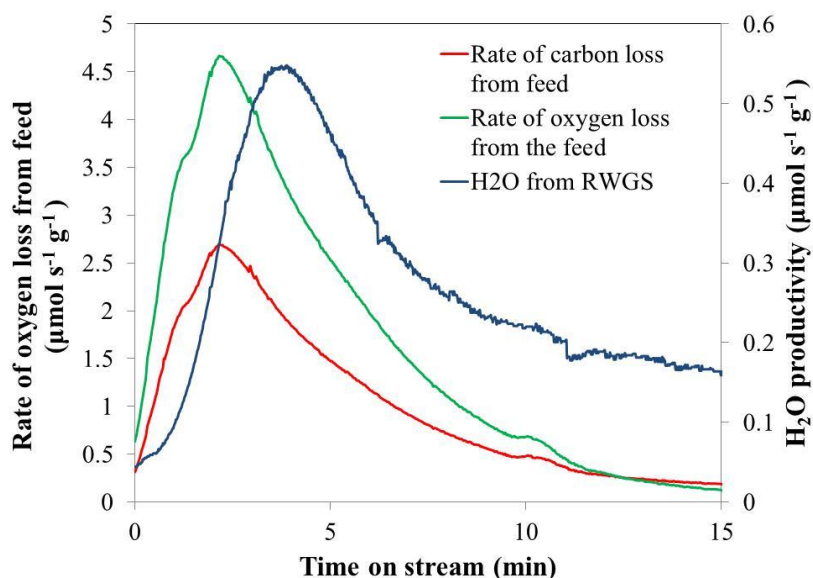


**Figure 6.12: Comparison on H<sub>2</sub>O productivity and rate of carbon and oxygen lost over the front 250 mg of a Cu/ZnO/Al<sub>2</sub>O<sub>3</sub> catalyst bed during the first 15 min operation under CO/CO<sub>2</sub>/H<sub>2</sub>/N<sub>2</sub> (3:3:67:27) at 7.5 L h<sup>-1</sup> (STP) at 25 bar, 473 K.**

Water productivity from RWGS is compared to the molar rate at which oxygen is lost from the feed. Both profiles follow a similar pattern, albeit there is a small delay between the rate of oxygen loss from the feed and that of water production from RWGS. This shows a direct link between oxygen lost from the feed to the catalyst surface and the RWGS reaction. Eq. (6.34), which denotes the dissociation of CO<sub>2</sub> over a vacant site, is the rate determining step for the RWGS in the steady state model of this study and in previous literature (Vanden Bussche and Froment, 1994). With this mechanism in mind, the delay in the two profiles may relate to this step following initial adsorption of CO<sub>2</sub> onto the catalyst surface. As the rate of oxygen lost from the feed drops in Figure 6.12, so does the rate of RWGS. This suggests that an increased build-up of oxygen (O.s type) species retards RWGS which is logical based on Eq. (6.34) and stresses the importance of a redox balance on the catalyst surface for this mechanism.

### 6.3.3 Binary formulations

Reaction testing of binary formulations was utilised to provide further understanding of copper-based catalyst functionality under CO/CO<sub>2</sub>/H<sub>2</sub> conditions. In Table 6.9, the reduction step and productivity of all three catalysts under reaction conditions are compared:

**Table 6.9: Comparison of binary and ternary copper-based formulations during reduction step and under CO/CO<sub>2</sub>/H<sub>2</sub>-feed reaction conditions (N.B.: values relate to a catalyst precursor charge of 500 mg)**

Catalyst precursor	Calculated oxygen within CuO component of precursor (mg)	Measured oxygen released during 2% H <sub>2</sub> /N <sub>2</sub> reduction	Steady state productivity at 473 K, 25 bar <sup>1</sup> (μmol g <sup>-1</sup> s <sup>-1</sup> )	
			CH <sub>3</sub> OH	H <sub>2</sub> O
CuO/ZnO/Al <sub>2</sub> O <sub>3</sub>	60	60	1.04	0.89
CuO/ZnO	34	36	0.44	0.59
CuO/Al <sub>2</sub> O <sub>3</sub>	25	26	0.06	0.37

<sup>1</sup>. Feed gas employed was (CO/CO<sub>2</sub>/H<sub>2</sub>/N<sub>2</sub>) = (3/3/67/27) at 7.5 L h<sup>-1</sup>

As with the CuO/ZnO/Al<sub>2</sub>O<sub>3</sub> catalyst precursor formulation, both the CuO/ZnO and CuO/Al<sub>2</sub>O<sub>3</sub> catalysts released an amount of oxygen during the reduction step (as H<sub>2</sub>O) that was almost equivalent to the oxygen content of CuO in the sample. This again suggests that the entire copper component is reduced to Cu<sup>0</sup> during this procedure. All three catalysts were subsequently tested under steady state CO/CO<sub>2</sub>/H<sub>2</sub> conditions at 473 K, 25 bar. Methanol productivity over a 500 mg bed followed the trend of Cu/ZnO/Al<sub>2</sub>O<sub>3</sub> > Cu/ZnO > Cu/Al<sub>2</sub>O<sub>3</sub>, which can be linearly correlated with the copper metal surface area of each of these three formulations, agreeing with the work of Chinchén *et al.*, (1988). Any correlation for RWGS and/or FWGS productivity is less clear from these data however and requires a cross-check with the steady state model developed earlier in this study.

Table 6.10 shows the fitted rate constant parameters for all terms in the steady state model of this study, using parallel difference test data at 25 bar, 473 K, for all three formulations:

**Table 6.10: Application of steady state parallel difference test data for binary and ternary copper-based formulations under reaction conditions using the kinetic model developed in this study<sup>1,2</sup>**

Model Parameter (x 10 <sup>3</sup> )	Cu/ZnO/Al <sub>2</sub> O <sub>3</sub>	Cu/ZnO	Cu/Al <sub>2</sub> O <sub>3</sub>
$k_{MeOH}$	13 ± 4	3.4 ± 1.1	0.8 ± 0.4
$k_2$	67 ± 23	95 ± 43	65 ± 28
$k_{MeOH}k_4$	4.8 ± 0.6	-	-
$K_{Carb}$	127 ± 40	-	-

<sup>1.</sup> Conditions (CO/CO<sub>2</sub>/H<sub>2</sub>/N<sub>2</sub>) = (3/3/67/27) at 7.5 L h<sup>-1</sup>, 473 K, 25 bar

<sup>2.</sup> R<sup>2</sup> values for all individual model responses were >0.99 for all three datasets

A comparison of all three  $k_2$  values show negligible differences in RWGS activity between the formulations (within the confidence intervals of the parameters). In Chinchén and Spencer (1991), it was found that WGS activity of copper-based formulations was not

linked to copper metal surface area, as the current study also suggests. Similarly, no correlation based on support choice can be made from these estimates. This suggests that more intrinsic catalyst formulation parameters may be at hand in determining this activity.

Neither of the binary formulations returned an estimated parameter for carbonate adsorption, suggesting the population of this species is negligible for these formulations under the applied reaction conditions. Given the lower methanol synthesis productivity of these catalysts compared to Cu/ZnO/Al<sub>2</sub>O<sub>3</sub> and the fact that carbonates are an intermediate in the mechanism, this is feasible. Cu/ZnO provided a  $k_{MeOH}$  parameter ~30% that of Cu/ZnO/Al<sub>2</sub>O<sub>3</sub>, which is comparable with the 42% lower methanol synthesis productivity measured.

## 6.4 Conclusions

In this chapter, the links between functionality and formulation of copper-based methanol synthesis catalysts has been investigated using CO/CO<sub>2</sub>/H<sub>2</sub> based feeds.

The copper components of two binary (CuO/ZnO and CuO/Al<sub>2</sub>O<sub>3</sub>) and one ternary (CuO/ZnO/Al<sub>2</sub>O<sub>3</sub>) precursor formulation(s) were all found to be reduced to copper metal during the initial reduction step in 2% H<sub>2</sub>/N<sub>2</sub> of the catalyst, as determined via mass balance. This provided a working model of a reduced copper surface prior to the onset of reaction conditions in this study.

The ternary Cu/ZnO/Al<sub>2</sub>O<sub>3</sub> catalyst was examined thoroughly under steady and non-steady state operation using gas feeds with P<sub>CO</sub>/P<sub>CO2</sub> between 1 and 10. An extensive dataset was developed in the low operation temperature range (453 – 493 K) which was applied against a backdrop of notable literature models. A successful model was developed based on Vanden Bussche and Froment, (1996) which postulated that carbonate species were populous on the surface under these conditions. Furthermore, the presence of a third reaction, a combined FWGS and methanol synthesis term, was developed which described the highly productive methanol synthesis behaviour witnessed primarily at P<sub>CO</sub>/P<sub>CO2</sub> ratios approaching 10. This provided new insight into the functional behaviour of this catalyst under these conditions.

Further to this, the reaction performance of the ternary catalyst was observed during reactor start-up when CO/CO<sub>2</sub>/H<sub>2</sub> is initially co-fed into the reactor. This provided an

understanding of the nature of the species adsorbed on the catalyst surface and the relative levels of oxygen added to the catalyst surface. The dynamics of the WGS reaction provided added insight into this as initial CO<sub>2</sub> adsorption (following a delay) led to an observation of water productivity from RWGS. The RWGS reaction was found to retard in line with increased oxygen build up on the catalyst surface, providing good support for the redox models quoted in literature for this reaction. Such an analysis, under real working conditions of the catalyst, is the first of its type.

Finally, the binary formulations were compared under reaction conditions to the ternary formulation. Methanol synthesis productivity was linked to copper surface area, in agreement with the literature. RWGS productivity showed no clear correlation and from kinetic modelling, was largely unchanged in activity between the samples, suggesting the link between this reaction and formulation is subtle. The working model for all three catalysts can now be taken forth into a dynamic pre-treatment study, whereby catalyst behaviour is probed under CO/H<sub>2</sub> conditions, which are inherently less well understood.

## 6.5 Appendices

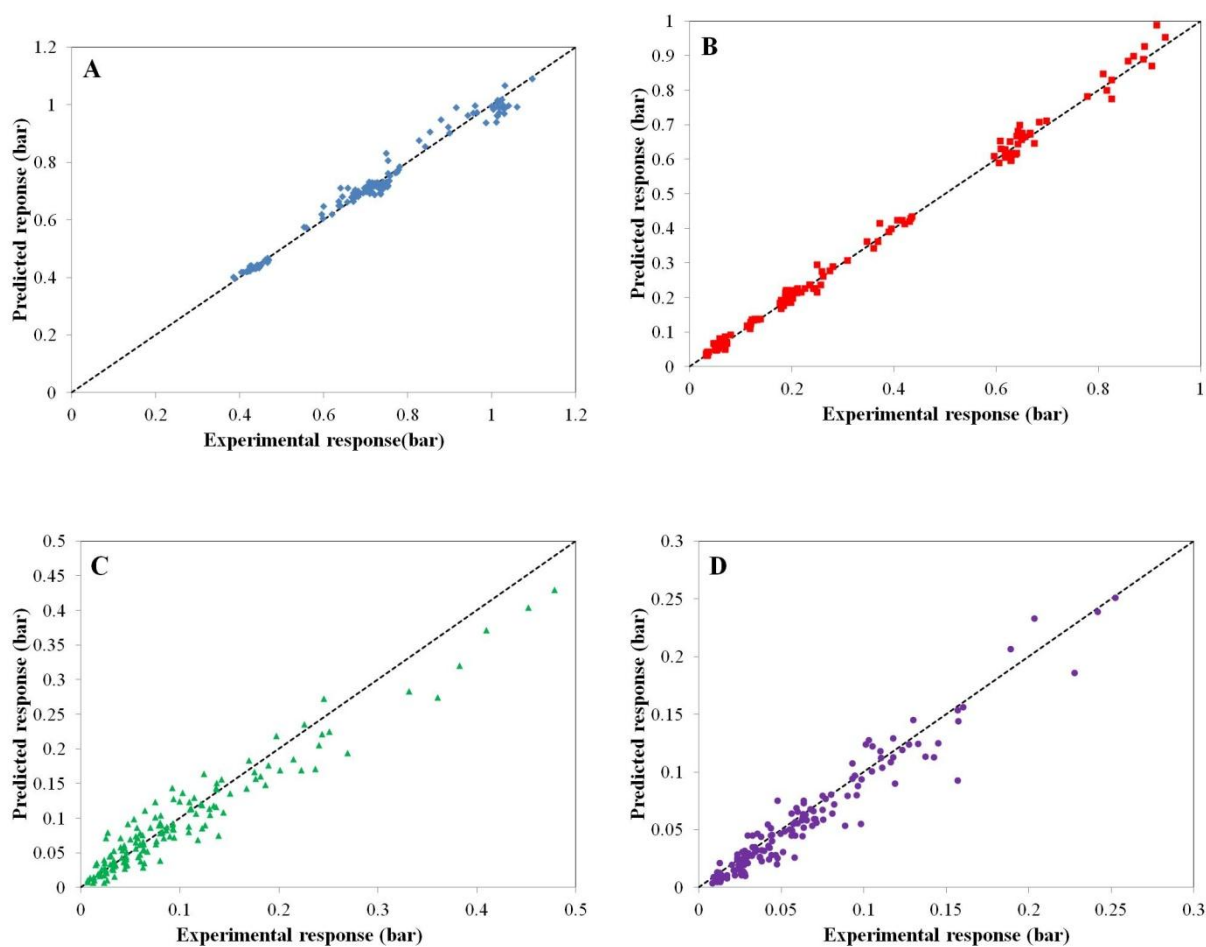


**Figure 6.13: Parity plots for response variables A) CO, B) CO<sub>2</sub> C) CH<sub>3</sub>OH and D) H<sub>2</sub>O.**

**Response variable predictions are provided by the 7-parameter, 3 reaction pathway model based on Vanden Bussche and Froment, (1996)**

**Table 6.11: Steady state testing results for parallel difference testing of Cu/ZnO/Al<sub>2</sub>O<sub>3</sub> under CO/CO<sub>2</sub>/H<sub>2</sub> conditions**

Temp. (K)	Total Pres. (bar)	H <sub>2</sub> In Feed (bar)	CO In Feed (bar)	CO <sub>2</sub> In Feed (bar)	Sector Number	CO Out (bar)	CO <sub>2</sub> Out (bar)	CH <sub>3</sub> OH Out (bar x 10 <sup>2</sup> )	H <sub>2</sub> O Out (bar x 10 <sup>2</sup> )
453	15	10.1	0.444	0.044	1	0.450	0.037	0.64	0.79
					2	0.447	0.033	1.24	1.02
					3	0.444	0.032	1.81	1.31
					4	0.437	0.032	2.52	1.33
453	15	10.1	0.444	0.143	1	0.446	0.138	0.66	0.87
					2	0.445	0.132	1.30	1.69
					3	0.444	0.125	1.90	2.11
					4	0.436	0.119	2.45	2.40

453	15	10.1	0.444	0.445	1	0.459	0.432	0.94	1.26
					2	0.465	0.430	1.69	2.32
					3	0.462	0.416	2.32	2.99
					4	0.464	0.421	2.92	3.51
453	25	16.8	0.750	0.071	1	0.752	0.059	1.47	1.71
					2	0.751	0.055	2.85	2.18
					3	0.741	0.052	4.01	2.75
					4	0.714	0.049	4.95	2.69
453	25	16.8	0.750	0.237	1	0.742	0.225	1.57	1.98
					2	0.731	0.202	2.98	3.79
					3	0.734	0.198	4.36	4.63
					4	0.720	0.188	5.52	5.08
453	25	16.8	0.723	0.710	1	0.722	0.666	2.38	2.96
					2	0.736	0.675	4.20	5.59
					3	0.731	0.651	5.71	7.03
					4	0.734	0.649	7.02	8.07
453	35	23.6	1.054	0.100	1	1.059	0.079	2.50	2.94
					2	1.032	0.068	4.70	3.22
					3	1.011	0.065	6.45	4.38
					4	0.986	0.067	9.35	4.29
453	35	23.6	1.040	0.338	1	1.040	0.309	2.72	3.23
					2	1.027	0.280	5.31	6.33
					3	1.012	0.259	7.46	7.49
					4	1.010	0.261	9.22	8.19
453	35	23.6	1.022	1.008	1	1.012	0.930	4.00	4.76
					2	1.016	0.888	7.51	9.63
					3	1.028	0.905	10.27	11.78
					4	1.017	0.869	12.42	13.27
463	25	16.8	0.741	0.238	1	0.742	0.218	2.32	2.75
					2	0.736	0.201	4.36	4.93
					3	0.724	0.190	6.18	5.58
					4	0.704	0.181	7.99	5.90
463	25	16.8	0.724	0.709	1	0.724	0.656	3.32	4.18
					2	0.728	0.629	5.93	7.49
					3	0.729	0.627	8.03	9.28
					4	0.729	0.629	9.94	10.51
463	25	16.8	0.748	0.071	1	0.751	0.056	2.07	2.18
					2	0.741	0.053	4.11	2.33
					3	0.719	0.052	5.93	2.81
					4	0.680	0.050	8.25	2.66
473	15	10.1	0.450	0.043	1	0.448	0.035	1.24	1.11
					2	0.444	0.035	2.32	1.11
					3	0.428	0.031	3.18	1.34
					4	0.414	0.034	4.29	1.24
473	15	10.1	0.441	0.143	1	0.442	0.127	1.36	1.62
					2	0.439	0.119	2.58	2.59
					3	0.431	0.118	3.50	2.93
					4	0.423	0.115	4.52	2.98

473	15	10.1	0.459	0.449	1	0.469	0.435	1.90	2.50
					2	0.465	0.406	3.39	4.18
					3	0.463	0.395	4.54	5.19
					4	0.458	0.389	5.55	5.81
473	25	16.8	0.748	0.071	1	0.748	0.053	3.14	2.54
					2	0.704	0.050	6.33	2.36
					3	0.673	0.050	9.25	2.69
					4	0.639	0.052	12.95	2.72
473	25	16.8	0.748	0.071	1	0.748	0.054	3.23	2.46
					2	0.715	0.052	6.24	2.31
					3	0.681	0.052	8.59	2.76
					4	0.634	0.051	13.01	2.60
473	25	16.8	0.736	0.238	1	0.742	0.210	3.32	3.79
					2	0.729	0.192	6.24	5.96
					3	0.696	0.180	9.25	6.35
					4	0.665	0.179	12.13	6.33
473	25	16.8	0.728	0.719	1	0.728	0.651	4.58	5.72
					2	0.741	0.637	8.09	9.84
					3	0.729	0.618	10.91	11.77
					4	0.708	0.605	13.70	12.97
473	25	16.8	0.741	0.241	1	0.744	0.210	3.26	3.69
					2	0.722	0.188	6.30	5.82
					3	0.693	0.178	9.22	6.28
					4	0.669	0.182	12.26	6.44
473	25	16.8	0.740	0.243	1	0.740	0.210	3.26	3.68
					2	0.718	0.187	5.96	5.61
					3	0.708	0.197	8.65	6.23
					4	0.681	0.193	11.13	6.30
473	25	16.8	0.728	0.719	1	0.726	0.642	4.51	5.62
					2	0.734	0.625	7.99	9.55
					3	0.729	0.617	10.97	11.64
					4	0.710	0.596	13.70	12.73
473	25	16.8	0.772	0.749	1	0.777	0.698	4.51	5.49
					2	0.774	0.666	8.09	9.01
					3	0.757	0.627	11.10	11.08
					4	0.751	0.640	13.67	12.31
473	35	23.6	1.054	0.101	1	1.019	0.058	5.53	3.95
					2	0.964	0.068	11.63	3.55
					3	0.895	0.065	17.52	4.34
					4	0.841	0.069	24.36	4.36
473	35	23.6	1.028	0.327	1	1.027	0.274	5.66	5.98
					2	1.005	0.256	11.41	9.44
					3	0.942	0.242	16.99	10.09
					4	0.899	0.249	22.57	10.30
473	35	23.6	1.024	0.999	1	1.023	0.890	7.86	9.30
					2	1.012	0.826	14.22	15.70
					3	1.003	0.826	19.71	18.88
					4	0.955	0.778	24.54	20.34

483	25	16.8	0.748	0.071	1	0.719	0.046	4.55	2.57
					2	0.680	0.053	9.37	2.40
					3	0.635	0.053	13.42	2.74
					4	0.597	0.054	17.62	2.65
483	25	16.8	0.734	0.237	1	0.730	0.190	4.55	4.74
					2	0.700	0.178	8.97	6.26
					3	0.655	0.181	13.64	6.84
					4	0.619	0.185	18.15	6.53
483	25	16.8	0.770	0.753	1	0.779	0.683	6.02	7.51
					2	0.769	0.639	10.88	11.87
					3	0.754	0.642	15.08	13.73
					4	0.711	0.607	18.94	14.48
493	15	10.1	0.442	0.142	1	0.445	0.121	2.62	2.78
					2	0.423	0.111	4.67	3.38
					3	0.407	0.118	6.70	3.40
					4	0.384	0.113	8.34	3.23
493	15	10.1	0.448	0.043	1	0.441	0.034	2.33	1.29
					2	0.423	0.035	4.39	1.09
					3	0.402	0.035	5.95	1.28
					4	0.386	0.035	7.55	1.10
493	15	10.1	0.435	0.429	1	0.444	0.372	3.37	4.72
					2	0.447	0.368	5.78	7.13
					3	0.427	0.347	7.64	7.67
					4	0.417	0.360	9.34	7.98
493	25	16.8	0.753	0.073	1	0.707	0.050	6.24	2.62
					2	0.643	0.052	12.26	2.33
					3	0.593	0.051	16.74	2.69
					4	0.558	0.055	21.47	2.67
493	25	16.8	0.737	0.238	1	0.730	0.188	6.36	5.80
					2	0.673	0.182	12.51	6.95
					3	0.599	0.176	18.62	6.77
					4	0.552	0.184	24.01	6.93
493	25	16.8	0.763	0.740	1	0.777	0.646	7.96	9.83
					2	0.753	0.609	14.39	14.23
					3	0.720	0.627	20.13	15.71
					4	0.670	0.617	25.08	16.00
493	35	23.6	1.026	0.331	1	0.998	0.248	10.89	8.86
					2	0.878	0.234	22.26	10.48
					3	0.747	0.245	36.04	11.04
					4	0.639	0.234	45.22	10.98
493	35	23.6	1.081	1.053	1	1.095	0.914	13.87	15.70
					2	1.031	0.858	26.95	22.78
					3	0.914	0.809	38.28	24.17
					4	0.826	0.816	47.85	25.22
493	35	23.6	1.046	0.101	1	0.960	0.068	11.81	4.24
					2	0.851	0.073	23.66	3.74
					3	0.752	0.072	33.15	4.41
					4	0.656	0.068	40.96	4.41

## 6.6 References

- Andrew S.P.S., (1980), at 'Post Congr. Symp. 7<sup>th</sup> Intern. Congr. Catal.', Osaka, Japan, 7<sup>th</sup> July 1980
- Bart J.C.J., Sneed R.P.A., (1987), '*Copper-zinc oxide-alumina methanol catalysts revisited*', Catal. Today, 2, 1-124
- Birtill J.J., (2003), '*But will it last until the shutdown? Deciphering catalyst decay!*', Catal. Today, 81, 531-545
- Bowker M., Hadden R.A., Houghton R.A., Hyland J.N.K., Waugh K.C., (1988), '*The mechanism of methanol synthesis on copper/zinc oxide/alumina catalysts*', J. Catal., 109, 263-273
- Caracotsios M., Stewart W.A.E., (1985), '*Sensitivity analysis of initial value problems with mixed ODEs and algebraic equations*', Comp. and Chem. Eng., 9, 4, 359-365
- Chinchen G.C., Waugh K.C., Whan D.A., (1986), '*The activity and state of the copper surface in methanol synthesis catalysts*', App. Cat., 25, 101-107
- Chinchen G.C., Hay C.M., Vandervell H.D., Waugh K.C., (1987), '*The measurements of copper surface areas by reactive frontal chromatography*', J. Catal., 103, 79-86
- Chinchen G.C., Spencer M.S., (1991), '*Sensitive and insensitive reactions on copper catalysts: The water-gas shift reaction and methanol synthesis from carbon dioxide*', Catal. Today, 10, 293-301
- Chu C.F. and Ng K.M., (1989), '*Flow in packed tubes with a small tube to particle diameter ration*' AIChE Jnl. 35, 148
- Coteron A., Hayhurst A.N., (1994), '*Kinetics of the synthesis of methanol from CO + H<sub>2</sub> and CO + CO<sub>2</sub> + H<sub>2</sub> over copper-based amorphous catalysts*', Chem. Eng. Sci., 49, 2, 209-221
- Ergun S., (1952) '*Fluid flow through packed columns*' Chem. Eng. Prog. 49, 89-94
- Graaf G.H., Sijtsema P.J.J.M., Stambuis E.J., Joosten G.E.H., (1986), '*Chemical equilibria in methanol synthesis*', Chem. Eng. Sci., 41, 11, 2883-2890

- Graaf G.H., Stamhuis E.J., Beenackers A.A.C.M., (1988), '*Kinetics of low-pressure methanol synthesis*', Chem. Eng. Sci., 43, 12, 3185-3195
- Hanken L., (1995), '*Optimization of methanol reactor*', Master's thesis, Norwegian University of Science and Technology
- Himelfarb P.B., Simmons G.W., Klier K., Herman R.G., (1985), '*Precursors of copper-zinc oxide methanol synthesis catalysts*', J. Catal., 93, 442
- Klier K., Chatikavanu V., Herman R.G., Simmons G.W., (1982), '*Catalytic synthesis of methanol from CO/H<sub>2</sub> – IV. The effects of carbon dioxide*', J. Catal., 74, 343-360
- Kung H.H., (1992), '*Deactivation of methanol synthesis catalysts – A review*', Catal. Today, 11, 443-453
- Leonov V.E., Karavaev M.M., Tsybina E.N., Petrischeva G.S., (1973), Kinet. Katal., 14, 848
- Liu G., Willcox D., Garland M., Kung H.H., (1985), '*The role of CO<sub>2</sub> in methanol synthesis on Cu-Zn oxide: An isotope labelling study*', J. Catal., 96, 251-260
- Løvik I., Rønnekleiv M., Olsvik O., Hertzberg T., (2001), '*Estimation of a deactivation model for the methanol synthesis catalyst from historic process data*', Eur. Sym. on Comp. Aided Process Engineering, 11, 219-224
- Marquardt D., '*An algorithm for least-squares estimation of nonlinear parameters*', (1963), S.I.A.M. K. App. Math., 11, 143
- Mochalin V.P., Lin G.I., Rozovskii A.Y., (1984), Khim. Promst., 1, 11
- Nakamura J., Campbell J.M., Campbell C.T., (1990), '*Kinetics and mechanism of the water gas shift reaction catalysed by the clean and Cs-promoted Cu(110) surface: a comparison with Cu(111)*', J. Chem. Soc. Faraday Trans., 86, 2725-2734
- Narita K., Takeyawa N., Kobayashi J., Toyoshima I., (1982), '*Adsorption of nitrous oxide on metallic copper catalysts*', Reac. Kin. Catal. Letters., 19, 91
- Ovesen C.V., Stoltze P., Nørskov J.K., Campbell C.T., (1992), '*A kinetic model of the water gas shift reactions*', J. Catal., 134, 445-468

Ovesen C.V., Clausen B.S., Schiøtz J., Stoltze P., Topsøe H., Nørskov J.K., (1997), '*Kinetic implications of dynamical changes in catalyst morphology during methanol synthesis over Cu/ZnO catalysts*', J. Catal., 168, 133-143

Parris G.E., Klier K., (1986), '*The specific copper surface areas in Cu/ZnO methanol synthesis by oxygen and CO chemisorption: evidence for irreversible CO chemisorption induced by the interaction of the catalyst components*', J. Catal., 97, 374-384

Perez-Ramirez J., Berger R.J., Mul G., Kapteijn F., Moulijn J.A., (2000) '*The six-flow reactor technology: A review on fast catalyst screening and kinetic studies*', Catalysis Today 60, 93-109

Peter M., Fichtl M.B., Ruland H., Kaluza S., Muhler M., Hinrichsen O., (2012), '*Detailed kinetic modelling of methanol synthesis over a ternary copper catalyst*', Chem. Eng. Jnl., 203, 480-491

Rasmussen D.B., Janssens T.V.W., Temel B., Bligaard T., Hinnemann B., Helveg S., Sehested J., (2012), '*The energies of formation and mobilities of Cu surface species on Cu and ZnO in methanol and water gas shift atmospheres studies by DFT*', J. Catal., 293, 205-214

Sahibzada M., Metcalfe I.S., Chadwick D., (1998), '*Methanol synthesis from CO/CO<sub>2</sub>/H<sub>2</sub> over Cu/ZnO/Al<sub>2</sub>O<sub>3</sub> at differential and finite conversions*', J. Catal., 174, 111-118

Soave G., (1972), '*Equilibrium constants from a modified Redlich-Kwong equation of state*', Chem. Eng. Sci., 27, 1197-1203

Twigg M.V., (1989), '*Catalyst handbook – 2<sup>nd</sup> edition*', Wolfe Publishing Ltd., Ch. 9

Vanden Bussche K.M., Froment G.F., (1994), '*Nature of the formate in methanol synthesis on Cu/ZnO/Al<sub>2</sub>O<sub>3</sub>*', App. Cat. A: Gen, 112, 37-55

Vanden Bussche K.M., Froment G.F., (1996), '*A steady-state kinetic model for methanol synthesis and the water gas shift reaction on a commercial Cu/ZnO/Al<sub>2</sub>O<sub>3</sub> catalyst*', J. Catal., 161, 1-10

Villa P., Forzatti P., Buzzi-Ferraris G., Garone G., Pasquon I., (1985), '*Synthesis of alcohols from carbon oxides and hydrogen. 1. Kinetics of low-pressure methanol synthesis*', Ind. Eng. Chem. Proc. Des. Dev., 24, 12-19

Waugh K.C., (1999), '*Prediction of global reaction kinetics by solution of the Arrhenius parameterised component elementary reactions: Microkinetic analysis*', Catal. Today, 53, 161-176

## Chapter 7:

### Functionality and formulation of copper-based methanol synthesis catalysts –

#### Part II: Dynamic behaviour under CO/H<sub>2</sub> and its relationship with performance under CO/CO<sub>2</sub>/H<sub>2</sub> conditions

*The methanol synthesis activity of copper-based catalysts has long been linked to the metric of available copper metal surface area. Whilst findings in Chapter 6 demonstrate general agreement with this finding under CO/CO<sub>2</sub>/H<sub>2</sub> conditions, debate exists around the nature of the active sites for methanol synthesis under CO/H<sub>2</sub>.*

*The reactor start-up of a H<sub>2</sub>/N<sub>2</sub> reduced Cu/ZnO/Al<sub>2</sub>O<sub>3</sub> catalyst under CO/H<sub>2</sub> conditions at elevated temperature and pressure is thoroughly investigated in this study. In contrast to a CO/CO<sub>2</sub>/H<sub>2</sub> feed start-up, the catalyst undergoes a loss of oxygen, believed to be from the ZnO component at the Cu-Zn interface, due to reduction via CO and H<sub>2</sub>. Reactor start-up temperature has a strong impact on these effects and the generation and/or stability of methanol synthesis activity under these conditions. If a reducible component is not present in the catalyst formulation (such as in Cu/Al<sub>2</sub>O<sub>3</sub>), the catalyst produces no methanol.*

*CO/H<sub>2</sub>-treated Cu/ZnO/Al<sub>2</sub>O<sub>3</sub> catalysts were subsequently exposed to CO/CO<sub>2</sub>/H<sub>2</sub> feeds which produced a transient over-production of methanol during the early stages of exposure, in stark comparison to the CO/CO<sub>2</sub>/H<sub>2</sub> feed start-up in Chapter 6. This over-production has been linked to the presence of oxygen vacancies on the catalyst surface, postulated to be at the interface between Cu and Zn. Detailed oxygen and carbon balance analysis reveals these vacancies are quickly oxidised via CO<sub>2</sub>, producing methanol in the process. At steady state, the Cu/ZnO/Al<sub>2</sub>O<sub>3</sub> catalyst adopts a similar surface population of carbon and oxygen to that demonstrated in Chapter 6, hence the effect of a CO/H<sub>2</sub> pre-treatment is reversible within the bounds of the study. The transient experiments presented in this study are new in the field of methanol synthesis catalysis and provide new insight into the link between catalyst formulation and functionality under different feeds.*

## 7. Introduction: ‘New active sites or old surface species?’

In the field of methanol synthesis catalysis over copper-based formulations, such as Cu/ZnO/Al<sub>2</sub>O<sub>3</sub>, debate still exists over the exact nature of the active sites required. It is known that copper alone can synthesise methanol using mixtures of CO/CO<sub>2</sub>/H<sub>2</sub> but catalyst activity can be greatly increased by the inclusion of ZnO (and to some extent Al<sub>2</sub>O<sub>3</sub>) in the catalyst formulation. Both ZnO and Al<sub>2</sub>O<sub>3</sub> show little and no methanol synthesis activity respectively when used individually and are often believed to merely act as structural promoters for the active copper phase (Twigg, 1989), thus enhancing copper metal surface area which has been directly linked to methanol synthesis activity under CO/CO<sub>2</sub>/H<sub>2</sub> reaction conditions (Chinchen *et al.*, 1986). There is however great breadth in the possible process conditions that can be applied and may impact on the state of a copper-based catalyst and/or its reaction pathway functionality:

- **Temperature:** The industrial process is typically operated at ~523 K but methanol synthesis activity has been demonstrated in the range 453 – 553 K in literature (Vanden Bussche and Froment, 1996).
- **Pressure:** Typically operated at 50 – 100 bar in industry but pressures as low as 1 bar have been used in literature. For Cu/ZnO catalysts operating under low pressure conditions, a different active site positioned at the Cu-Zn interface is believed to be active for methanol synthesis (Vanden Bussche and Froment, 1994).
- **Gas phase composition:**  $P_{CO}$  to  $P_{CO_2}$  feed ratio has a significant impact on the reaction pathway functionality of copper-based catalysts. In Chapter 6, this was clearly demonstrated between ratios of 1 to 10, whereby the direction of the water gas shift (WGS) reaction has an impact on the methanol synthesis pathway.

In Chapter 6, reactor start-up analysis under CO/CO<sub>2</sub>/H<sub>2</sub> conditions provided an insight into the development of active sites for methanol synthesis. Critical to this process was the addition of oxygen to the surface (specifically assumed to relate to copper metal based on extensive literature agreement) via CO<sub>2</sub> dissociation in the reverse water gas shift (RWGS) reaction. A postulated redox balance between vacant ( $s$ ) and surface oxygen ( $O.s$ ) sites is eventually developed at steady state which can allow the methanol synthesis mechanistic pathway to take place via bi-dentate CO<sub>2</sub> adsorption over two sites ( $s + O.s$ ).

The next step is to examine how catalytic activity can be generated over copper-based formulations in CO/H<sub>2</sub> feeds and, if methanol can be synthesised, what mechanism this involves. Coteron and Hayhurst, (1994) concluded that it was insufficient to describe the behaviour under both CO/H<sub>2</sub> and CO/CO<sub>2</sub>/H<sub>2</sub> feeds by using the same steady state kinetic model. Indeed this may suggest that the formate route for methanol synthesis, the predominant reaction pathway from CO<sub>2</sub> under CO/CO<sub>2</sub>/H<sub>2</sub> conditions, may not be the functional route under CO/H<sub>2</sub>.

The literature review presented in the next section will address previous literature studies concerning CO/H<sub>2</sub> based operation. This will be linked with dynamic methods which have been used in attempt to discern differences in both catalyst surface and reaction mechanisms generated under CO/H<sub>2</sub> and CO/CO<sub>2</sub>/H<sub>2</sub>.

## **7.1 Approaches to examining the generation and loss of methanol synthesis functionality over copper-based formulations**

### **7.1.1 Steady-state kinetics under CO/H<sub>2</sub>**

The fundamental reaction mechanism behind the synthesis of methanol under CO/H<sub>2</sub> conditions over Cu/ZnO/Al<sub>2</sub>O<sub>3</sub> is poorly understood. The active site for methanol synthesis under these conditions is a matter of debate with proposals including Cu metal, Cu<sup>δ+</sup> species over defective ZnO (Ponec, 1992), CuZn alloys (Topsøe and Topsøe, 1999) and a Schottky junction between Cu and ZnO (Frost, 1988).

There are few published detailed kinetic modelling studies under these conditions and they are confined to steady state operation. Example models, some of which had limited success are shown in Table 7.1. The models of Bos *et al.*, (1989) were based on experimental reaction performance data of a Cu/ZnO/Al<sub>2</sub>O<sub>3</sub> catalyst in an internally recycled gradientless reactor. No definitive model could be elucidated from the four shown in Eq. (7.1-4), all of which assumed the synthesis of methanol to be the rate determining step. Similarly, a positive value was seen for heats of adsorption in Eq. (7.1-3), which violates the thermodynamic laws (Boudart, 1972). The authors dramatically concluded that reaction mechanisms under CO/H<sub>2</sub> conditions could never be expected to be understood from kinetic experiments. It was conceded however that trace levels of CO<sub>2</sub> and H<sub>2</sub>O eluted during the experiment required more investigation.

**Table 7.1: Kinetic models for methanol synthesis under CO/H<sub>2</sub> conditions over Cu/ZnO/(Al<sub>2</sub>O<sub>3</sub>) taken from literature**

Model	Model for CO → CH <sub>3</sub> OH	Experimental conditions tested	Fitted activation energies or heat of adsorption (kJ mol <sup>-1</sup> )
<b>Bos et al., (1989) (7.1-4)</b>	$r_3 = \frac{k_r K_{CO} K_{H_2}^2 (P_{CO} P_{H_2}^2 - P_{MeOH} / K_3^*)}{(1 + K_{CO} P_{CO} + K_{H_2} P_{H_2})^3}$	30 – 70 bar 503 – 553 K 4 – 22% CO in H <sub>2</sub>	E <sub>a,r</sub> = 26.9 ΔH <sub>ads,CO</sub> = 28.5 ΔH <sub>ads,H<sub>2</sub></sub> = 38.6
	$r_3 = \frac{k_r (P_{CO} P_{H_2}^2 - P_{MeOH} / K_3^*)}{(1 + K_{CO} P_{CO} + K_{H_2} P_{H_2} P_{CO})}$	Gradientless reactor	E <sub>a,r</sub> = 86.0 ΔH <sub>ads,CO</sub> = -143.0 ΔH <sub>ads,H<sub>2</sub></sub> = 39.0
	$r_3 = \frac{k_r (P_{CO} P_{H_2}^2 - P_{MeOH} / K_3^*)}{P_{H_2} (1 + K_{CO} P_{CO} + K_{H_2} P_{H_2})^2}$		E <sub>a,r</sub> = 98.6 ΔH <sub>ads,CO</sub> = 23.1 ΔH <sub>ads,H<sub>2</sub></sub> = 67.7
	$r_3 = \frac{k_r (P_{CO} P_{H_2}^2 - P_{MeOH} / K_3^*)}{P_{H_2}}$		E <sub>a,r</sub> = 93.9
<b>Coteron and Hayhurst, (1994) (7.5)</b>	$r_3 = \frac{k_r K_{CO} K_{H_2}^2 K_{CH}}{1 + K_{CO} P_{CO} + K_{CO} K_{H_2}^{3/2} K_{CH} P_{CO} P_{H_2}^{3/2}}$	10 bar 473 – 523 K 10 – 40 % CO in H <sub>2</sub> Differential operation	E <sub>a,r</sub> = 65.1 ΔH <sub>ads,CO</sub> = -3.2 ΔH <sub>ads,H<sub>2</sub></sub> = -6.3

Coteron and Hayhurst, (1994) attempted a considerably more synergistic kinetic study over both a  $\text{Cu}_{30}\text{Zr}_{70}$  and  $\text{Cu}_{30}\text{Zn}_{70}$  catalyst. In this work, separate rate expressions were derived for methanol production under  $\text{CO}/\text{H}_2$  and  $\text{CO}/\text{CO}_2/\text{H}_2$ , and suggested that  $\text{CO}$  and  $\text{CO}_2$  hydrogenation proceeded via different mechanisms. Indeed  $\text{CO}_2$  hydrogenation was found to be the only prevalent route to synthesise methanol under  $\text{CO}/\text{CO}_2/\text{H}_2$ . The basis for  $\text{CO}$  hydrogenation in this work was a stepwise hydrogenation of  $\text{CO}$ , whereby  $\text{CO}$  is adsorbed on a  $\text{Cu}$  site and  $\text{H}_2$  is dissociatively adsorbed on a zinc site. Unlike the work of Bos *et al.*, (1989), the final model parameters obeyed thermodynamic constraints. Unfortunately, the work did not allude to product  $\text{CO}_2$  or  $\text{H}_2\text{O}$  generated under  $\text{CO}/\text{H}_2$  conditions or if non-steady state behaviour was observed during the test programme.

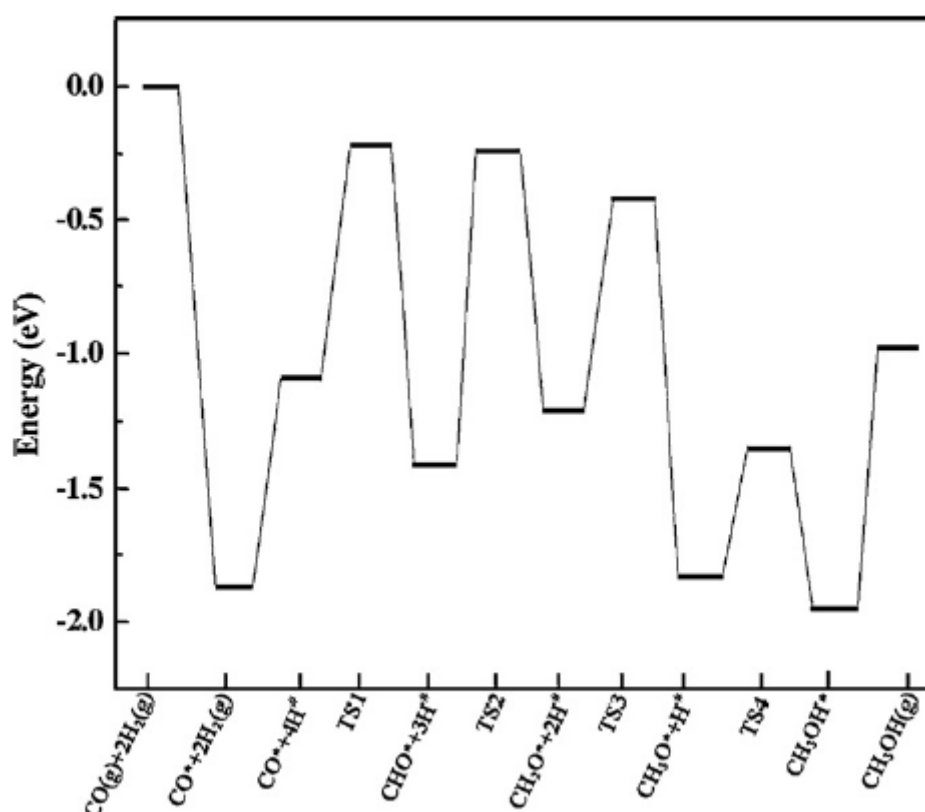


**Figure 7.1: Potential energy diagram for the methanol synthesis reaction on the  $\text{Cu}/\text{ZnO}$  interface (1 0 1 0) from  $\text{CO}$  hydrogenation. ‘TS’ represents transition state, # and \* correspond to Zn and Cu sites, respectively (Zuo *et al.*, 2012)**

Density functional theory (DFT) simulations have also provided some insight into possible routes to synthesise methanol from  $\text{CO}/\text{H}_2$ . Zuo *et al.*, (2012) (see Figure 7.1) simulated the direct and stepwise hydrogenation of  $\text{CO}$ , which was found to prevail over a

$\text{Cu}^{\delta+}$  at an interface with a Zn site. The hydrogenation of CHO at was found to be the rate determining step with an energy barrier of 1.17 eV (115 kJ mol<sup>-1</sup>). In other works (Greeley *et al.*, (2003)), the interaction of CO with both partially oxidised and reduced Cu(1 1 1) surfaces has been simulated. It was found that Zn and/or ZnO species in proximity to the Cu sites were important in enhancing CO interaction with the surface.

### 7.1.2 *In situ* gas-phase pre-treatments

The work of Wilmer and Hinrichsen (2002) investigated the effect of gas-phase conditions on methanol synthesis activity of a Cu/ZnO/Al<sub>2</sub>O<sub>3</sub> catalyst by inducing a selection of different pre-treatments on the catalyst prior to exposure under reference methanol synthesis conditions (CO/CO<sub>2</sub>/H<sub>2</sub>/He) (Figure 7.2):

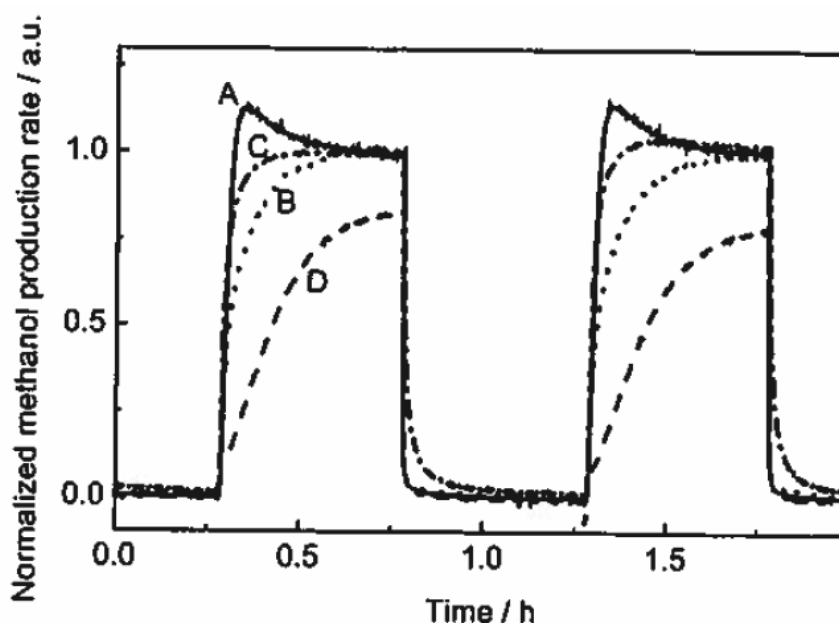


**Figure 7.2: Normalised methanol production rate in a tubular reactor after pre-treatment of a Cu/ZnO/Al<sub>2</sub>O<sub>3</sub> catalyst for 0.5 h with (A) CO/He, (B) He, (C) pure H<sub>2</sub> and (D) CO<sub>2</sub>/He with a subsequent switch to syngas (CO/CO<sub>2</sub>/H<sub>2</sub>/He: 4/14/72/10).**

**Experimental conditions: temperature: 473 K, pressure: 1 bar, flow rate: 7.5 ml min<sup>-1</sup> (STP), catalyst mass: 0.2 g (Wilmer and Hinrichsen, 2002)**

As shown in Figure 7.2, different pre-treatment gases result in a different time-dependent methanol synthesis performance response when switching back to CO/CO<sub>2</sub>/H<sub>2</sub>/He. A CO/He pre-treatment was found to induce a transient maximum in methanol production

before dropping to a lower value. The He and pure H<sub>2</sub> pre-treatments also approached the same final activity but without the maximum, much in the same vein as the CO/CO<sub>2</sub>/H<sub>2</sub> start-up following a 2% H<sub>2</sub>/N<sub>2</sub> reduction step in Chapter 6. CO<sub>2</sub>/He pre-treatments also resulted in initial transient behaviour as well as a lower final activity compared to the other pre-treatments. This was linked to over-oxidation of the catalyst under these pre-treatment conditions (Hinrichsen *et al.*, 2000). All phenomena observed were found to be reversible barring the CO<sub>2</sub>/He pre-treatment.

Neither kinetic analysis nor measure of carbon and oxygen balances during pre-treatment and dynamic operation, which may have helped explain the time dependent behaviours observed, were included in this work. The work does show the strong sensitivity of the catalyst to different gas-phase conditions in generating catalytic activity, evidenced by the significant differences between the CO/He and CO<sub>2</sub>/He pre-treatments.

In Vesborg *et al.*, (2009), pre-treatment mixtures of CO and H<sub>2</sub> produced varied but completely reversible transient methanol production profiles, as shown in Figure 7.3:

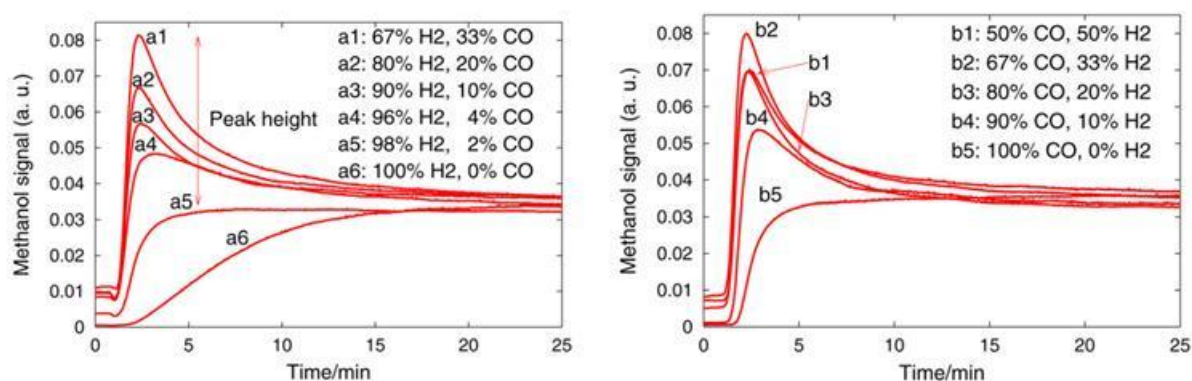


**Figure 7.3: Methanol production over a Cu/ZnO/Al<sub>2</sub>O<sub>3</sub> catalyst in a tubular reactor as a function of time following different 2 h pre-treatments comprising mixtures of CO and H<sub>2</sub>. After the pre-treatment (t = 0 min), the gas mixture is changed to syngas (CO/CO<sub>2</sub>/H<sub>2</sub>/He: 30/5/40/25).**

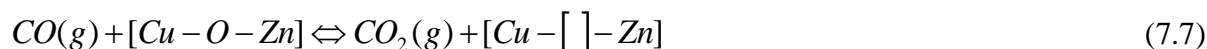
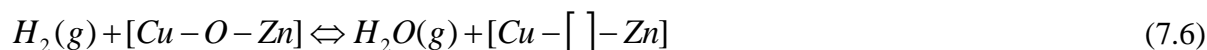
**Experimental conditions: temperature: 500 K, pressure: 4 bar, flow rate: 100 ml min<sup>-1</sup> (STP), catalyst mass: 1.0 g (Vesborg *et al.*, 2009)**

Again this work did not carry out kinetic modelling or mass balance analysis on the dynamic periods of operation but did link the transient methanol maxima for each CO/H<sub>2</sub> gas mix to surface copper nanoparticle shape calculated from a Wulff construction framework

(which calculates copper particle ‘wetting’ on a ZnO support) and environmental transmission electron microscopy (ETEM) imaging. The work linked the findings to reduction potential of the gas inducing greater flatness of surface copper particles (i.e. increased copper metal area) but could not explain the implied synergistic effect of CO/H<sub>2</sub> leading to a transient methanol production maximum at a 0.66:1 or 1:0.66 CO:H<sub>2</sub> ratio. Interestingly, CO/H<sub>2</sub> treatments have also been shown to induce a subsequent maximum when switching to methanol reforming conditions over Cu/ZnO/Al<sub>2</sub>O<sub>3</sub> (Peppley *et al.*, 1999).

### 7.1.3 Dynamic kinetic modelling

In recent years, significant emphasis has been placed on developing kinetic models for methanol synthesis over Cu/ZnO/(Al<sub>2</sub>O<sub>3</sub>) that account for changes in surface morphology of copper particles based on gas-phase conditions (Ovesen *et al.*, 1992; Ovesen *et al.*, 1997; Vesborg *et al.*, 2009). Surface morphology of copper particles is assumed to change based on the following reactions at the Cu-O-Zn interface (Ovesen *et al.*, 1997):



Combined with the Wulff construction framework, these dynamic kinetic models account for the changing copper metal surface area of the catalyst based on gas phase conditions and link this through to methanol synthesis activity. Figure 7.4 shows some of the extents of changes to the copper particles and interaction with ZnO that may take place. The model’s limitations are that it can only account for reversible changes to the catalyst based on conditions and does not afford an explanation for behaviour under CO/H<sub>2</sub> conditions which are in effect, highly reducing. The kinetic model also only considers various copper metal facets, such as Cu(100), Cu(110) and Cu(111) as active sites rather than the effect of changes in charge distribution in the copper particles, based on reduction potential, which could potentially lead to Cu<sup>δ+</sup>.

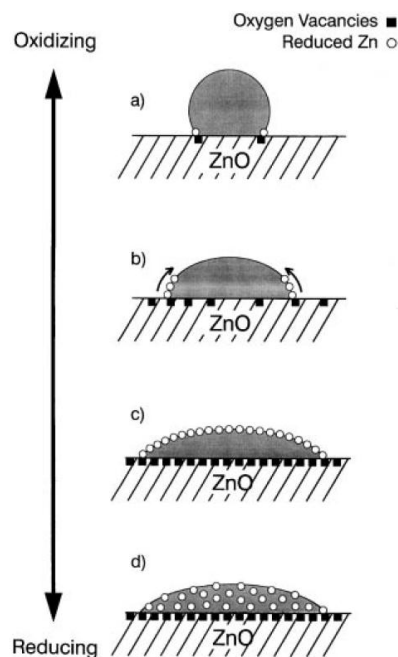


**Figure 7.4: Model diagram for the wetting/non-wetting of Cu-particles on a Zn support, surface alloying and bulk alloy formation: a) round shaped particle under oxidising syngas conditions, b) disk-like particle under more reducing conditions, c) surface Zn-Cu alloying due to stronger reducing conditions, d) brass alloy formation due to severe reducing conditions (Grunwaldt *et al.*, 2000; Verborg *et al.*, 2009)**

#### 7.1.4 Co-adsorption and temperature programmed desorption (TPD) studies

Reactant co-adsorption and TPD studies have been instrumental in probing the nature of the active sites for methanol synthesis on a Cu/ZnO/Al<sub>2</sub>O<sub>3</sub> surface. In Vanden Bussche and Froment, (1994), a Cu/ZnO/Al<sub>2</sub>O<sub>3</sub> catalyst was fully reduced in CO at 1 bar, 523 K and subsequently exposed to CO<sub>2</sub>/H<sub>2</sub> at 373 K. A subsequent TPD under argon showed two distinct evolution peaks of gas-phase species (see Figure 7.5), namely CO<sub>2</sub> and H<sub>2</sub> at 448 K and CO and H<sub>2</sub> at 483 K. Both were linked to different types of formate species, at Cu-Cu and Cu-Zn interfaces respectively. As discussed in Chapter 6, hydrogenation of the formate is the rate determining step for methanol synthesis from CO<sub>2</sub>. This therefore suggested that two different active sites can be prevalent for methanol synthesis. The Cu-Zn formate was found to prevail under low pressure conditions on a reduced catalyst. Under typical industrial conditions, which feature a more oxidising environment, the Cu-Cu formate prevails.

H<sub>2</sub> adsorption-TPD experiments have also provided insight into the nature of active sites on reduced catalyst surfaces following CO pre-treatments. H<sub>2</sub> adsorption capacity was found to decrease over Cu/ZnO/Al<sub>2</sub>O<sub>3</sub> with increasingly reducing pre-treatment conditions suggesting a decrease in copper metal area in this direction (Wilmer and Hinrichsen, 2000; Wilmer *et al.*, 2003). This is contrary to the work of Ovesen *et al.*, (1999) and Vesborg *et al.*, (2009) and may suggest that under reducing conditions, the apparent increase copper metal observed by ETEM may in fact be in a different state, such as Cu<sup>δ+</sup>. This would support a number of literature arguments that removal of oxygen from Cu-O-Zn interfaces, leading to defective ZnO<sub>1-x</sub>, induces an electron attraction and distortion of nearby copper atoms, termed V<sub>0</sub><sup>++</sup> (Parris and Klier, 1986; Bowker *et al.*, 1988; Vanden Bussche and Froment, 1994).

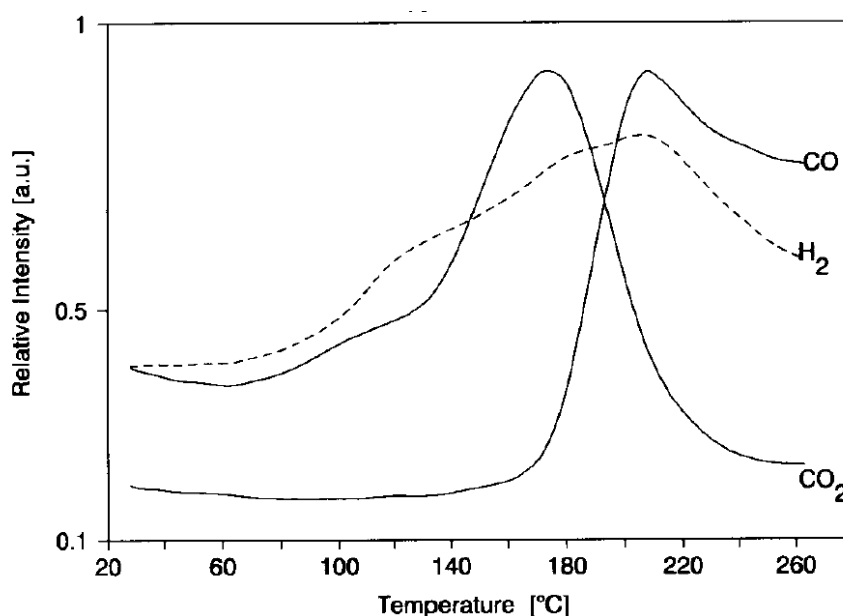


**Figure 7.5: TPD profiles obtained after coadsorption of CO<sub>2</sub> and H<sub>2</sub> (1:9) at 100°C, 8 bar on a reduced commercial Cu/ZnO/Al<sub>2</sub>O<sub>3</sub> catalyst with a heating rate of 3 K min<sup>-1</sup>. Prior reduction was carried out at 523 K, 1 bar in a flow of pure CO (15 ml min<sup>-1</sup> (STP)) for 2 h (Vanden Bussche and Froment, 1994)**

### 7.1.5 *In situ* characterisation studies

ETEM has been used to validate Wulff construction framework calculations (Derouane *et al.*, 1981). In Vesborg *et al.*, (2009), ETEM is used to observe the morphology of surface copper nanoparticles under a variety of conditions, with flatter, disk-like, shapes observed under reducing (CO, H<sub>2</sub> or CO/H<sub>2</sub>) conditions and rounder shapes observed under more oxidising conditions containing CO<sub>2</sub> or H<sub>2</sub>O.

Elsewhere, *in situ* extended x-ray adsorption fine structure (EXAFS) techniques have been used to understand the co-ordination of surface copper on Cu/ZnO and link this to morphological changes on the catalyst surface (Grunwaldt *et al.*, 2000). Cu-Cu co-ordination number was found to decrease under more reducing conditions and was linked to spreading of copper on ZnO. The Cu-Cu co-ordination number of a different formulation, Cu/SiO<sub>2</sub> was found to be unaffected by the changes in the reduction potential of the gas, suggesting a reducible support such as ZnO is important in permitting morphological changes based on process gas conditions.

### 7.1.6 Chapter Objectives

This review has demonstrated that Cu/ZnO/(Al<sub>2</sub>O<sub>3</sub>) catalysts have surfaces which are highly sensitive to the gas phase conditions that they are exposed to. This is particularly pronounced when these catalysts are initially treated under CO/H<sub>2</sub> and then exposed to a CO/CO<sub>2</sub>/H<sub>2</sub> feed leading to dynamic changes in methanol productivity. Few studies on the kinetic modelling of these pre-treatment experiments are present in the literature yet this approach could be successful in enabling fundamental understanding of the dynamic behaviour of these catalysts. This could also shed further light on the differences in catalytic functionality under CO/H<sub>2</sub> and CO/CO<sub>2</sub>/H<sub>2</sub> behaviour respectively. Hence, the aims for this study are thus:

- Undertake a thorough non-steady (reactor start-up) and steady state kinetic analysis of Cu/ZnO/Al<sub>2</sub>O<sub>3</sub> under CO/H<sub>2</sub> to understand the generation of methanol synthesis activity under these conditions.
- Apply experimental methods and develop models to understand the effect of CO/H<sub>2</sub> conditions on the subsequent behaviour of Cu/ZnO/Al<sub>2</sub>O<sub>3</sub> under CO/CO<sub>2</sub>/H<sub>2</sub>.
  - Utilise high pressure conditions (~25 bar) which are closer to that of the real industrial methanol synthesis process to challenge and/or support findings at lower pressure from literature.
  - Link findings to the nature of active sites on the catalyst surface under each of these conditions.
- Apply non-steady state kinetic models to binary catalysts and further infer the impact of formulation on catalyst functionality and presence of active sites.

- Evaluate conclusions from this study with those from Chapter 6 to gain an improved understanding of the link between catalyst formulation, gas phase conditions and catalyst reaction performance.

## 7.2 Materials and methods

### 7.2.1 Sample preparation and properties

Three catalysts precursors, a CuO/ZnO/Al<sub>2</sub>O<sub>3</sub>, CuO/ZnO and CuO/Al<sub>2</sub>O<sub>3</sub> were utilised in this study. Readers are directed to Chapter 6, section 6.2.1 for further characteristic information.

### 7.2.2 Micro-reactor test rig

For full information on the detail and operation of the micro reactor test rig in this chapter, readers are directed to Section 6.2.2. Notable differences in this chapter firstly relate to the types of feed gas employed, which are tabulated in Table 7.2.

**Table 7.2: List of feed-gas compositions used in this study**

Feed-gas type	v/v composition (%)			
	CO	CO <sub>2</sub>	H <sub>2</sub>	N <sub>2</sub>
CO/CO <sub>2</sub> /H <sub>2</sub> gas	3	3	67	27
CO/H <sub>2</sub> gases	3	0	67	30
	10	0	67	23

The majority of experimental testing and analysis in this study involves transient behaviour and, using the feed-gas types listed in Table 7.2 will involve the following transitions:

- Start-up in CO/H<sub>2</sub>
- Start-up in CO/H<sub>2</sub>, then switch to CO/CO<sub>2</sub>/H<sub>2</sub>

In effect, all non-steady state behaviour experiments in this study were triggered by a change in feed conditions over the catalyst beds. As in Chapter 6, a detailed set of blank measurements were carried out for these changes in feed conditions including:

- Checking all 6 reactors individually.
- Checking the effect of reactor packing.
- Examining the effect of temperature and pressure on the measured feed break-through profile.

A study of the above nature ensured carbon and oxygen could be fully tracked during non-steady state operation during catalyst reaction testing. Relevant blank feed change profiles will be included in the results presentation in Section 7.3. It is noted that catalysts were also exposed to CO/H<sub>2</sub> following exposure to CO/CO<sub>2</sub>/H<sub>2</sub>, however this was carried out following flushing of the reactors with N<sub>2</sub>.

### 7.3 Results and discussion

Figure 7.6 (below) shows the gas-phase conditions explored in this chapter and the transitions between them. Relevant findings from the conditions explored in Chapter 6 will be linked as necessary.

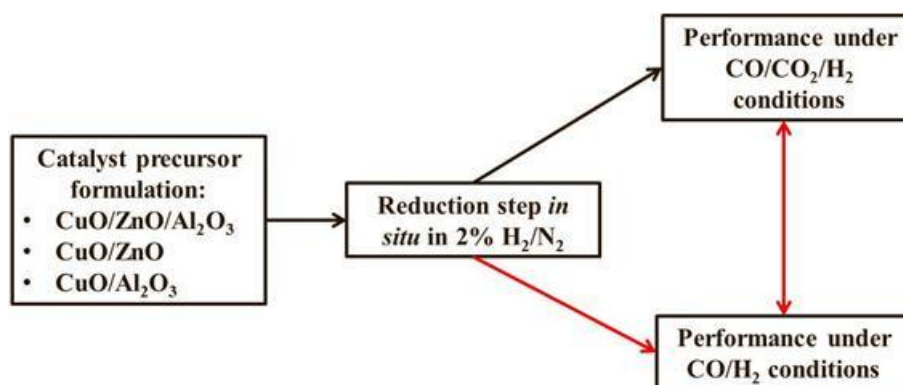


**Figure 7.6: Transitions of gas-phase conditions over copper-based catalysts explored in Chapter 6 (→) and Chapter 7 (→)**

### 7.3.1 Kinetic analysis of Cu/ZnO/Al<sub>2</sub>O<sub>3</sub> under CO/H<sub>2</sub> feeds

#### 7.3.1.1 Start-up in CO/H<sub>2</sub> feeds

The start-up of a Cu/ZnO/Al<sub>2</sub>O<sub>3</sub> catalyst in CO/H<sub>2</sub> shows a highly transient profile with time on stream (Figure 7.7A):

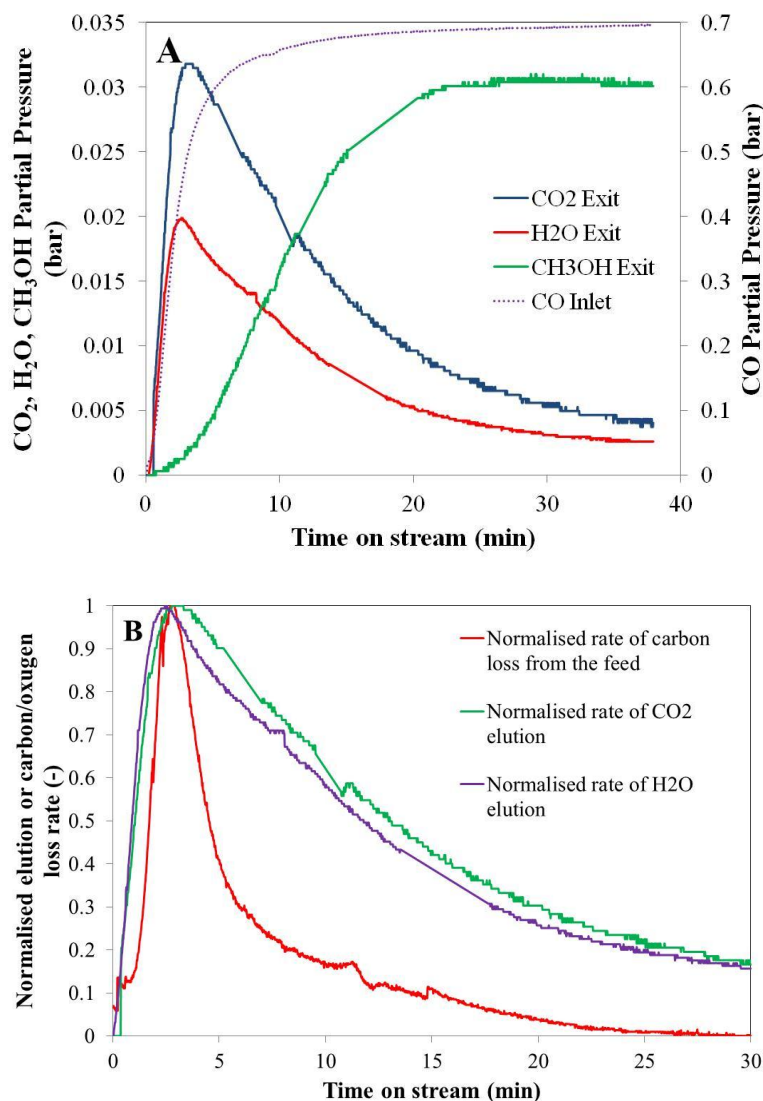


**Figure 7.7: A) Reaction performance of a 500 mg of Cu/ZnO/Al<sub>2</sub>O<sub>3</sub> catalyst upon feeding CO/H<sub>2</sub>/N<sub>2</sub> (3:67:30) at 7.5 L h<sup>-1</sup> (STP) at 25 bar, 473 K. The catalyst had undergone reduction in 2% H<sub>2</sub>/N<sub>2</sub> as shown in Section 6.3.1 prior to this exposure.**

**B) Comparison of normalised carbon loss rates with CO<sub>2</sub> and H<sub>2</sub>O elution in the same experiment. Maxima occur 1.29, 0.24 and 0.15 μmol s<sup>-1</sup> g<sup>-1</sup> for carbon loss, CO<sub>2</sub> and H<sub>2</sub>O elution respectively**

Figure 7.7A shows an example of this during initial exposure of a 500 mg catalyst bed to 3% CO / 67% H<sub>2</sub> / 30% N<sub>2</sub> at 473 K. As CO (and H<sub>2</sub>) are fed into the reactor at t = 0 min, a concomitant and time dependent evolution of CO<sub>2</sub> and H<sub>2</sub>O is witnessed.

Both evolution profiles reach a peak level before declining to a residual value. In a similar manner to the start-up under CO/CO<sub>2</sub>/H<sub>2</sub> conditions, methanol production is initially delayed before increasing up to a steady state productivity level of 0.22 μmol s<sup>-1</sup> g<sup>-1</sup>. This productivity is an order of 4 times smaller than under the same conditions in 3% CO / 3% CO<sub>2</sub> / 67% H<sub>2</sub> / 27% N<sub>2</sub> which agrees with literature (Klier *et al.*, 1982; Sahibzada *et al.*, 1998).

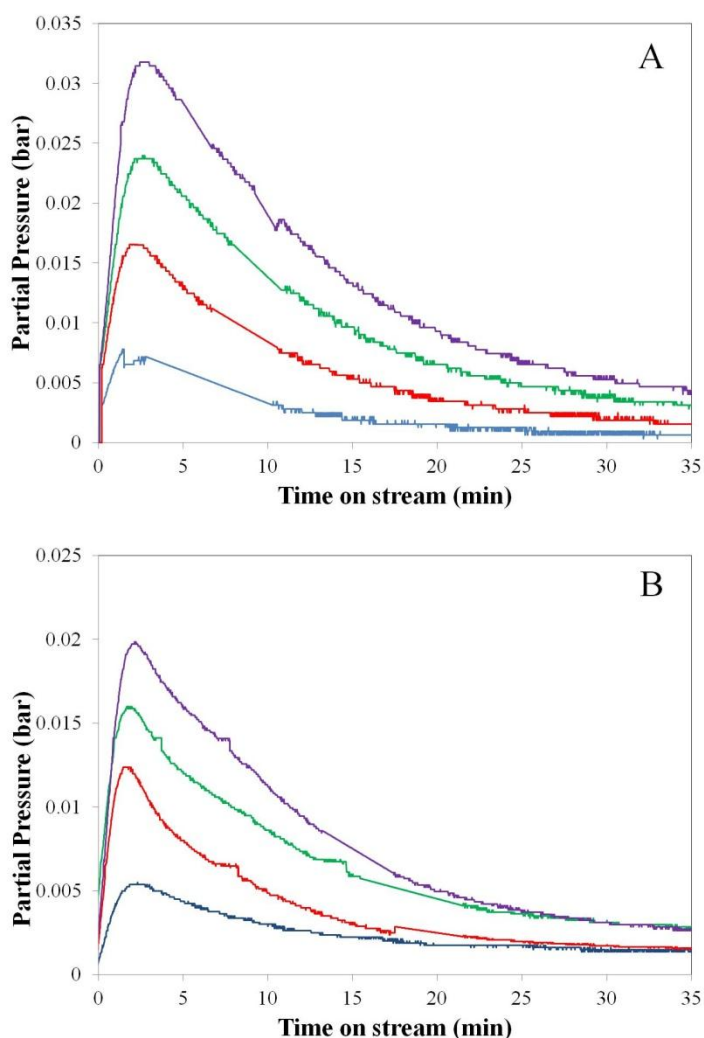
The carbon and oxygen mass balance over the catalyst bed was also checked during the start-up period. The carbon balance was calculated using Eq. (6.14) with the incorporation of an accumulation term which describes the loss of carbon from the feed. The oxygen balance is complicated by possible loss of oxygen from the catalyst itself and hence relied on the following assumptions:

- The Boudouard Reaction, which involves the disproportionation of two CO molecules into C and CO<sub>2</sub> was assumed to not occur under these conditions.
- The addition of oxygen to CO and/or H<sub>2</sub> to form CO<sub>2</sub> and/or H<sub>2</sub>O is therefore supplied from the catalyst itself. Hence, oxygen released from the catalyst is the sum of H<sub>2</sub>O and the extra oxygen in CO<sub>2</sub>.
- H<sub>2</sub>O and CO<sub>2</sub> released do not re-adsorb along the catalyst bed (this assumption will be discussed at a later point).

In Figure 7.7B, an analysis of normalised rates for carbon loss, CO<sub>2</sub> and H<sub>2</sub>O elution with time on stream reveal that all three measurements reach a maximum after approximately 2.5 min. Whilst the magnitude of carbon loss is only slightly higher than that of combined CO<sub>2</sub> and H<sub>2</sub>O elution (estimated, with 10% error, at 196 ± 13 μmol compared to 160 ± 15 μmol over 30 min), the pattern of rate decline for these measurements is very different following these maxima. This suggests that the process associated with carbon loss from the feed is different to that of CO<sub>2</sub> and H<sub>2</sub>O elution. The carbon loss observed under these conditions is lower than that during CO/CO<sub>2</sub>/H<sub>2</sub> start-up at the same temperature and pressure (361 ± 40 μmol).

From these initial observations, three key questions arise regarding, firstly, the origin of the eluted  $\text{CO}_2$  and  $\text{H}_2\text{O}$ , secondly, the manner in which carbon and oxygen adsorb onto the surface and finally, which catalyst transformations during the start-up period drive the progressive generation of methanol synthesis activity.

Figure 7.8 shows parallel difference test reactor outlet results for the start-up profile shown in Figure 7.7A. Figures 7.8A and 7.8B show an even trend with axial length along the catalyst bed for  $\text{CO}_2$  and  $\text{H}_2\text{O}$  production. Hence, the proportion of the two products does not change during initial operation at all points of the catalyst bed. This observation, also seen for a wider range of  $\text{CO}/\text{H}_2$  start-up profiles at temperatures between 453 and 493 K, suggests that  $\text{CO}_2$  and  $\text{H}_2\text{O}$  do not appear to re-adsorb along the catalyst bed following release.



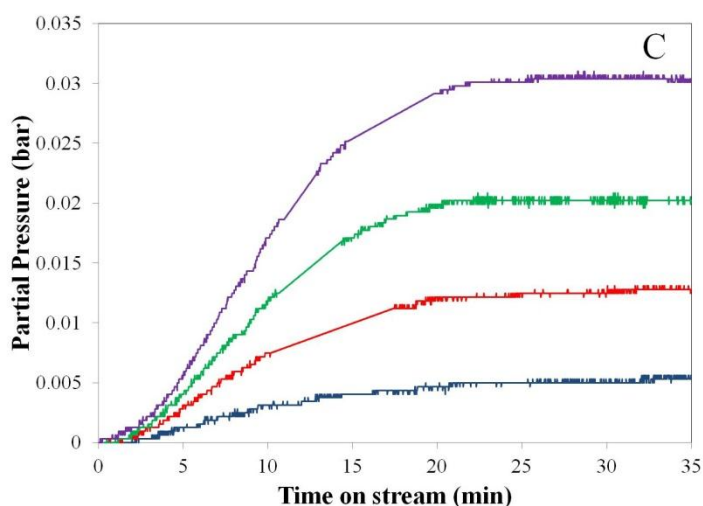


**Figure 7.8: Reactor outlet observations of A) CO<sub>2</sub>, B) H<sub>2</sub>O and C) CH<sub>3</sub>OH of (--) 125 mg, (--) 250 mg, (--) 375 mg and (--) 500 mg of Cu/ZnO/Al<sub>2</sub>O<sub>3</sub> catalyst upon feeding CO/H<sub>2</sub>/N<sub>2</sub> (3:67:30) at 7.5 L h<sup>-1</sup> (STP) at 25 bar, 473 K.**

The ratio of CO<sub>2</sub> to H<sub>2</sub>O eluted remains in the range of 1.4 – 1.6 throughout the 473 K start-up under 3% CO/H<sub>2</sub>. Using these ratios, this would set the RWGS equilibrium term,  $\beta_2^*$ , between 6.3 and 7.2; strongly in favour of the FWGS reaction. Hence the presence of WGS catalysis can be largely ruled out as a proportional shift towards CO<sub>2</sub> formation from H<sub>2</sub>O would be expected along the catalyst bed if this reaction was prevalent. For methanol production in Figure 7.8C, productivity increases along the catalyst bed ranging from 0.14  $\mu\text{mol s}^{-1} \text{g}^{-1}$  in the 1<sup>st</sup> sector to 0.28  $\mu\text{mol s}^{-1} \text{g}^{-1}$  in the 4<sup>th</sup> sector after 30 min operation.

Using 500 mg catalyst datasets for start-up in 3% CO/H<sub>2</sub> in the temperature range 453 – 493 K, an estimation of the energies associated with carbon loss, CO<sub>2</sub> and H<sub>2</sub>O formation can be made. To achieve this, three first order rate equations were devised:

$$r_{C_{loss}} = k_{C_{loss}} P_{CO} \theta_{v,C_{ads}} \quad (7.8)$$

$$r_{CO_2} = k_{CO_2} P_{CO} \theta_O \quad (7.9)$$

$$r_{H_2O} = k_{H_2O} P_{H_2} \theta_O \quad (7.10)$$

Hence, the  $r_{C_{loss}}$  (carbon loss rate,  $\mu\text{mol s}^{-1} \text{g}^{-1}$ ) and  $r_{CO_2}$  (CO<sub>2</sub> formation rate,  $\mu\text{mol s}^{-1} \text{g}^{-1}$ ) were assumed to be first order in CO and  $r_{H_2O}$  (H<sub>2</sub>O formation rate,  $\mu\text{mol s}^{-1} \text{g}^{-1}$ ) was assumed to be first order in H<sub>2</sub>. As all three processes are time dependent, they were assumed to relate to some surface site availability; namely vacant adsorption site for carbon loss ( $\theta_{v,C}$

*ads*) and an oxygenated site for CO<sub>2</sub> and H<sub>2</sub>O formation ( $\theta_O$ ). As the exact nature of these sites is unknown and cannot be quantified at this point, rate constants were estimated based on initial rates observed:

- For  $r_{C\ loss}$ , an  $E_a$  of  $47 \pm 3$  kJ mol<sup>-1</sup> was estimated. This energy was measured consistently for the first 6 min on stream ( $R^2 > 0.95$ ). Following this both  $E_a$  and  $R^2$  decreased in tandem.
- For  $r_{CO_2}$ , an  $E_a$  of  $63 \pm 2$  kJ mol<sup>-1</sup> was estimated. This energy was measured consistently for the first 3 min on stream ( $R^2 > 0.95$ ) before decreasing.
- For  $r_{H_2O}$ , an  $E_a$  of  $51 \pm 3$  kJ mol<sup>-1</sup> was estimated. This energy was measured consistently for the first 3 min on stream ( $R^2 > 0.95$ ) before decreasing.

Coupled with these  $E_a$  measurements, the cumulative oxygen lost from the catalyst in the form of CO<sub>2</sub> and H<sub>2</sub>O and the carbon species adsorbed onto the catalyst from the feed were calculated over the first 30 min operation under a variety of conditions. As Table 7.3 shows, the levels of both oxygen loss and carbon adsorption increase with start-up temperature. The levels of carbon adsorbed at temperatures 453 – 493 K are within the range of the as received copper metal surface area of the catalyst (32.4 m<sup>2</sup> g<sup>-1</sup>). The coverage of oxygen lost is considerably smaller than this and may relate to interfacial Cu-O-Zn or bulk Zn-O-Zn sites which are not reduced under initial reduction (2% H<sub>2</sub>/N<sub>2</sub>) conditions.

The values measured for a 250 mg bed at 473 K are similar to its 500 mg counterpart, suggesting there is no significant gradient of these effects along the catalyst bed. Increasing the concentration of CO to 10% v/v in the feed stream only produces a small increase in oxygen released from the catalyst but a doubling of the surface coverage of carbon species.

**Table 7.3: Calculated surface coverage of oxygen removed and carbon adsorbed onto a Cu/ZnO/Al<sub>2</sub>O<sub>3</sub> catalyst surface during the first 30 min operation under CO/H<sub>2</sub> (Conditions are 25 bar, 3% CO / 67% H<sub>2</sub> / N<sub>2</sub>, 500 mg catalyst unless otherwise stated).**

Reactor start-up temperature (K)	Oxygen lost from catalyst (total after 30 min on stream) assuming 10% error in measurements		Carbon species adsorbed on catalyst (total after 30 min on stream) assuming 10% error in measurements	
	Moles of oxygen lost ( $\mu\text{mol}$ )	Surface coverage <sup>1</sup> ( $\text{m}^2 \text{g}^{-1}$ )	Moles of carbon species adsorbed ( $\mu\text{mol}$ )	Surface coverage <sup>2</sup> ( $\text{m}^2 \text{g}^{-1}$ )
<b>453</b>	103 ± 5	2.2 ± 0.1	146 ± 15	10.8 ± 1.1
<b>463</b>	140 ± 9	3.1 ± 0.2	182 ± 18	13.5 ± 1.3
<b>473</b>	160 ± 14	3.5 ± 0.3	196 ± 13	14.6 ± 1.0
<b>483</b>	181 ± 18	4.0 ± 0.4	227 ± 20	16.8 ± 1.5
<b>493</b>	239 ± 46	5.2 ± 1.0	334 ± 55	24.8 ± 4.1
<b>473 (250 mg catalyst)</b>	72 ± 7	3.2 ± 0.3	85 ± 7	12.6 ± 1.8
<b>473 (10% CO / 67% H<sub>2</sub> / N<sub>2</sub>)</b>	193 ± 18	4.2 ± 0.4	474 ± 67	35.1 ± 3.0

1. Surface area of oxygen vacancies, using the assumption that one oxygen atom has a molecular diameter of 1.5 Å.
2. Surface area of carbon coverage assumed species to be CO-type molecules, with molecular diameter of 2.8 Å.

In Figure 7.9, it can be observed that whilst increased reaction temperatures lead to greater methanol outputs, a performance decline from ~10 – 15 min on stream is observed in the 483 and 493 K experiments. Hence, whilst it is tempting to link loss of oxygen from the catalyst and/or carbon species build up to methanol synthesis functionality of the catalyst, the

link may not necessarily be linear. Furthermore, the catalyst start-up under 10% CO in the feed at 473 K generates the highest carbon species surface population but does not have the highest methanol synthesis performance. The methanol synthesis productivity of this catalyst is however 66% higher than one exposed initially to 3% CO-based feeds at 473 K. Hence, some link may be afforded between CO partial pressure, surface carbon coverage and methanol synthesis activity.

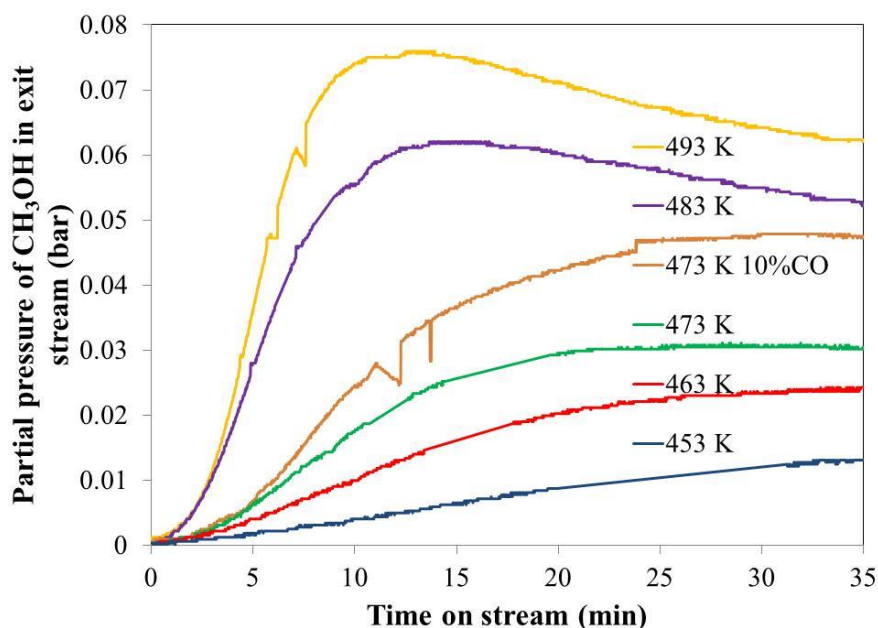


**Figure 7.9: Outlet methanol profiles for a 500 mg Cu/ZnO/Al<sub>2</sub>O<sub>3</sub> catalyst bed upon feeding CO/H<sub>2</sub>/N<sub>2</sub> (3:67:30) (unless stated) at 7.5 L h<sup>-1</sup> (STP) at 25 bar for 35 min**

The  $E_a$  value observed for  $r_{C,loss}$  is within range of literature values for CO adsorption on a reduced copper surface (Ovesen *et al.*, 1992; Waugh *et al.*, 1999). Similarly the  $E_a$  values observed for  $r_{CO_2}$  and  $r_{H_2O}$  are similar to the same previous literature models for CO oxidation from surface oxygen on copper and H<sub>2</sub>O desorption from a copper surface respectively. The initial catalyst surface before exposure of 3% CO/H<sub>2</sub> has been estimated to be one of fully reduced copper metal however which questions the origin for the oxygen in CO<sub>2</sub> and H<sub>2</sub>O.

Alternative arguments may relate to CO adsorption over a ZnO surface, which has been found in the range of 25 – 80 kJ mol<sup>-1</sup> (Sloczynski *et al.*, 1991) and 7 – 44 kJ mol<sup>-1</sup> (Giamello and Fubini, 1983). The large measured range on these measurements is ascribed to

the fact that CO is more likely to defect the surface, forming CO<sub>2</sub> and ZnO<sub>1-x</sub> than adsorb onto it. Furthermore, Bowker *et al.*, (1981) found that CO adsorption does not occur on a completely reduced ZnO surface.

It is therefore important to compare synergistic observations in Cu/ZnO systems to this work. As mentioned earlier, Frost (1988) linked the creation of defects in ZnO and their stabilisation by electron transfer from the neighbouring Cu metal leading to Cu<sup>δ+</sup>, suggesting these defects are the site for methanol synthesis under CO/H<sub>2</sub>. In the observations in Figure 7.9 of the current work, a parallel may be drawn here as increased oxygen loss from the catalyst could be linked to the creation of defects in ZnO and increasing methanol synthesis performance with temperature. The instabilities seen at higher temperatures may follow from Bowker *et al.*, (1981) suggesting that creating an overly defective ZnO structure may cause a loss in activity. It is possible that an optimised level of defects is needed in the ZnO structure to balance activity and stability.

### 7.3.1.2 Steady state apparent kinetics

Obtaining useful steady state measurements for kinetic modelling purposes under CO/H<sub>2</sub> conditions was found to be more difficult than under CO/CO<sub>2</sub>/H<sub>2</sub>. Initially, a Cu/ZnO/Al<sub>2</sub>O<sub>3</sub> catalyst which was started up in 3% CO/H<sub>2</sub> at 473 K was equilibrated over a 10 h period before temperature step change testing. Upon testing the catalyst under higher temperatures however, increased elution of CO<sub>2</sub> and H<sub>2</sub>O was observed and the catalyst suffered noticeable losses in methanol synthesis productivity, evidenced clearly when returned to the reference 473 K temperature. This finding echoes the conclusions from Bos *et al.*, (1989), which noted the impact of CO<sub>2</sub> and H<sub>2</sub>O elution on obtaining reliable steady state kinetics. Linking with current analysis in Section 7.3.1.1, this again shows that higher temperatures result in an increased oxygen loss from the catalyst, resulting in a more defective structure.

Steady state data were eventually obtained using a catalyst that had been conditioned at 493 K for 20 h on stream. Apparent  $E_a$  values for methanol formation were calculated for a 125 and 500 mg catalyst bed and are compared in Figure 7.10 with counterpart values from the conditions tested in Chapter 6 using CO/CO<sub>2</sub>/H<sub>2</sub> mixtures at 453 – 493 K and 25 bar. A striking difference is seen between 3% CO/H<sub>2</sub> and the other CO<sub>2</sub>-containing feeds, with the former displaying much lower activation energies of 37 and 44 kJ mol<sup>-1</sup> for the 125 and 500

mg beds respectively. This may suggest a different reaction pathway or active site is responsible for methanol synthesis activity under CO/H<sub>2</sub> conditions.

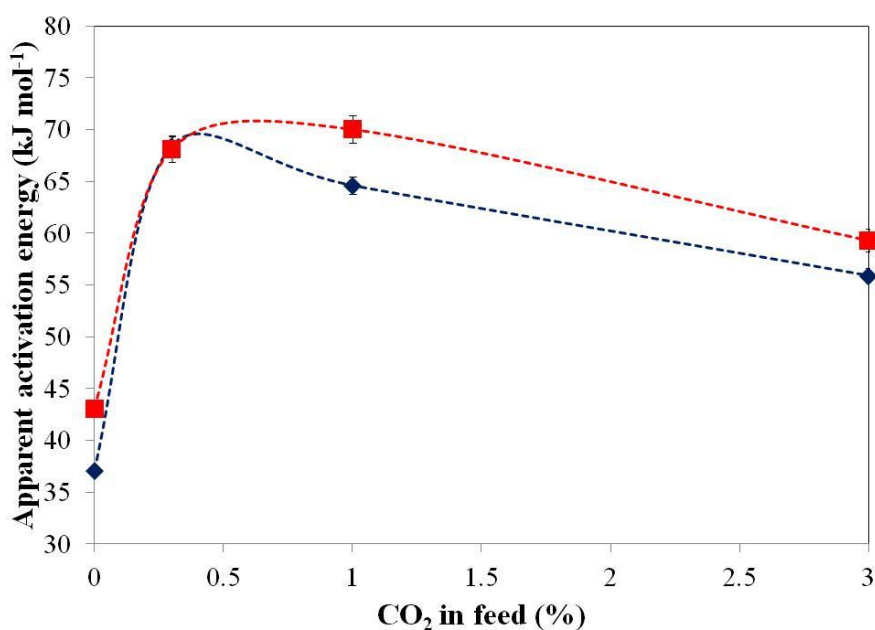


**Figure 7.10: Apparent  $E_a$  values for methanol formation across 125 and 500 mg Cu/ZnO/Al<sub>2</sub>O<sub>3</sub> catalyst beds under 3% CO/ X% CO<sub>2</sub>/ 67% H<sub>2</sub>/ 30-X% N<sub>2</sub> at 7.5 L h<sup>-1</sup> (STP) at 25 bar in the temperature range 453 – 493 K. (◆) and (■) denote 125 and 500 mg catalyst beds respectively. N.B.: R<sup>2</sup> for all Arrhenius plots was > 0.99.**

The gradual  $E_a$  changes in the feeds containing 0.3 – 3% CO<sub>2</sub> can be explained by shifts in the activity of reaction pathways  $r_1$  and  $r_4$  (which were proposed in the steady state model for CO/CO<sub>2</sub>/H<sub>2</sub> in Chapter 6). The net energy barrier for  $r_4$  was estimated to be higher than  $r_1$ ; as a result higher apparent  $E_a$  values are seen in conditions where  $r_4$  dominates over  $r_1$  (i.e. high P<sub>CO</sub>/P<sub>CO<sub>2</sub></sub> ratios and back sectors of the catalyst bed). Meanwhile, the apparent  $E_a$  for 3% CO/H<sub>2</sub> appears to represent a dramatic shift in the key energy barrier to methanol formation. Two possibilities for this value are thus:

- CO adsorption on a Cu or ZnO surface as earlier discussed. The apparent  $E_a$  values measured in this section are within range of literature values (Giamello and Fubini, 1983, Sloczynski *et al.*, 1991).
- Dissociative adsorption of hydrogen over a reduced copper surface has been measured in the range of 42 – 50 kJ mol<sup>-1</sup> over a variety of copper-based on ZnO and/or Al<sub>2</sub>O<sub>3</sub>

catalysts (Wilmer *et al.*, 2003). In this work, the hydrogen adsorption capacity of Cu/ZnO/Al<sub>2</sub>O<sub>3</sub> was shown to decrease approximately five-fold following an extended reductive pre-treatment in CO/He. Methanol formation levels under 3% CO/H<sub>2</sub> are typically 3 – 5 times lower than that under CO/CO<sub>2</sub>/H<sub>2</sub> in the current work providing support to the argument that availability of surface hydrogen may be rate limiting.

### **7.3.2 Dynamic analysis under CO/CO<sub>2</sub>/H<sub>2</sub> conditions following CO/H<sub>2</sub> pre-treatments over a Cu/ZnO/Al<sub>2</sub>O<sub>3</sub> catalyst**

#### **7.3.2.1 Initial parallel difference test analysis**

The effect of a CO/H<sub>2</sub> pre-treatment on a 500 mg Cu/ZnO/Al<sub>2</sub>O<sub>3</sub> catalyst bed during subsequent exposure to CO/CO<sub>2</sub>/H<sub>2</sub> conditions is explored in Figure 7.11. Both the CO/H<sub>2</sub> and CO/CO<sub>2</sub>/H<sub>2</sub> based gases contained 3% CO and 67% H<sub>2</sub> and so the start-up profile in Figure 7.11 is, in effect, showing the impact of doping 3% CO<sub>2</sub> into the feed stream.

In Figure 7.11, the CO/H<sub>2</sub> pre-treated catalyst shows a distinct transient methanol outlet profile with time on stream, passing through a maximum level at ~2.5 min before declining towards a steady state level. This profile observed is consistent with observations made in Vesborg *et al.*, (2009) using a similar methodology. A comparison is made with the methanol outlet profile observed during a CO/CO<sub>2</sub>/H<sub>2</sub> start-up following exposure to a H<sub>2</sub>/N<sub>2</sub> atmosphere, as analysed in Chapter 6, where a very different approach to steady state is seen. Over 40 min on stream, the CO/H<sub>2</sub> pre-treated 500 mg catalyst produces  $412 \pm 126$   $\mu\text{mol}$  more methanol than the H<sub>2</sub>/N<sub>2</sub> pre-treated one. For the rest of this study this difference will be referred to as ‘additional methanol’.

Whilst similar in the manner of approach to steady state, H<sub>2</sub>O production and CO<sub>2</sub> consumption over the CO/H<sub>2</sub> pre-treated catalyst is greater than over the non pre-treated one over the first 40 min on stream. This amounts to  $57 \pm 21$   $\mu\text{mol}$  more H<sub>2</sub>O produced and  $167 \pm 43$   $\mu\text{mol}$  more CO<sub>2</sub> consumed, respectively. Interestingly, the extra CO<sub>2</sub> uptake is very close in value to the molar loss of oxygen from the catalyst under CO/H<sub>2</sub> over a 30 min period ( $160 \pm 15$   $\mu\text{mol}$ ) hence it is possible that both effects could be linked.

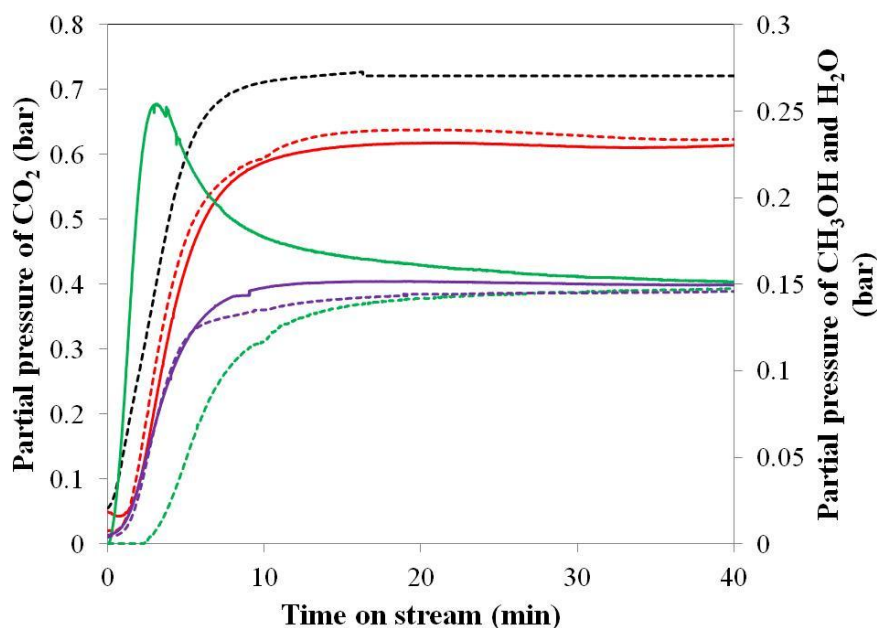


**Figure 7.11: Start-up comparison of 500 mg Cu/ZnO/Al<sub>2</sub>O<sub>3</sub> catalyst pre-treated for 6 h at 473 K, 25 bar, 7.5 L h<sup>-1</sup> in A) CO/H<sub>2</sub>/N<sub>2</sub>: 3/67/30 (solid lines) and B) H<sub>2</sub>/N<sub>2</sub> : 2/98 (dashed lines). Start-up conditions were 473 K, 25 bar, 7.5 L h<sup>-1</sup> using feed gas (CO/CO<sub>2</sub>/H<sub>2</sub>/N<sub>2</sub>: 3/3/67/27). (---) denotes inlet CO<sub>2</sub>, (---) outlet CO<sub>2</sub>, (---) outlet CH<sub>3</sub>OH and (---) outlet H<sub>2</sub>O.**

Figure 7.12 examines the evolution of the additional CH<sub>3</sub>OH or H<sub>2</sub>O productivity and CO<sub>2</sub> consumption with time on stream. Using a normalised scale, it can be seen that the evolution patterns for both values are concomitant over the first 10 min however CO<sub>2</sub> consumption subsequently follows a different pattern. Examination of additional water produced over the CO/H<sub>2</sub> pre-treated catalyst appears to be linked to this.

Similar start-up profiles were analysed over 125, 250 and 375 mg catalyst beds following a CO/H<sub>2</sub> pre-treatment. This enabled a four sector profile of transient reactor performance to be obtained over the full 500 mg catalyst bed. Figure 7.13A shows a breakdown of sector methanol productivities during the first 20 min on stream following exposure to CO/CO<sub>2</sub>/H<sub>2</sub> based gas. It can be seen that whilst the 1<sup>st</sup> sector quickly reaches an apparent plateau level of productivity, sectors 2 – 4 all progress through a transient maxima with time on stream before declining towards a steady state level.

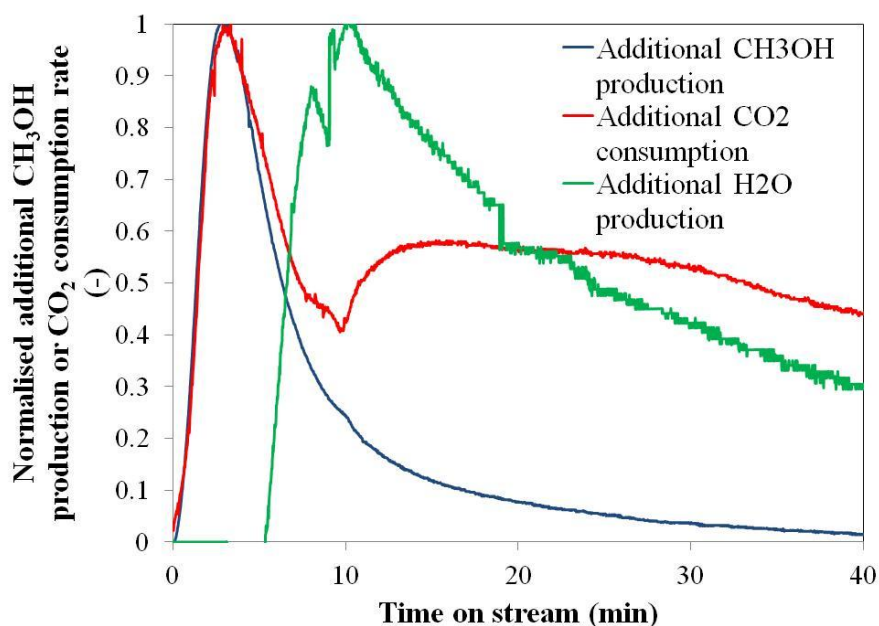


**Figure 7.12: Comparison of normalised ‘additional’ CH<sub>3</sub>OH and H<sub>2</sub>O production and CO<sub>2</sub> consumption rates over a CO/H<sub>2</sub> pre-treated 500 mg Cu/ZnO/Al<sub>2</sub>O<sub>3</sub> catalyst in comparison to a H<sub>2</sub>/N<sub>2</sub> pre-treatment at 473 K, 25 bar, 7.5 L h<sup>-1</sup> using feed gas (CO/CO<sub>2</sub>/H<sub>2</sub>/N<sub>2</sub>: 3/3/67/27). Maxima occur 1.82, 0.10 and 0.66 μmol s<sup>-1</sup> g<sup>-1</sup> for additional CH<sub>3</sub>OH, H<sub>2</sub>O production and CO<sub>2</sub> consumption rates respectively.**

To gain further understanding of these sector profiles, the following simple rate assumption was applied to methanol productivity during start-up to measure an apparent rate constant for each sector. This assumption was based on the steady state kinetic model developed for CO/CO<sub>2</sub>/H<sub>2</sub> conditions in Chapter 6:

$$r_{MeOH} = k_{MeOH} P_{CO_2} (1 - \beta_1^*) \quad (7.11)$$

Where  $r_{MeOH}$  is the observed rate (μmol s<sup>-1</sup> g<sup>-1</sup>) and  $k_{MeOH}$  is the apparent first order rate constant (s<sup>-1</sup>) of methanol synthesis respectively and  $\beta_1^*$  is the equilibrium term for methanol synthesis from a CO<sub>2</sub> source (see Eq. (6.25)). Application of Eq. (7.11) to show evolution of  $k_{MeOH}$  with time on stream is shown in Figure 7.13B and reveals that all four sectors pass through a transient maximum and decline similarly. The peak of the transient maxima in Figure 7.13A is greatest for the 4<sup>th</sup> sector and smallest for the 1<sup>st</sup>. Hence whilst the simple first order assumption of Eq. (7.11) is effective, it does not fully describe the evolution of  $k_{MeOH}$  with time on stream across the entire catalyst bed. Whilst experimental error may

influence these differences (taken at 10% for parallel difference test analysis in this chapter), other mechanistic effects are feasible:

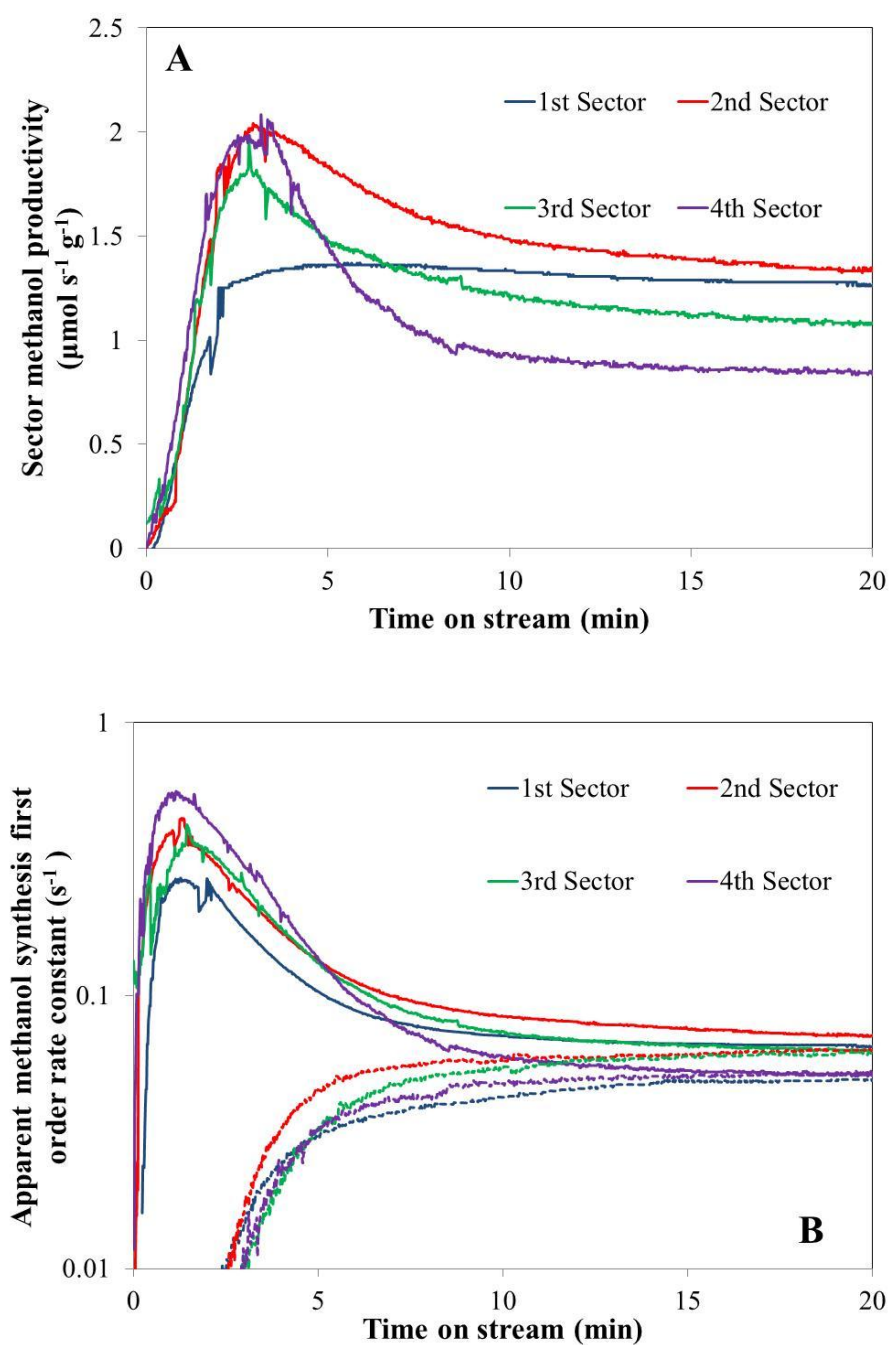


**Figure 7.13: Time on stream sector evolution of A) Methanol productivity, B) Apparent methanol synthesis first order rate constant of a Cu/ZnO/Al<sub>2</sub>O<sub>3</sub> catalyst (500 mg total bed) during start-up under (CO/CO<sub>2</sub>/H<sub>2</sub>/N<sub>2</sub>: 3/3/67/27) following a 6 h pre-treatment under (CO/H<sub>2</sub>/N<sub>2</sub>: 3/67/30) (solid lines) and (H<sub>2</sub>/N<sub>2</sub>: 2/98) (dotted lines) both at 473 K, 25 bar, 7.5 L h<sup>-1</sup>.**

- Increased carbon species surface population along the catalyst bed, enabling an increased titration of species. Table 7.3 suggested the carbon species population increased slightly along a catalyst bed pre-treated under CO/H<sub>2</sub>, however this difference could not be declared with confidence due to error bars.
- A kinetic effect relating to increased activity of the lumped forwards water gas shift (FWGS) and methanol synthesis reaction with increased axial distance along the catalyst bed. Dynamic changes in CO consumption were not seen during this transient maximum however.

In Figure 7.13B, it is clear that the pre-treatment of a Cu/ZnO/Al<sub>2</sub>O<sub>3</sub> catalyst under CO/H<sub>2</sub> produces a very different  $k_{MeOH}$  profile to a catalyst prior treated under H<sub>2</sub>/N<sub>2</sub>. In the latter, activity evolution of all sectors is initially delayed (as shown in Chapter 6) and all sectors show a similar trend in reaching steady state.

Analysis of changes in carbon and oxygen species on the catalyst surface was also carried out over a CO/H<sub>2</sub> pre-treated Cu/ZnO/Al<sub>2</sub>O<sub>3</sub> catalyst over the first 20 min of exposure to CO/CO<sub>2</sub>/H<sub>2</sub>/N<sub>2</sub>. As Figure 7.14 shows, the front and back 250 mg sectors of the catalyst bed develop surface populations of carbon and oxygen differently. The front 250 mg gains an increased amount of both species with time, during which the O/C ratio of these species remains above 2. This high ratio suggests that surface adsorption of CO<sub>2</sub> is not the sole mechanism at hand over this sector and further oxygen is added to the catalyst surface. This further suggests that the oxygen lost from the catalyst structure under CO/H<sub>2</sub> is replaced when CO<sub>2</sub> is added to the feed.

In Figure 7.14, the back 250 mg shows a maximum in cumulative oxygen and carbon surface populations at ~3 min before moving towards a net decline in both populations after 20 min on stream. The maximum coincides with the maximum in methanol productivity seen across the full catalyst bed.

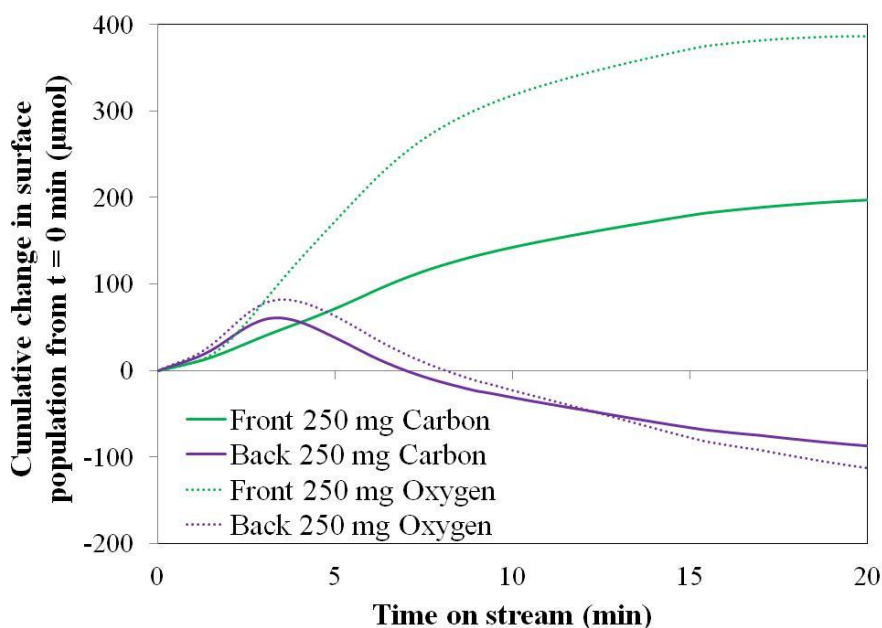


**Figure 7.14: Measured changes in molar surface population of carbon and oxygen species during start-up under (CO/CO<sub>2</sub>/H<sub>2</sub>/N<sub>2</sub>: 3/3/67/27) following a 6 h pre-treatment under (CO/H<sub>2</sub>/N<sub>2</sub>: 3/67/30) both at 473 K, 25 bar, 7.5 L h<sup>-1</sup>.**

In the earlier analysis of a Cu/ZnO/Al<sub>2</sub>O<sub>3</sub> start-up under CO/H<sub>2</sub> conditions at 473 K in Section 7.3.1.1, the front and back 250 mg of the catalyst bed were found to contain  $85 \pm 14$  and  $111 \pm 14$   $\mu\text{mol}$  of carbon and oxygen species respectively after 30 min exposure. Whilst these values are similar within error, the change observed in Figure 7.14 suggests a large skew towards high surface populations at the front of the catalyst bed and a smaller one at the back. In Chapter 6, this was seen for start-up of the same catalyst following H<sub>2</sub>/N<sub>2</sub> exposure under the same conditions ascribed in Figure 7.14; the front and back 250 mg contained  $260 \pm 21$  and  $100 \pm 36$   $\mu\text{mol}$  of carbon species respectively. Whilst the mass balance cannot be quantitatively closed between the two pre-treatments in this case (the former catalyst was conditioned in CO/H<sub>2</sub> for 6 h but reliable species analysis was only possible over the first 30 min), the trend in surface coverage obtained when approaching steady state operation under CO/CO<sub>2</sub>/H<sub>2</sub> appears to be similar for both prior treatments. This suggests that the CO/H<sub>2</sub> pre-treatment employed does not induce any irreversible changes to the catalyst that may change its performance under CO/CO<sub>2</sub>/H<sub>2</sub>. This is supported by similar methanol productivities for both CO/H<sub>2</sub> and H<sub>2</sub>/N<sub>2</sub> pre-treated catalysts after 40 min on stream in Figure 7.11, agreeing with Vesborg *et al.*, (2009).

### 7.3.2.2 Reversibility and stability

To support findings in Section 7.3.2.1, a Cu/ZnO/Al<sub>2</sub>O<sub>3</sub> catalyst was exposed to successive CO/H<sub>2</sub> → CO/CO<sub>2</sub>/H<sub>2</sub> exposure cycles. Figure 7.15A and 7.15B, show parallel difference test results for outlet methanol and water partial pressures for all 4 catalyst beds employed with successive pre-treatments.

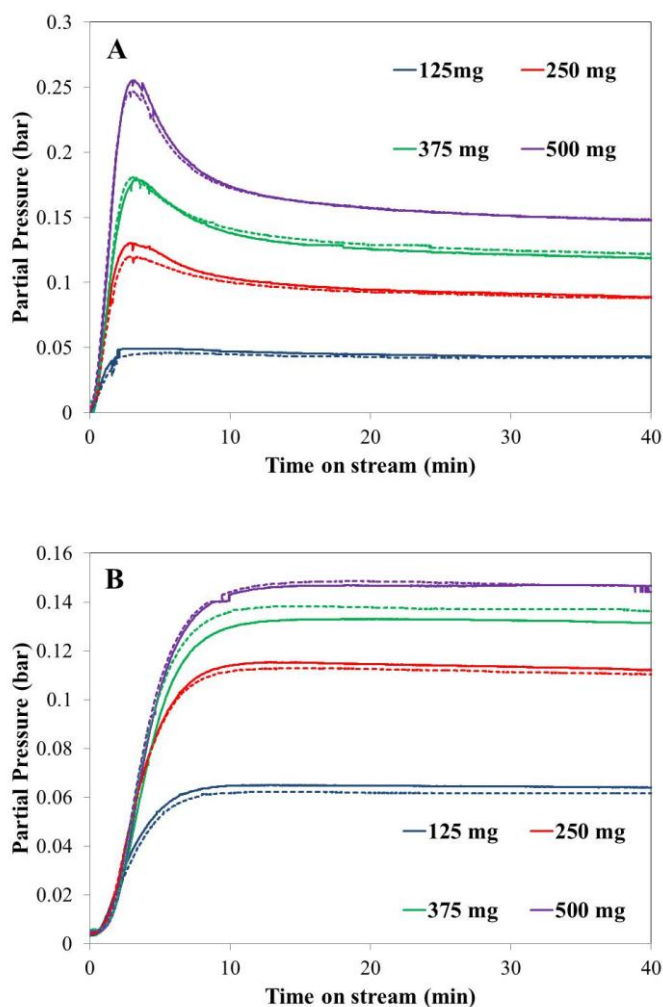


**Figure 7.15: A) Outlet CH<sub>3</sub>OH and B) Outlet H<sub>2</sub>O partial pressures of four Cu/ZnO/Al<sub>2</sub>O<sub>3</sub> catalyst beds of different masses during start-up under (CO/CO<sub>2</sub>/H<sub>2</sub>/N<sub>2</sub>: 3/3/67/27) following a 6 h pre-treatment under (CO/H<sub>2</sub>/N<sub>2</sub>: 3/67/30) both at 473 K, 25 bar, 7.5 L h<sup>-1</sup>. Solid lines denote results following first pre-treatment and dotted lines results following a second successive pre-treatment in the same experiment.**

The transient effects seen during initial exposure of a CO/H<sub>2</sub> pre-treated catalyst to CO/CO<sub>2</sub>/H<sub>2</sub> are almost entirely reproduced following a successive CO/H<sub>2</sub> pre-treatment. This was again shown on further repeat cycles. Similarly, transient performance profiles of the

same catalyst under CO/H<sub>2</sub> conditions were also found to be almost entirely reproducible over successive runs on the same sample. This suggests that the catalyst state developed under CO/CO<sub>2</sub>/H<sub>2</sub> involves the full reinstatement of the oxygen lost from the catalyst under the prior CO/H<sub>2</sub> treatment.

Whilst early stages (40 min on stream or less) of catalyst behaviour under CO/CO<sub>2</sub>/H<sub>2</sub> have been a key focus in this section it is critical to assess the impact that either a CO/H<sub>2</sub> or H<sub>2</sub>/N<sub>2</sub> pre-treatment has on the longer term performance of a Cu/ZnO/Al<sub>2</sub>O<sub>3</sub> catalyst. Figure 7.16 examines the performance of 125 mg of catalyst with 30 h on stream under CO/CO<sub>2</sub>/H<sub>2</sub>. The results show that outlet partial pressures of methanol and water are almost the same after 30 h; hence neither pre-treatment has a discernible long term effect on the catalyst operating state.

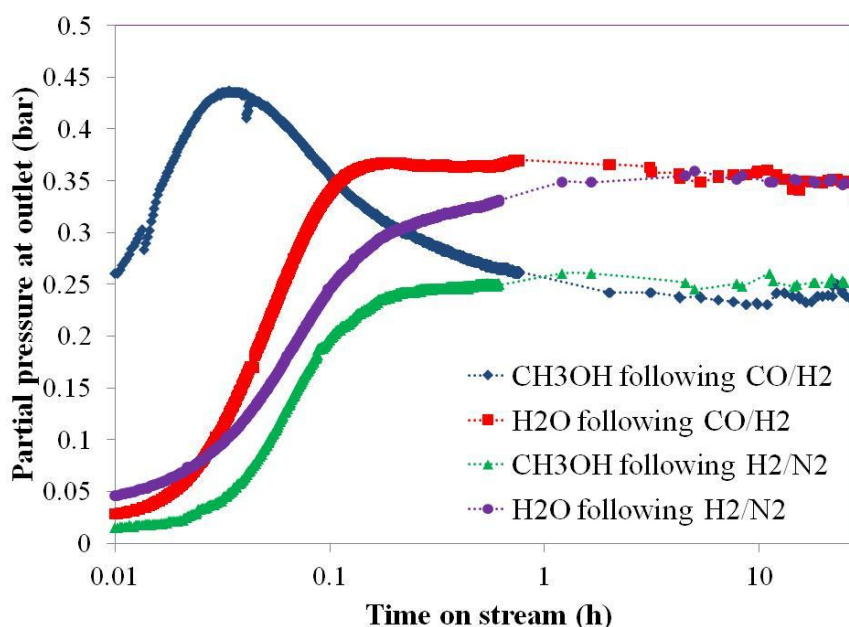


**Figure 7.16: Outlet CH<sub>3</sub>OH and H<sub>2</sub>O partial pressures at the reactor outlets of a 125 mg Cu/ZnO/Al<sub>2</sub>O<sub>3</sub> catalyst bed over 30 h on stream following a 6 h pre-treatment under (CO/H<sub>2</sub>/N<sub>2</sub>: 3/67/30) or (H<sub>2</sub>/N<sub>2</sub>: 2/98). Reaction conditions were (CO/CO<sub>2</sub>/H<sub>2</sub>/N<sub>2</sub>: 3/3/67/27) at 473 K, 25 bar, 7.5 L h<sup>-1</sup>. N.B.: Time on stream values on a log scale.**

### 7.3.2.3 Impact of pre-treatment temperature

To further understand the impact of pre-treatment conditions on the state of a Cu/ZnO/Al<sub>2</sub>O<sub>3</sub> catalyst, seven different CO/H<sub>2</sub>-based pre-treatments, largely varying in

temperature, were carried out on 500 mg of catalyst in separate experiments and subsequent behaviour under CO/CO<sub>2</sub>/H<sub>2</sub> observed, as shown in Figure 7.17:

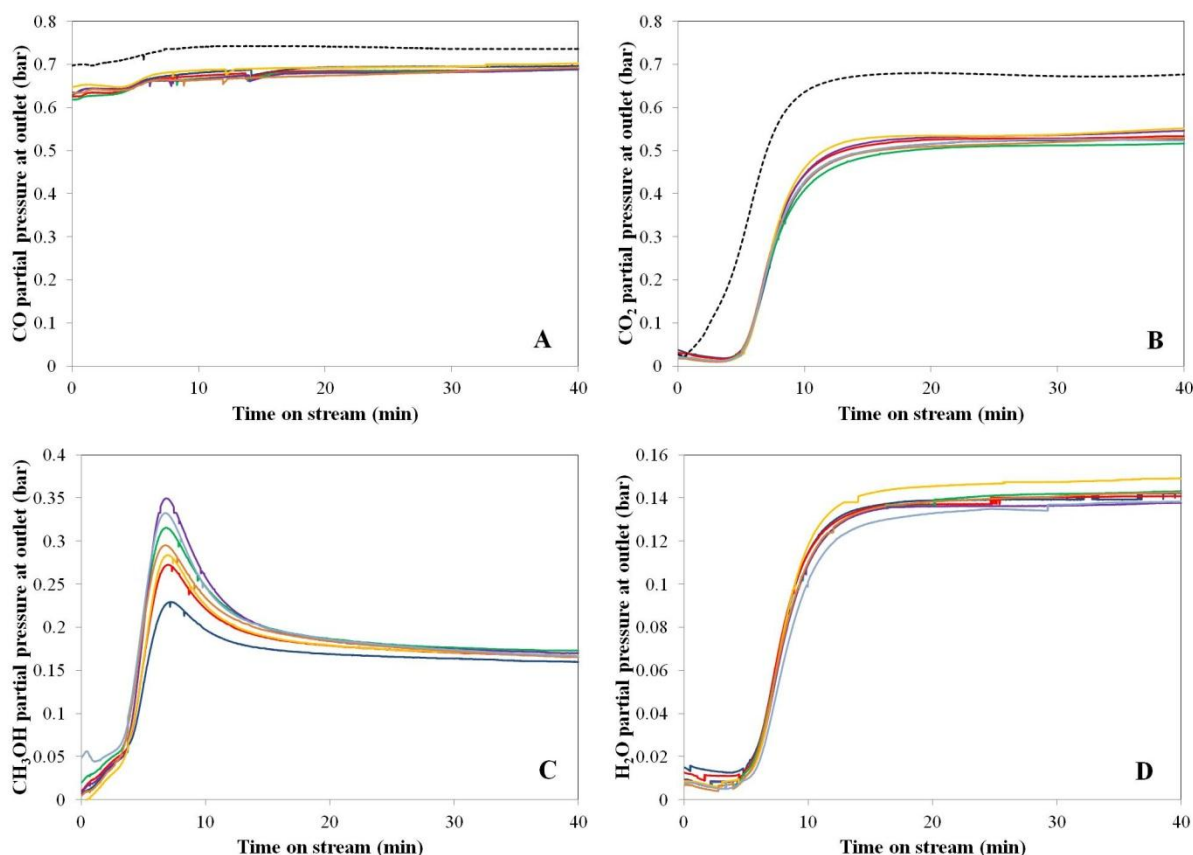


**Figure 7.17: Partial pressure outlet responses over a 500 mg Cu/ZnO/Al<sub>2</sub>O<sub>3</sub> catalyst bed for A) CO, B) CO<sub>2</sub>, C) CH<sub>3</sub>OH, D) H<sub>2</sub>O with time on stream under (CO/CO<sub>2</sub>/H<sub>2</sub>/N<sub>2</sub>: 3/3/67/27) at 473 K, 25 bar, 7.5 L h<sup>-1</sup> following 30 min pre-treatments using (CO/H<sub>2</sub>/N<sub>2</sub>: 3/67/30) at (—) 453 K, (—) 463 K, (—) 473 K, (—) 483 K, (—) 493 K, (—) 503 K and (CO/H<sub>2</sub>/N<sub>2</sub>: 10/67/23) at (—) 473 K at 25 bar, 7.5 L h<sup>-1</sup>. (---) denotes CO or CO<sub>2</sub> reactor inlet partial pressures.**

Figure 7.17A – 7.17D shows the CO, CO<sub>2</sub>, CH<sub>3</sub>OH and H<sub>2</sub>O responses in these experiments respectively. In Figure 7.17A, CO consumption across the 500 mg catalyst bed is the same regardless of pre-treatment conditions and changes very little with time on stream. In Figure 7.17B, the CO<sub>2</sub> evolution curves all follow a similar pattern with time on stream. Small differences are seen based on different pre-treatment conditions although these observations appear to relate to no distinct trend.

In Figure 7.17C, distinct differences are seen in the production of methanol with time on stream. All experiments, regardless of pre-treatment condition, show a maximum in methanol evolution at the same time however all maxima vary in magnitude. Methanol maxima increase with temperature between 453 and 483 K but drop at 493 and 503 K. Meanwhile, water production in Figure 7.17D with time on stream is largely the same for all pre-treated catalysts. Hence, transient methanol production appears to be the key variable affected by pre-treatments in CO/H<sub>2</sub> at different temperatures.

Figure 7.18 compares the extent of oxygen loss from the catalyst with subsequent additional methanol produced under CO/CO<sub>2</sub>/H<sub>2</sub> (in comparison to start-up of a H<sub>2</sub>/N<sub>2</sub> pre-treated catalyst) as a function of CO/H<sub>2</sub> pre-treatment temperature. The trend seen in the additional methanol plot draws strong parallels with the TPD experiments carried out in Vanden Bussche and Froment, (1994). The greatest methanol maxima observed in the current study at 483 K coincides with a formate decomposition maxima (yielding CO and H<sub>2</sub>) in this study (See Figure 7.5). This suggests that the transient methanol profile observed may be linked to hydrogenation of formates at a reduced Cu-Zn interface, upon the introduction of CO<sub>2</sub>, by the following reaction route:

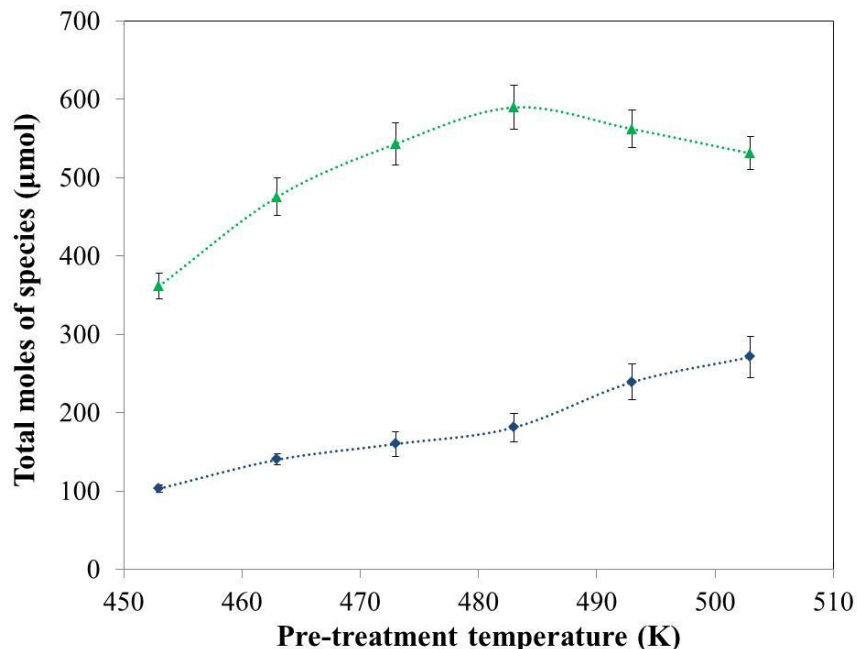
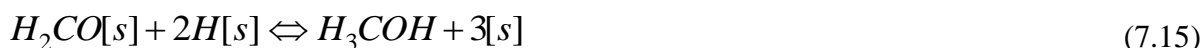
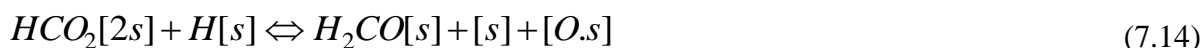


**Figure 7.18: Comparison of total oxygen lost from catalyst during pre-treatments in (CO/H<sub>2</sub>/N<sub>2</sub>: 3/67/30) at different temperatures for 30 min (◆) with subsequent ‘additional methanol’ produced (▲) during the first 30 min operation under (CO/CO<sub>2</sub>/H<sub>2</sub>/N<sub>2</sub>: 3/3/67/27) at 473 K, 25 bar, 7.5 L h<sup>-1</sup> over 500 mg Cu/ZnO/Al<sub>2</sub>O<sub>3</sub>.**



Where [s] and [O.s] are vacant and oxygenated Cu-Zn interfacial sites. It is noted in Eqs. (7.12-15) that one [O.s] site is needed to initiate this reaction whilst two [O.s] sites are subsequently produced. This constitutes a net increase in one [O.s] site which can be linked to oxidation of interfacial Cu-Zn vacancies which are reduced under CO/H<sub>2</sub>. This would also explain the initial lack of water production in contrast to methanol production as subsequent reduction of oxidised Cu-Zn interfacial sites to form water would be highly unfavourable in oxidising CO/CO<sub>2</sub>/H<sub>2</sub> conditions (Bowker *et al.*, 1981; Ponec, 1991; Ponec, 1992):



In keeping with the findings in Vanden Bussche and Froment, (1994), the trend for transient methanol maximum with temperature is seen to follow that of increased oxygen loss from the catalyst, up to 483 K. Above this temperature however, additional methanol production declines although extent of catalyst oxygen loss continues to increase with temperature. Furthermore, the total additional methanol produced is much greater than the amount of missing oxygen in the catalyst. This suggests that whilst the Cu-Zn vacancy oxidation mechanism shown in Eq. (7.12-15) may be prevalent, there are simply not enough vacant sites to equate to the total additional methanol formed.

The disparity in additional methanol and oxygen vacancies in the catalyst suggests that CO/H<sub>2</sub> pre-treatments at different temperatures may also impact on other active sites on the catalyst surface. A prime candidate here may be the active site at Cu-Cu surfaces, discussed by many to be the dominant site for methanol synthesis under CO/CO<sub>2</sub>/H<sub>2</sub> conditions. Previous literature has discussed the impact of catalyst reduction potential on the copper surface (Ovesen *et al.*, 1997; Vesborg *et al.*, 1997). Highly reducing (CO and H<sub>2</sub>) dominated feeds have been suggested to increase copper surface area via a surface wetting mechanism by reduction of Cu-[O]-Zn interfacial sites. This in turn may play a role in the

large additional methanol productivity observed during the first 30 min on stream under CO/CO<sub>2</sub>/H<sub>2</sub>.

The reduction potential argument is however not satisfactory in describing why additional methanol productivity is not completely linear with pre-treatment temperature. Whilst some works on reduction potential have suggested that over-reduction can lead to irreversible Cu-Zn alloying or brass formation (Ovesen *et al.*, 1997; Grunwaldt *et al.*, 2001), this is countered by the observations of complete reversibility of pre-treatment effects in Section 7.3.2.2. It is therefore worthwhile to consider the mechanism for methanol formation at a Cu-Zn interface; the initiation step in Eq. (7.12) requires both one oxidised and one reduced Cu-Zn interfacial site. The generation of too many reduced, [s] sites in comparison to oxidised, [O.s] sites may have a negative impact on the overall reactivity of the pre-treated catalyst via this pathway. This is logical as a balance of [O.s] and [s] may be required to initiate the formation of carbonates at these interfaces, in a similar manner to the balance required at Cu-Cu interfaces, which was discussed for the CO/CO<sub>2</sub>/H<sub>2</sub> start-up of a H<sub>2</sub>/N<sub>2</sub> pre-treated catalyst in Chapter 6.

Returning to earlier assessments of carbon and oxygen coverage of the Cu/ZnO/Al<sub>2</sub>O<sub>3</sub> surface under both CO/H<sub>2</sub> and CO/CO<sub>2</sub>/H<sub>2</sub> conditions, a complete assessment is made in Table 7.4. As found in Section 7.3.1, coverage of carbon and oxygen (from adsorbed CO) and formation of catalyst oxygen vacancies were found to increase with temperature in the 453 – 493 K range for CO/H<sub>2</sub> pre-treatments over 30 min. Subsequently, net adsorbed carbon and oxygen was calculated over the same pre-treated catalysts when exposed for 30 min to CO/CO<sub>2</sub>/H<sub>2</sub> at 473 K and added to the surface populations generated during the pre-treatments. After this time, a carbon and oxygen balance of 100 ± 1 % was obtained in all cases. As Table 7.4 shows, the total carbon and oxygen adsorbed for catalysts pre-treated under CO/H<sub>2</sub> at different temperatures are mostly within 10% experimental error range of that found on a catalyst pre-treated in H<sub>2</sub>/N<sub>2</sub> and exposed to CO/CO<sub>2</sub>/H<sub>2</sub> at 473 K.

**Table 7.4: Carbon and oxygen surface population balance evaluation over 500 mg Cu/ZnO/Al<sub>2</sub>O<sub>3</sub> during CO/H<sub>2</sub>/N<sub>2</sub> pre-treatment and subsequent CO/CO<sub>2</sub>/H<sub>2</sub>/N<sub>2</sub> exposure step. A comparison is made with the same catalyst, pre-treated in H<sub>2</sub>/N<sub>2</sub> and exposed to CO/CO<sub>2</sub>/H<sub>2</sub>/N<sub>2</sub> at 473 K. N.B.: All error bars (including accumulated errors) are made assuming 10% error in measurements**

Temperature during CO/H <sub>2</sub> /N <sub>2</sub> conditions (K)	Species adsorbed and/or oxygen lost on 500 mg catalyst surface following 30 min under CO/H <sub>2</sub> /N <sub>2</sub> : 3/67/30 (μmol)	
	Total carbon species adsorbed	Oxygen lost from catalyst as CO <sub>2</sub> or H <sub>2</sub> O
453	146 ± 15	103 ± 5
463	182 ± 18	140 ± 7
473	196 ± 14	160 ± 16
483	227 ± 20	181 ± 18
493	334 ± 34	239 ± 23
Treatment conditions prior to CO/CO <sub>2</sub> /H <sub>2</sub> /N <sub>2</sub> exposure	Species adsorbed on 500 mg catalyst surface following subsequent 30 min exposure under CO/CO <sub>2</sub> /H <sub>2</sub> /N <sub>2</sub> : 3/3/67/27 at 473 K (μmol)	
	Total carbon adsorbed	Total oxygen adsorbed
453 K (CO/H <sub>2</sub> /N <sub>2</sub> )	386 ± 39	629 ± 78
463 K (CO/H <sub>2</sub> /N <sub>2</sub> )	338 ± 34	533 ± 74
473 K (CO/H <sub>2</sub> /N <sub>2</sub> )	313 ± 26	508 ± 77
483 K (CO/H <sub>2</sub> /N <sub>2</sub> )	309 ± 28	481 ± 81
493 K (CO/H <sub>2</sub> /N <sub>2</sub> )	471 ± 48	581 ± 106
473 K (H <sub>2</sub> /N <sub>2</sub> )	(361 ± 40)	(498 ± 49)

The overall similarity of the final surface carbon and oxygen species inventories for the CO/H<sub>2</sub> pre-treated catalysts compared to the H<sub>2</sub>/N<sub>2</sub> pre-treated one provides further confidence in the reversibility of the pre-treatment effects tested and allows the population balance to be closed within error bars of the analysis. Whilst such species population studies under high pressure reaction conditions are not currently present in the literature, the closure of these balances within good confidence intervals adds weight to the findings in the study.

### 7.3.3 Binary formulations

To complement results and discussion in Sections 7.3.1 and 7.3.2, binary copper-based formulations were also tested under CO/H<sub>2</sub> conditions. The results shown in Table 7.5 show distinct differences between the Cu/ZnO and Cu/Al<sub>2</sub>O<sub>3</sub> catalyst, namely that the latter is unable to produce any methanol and releases no structural oxygen in the form of CO<sub>2</sub> or H<sub>2</sub>O. The Cu/ZnO catalyst was found to behave in a similar manner to that of Cu/ZnO/Al<sub>2</sub>O<sub>3</sub> whereby methanol synthesis activity increases over a 30 min period with time on stream. The methanol productivity of both Cu/ZnO and Cu/ZnO/Al<sub>2</sub>O<sub>3</sub> was found to be similar even though the former has a considerably lower copper surface area in comparison to the latter (32.4 vs. 16.0 m<sup>2</sup> g<sup>-1</sup> based on as received mass). This suggests that copper surface area is not necessarily a direct metric for methanol synthesis performance of copper-based catalysts under CO/H<sub>2</sub>. Instead, the presence of a reducible support appears to be critical as Cu/Al<sub>2</sub>O<sub>3</sub> (featuring an irreducible support) is unable to synthesise methanol. Future work should attempt to measure the total available area of Cu-Zn interfaces with the aim to demonstrate a quantitative relationship with methanol synthesis performance under CO/H<sub>2</sub>.

**Table 7.5: Comparison of performance of 500 mg of copper-based formulations under (CO/H<sub>2</sub>/N<sub>2</sub>: 3/67/30) at 473 K, 25 bar, 7.5 L h<sup>-1</sup>.**

	<b>Cu/ZnO/Al<sub>2</sub>O<sub>3</sub></b>	<b>Cu/ZnO</b>	<b>Cu/Al<sub>2</sub>O<sub>3</sub></b>
<b>Methanol productivity after 30 min on stream (μmol s<sup>-1</sup> g<sup>-1</sup>)</b>	0.22	0.19	0
<b>Total CO<sub>2</sub> eluted after 30 min on steam (μmol)</b>	117	57	0
<b>Total H<sub>2</sub>O eluted after 30 min on steam (μmol)</b>	79	59	0

Both CO/H<sub>2</sub> pre-treated binary formulations were subsequently exposed to CO/CO<sub>2</sub>/H<sub>2</sub>-based gas (Figure 7.19). Again a striking difference is seen whereby methanol

produced over Cu/ZnO passes through a large transient maximum, an effect which is not seen over the Cu/Al<sub>2</sub>O<sub>3</sub> catalyst. Water production is different in magnitude over both catalysts, however the response appears to follow a similar trend in both cases.

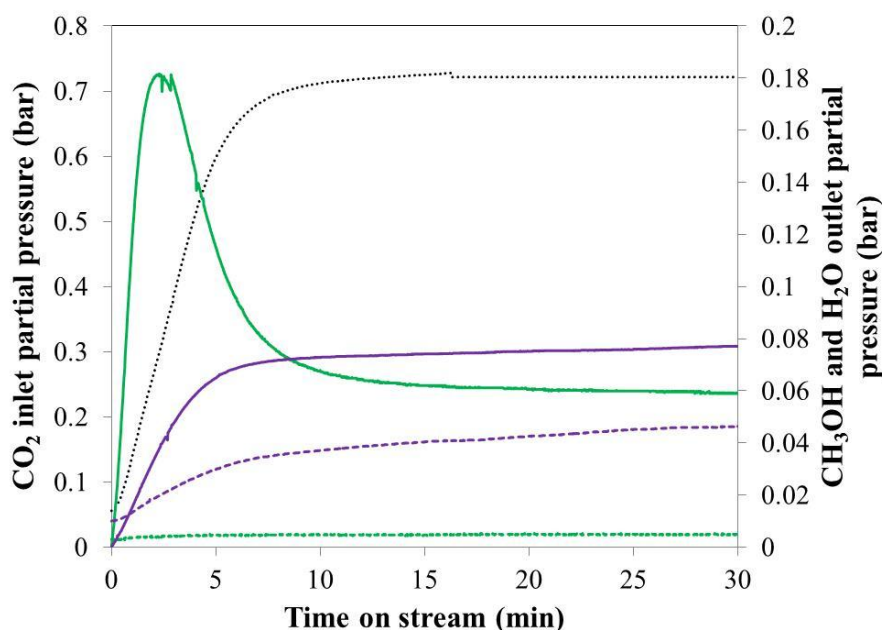


**Figure 7.19: Start-up of 500 mg Cu/ZnO (solid lines) and Cu/Al<sub>2</sub>O<sub>3</sub> (dashed lines) in (CO/CO<sub>2</sub>/H<sub>2</sub>/N<sub>2</sub>: 3/3/67/27) at 473 K, 25 bar, 7.5 L h<sup>-1</sup> following pre-treatment in (CO/H<sub>2</sub>/N<sub>2</sub>: 3/67/30) under the same conditions. (···) denotes inlet CO<sub>2</sub>, (—) outlet CH<sub>3</sub>OH and (—) outlet H<sub>2</sub>O**

Observations in Figure 7.19 again suggest that the creation of vacancies due to oxygen loss from the catalyst under CO/H<sub>2</sub> conditions is critical in generating increased methanol synthesis activity during initial operation when returning to a CO/CO<sub>2</sub>/H<sub>2</sub>-based feed. The presence of ZnO is critical to this effect as the creation of surface defects under CO/H<sub>2</sub> appears to lead to the presence of Cu-Zn interfacial sites for methanol synthesis. These are re-oxidised during transient methanol production when switching back to CO/CO<sub>2</sub>/H<sub>2</sub>.

## 7.4 Conclusions

In this chapter, the dynamic reaction performance behaviour of copper-based methanol synthesis catalysts has been explored via exposure to CO/H<sub>2</sub> conditions, with the aim of further understanding the generation and loss of active sites with these formulations.

Building on the approach carried out for a CO/CO<sub>2</sub>/H<sub>2</sub> feed reactor start-up in Chapter 6, the development of surface species and methanol synthesis performance under CO/H<sub>2</sub> has been quantified. Testing of a model Cu/ZnO/Al<sub>2</sub>O<sub>3</sub> catalyst showed that three mechanisms occur in tandem upon CO/H<sub>2</sub> exposure. Two of these relate to reduction of the catalyst itself, believed to be the removal of oxygen from Cu-Zn interfaces, via H<sub>2</sub> and CO to form H<sub>2</sub>O and CO<sub>2</sub>. Both reactions are competitive and their extent depends on the start-up temperature employed. The third mechanism involves the adsorption of CO-type species onto the catalyst, the magnitude of which increases with start-up temperature.

Whilst the exact origin and reaction mechanism of methanol formed under these conditions cannot be fully ascertained in this study, there appears to be a link between extent of catalyst reduction, species adsorbed and methanol synthesis activity. Whilst these findings agree with works such as Parris and Klier (1986) and Frost (1988), the effect is non-linear with catalyst reduction extent as higher start-up temperatures result in methanol synthesis performance instabilities. Overly defective ZnO structures can inhibit CO adsorption (Bowker *et al.*, 1981) or cause destabilisation of Cu<sup>δ+</sup> species (Ponec, 1992) which may support observations in the current study.

Steady state analysis of CO/H<sub>2</sub> conditions in this study echoes statements made in Bos *et al.*, (1989), which expressed the importance of understanding the origin of CO<sub>2</sub> and H<sub>2</sub>O. Obtaining a stable catalyst under these conditions is difficult and the activity of the catalyst surface appears to be dependent upon the start-up temperature, due to the impact of surface reduction effects by CO and H<sub>2</sub>, which are kinetically driven. This is in stark contrast to performance of copper-based formulations under CO/CO<sub>2</sub>/H<sub>2</sub> in Chapter 6, whereby steady state methanol synthesis and water gas shift performance is reversible over a wide temperature, pressure and feed gas operating window. In this work, these differences have been successfully demonstrated, a discrimination not previously shown in the literature, particularly via the use of transient analysis methods.

Exposure of a CO/H<sub>2</sub> pre-treated Cu/ZnO/Al<sub>2</sub>O<sub>3</sub> catalyst to CO/CO<sub>2</sub>/H<sub>2</sub>-based feeds provided further understanding of generation and loss of active sites. The introduction of CO<sub>2</sub> resulted in a transient methanol production over ~30 min on stream, passing through a maximum. A comparison with a H<sub>2</sub>/N<sub>2</sub> pre-treated catalyst (as described in Chapter 6) shows that the CO/H<sub>2</sub> pre-treated catalyst produces significantly more methanol during this period and also consumes more CO<sub>2</sub>. This additional consumption has been linked with re-oxidation

of vacancies at the Cu-Zn interface and parallel production of methanol. The analysis method used in this study, is the first of its kind to track changes in population of surface species with time on stream. This has enabled the extent of catalyst reduction ( $\text{CO}_2$  and  $\text{H}_2\text{O}$  release under  $\text{CO}/\text{H}_2$  conditions) to be quantitatively linked to the additional  $\text{CO}_2$  consumption observed under initial exposure to  $\text{CO}/\text{CO}_2/\text{H}_2$ .

$\text{CO}/\text{H}_2 \rightarrow \text{CO}/\text{CO}_2/\text{H}_2$  cycling experiments have revealed that pre-treatment effects employed are completely reversible, negating any notion of alloying effects at the catalyst surface which could compromise activity. Similarly,  $\text{CO}/\text{H}_2$  pre-treatments do not impact catalyst behaviour during long term  $\text{CO}/\text{CO}_2/\text{H}_2$  operation in comparison to  $\text{H}_2/\text{N}_2$  pre-treated catalysts. Whilst such reversible effects have been alluded to in Wilmer and Hinrichsen, (2000) and Vesborg *et al.*, (2009), they have been systematically shown across a wider operation scope in this study and backed up by quantitative analysis.

A detailed carbon and oxygen balance analysis of  $\text{CO}/\text{H}_2$  pre-treated catalysts during  $\text{CO}/\text{CO}_2/\text{H}_2$  exposure show a restructuring of surface populations, returning to that observed for a  $\text{CO}/\text{CO}_2/\text{H}_2$  start-up population balance in Chapter 6. Closure of these balances, within 10% error, validates the reversibility of these effects. Coupled with this, a mechanistic link is afforded between additional methanol production during start-up and extent of catalyst reduction under  $\text{CO}/\text{H}_2$ . Agreeing with Vanden Bussche and Froment, (1994), these factors correlate linearly up to 483 K but transient methanol productivity is lower above this pre-treatment temperature. This suggests that a balance between reduced and oxidised sites may be needed to enable methanol synthesis from  $\text{CO}_2$  via the formation of carbonate structures. From this perspective, Cu-Zn and Cu-Cu interfacial sites are no different in their mechanism; it is simply a case that the former can only be readily generated following a more reductive procedure on the catalyst surface.

Critically, assessment of binary copper-based formulations revealed that Cu/ZnO was able to synthesise methanol under  $\text{CO}/\text{H}_2$  but Cu/ $\text{Al}_2\text{O}_3$  could not. Similarly, only Cu/ZnO showed a transient initial overproduction of methanol when switching back to  $\text{CO}/\text{CO}_2/\text{H}_2$  conditions. This shows that the presence of a reducible support, such as ZnO, is critical in the generation of methanol synthesis activity under  $\text{CO}/\text{H}_2$  and also in the development of alternative interfacial sites for methanol synthesis due to support vacancy creation.

Detailed analysis of both transient and steady state operation of copper-based methanol synthesis catalysts has developed an increased understanding of the operating scope of these formulations. A novel analysis of start-up under both CO/CO<sub>2</sub>/H<sub>2</sub> and CO/H<sub>2</sub> conditions has been demonstrated at elevated pressures and has shown clear differences in the surfaces generated for methanol synthesis catalysis. CO/H<sub>2</sub> → CO/CO<sub>2</sub>/H<sub>2</sub> switching experiments have been instrumental in reconciling differences between these two modes of operation and identifying the presence of alternative active sites for methanol synthesis.

## 7.5 References

- Bowker M., Houghton H., Waugh K.C., (1981), '*Mechanism and kinetics of methanol synthesis on ZnO*', J. Chem. Soc. Faraday Trans., 77, 3023-3036
- Bowker M., Hadden R.A., Houghton R.A., Hyland J.N.K., Waugh K.C., (1988), '*The mechanism of methanol synthesis on copper/zinc oxide/alumina catalysts*', J. Catal., 109, 263-273
- Bos A.N.R., Borman P.C., Kuczynski M., Westerterp K.R., (1989), '*The kinetics of the methanol synthesis on a copper catalyst: An experimental study*', Chem. Eng. Sci., 44, 11, 2435-2449
- Boudart M., (1972), '*Two-step catalytic reactions*', AIChE Jnl., 18, 465-478
- Chinchen G.C., Waugh K.C., Whan D.A., (1986), '*The activity and state of the copper surface in methanol synthesis catalysts*', App. Cat., 25, 101-107
- Coteron A., Hayhurst A.N., (1994), '*Kinetics of the synthesis of methanol from CO + H<sub>2</sub> and CO + CO<sub>2</sub> + H<sub>2</sub> over copper-based amorphous catalysts*', Chem. Eng. Sci., 49, 2, 209-221
- Derouane E.G., Baker R.T.K., Dumesic J.A., Sherwood R.D., (1981), '*Direct observation of wetting and spreading of iridium particles on graphite*', J. Catal., 69, 101-110
- Frost J.C., (1988), '*Junction effect interactions in methanol synthesis catalysts*', Nature, 334, 577-580
- Giamello E., Fubini B., (1983), '*Heat of adsorption of carbon monoxide on ZnO pretreated by various methods*', J. Chem. Soc. Faraday Trans., 79, 1995-2003

- Greeley J., Gokhale A.A., Kreuser J., Dumesic J.A., Topsøe H., Topsøe N.-Y., Mavrikakis M., (2003), '*CO vibrational frequencies on methanol synthesis catalysts: A DFT study*', J. Catal., 213, 62-72
- Grunwaldt J.-D., Molenbroek A.M., Topsøe N.-Y., Topsøe H., Clausen B.S., (2000), '*In situ investigations of structural changes in Cu/ZnO catalysts*', J. Catal., 194, 452-460
- Hinrichsen O., Genger T., Muhler M., (2000), '*Probing the elementary steps of the water-gas shift reaction over Cu/ZnO/Al<sub>2</sub>O<sub>3</sub> with transient experiments*', Stud. in Surf. Sci and Cat., 130, 3825-3830
- Klier K., Chatikavanu V., Herman R.G., Simmons G.W., (1982), '*Catalytic synthesis of methanol from CO/H<sub>2</sub> – IV. The effects of carbon dioxide*', J. Catal., 74, 343-360
- Ovesen C.V., Stoltze P., Nørskov J.K., Campbell C.T., (1992), '*A kinetic model of the water gas shift reaction*', J. Catal., 134, 445-468
- Ovesen C.V., Clausen B.S., Schiøtz J., Stoltze P., Topsøe H., Nørskov J.K., (1997), '*Kinetic implications of dynamical changes in catalyst morphology during methanol synthesis over Cu/ZnO catalysts*', J. Catal., 168, 133-143
- Parris G.E., Klier K., (1986), '*The specific copper surface areas in Cu/ZnO methanol synthesis by oxygen and CO chemisorption: evidence for irreversible CO chemisorption induced by the interaction of the catalyst components*', J. Catal., 97, 374-384
- Peppley B.A., Amphlett J.C., Kearns L.M., Mann R.F., (1999), '*Methanol-steam reforming on Cu/ZnO/Al<sub>2</sub>O<sub>3</sub>. Part I: the reaction network*', App. Cat., A: Gen, 179, 21-29
- Ponec V., (1991), '*On the so called junction effect in methanol synthesis*', Catal. Lett., 11, 249-250
- Ponec V., (1992), '*Active centres for synthesis gas reactions*', Catal. Today, 12, 227-254
- Sahibzada M., Metcalfe I.S., Chadwick D., (1998), '*Methanol synthesis from CO/CO<sub>2</sub>/H<sub>2</sub> over Cu/ZnO/Al<sub>2</sub>O<sub>3</sub> at differential and finite conversions*', J. Catal., 174, 111-118

Sloczynski J., Grabowski R., Janas J., Skrzypek J., (1991), '*Adsorption model of methanol synthesis reactants on CuO-ZnO-Al<sub>2</sub>O<sub>3</sub> catalyst – II. Adsorption on the individual components of the catalyst*', Chem. Eng. Sci., 46, 10, 2611-2623

Topsøe N.-Y., Topsøe H., (1999), '*On the nature of surface structural changes in Cu/ZnO methanol synthesis catalysts*', Top. Catal., 8, 267

Twigg M.V., (1989), '*Catalyst handbook – 2<sup>nd</sup> edition*', Wolfe Publishing Ltd., Ch. 9

Vanden Bussche K.M., Froment G.F., (1994), '*Nature of the formate in methanol synthesis on Cu/ZnO/Al<sub>2</sub>O<sub>3</sub>*', App. Cat. A: Gen, 112, 37-55

Vanden Bussche K.M., Froment G.F., (1994), '*A steady-state kinetic model for methanol synthesis and the water gas shift reaction on a commercial Cu/ZnO/Al<sub>2</sub>O<sub>3</sub> catalyst*', J. Catal., 161, 1-10

Vesborg P.C.K., Chorkendorff I., Knudsen I., Balmes O., Nerlov J., Molenbroek A.M., Clausen B.S., Helveg S., (2009), '*Transient behaviour of Cu/ZnO-based methanol synthesis catalysts*', J. Catal., 262, 65-72

Waugh K.C., (1999), '*Prediction of global reaction kinetics by solution of the Arrhenius parameterised component elementary reactions: Microkinetic analysis*', Catal. Today, 53, 161-176

Wilmer H., Hinrichsen O., (2002), '*Dynamical changes in Cu/ZnO/Al<sub>2</sub>O<sub>3</sub> catalysts*', Catal. Letters, 82, 1-2, 117-122

Wilmer H., Genger T., Hinrichsen O., (2003), '*The interaction of hydrogen with alumina-supported copper catalysts: a temperature-programmed adsorption/temperature-programmed desorption/isotopic exchange reaction study*', J. Catal., 215, 188-198

Zuo Z.-J., Han P.-D., Li Z., Hu J.-S., Huang W., (2012), '*Can methanol be synthesized from CO by direct hydrogenation over Cu/ZnO catalysts?*', App. Surf. Sci., 261, 640-646

## Chapter 8:

### Reaction kinetics in formulated industrial catalysts:

#### Conclusions and future work

*The key objective in this thesis was to develop reaction kinetics strategies, using experimental and modelling methods, to understand the fundamental link between performance of catalysts and their formulation. Reactor start-up operation and other transient operation methods were identified as key approaches to meeting these objectives in detail. Three major studies formed the basis of this thesis and development of such strategies: the selective oxidation of n-butane over vanadium phosphorus oxides (VPOs), selective catalytic reduction of NO<sub>x</sub> over vanadia-titania-tungsta and methanol synthesis over copper-based catalysts. In this chapter, the outcomes from these studies and the thesis work as a whole are discussed in light of the aims set out in the introduction. Critically, this thesis has found that a combinatorial approach of experimental, characterisation and kinetic modelling studies, in particular for assessing catalysts under non-steady state operation, was highly effective in understanding generation and loss of specific active sites in catalysts. Such assessments have been linked to changes in the physico-chemical structure of catalyst formulations themselves. The end of this chapter offers future directions beyond this thesis, comprising expansion of experimental methodologies, assessment at different scales and on different reactor technologies.*

## 8. Conclusions Overview

A diverse range of catalyst formulations exist which have application in a wide range of catalytic processes, crossing industries such as chemicals, pharmaceuticals and petrochemicals. This doctoral thesis has utilised a wide portfolio of different catalyst formulations and reactions systems to provide insight into the link between the fundamental reaction kinetics of catalysts and their formulation. For any solid catalyst, surface active sites are at the heart of any intended (or unintended) catalytic process under reaction conditions. Understanding the nature of these sites, their link with reaction pathways and how to form them based on formulation and/or pre-treatment processes is essential to developing a good catalyst. This thesis has used both steady and non-steady state studies carved out of rigorous experimental, characterisation and modelling methods to interrogate the fundamental nature of active sites in a range of catalytic systems.

In the introduction chapter, a series of specific and overall project aims were set out to cover this topic. In the following sections, a reflection will be made on the learning gained from this thesis study and how well these original aims have been addressed. Following this, the work will be placed in the context of the wider kinetics and reaction engineering field, with indications of future works building on this thesis.

### 8.1 Reflection on the specific project aims

*In the pursuit of understanding reaction kinetics of formulated industrial catalysts, develop experimental methods to rigorously probe catalysts under reaction conditions.*

- a. Design lab-based experiments to ensure the absence of heat/mass transport and flow regime limitations so that catalyst testing data are intrinsic in nature and explore 'true' reaction behaviour.*

Elimination of transport limitations and undesired flow regimes to enable the measurement of intrinsic performance data has been at the heart of all experimental studies in this thesis. The review in Chapter 2 identified *a priori* and experimental methods which acted as criteria to ensure such limitations were minimised. The greatest challenge in meeting this aim was found in the VPO selective oxidation study in Chapter 4. This highly exothermic reaction system presented a large barrier to obtaining intrinsic testing conditions however careful experimental design and use of methods from Chapter 2 tempered such effects.

- b. Design experimental methods that are simple to implement so that they can have wider use in future industrial catalyst development programmes or academic studies.***

The parallel difference test, utilising a series of fixed catalyst beds of varied mass under operation in tandem, saw significant development in this thesis. On a simpler level, the method was utilised in steady state studies (such as methanol synthesis and water gas shift kinetics over Cu/ZnO/Al<sub>2</sub>O<sub>3</sub> in Chapter 6) to provide axial performance profiles of catalyst performance at different operating conditions. This enabled a more thorough dataset to be gathered for such purposes. The subsequent aim in this section will explore the benefits of this method for catalysts operating under non-steady state operation.

Choice of reactor outlet composition analysis method is critical in any catalyst study, particularly when non-steady state operation is probed. It is critical that the analyser used can both suitably analyse the components of an outlet stream and achieve it on a relevant time scale. Regarding the latter, gas chromatography was suitable to monitor VPO evolution (analysis time: 5 – 10 min; catalyst evolution period: 10 – 100 h) but would have been highly unsuitable to measure transient methanol synthesis performance (catalyst evolution period: 10 – 60 min). In this thesis, the methods used provided suitable data density for the catalyst performance evolution phenomena under study.

***Develop non-steady state experimental approaches which can provide further depth of understanding of catalyst systems, in particular to probe the following:***

- a. Generation and loss of catalytically active sites during catalyst pre-cursor activation and/or initial operation under reaction conditions (reactor start-up).***

The parallel difference test was utilised to describe four different non-steady state scenarios: a fresh VPO catalyst under *n*-butane-air, reduction of copper-based catalysts in H<sub>2</sub>/N<sub>2</sub>, exposure of reduced copper-based catalysts in CO/H<sub>2</sub> and CO/CO<sub>2</sub>/H<sub>2</sub>. This method allowed the performance evolution of a ‘full’ integral catalyst bed to be monitored in smaller segments.

In the case of the VPO catalyst, this enabled an understanding of active site evolution of the catalyst by applying kinetic models to discrete time on stream datasets. For the reduction of copper-based catalysts, a ‘wave-like’ reduction effect of the catalyst bed could

be clearly seen and a mass balance of all bed sectors revealed a homogeneous catalyst reduction at the end of the procedure.

For copper-based catalysts under CO/H<sub>2</sub> and CO/CO<sub>2</sub>/H<sub>2</sub>, dynamic changes in surface species (based on carbon and oxygen balances) could be identified across the catalyst bed and this was linked to evolution of different reaction pathways. Under CO/H<sub>2</sub>, a Cu/ZnO/Al<sub>2</sub>O<sub>3</sub> catalyst undergoes ZnO reduction (postulated to be at Cu-Zn interfaces) as well as surface adsorption of CO in a homogenous manner. Meanwhile, under CO/CO<sub>2</sub>/H<sub>2</sub> this reduction step does not occur due to a more oxidising atmosphere and a population of CO<sub>x</sub>-type species develop on the surface. In contrast to CO/H<sub>2</sub> operation, analysis showed that the overall population of the latter were largely present at the front of the full catalyst bed. Such findings would be less clear if only a standard integral bed was utilised without a sector breakdown.

***b. Dynamic behaviour of catalysts following a change in process conditions (transient response experiments).***

These methods saw significant development for copper-based catalysts (introduction of CO<sub>2</sub> into a CO/H<sub>2</sub> feed) and for NH<sub>3</sub> adsorption and desorption testing (under NH<sub>3</sub>/He feeds). Dynamic analysis of these systems permitted an understanding of changes in surface populations of these catalysts. Closure of carbon and oxygen (for copper-based catalysts) and nitrogen balance (for V<sub>2</sub>O<sub>5</sub>-WO<sub>3</sub>/TiO<sub>2</sub> catalysts) was successfully demonstrated between step changes.

A key learning from these studies is that it is of critical importance to characterise empty reactors when exposed to a step change in conditions. Due to the setup of the equipment utilised, the imposed changes in conditions were rarely immediate step changes and had to be themselves described with time on stream. Whilst this implementation was successful and improved interpretation of data, minimising transient effects in inlet feeds upon a step change is advisable if the equipment allows.

***c. Generation and loss of catalytically active sites during longer-term ageing of catalyst formulations.***

V<sub>2</sub>O<sub>5</sub>-WO<sub>3</sub>/TiO<sub>2</sub> formulations for NH<sub>3</sub> selective catalytic reduction of NO<sub>x</sub> evolve slowly with time on stream and are an example of a catalyst which requires accelerated ageing to measure long term loss of activity. In Chapter 5, the steady state kinetic

development of these catalysts was measured at different stages of ageing. This allowed the evolution of kinetic model parameters to be understood with time on stream providing a strong link between ageing phenomena and changes in catalyst performance.

***Develop appropriate steady-state and dynamic kinetic modelling techniques in order to fit experimental data to mechanistically-based kinetic models and estimate key parameters surrounding catalytic reaction behaviour (e.g. activation energies).***

Athena Visual Studio, a parameter estimation modelling tool, was applied for both steady-state and dynamic kinetic modelling pursuits in this thesis. Steady-state kinetic models were solved using either explicit methods (typically for modelling one reaction pathway) or implicit methods (for multiple and/or complex reaction systems). In general, the latter saw greater use due to the prevalence of a number of networks where reactants and products were dependent on multiple reactions, hence direct reaction rates were unknown.

For modelling of catalyst performance evolution, a non-steady state model basis was found to be most appropriate where dynamic changes in surface species population were prevalent (e.g. NH<sub>3</sub> adsorption-desorption work). For slower evolving systems, such as the steady state work over V<sub>2</sub>O<sub>5</sub>-WO<sub>3</sub>/TiO<sub>2</sub> or the start-up evolution of VPO, changes in surface populations and/or activity were negligible over discrete points of performance analysis allowing pseudo-steady state modelling methods to be utilised successfully.

***Develop rigorous statistical analysis methods to interrogate both quality of data and kinetic modelling parameter estimation results in order to develop more robust model descriptions of catalyst reaction performance.***

***a. Include critical examination of estimated parameters from kinetic modelling studies to understand these outputs in a real, physical sense.***

In Chapter 3, methods were developed using batch hydrogenation data, based on literature approaches, which examined the quality of parameter estimations when data were fitted to kinetic models. The approach was successful in eliminating statistically insignificant parameters by use of sensitivity values and then checking the impact of removing parameters by use of the global *F*-test. The approach had subsequent use throughout the thesis chapters concerning catalyst performance evolution.

A large emphasis has been placed on combining an understanding and appreciation of chemistry and statistics in this thesis. At every stage of the kinetic modelling process, values of estimated parameters were questioned, based not only on their statistical integrity but also their meaning in a physico-chemical sense. For example, in Chapter 3, an activation energy was identified as an insignificant parameter; its removal was statistically valid but not chemically valid and was instead equated to another activation energy which described the same reaction pathway in a different position of the reaction network.

***Employ appropriate catalyst characterisation methods to provide supporting evidence to kinetic models and findings from experimental reaction studies.***

Catalyst characterisation methods were found to be highly useful and confirming or refuting possible physico-chemical phenomena taking place which may link to catalyst performance evolution changes. In the study of VPO catalysts, bulk phase and oxidation state changes observed from XRD, Raman and auto-titration methods were found to take place on a considerably slower time-scale than the observed performance changes, whilst subtle changes in the XPS spectra with time on stream, relating to surface oxidation state, were more closely linked.

The nature of the catalyst state with respect to operating conditions was found to be a key driver behind characterisation techniques used. Characterisation of copper-based catalysts with respect to performance evolution was the most challenging as the active catalyst is developed *in situ*. In this study, reactive frontal chromatography was used to measure copper metal surface area. This provided measurements which were later linked to carbon and oxygen coverages under operation conditions. The use of *in situ* and *operando* techniques could certainly be expanded from this thesis and will be discussed in future work.

## **8.2 Reflection on the overall project aims: ‘A tale of two active sites’**

***Combine experimental, characterisation and kinetic modelling approaches to fundamentally understand reaction pathway functionality and the nature of active sites on the surfaces of catalyst formulations.***

Drawing on the specific aims summarised in Section 8.1, a combinatorial approach has been attempted with good success throughout this thesis. As initially discussed in Chapter 2, a broad range of options are available for experimental, characterisation and modelling

pursuits. By utilising a wide portfolio of catalyst systems in this thesis, this has allowed a deeper understanding of relevant combinatorial strategies to be developed. Experimentally, obtaining good steady state experimental test data was an essential basis for developing kinetic models in the VPO, V<sub>2</sub>O<sub>5</sub>-WO<sub>3</sub>/TiO<sub>2</sub> and Cu-based catalyst studies. For transient studies, the timescale of catalyst performance evolution phenomena observed had a strong impact on the methodologies used.

In this thesis, experimental, characterisation and modelling studies have been intrinsically linked. Due to this, specific emphasis has been placed on the limitations and induced errors in all three aspects. For example, a poorly designed experiment featuring unintended heat gradients over the catalyst under observation may impact on its physical state for subsequent characterisation, thus providing misleading results. Similarly, understanding error variation in experimental measurements has a direct impact on confidence in kinetic model parameters when data are fitted.

***By examining a range of catalyst formulations for use in a particular reaction system, understand the critical structural components that deliver catalytic functionality in these formulations. This should be linked with the scope of reaction conditions employed for the catalytic process in question.***

A primary deliverable of this thesis is to link findings from experimental, characterisation and kinetic modelling with catalytic functionality and formulation. In this thesis, the analysis of catalysts under transient operation has been particularly fruitful in identifying the development and/or loss of active site populations (relating to specific reactions) at the catalyst surface.

In some studies, a strong link has been forged between reaction conditions, catalyst functionality and formulations. For Cu-based catalysts, it was demonstrated that the copper component was key to methanol synthesis functionality under CO/CO<sub>2</sub>/H<sub>2</sub> conditions but a reducible support was essential for the same functionality under CO/H<sub>2</sub>. Similarly in this study, reaction temperature had a time-dependent impact on catalyst activity under CO/H<sub>2</sub> but not under CO/CO<sub>2</sub>/H<sub>2</sub>.

In the case of the VPO catalyst, the link between reaction conditions, catalyst functionality and formulation is more subtle. Reaction conditions employed over the fresh catalyst during start-up all had the same time dependent effect and to the same degree within

the bounds of the study (which covered industrially relevant conditions). Kinetic modelling played a strong role in this study in discerning the development of two distinct active sites, the second of which was linked to the re-oxidation of product maleic anhydride (MA) and was quickly lost under *n*-butane/air with time on stream.

***By studying a range of catalyst systems and in meeting the above aims, assess common themes and differences between different types of catalytic system.***

The three key studies of this thesis have all employed mixed metal oxide catalysts for very different catalytic chemistries. An interesting common theme between all three studies have been the prevalence of two key active sites which can either be developed or lost as a function of reaction conditions and/or time on stream:

- **VPO catalysts:** Two sites, one for *n*-butane oxidation and one for MA oxidation in fresh catalyst. The fresh catalyst is highly active but less selective to MA production. Activity of the latter pathway decays severely with time on stream resulting in a less active but more selective catalyst.
- **V<sub>2</sub>O<sub>5</sub>-WO<sub>3</sub>/TiO<sub>2</sub>:** The relative population of NH<sub>3</sub> adsorption and activation (reactive) sites has a strong impact on catalyst performance. Control of the catalyst formulation procedure can maximise the latter, increasing activity, but retaining a high proportion of these sites is difficult over long term operation.
- **Cu-based catalysts:** Under CO/CO<sub>2</sub>/H<sub>2</sub> conditions, methanol synthesis largely takes place over Cu-Cu-type sites. An alternative site, postulated to be at the Cu-Zn interface is generated following a CO/H<sub>2</sub> pre-treatment which is highly active in methanol production under CO/CO<sub>2</sub>/H<sub>2</sub> but is lost in the process of this catalytic reaction taking place.

From this summary of each study, the catalyst formulation and/or pre-treatment procedure have an impact on the nature of sites initially generated. It appears that high initial catalyst activity is somewhat linked with instability and often formulations cannot maintain this level of performance under the conditions employed. This thesis has been successful in identifying discrete active sites for different catalysts however, opening up new possibilities in the catalyst formulation process, which will be discussed in Section 8.3.

The methods developed to investigate reaction kinetics in industrial catalyst formulations in this thesis have led the way to novel findings during each catalyst case study, particularly around the fundamental catalytic chemistry taking place. For example, the insight given in the VPO study provided a clear identification and discrimination of two different active sites. Whilst the presence of these distinct sites has been alluded to in the literature, transient kinetic analysis of fresh catalyst evolution under reaction conditions has provided strong evidence to these assertions. Elsewhere, the approach demonstrated in Chapters 6 and 7 for copper-based methanol synthesis catalysts is the first of its kind to concisely track surface species population levels and the extent of catalyst reduction/oxidation under a range of industrially relevant reaction conditions. Combining these findings with kinetic modelling has yielded greater understanding of the generation and loss of catalytically active sites over these materials.

### **8.3 Context and future work**

Returning to the introduction chapter, the importance of grasping complexity in catalysis was discussed. This is necessary when linking fundamental understanding of catalyst performance to its formulation as these two factors change as a function of a wide range of possibilities, from manufacturing process to conditions employed in the reactor. The use of non-steady state operation has in particular met this need; for example, analysis of fresh catalyst formulations during start-up under reaction conditions has provided new insight around the development and loss of catalytically active sites. The problem is inherently more complex than a steady state study, requiring careful and more detailed kinetic analysis, but the outcome was a clear picture of key active sites developed in catalyst formulations and a good measure of their activity and stability. The use of different catalyst formulations in this process (such as a range of copper-based catalysts) strengthened the links between reaction kinetics, active sites and formulation.

In the wider reaction engineering field, the studies in this thesis have presented a number of novel methods, chiefly including:

- New types of non-steady state analysis methods in heterogeneous catalysis; in particular analysis of reactor start-up performance of fresh catalysts.

- Development of rigorous and high throughput experimental methods; in particular the parallel difference test, which can be applied to a wide range of fixed-bed type catalytic systems, beyond this thesis scope.
- A key focus around non-steady state performance under industrially relevant reaction conditions; for example the study of copper-based catalysts under CO/H<sub>2</sub> and CO/CO<sub>2</sub>/H<sub>2</sub> is a first in fully quantifying dynamic behaviour at elevated pressures.
- Systematic procedures to develop statistically and physico-chemically sound kinetic models utilising experimental data.

In light of these developments, there lie further opportunities in this area for the reaction engineering community which can serve to further improve understanding of the links between reaction kinetics, catalyst functionality and formulation:

- **Integration of *operando* techniques:** Further technique development may permit greater understanding of some of the thesis findings. An example would incorporate an oxygen or carbon labelling study for the Cu-based catalysts, particularly to improve interpretation of the CO/H<sub>2</sub> → CO/CO<sub>2</sub>/H<sub>2</sub> switching experiments.
- **Further redox studies (i.e for systems such as VPO selective oxidation):** Catalyst reduction and re-oxidation activity over catalysts at different stages of their lifetime can be assessed separately. For example, transient performance under reducing conditions (e.g. organic/inert) only can be observed followed by switching to oxidising conditions (e.g. oxygen /inert). Kinetic modelling of these performance observations can be used to extract further mechanistic information about catalyst behaviour. By examining a catalyst at different stages of its lifetime, evolution of active site populations can be understood with greater clarity.
- **Understanding development and loss of catalyst activity with scale:** Understanding the impact of heat/mass transport and flow regime effects on the development and loss of catalytic activity, during both start-up and long term operation.
- **Practical start-up and shut-down aspects:** Linking to the above, develop practical methods to effectively start-up (and shut-down) catalytic reactors so that adverse effects are minimised and the start-up procedure delivers maximised catalyst activity.
- **Links with computational chemistry:** A number of mechanisms have been proposed throughout this thesis for the development and loss of catalytically active sites. Such

mechanisms could be tested using computational chemistry, such as the interaction of reactants with postulated active sites/surfaces and the subsequent reactions encountered.

- **Alternative reactor technologies:** The bulk of this thesis has largely developed techniques around fixed-bed gas phase operation. Subsequent steps may be to apply and develop methods to systems such as trickle beds (three phase systems), fluidised beds and riser-regeneration systems.
- **Integrated approach with the catalyst formulation process:** This thesis has laid down the main mechanistic lines for the generation and loss of activity of catalyst formulations for a number of processes. These findings can be linked to the manipulation of key parameters of the catalyst formulation process which could be explored more deeply. New formulations should be explored against a key catalyst testing metric, for example start-up under a defined set of conditions with results applied to existing models.